Assessing water colour of lakes with high and medium spatial resolution remote sensing data

Dissertation

zur Erlangung des Doktorgrades
der Mathematisch-Naturwissenschaftlichen-Fakultät
der Christian-Albrechts-Universität zu Kiel

vorgelegt von
Katja Judith Dörnhöfer

Kiel, 2018

Erste Gutachterin: Prof. Dr. Natascha Oppelt

Zweite Gutachterin: PD Dr. Angela Lausch

Termin der mündlichen Prüfung: 12. Juni 2018
Zum Druck genehmigt: 12. Juni 2018

gez. Prof. Dr. Natascha Oppelt, Dekanin

Danksagung

An dieser Stelle bedanke ich mich bei allen Personen, die dazu beigetragen haben, dass ich diese Dissertation abschließe.

In erster Linie bedanke ich mich herzlich bei meiner Betreuerin Prof. Dr. Natascha Oppelt für ihre Beratung und Geduld in den letzten vier Jahren. Ihre Art und Weise hat so ein angenehmes Arbeitsumfeld, aber auch genügend Druck geschaffen, um voranzukommen. Im Rahmen des BMWi geförderten Projekts LAKESAT hat sie mir die Möglichkeit gegeben, viel Erfahrung in der Gewässerfernerkundung, sei es beim Messen oder Modellieren, zu sammeln. Auf Konferenzen/ Workshops hatte ich die Gelegenheit mich in der Community auszutauschen.

Ein lieber Dank geht an PD Dr. Angela Lausch (UFZ Leipzig) für die Begutachtung meiner Dissertation. Die (Mess-) Workshops der Fernerkundungs-Binnengewässergruppe, bei denen ich sie kennen gelernt habe, brachten mir viele Ideen und Erkenntnisse. Meinen Arbeitskollegen der AG Earth Observation and Modelling (Marcel König, Dr. Alireza Taravat, Florian Uhl, Matthias Wagner) danke ich für den Arbeitsalltag auflockernde Diskussionen und gegenseitige Unterstützung. Stenka Vulova danke ich für sprachliche Anmerkungen.

Während der Promotionsszeit habe ich viele Messkampagnen durchgeführt, die ohne die Hilfe anderer nicht umsetzbar gewesen wären. Mehrere Hilfskräfte und Geographie-Studierende unterstützten mich durch Studienprojekte und Abschlussarbeiten dabei. Ein besonderer Dank geht hier an meine ehemalige Arbeitskollegin Thea-Lina Merkens, die stets zur Stelle war und oft bis spät in die Nacht im Labor der Abteilung Hydrologie und Wasserwirtschaft mit mir zusammen Wasserproben filtriert hat.

Bei Ilona Korczynski bedanke ich mich für die unkomplizierte Bereitstellung von Mess- und Geodaten vom Kummerower See durch das Ministerium für Landwirtschaft und Umwelt Mecklenburg-Vorpommern. Für den Starnberger See erhielt ich dankenswerterweise Messdaten von Dr. Peter Gege und Anna Göritz vom DLR Oberpfaffenhofen. In diesem Zusammenhang sei auch den Kooperationspartner von LAKESAT der TU München, Dr. Thomas Schneider und Christine Fritz, für Laboranalysen, Daten- und Wissensaustausch gedankt. Mit Christine Fritz hat mich eine verlässliche Projektpartnerin begleitet. In den letzten vier Jahren haben wir uns nicht nur am Telefon oft gegenseitig motiviert und unterstzützt.

In dieser kumulativen Dissertation sei meinen Co-Autoren (Dr. Peter Gege, Anna Göritz, Dr. Thomas Heege, Philip Klinger, Prof. Dr. Natascha Oppelt, Bringfried Pflug, Jorrit Scholze, Kerstin Stelzer) für ihre Zuarbeit gedankt. Die kritischen Kommentare im Vorfeld haben so zu meist hilfreichen Reviewer-Kommentaren geführt und damit zur erfolgreichen Veröffentlichung beigetragen.

Beim Graduiertenzentrum der Christian-Albrechts-Universität zu Kiel bedanke ich mich für das umfassende Kursprogramm zur Weiterbildung für Promovierende. Insbesondere Katharine Simmons und Ulf Evert von der Science Show danke ich für das Coaching in den letzten eineinhalb Jahren, durch das ich gelernt habe und die Möglichkeit hatte, mein Dissertationsthema allgemein verständlich einem breitem Publikum vorzustellen.

Meinem Freund Michael Kuhwald gebührt außerordentlicher Dank für sein ungebrochenes Verständnis und die moralische Unterstzützung in allen erdenklichen Lagen. Vielen Dank für deine stets kritischen Nachfragen und Anmerkungen.

Summary

Lakes form essential ecosystems, play an important role in the Earth's biogeochemical cycles and provide various ecosystem services to humans. Lakes undergo natural and human-induced changes which may influence their ecological integrity and are therefore often monitored with traditional point-based samplings. Remote sensing techniques can assist the traditional approaches by supplying spatial information on optically active lake ecology indicators. These are namely chlorophyll-a (CHL), total suspended matter (TSM), coloured dissolved organic matter (CDOM), and, especially in optically shallow waters, water depth and substrate composition.

The current generation of land observation satellites with their improved radiometric characteristics, such as Sentinel-2 and Landsat 8, offer a high potential for a remote sensing based lake monitoring at high spatial resolution (10-60 m). A comprehensive literature review, conducted in the present thesis, provides an overview on the current research status concerning lake remote sensing and its added value for lake ecology. The primary focus was on indicators associated with the lake properties transparency, biota, hydrology, ice phenology and water temperature. The review shows that time series analyses of indicators derived from archived and operational sensors offer great benefits for lake ecology analyses and monitoring. In view of new sensors, the present thesis aims at investigating the suitability of Sentinel-2 and Landsat 8 for lake monitoring as well as their combination with spatially lower resolved sensors and archived imagery. Two study areas with highly different optical characteristics served as test sites, i.e. the oligotrophic Lake Starnberg (southern Germany) and the mesotrophic-eutrophic Lake Kummerow (northern Germany).

Various measurement campaigns were conducted at both lakes to provide a data basis for sensor evaluations. Using the bio-optical model WASI-2D, Sentinel-2A turned out to be suited for retrieving low TSM and CDOM concentrations. CHL estimations performed better for higher CHL concentrations. The high spatial resolution enabled the differentiation between bare ground and areas covered by submerged aquatic vegetation. Water depth estimations performed well until half Secchi disk depth. Combining CHL, retrieved with the Modular Inversion and Processing System, from different satellite sensors (MODIS, Landsat 7/ 8, Sentinel-2A) underlined the synergetic use of remote sensing and *in situ* data for observing phytoplankton development at Lake Kummerow. This synergetic data composite enabled detailed observations of phytoplankton development and the integration of satellite data into trophic state assessment. Cross-sensor comparisons demonstrated high correlation of CHL among timely acquired, spatially high and medium resolved sensors. Evaluations with *in situ* data showed that most of the sensor-*in situ* match-ups were within an uncertainty range of *in situ* measurements. Analysing a 9-year MERIS time series with FUB/WeW revealed unprecedented information on temporal trends and seasonal behaviour of CHL, TSM and CDOM at the study area Lake Kummerow.

The present thesis demonstrates the suitability of Sentinel-2A and Landsat 8 for mapping lake ecology indicators. It further shows the importance of including *in situ* measurement uncertainties into sensor and algorithm evaluations. A synergetic combination of multiple sensors necessitates sensor-independent algorithms for atmospheric correction over water bodies and for indicator retrieval. Such combinations are a step forward to future lake analyses which may integrate remote sensing data, *in situ* measurements and environmental modelling.

Zusammenfassung

Als elementarer Teil biogeochemischer Kreisläufe der Erde bilden Seen wichtige Ökosysteme und stellen uns Menschen verschiedene Ökosystemleistungen zur Verfügung. Seen durchlaufen natürliche aber auch vom Menschen verursachte Veränderungen, die ihre ökologische Integrität beeinflussen können. Um dies zu beobachten, werden häufig Indikatoren dieses Zustands mit etablierten, punktbasierten Messmethoden erfasst. Fernerkundungstechniken können diese Ansätze unterstützen. Sie stellen räumliche Informationen über optisch aktive Indikatoren der Seeökologie bereit: Chlorophyll-a (CHL), die Gesamtmenge der suspendierten Partikel (TSM) und die farbgebende Komponente des gelösten organischen Kohlenstoffs (CDOM). Im Flachwasser kommen die Wassertiefe und die Untergrundbedeckung hinzu.

Die aktuelle Generation der Erdbeobachtungssatelliten, wie Sentinel-2 und Landsat 8, weist verbesserte radiometrische Eigenschaften auf bei gleichzeitiger, hoher räumlicher Auflösung (10-60 m) und bietet damit ein großes Potenzial für ein fernerkundliches Seenmonitoring. In dieser Dissertation wurde eine umfassende Literaturrecherche durchgeführt, die einen Überblick über den aktuellen Forschungsstand im Bereich der Seenfernerkundung und deren Mehrwert für die Gewässerökologie gibt. Dabei kam heraus, dass Zeitreihenanalysen auf Basis archivierter und operationeller Sensoren große Vorteile für die Analyse und Beobachtung der Gewässerökologie mit sich bringen.

Im Hinblick auf die neuen Sensoren zielt die vorliegende Dissertation darauf ab, die Möglichkeiten von Sentinel-2 und Landsat 8 für das Seenmonitoring zu untersuchen und inwiefern diese mit anderen Sensoren und archivierten Daten kombiniert werden können. Als Untersuchungsgebiete dienten zwei Seen mit jeweils sehr unterschiedlichen optischen Eigenschaften: der oligotrophe Starnberger See (Süddeutschland) und der mesotrophe-eutrophe Kummerower See (Norddeutschland). Dort wurden mehrere Messkampagnen durchgeführt um eine Datengrundlage für die Evaluierung der Sensoren zu schaffen. Unter Verwendung des bio-optischen Models WASI-2D erwies sich Sentinel-2A als geeignet um niedrige TSM- und CDOM-Konzentrationen abzuleiten. CHL ließ sich unter höheren CHL-Konzentrationen besser bestimmen. Im Flachwasser ermöglichte die hohe räumliche Auflösung eine Unterscheidung zwischen unbewachsenem Boden und mit Makrophyten bedeckten Flächen sowie die Bestimmung der Wassertiefe bis etwa halbe Sichttiefe. Zudem sind CHL Produkte mit dem 'Modular Inversion and Processing System' aus verschiedenen Satellitensensoren (MODIS, Landsat 7/ 8, Sentinel-2A) bestimmt worden. Deren Kombination mit *in situ* Daten verdeutlichte wie eine solche synergetische Nutzung zur Beobachtung der Phytoplanktonentwicklung am Kummerower See eingesetzt werden kann und zeigte, dass Satellitendaten in die trophische Zustandsbewertung integriert werden können. Die meisten Match-ups der Evaluierung lagen innerhalb eines Unsicherheitsbereich der *in situ* Messungen. Aus der Analyse (FUB/WeW) einer 9-jährigen MERIS Zeitreihe ergaben sich bisher nicht vorhandene Informationen über zeitliche Trends und saisonales Verhalten von CHL, TSM und CDOM am Kummerower See.

Die vorliegende Arbeit zeigt, dass Sentinel-2A und Landsat 8 für die fernerkundliche Bestimmung von Indikatoren der Seeökologie geeignet sind. Sie zeigt ferner, wie wichtig es ist, *in situ* Messunsicherheiten in Evaluierungen von Sensoren und Algorithmen einzubeziehen. Eine synergetische Nutzung mehrerer Sensoren benötigt aber sensorunabhängige Algorithmen zur Atmosphärenkorrektur speziell über Gewässern und zur Indikatorableitung. Solche Kombinationen weisen in Richtung einer zukunftsorientierten Analyse von Seen, die Fernerkundungsdaten mit *in situ* Messungen und Umweltmodellierung verknüpft.

Contents

List of Figures

List of Tables

Abbreviations

CHL chlorophyll-a.

N nitrogen.

P phosphorous.

TOC total organic carbon.

Chapter 1

Introduction

1.1 Monitoring of lakes and assessing water colour

Lakes are highly productive ecosystems with a high biodiversity and play an important role in the Earth's biogeochemical cycles (Moss, 2012; Tranvik et al., 2009). Lakes provide essential habitats for a variety of species. Around 117 million lakes (area > 0.002 km^2) cover 3.7 % of the Earth's non-glaciated surface ($5{\cdot}10^6$ km^2, Verpoorter et al. 2014). Currently, around 50 % of the Earth's population lives in close vicinity (< 3 km) to lakes or rivers (Politi et al., 2016) since humans benefit from a variety of ecosystem services provided by lakes. For instance, we extract lake water for drinking water and irrigation, enjoy lakes for recreational activities, generate energy from hydropower and benefit from climate regulation (Anzaldua et al., 2018; Millennium Ecosystem Assessment, 2005). Nevertheless, anthropogenic influence subjects lakes to manifold pressures, such as climate change, eutrophication, harmful algal blooms (HAB), invasive species, and morphological alterations which affect their ecological integrity and water quality (Anzaldua et al., 2018; Brönmark and Hansson, 2002; Brooks et al., 2016). Apart from direct interventions, interferences in their catchment also have an indirect impact on lakes; lakes therefore are often considered as sentinels of change in their catchment (Adrian et al., 2009).

Detecting changes in the ecological integrity and water quality of lakes requires a monitoring of indicators which describe and respond to changes in a lake's status (Poikane et al., 2014; Tuvikene et al., 2011). Lake management which aims to preserve or restore a lake's status also necessitates monitoring to observe amelioration or deterioration (e.g. Jeppesen et al., 2005; Spears et al., 2016). Prominent indicators measured in lakes provide information on physico-chemical state (e.g. pH, nutrients, electric conductivity, oxygen, harmful substances), on hydro-morphological conditions (size, water depth, substrate, mixing character, water residence time, shoreline structure) and on biological state (e.g. phytoplankton composition and biomass, aquatic vegetation, fish, macroinvertebrates) (European Commission, 2000). Hitherto, *in situ* monitoring of such indicators has mainly relied on individual point-based sampling or diver's mapping (Pasztaleniec, 2016). Traditional lake monitoring approaches, however, reach their limitations and are hardly able to tackle the challenges of global and climate change alone (e.g. Bertani et al., 2017; Brooks et al., 2016; Politi et al., 2016). Prominent constraints are a limited spatial coverage and temporal frequency which fail to capture for instance short-living cyanobacterial or phytoplankton blooms (Reyjol et al., 2014), the spatial expansion of submerged aquatic vegetation (SAV) (Shuchman et al., 2013b) or reoccurring events of high total suspended matter concentrations hindering SAV colonisation (Giardino et al., 2010a). Costs and

logistics of *in situ* sampling cause trade-offs between the ideal and implemented monitoring strategy (Pasztaleniec, 2016; Schaeffer et al., 2013). Different sampling and analysis protocols constrain comparative studies among different lakes (Cao and Hawkins, 2011; Diamond et al., 2012). The European Union's Water Framework Directive (WFD) aimed to achieve comparable assessments of all water bodies among the European Union's member states (Poikane et al., 2015). Nevertheless, Birk et al. 2012 entitled their paper 'three hundred ways to assess Europe's surface waters' which summarised biological methods applied in the WFD.

Remote sensing may help to overcome the lack of comparability and to fill gaps in lake assessment systems. Satellites provide spatially synoptic data covering entire lakes in temporally regular intervals. Indicators can be retrieved from standardised products or with standardised algorithms. Indeed, passive remote sensing can only derive indicators, which have an influence on the radiometric characteristics of a lake detectable by a remote sensor and depends on cloud free data (e.g. Hestir et al., 2015a; Mouw et al., 2015; Palmer et al., 2015b). Being aware of the constraints and benefits, remote sensing offers a great potential for lake monitoring (details in Chapter 3). In combination with *in situ* sampling and complex lake models, remote sensing can support the detection of changes in water quality and improve lake management (e.g. Bertani et al., 2017; Politi et al., 2016; Tyler et al., 2016).

The principle of lake (or inland waters which may also include rivers) remote sensing originates from ocean remote sensing research which started in the 1960s (Morel and Gordon, 1980; Ogashawara et al., 2017b). Compared to lakes, oceans are relatively clear waters. The main optically active constituent, which contributes to the water colour is phytoplankton, in particular the photosynthetic active pigment chlorophyll-a (CHL). If present, other constituents, such as total suspended matter (TSM) or coloured dissolved organic matter (CDOM) highly covary with chlorophyll-a (CHL) in the open ocean (Morel and Prieur, 1977). In contrast, CHL, TSM and CDOM occur independently in different concentrations and relationships in lakes and other inland waters. The optically shallow waters of lakes, where the bottom is visible, introduce a further complexity, i.e. the influence of the bottom substrates (e.g. macrophytes and bare sediment) and the water depth or bathymetry. Due to these diverse optical characteristics, lakes are called optically complex (Mouw et al., 2015). Remote sensing of lakes focuses on the physical relationships between concentrations of optically active water constituents (in optically shallow water additionally bottom and water depth) and the shape and intensity of the water-leaving radiance, i.e. the water colour (details in section 3.2.1). CHL-rich waters, for instance, appear in greenish colours owing to a maximum of water-leaving radiance in green wavelengths; relatively clear waters are rather blueish and the strong absorbing behaviour of CDOM results in a very dark brownish water colour. In shallow water, the water colour darkens with increasing water depth assuming a homogeneous bottom type; shallow water areas with bare sediment appear lighter than areas where macrophytes grow. Remote sensing sensors on different platforms such as spaceborne satellites, airplanes or unmanned aerial vehicles gather the scattered radiation as a physically measurable quantity of the water colour.

Lakes scatter low amounts of radiation since water is a strong absorber. Additionally, the atmosphere and water surface contribute to about 90-98 % of the radiation obtained by a sensor (Gitelson and Kondratyev, 1991). Remote sensing of lakes therefore requires sensors which offer spectral and radiometric characteristics sensitive enough to gather the low radiometric signal from the water (Mouw et al., 2015). Furthermore, an accurate atmospheric correction is the basis to remove undesired effects from the atmosphere (e.g. absorption and scattering, adjacency effects) and water surface (e.g. sun and sky glint) to obtain the desired remote sensing reflectance (R_{rs}) of

the water body (Gege, 2017; Moses et al., 2017). Various remote sensing algorithms exist which use this reflectance to derive quantitative information on water constituents, bottom or water depth (details in Chapter 3).

In the last 30 years, significant progress has been made in developing such algorithms for lake remote sensing (Ogashawara et al., 2017b). Ogashawara et al. (2017b) recently classified available approaches into empirically based, semi-empirical, semi-analytical, quasi-analytical and analytical algorithms. Most scientific studies using these algorithms, however, were based on spatially medium to low resolved ($\geq$ 300 m x 300 m) data from ocean colour data such as Medium Resolution Imaging Spectrometer (MERIS), Moderate Resolution Imaging Spectrometer (MODIS) or SeaWiFS and were therefore concentrated on larger lakes (e.g. Lake Balaton, Lake Taihu, Great Lakes; Dörnhöfer and Oppelt, 2016; Odermatt et al., 2012) and rarely on small lakes (Lake Zeekoevlei: $\sim$ 2.5 km^2; Matthews, 2014; Matthews et al., 2010). Analyses of smaller lakes involved less radiometric and spectrally sensitive sensors such as Landsat 5 (L5)/ Landsat 7 (L7) (Bonansea et al., 2015; Hicks et al., 2013; Kutser, 2012), RapidEye (Roessler et al., 2013) or WorldView/ Quickbird (Heblinski et al., 2011; Yuzugullu and Aksoy, 2014). Individual campaigns acquiring airborne hyperspectral data also represented one main data source for lake remote sensing (e.g. Giardino et al., 2015; Hunter et al., 2010b).

The advent of new sensors such as Landsat 8 (L8) in February 2013, Sentinel-2A (S2A) in June 2015 or Sentinel-2B (S2B) in March 2017 opened a new era for lake remote sensing. Although these sensors are technically designed for land applications, they offer improved radiometric and spectral characteristics at relatively high spatial resolution attributing a potential usage for analysing lakes at high spatial detail. Constellations of multiple sensors which are identical in construction such as S2A and S2B have a higher revisit time and increase the probability of cloud-free images. The new spatially high resolved sensors may be synergetically combined with ocean-colour sensors to derive temporally high resolved time series of lakes.

Along with these new possibilities, several issues arose or are still outstanding. They have to be investigated and resolved in order to encourage the widespread use of remote sensing in lake monitoring:

- Raising awareness and encouraging integration of remote sensing techniques in the lake ecology community requires a synthesis on studies connecting remote sensing outcomes with processes investigated in lake ecology.

- The suitability of newly available sensors was theoretically modelled and discussed. With the availability of image data, the real performance of different sensors and algorithms should be evaluated. Since inland waters have diverse optical characteristics, such evaluations should consider lakes with different optical characteristics.

- Evaluation and validation exercises rely on *in-situ* data acquired timely ($\pm$ 2 hours) to satellite data take. Whereas satellite retrievals are generally evaluated in comparison to established *in-situ* methods, evaluations often ignore instrumental, methodological or simply positional uncertainties associated with *in-situ* data.

- Combining data from multiple sensors requires algorithms for retrieving water constituents, SAV and water depths which are sensor-independent and transferable to varying lake conditions. The majority of available algorithms is based on empirical data which are hardly ap-

plicable to other sensors and lake conditions. Analytical approaches may overcome these constraints but are rarely used by users due to their complexity (Odermatt et al., 2012).

- Analytical approaches rely on the spectral shape and intensity of lake reflectance and therefore require an accurate atmospheric correction. Now, image- and look-up-table-based approaches are available (e.g. Sen2Cor for Sentinel-2 (S2); Müller-Wilm (2016)) and also specifically designed for atmospheric correction over water bodies (e.g. ACOLITE for S2 and L8 Vanhellemont and Ruddick (2015, 2016); MIP Heege et al. (2014); iCOR previously OPERA Sterckx et al. (2015a)). These approaches should be tested for their applicability with analytical retrieval algorithms.

The research objectives of this thesis consider the listed issues in order to contribute to the research progress in the field of lake remote sensing.

1.2 Research objectives and structure of the thesis

Inland water remote sensing gained increasing awareness in the remote sensing community. Special issues initiated by highly ranked journals such as *Remote Sensing of Environment* (Palmer et al., 2015b) or *Remote Sensing* (Zhang et al., 2017) and large research projects (e.g. GloboLakes, INFORM, GLaSS) have contributed to a rising number of scientific publications. The prospect of the launch of new sensor systems such as S2 and L8, and Sentinel-3 (S3) as a successor of MERIS boosted research activities in remote sensing of lakes and other inland waters. Algorithms for analysing water colour of lakes required adaptations and advancement with respect to these new sensors. The launch of L8 in 2013 and S2A in 2015 and subsequent data availability demanded for assessing sensor and algorithm performance under on-orbit conditions. Evaluating the performance of the new sensors necessitate timely *in situ* data from lakes with different optical characteristics. Outlining open research issues in Section 1.1 pointed out that scaling issues and *in situ* data uncertainties should be considered in such evaluations. The availability of several sensors potentially well-suited for lake monitoring from space creates the opportunity for multi-sensor data combination. Synergetically combining different satellite sensors, however, faces a variety of challenges: different sensor characteristics lead to different accuracies and require separate evaluations. Additionally, sensor-independent algorithms for atmospheric correction and indicator retrieval must be the basis for the analysis to avoid algorithm-induced differences.

In this context, the main research questions of this thesis were (1) whether the new sensors fulfil the promise on their predicted suitability and (2) whether different satellite sensors can be synergetically used to contribute to lake monitoring.

To answer the main research questions and address anticipated challenges, this thesis focuses on four specific objectives:

1) Reviewing the research status of optical remote sensing for lake ecology and outlining future directions

2) Evaluating the suitability of the new S2Asatellite for mapping lake ecology indicators

3) Combining multi-sensor data (MODIS-AQUA (MODAQ), MODIS-TERRA (MODTE), L7, L8, S2A) for phytoplankton monitoring

4) Assessing the value of archived MERIS satellite imagery for monitoring lake ecology indicators

The assessed indicators of lake ecology were CHL, total suspended matter (TSM), coloured dissolved organic matter (CDOM), water depth and substrate composition. To retrieve these indicators different algorithms for water constituent retrieval and shallow water analyses were tested and evaluated, i.e. the bio-optical inversion models WASI-2D (Water Colour Simulator; Gege (2014b)) and MIP (Modular Inversion and Processing System; Heege (2000); Heege et al. (2014)) and a neural network approach FUB/WeW (Case-2 water Properties Processor from Free University of Berlin; Schroeder et al. (2007a,b)). Furthermore, different atmospheric correction algorithms, i.e. Sen2Cor (Müller-Wilm, 2016), ACOLITE (Vanhellemont and Ruddick, 2015, 2016) and MIP (Heege, 2000; Heege et al., 2014), were compared to radiometric *in situ* measurements. This thesis further emphasised the consideration of *in situ* data uncertainty in evaluation exercises conducted at two lakes with different optical characteristics (Chapter 2).

The thesis is structured into seven main chapters. Chapter 1 provides the reader with a brief introduction to the scientific background of monitoring lakes and remote sensing. It highlights the research motivation and the research objectives. Chapter 2 gives an overview on the studied lakes, the conducted field measurements and underlines the differences in optical characteristics between the two lakes.

Chapter 3 summarises the theoretical background of lake remote sensing and lists suitable sensors for application. The review about the research status focuses on case studies retrieving and analysing indicators of lake ecology, i.e. water transparency (suspended particulate matter (SPM), CDOM, Secchi disk depth, diffuse attenuation coefficient, turbidity), biota (phytoplankton, cyanobacteria, submerged and emergent aquatic vegetation), water depth, water temperature (surface temperature) and ice phenology (ice cover, ice-on, ice-out). The discussion delineates present challenges and assets of integrating remote sensing into lake monitoring. This chapter is published as *Dörnhöfer K., Oppelt N. (2016) Remote sensing for lake research and monitoring – Recent advances. Ecological Indicators 64:105-122. doi: 10.1016/j.ecolind.2015.12.009*.

Chapter 4 focuses on the suitability of S2A for mapping water constituents, substrate composition and water depth in the relatively clear waters of the oligotrophic Lake Starnberg. This analysis comprises a comparison between three different atmospheric correction approaches to radiometric *in situ* data. Adapting WASI-2D (Gege, 2014b) to S2A's spectral characteristics enabled the retrieval of SPM and CDOM in optically deep waters; water depths, substrate composition (SAV and bare sediment) and CDOM were derived in optically shallow water. A specific emphasis was placed on the consideration of sun glint during bio-optical inversion. This chapter is published as *Dörnhöfer K., Göritz A., Gege P., Pflug B., Oppelt N. (2016) Water Constituents and Water Depth Retrieval from Sentinel-2A – A First Evaluation in an Oligotrophic Lake. Remote Sensing 8:941. doi: 10.3390/rs8110941*

Chapter 5 concentrates on the combination of different data sources for monitoring phytoplankton development in the CDOM-rich and eutrophic Lake Kummerow. The analysis combines different *in situ* data (CHL and cyanobacteria biomass) from own measurement campaigns (group Earth Observation and Modelling (EOM) of Christian-Albrechts-Universität zu Kiel (CAU)) and official lake monitoring programme (LU-MV, 2015b) with satellite data. Comparing own water sampling results with results from an external laboratory allowed the estimation of an *in situ* data uncertainty range. Using products from the sensor-independent, physical model Modular Inversion and Processing System (MIP) (Heege, 2000; Heege et al., 2014) allowed a combination of high and low spatial and temporal resolution satellite sensors, i.e. MODAQ, MODTE, L7, L8 and S2A. CHL concentration

and an indicator on potential harmful algal bloom (eoHAB), both derived from satellite data, were compared to *in situ* data. The combined time series of *in situ* and satellite data revealed benefits of combining both approaches but also methodological discrepancies. This chapter is published as *Dörnhöfer K., Klinger P., Heege T., Oppelt N. (2018) Multi-sensor satellite and in situ monitoring of phytoplankton development in a eutrophic-mesotrophic lake. Science of The Total Environment 612:1200-1214. doi: 10.1016/j.scitotenv.2017.08.219*

Chapter 6 contains a nine-year time series of the MERIS archive and underpins the information gain on water constituent development at Lake Kummerow exploiting non-operational, archived satellite data. CHL, TSM and CDOM were retrieved with an established neural-network approach, the FUB/WeW (Schroeder et al., 2007a,b). Using this time series allowed the calculation of trends and seasonal behaviour of water constituent concentrations. Qualitative and quantitative evaluations revealed the need for permanent measurement sites. This chapter is accepted for publication as *Dörnhöfer K., Scholze J., Stelzer K., Oppelt N. (2018) Water colour analysis of Lake Kummerow using time series of remote sensing and in situ data. Journal of Photogrammetry, Remote Sensing and Geoinformation Science. doi: 10.1007/s41064-018-0046-3*

Finally, Chapter 7 provides a synthesised summary of the key achievements from Chapter 3 to 6 and discusses them in relation to the specific objectives and main research questions. Furthermore, Chapter 7 points out still unresolved challenges that need to be addressed in order to advance lake remote sensing research.

Chapter 2

Description of study areas and measurements

Since lakes are known as optically complex waters, remote sensing studies advancing retrieval algorithms and evaluating sensor performance consider more than one lake covering a range of optical characteristics. This thesis included two different lakes located in northern and southern Germany (Fig. 2.1). Lake Starnberg (47.896° N, 11.313 ° E), an oligotrophic lake, formed during the last glacial period in the pre-alpine region. The second studied lake, Lake Kummerow (53.808° N, 12.856° E), also formed during the last glacial period as a proglacial lake but in the northern German lowlands and exhibits a mesotrophic-eutrophic character.

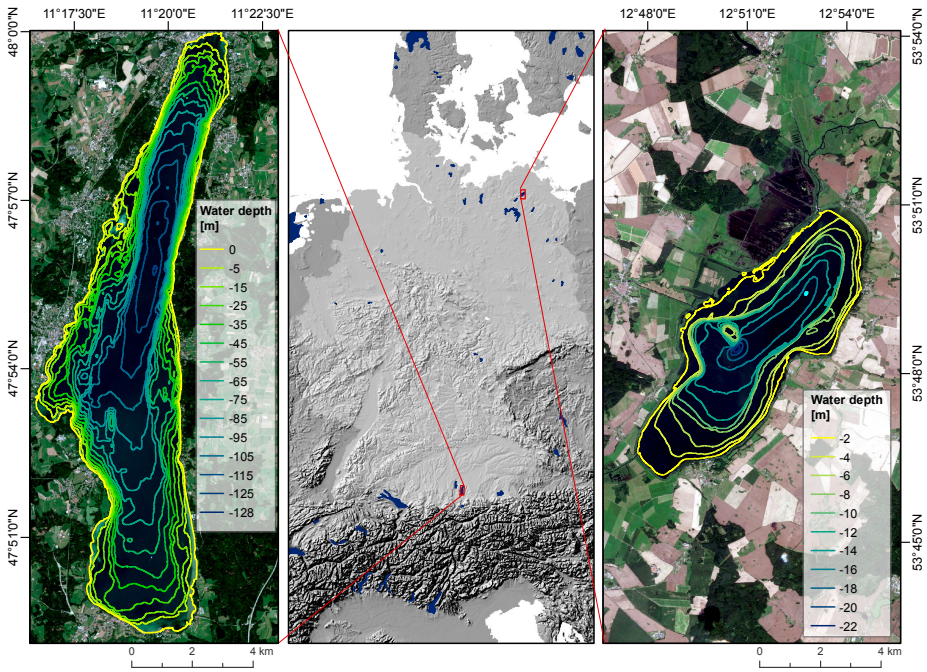

Figure 2.1: Location and official bathymetry contours of both study areas, i.e. Lake Starnberg (left; data source: Bavarian Environmental Agency, 2000) and Lake Kummerow (right; data source: LU-MV, 2002b). Background: Sentinel-2A true-colour-composite acquired on 3 Aug 2015 (left) and 6 Aug 2015 (right), hillshade elevation map of Europe and large lakes (middle; data source: European Environmental Agency).

2.1 Lake Kummerow

General information

Lake Kummerow's size of about 33 km^2 and oval shape is advantageous for satellite based remote sensing studies since high- and medium-scale satellite data cover the lake. Its close location to the remote sensing calibration and validation site Durable Environmental Multidisciplinary Monitoring Information Network (DEMMIN) which belongs to Terrestrial Environmental Observatories (TERENO) Northeastern German Lowland Observatory increases the chance for on-demand satellite data and airborne hyperspectral image acquisitions for research purposes.

With an average depth of 8 m, the lake is relatively shallow (maximum depth: $\sim$ 24 m; Fig. 2.1). The lake is located in the northeastern German young moraine landscape within the natural park 'Mecklenburg Schweiz and Lake Kummerow'. The wind-exposed location and shallow depth result in a polymictic mixing character meaning that the lake is entirely mixed most of the year. The lake rarely develops thermal stratification, generally following several windless, hot summer days (see alsp Sections 5.2.1 and 6.2). Naturally, the Lake Kummerow is mesotrophic and has a short water residence time (< 2 years). Inflows from agriculturally used areas ($\sim$ 50 % of the catchment) have led to increased nutrient levels (eutrophic conditions; Wöbbecke et al., 2003). After periods with intense easterly winds, the low gradient between the outflow at the northern end of the lake (Peene river) and the Baltic Sea leads to backwater effects (Wöbbecke et al., 2003). Mean annual precipitation measured at German Weather Service (DWD) station Teterow (within the catchment) is about 556 mm, i.e. lower than the German average. Precipitation is lowest during the first months of the year (February to April: $\sim$ 30 mm per month). Mean annual air temperature is 8.2 °C (Deutscher Wetterdienst, 2016b).

Water quality monitoring

At Lake Kummerow, the Department of lakes Mecklenburg-Western Pomerania (LU-MV) conducts measurements at two sampling sites within the lake monitoring programme of the federal state Mecklenburg-Western Pomerania. Fig. 2.2 summarises monthly average values about nutrients, total organic carbon (TOC), CHL and Secchi disk depth between 2005 and 2015.

Between March and October, total phosphorous (P) concentrations rise from 0.05 $g{\cdot}m^{-3}$ up to 0.18 $g{\cdot}m^{-3}$. In contrast, total nitrogen (N) exhibits a decreasing behaviour (from 2 to 1 $g{\cdot}m^{-3}$) in the same period (Fig. 2.2). Several peat bogs and wetlands draining into the lake explain the high total organic carbon (TOC) concentrations (> 10 $g{\cdot}m^{-3}$). Secchi disk depth varies between 1.5 and 2.5 m and negatively correlates with CHL concentrations. Higher CHL concentrations, for instance during spring blooms (March) and summer (August/September), are accompanied by lower Secchi disk depths. Phytoplankton analyses from LU-MV revealed a seasonally varying composition: during spring, diatoms predominate phytoplankton biomass; during late summer/autumn, the composition shows a mixture of different classes whereas cyanobacteria have the highest share (Fig. 2.3).

This strong variation in phytoplankton composition, the pronounced CHL cycle with a spring bloom followed by a clear water phase and massive phytoplankton development during summer provide in seasonally varying optical characteristics within one lake. The high TOC concentrations lead to a strongly absorbing water body which is challenging for lake ecology indicator retrieval with remote sensing. These conditions, however, make the lake highly interesting for remote sensing analyses.

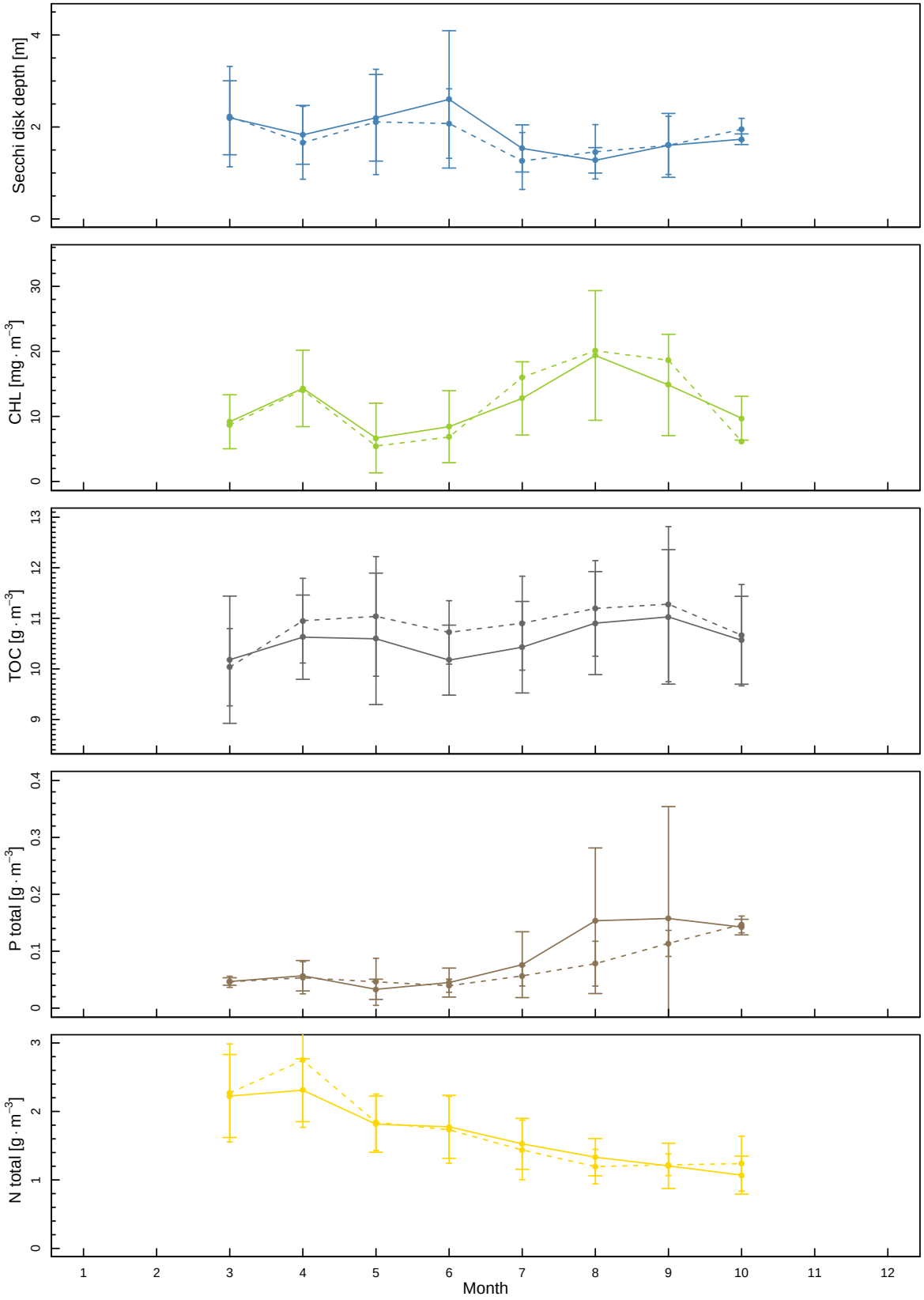

Figure 2.2: Monthly average values of Secchi disk depth (a), chlorophyll-a (CHL) (b), total organic carbon (TOC) (c), total phosphorous (P) (d) and total nitrogen (N) (e) at the two sampling sites 'deepest point' (solid line) and 'Höhe Gorschendorf' (dashed line) at Lake Kummerow between 2005 and 2015. Vertical error bars depict the standard deviation (data source: LU-MV, 2016). Modified from Dörnhöfer and Oppelt (2018).

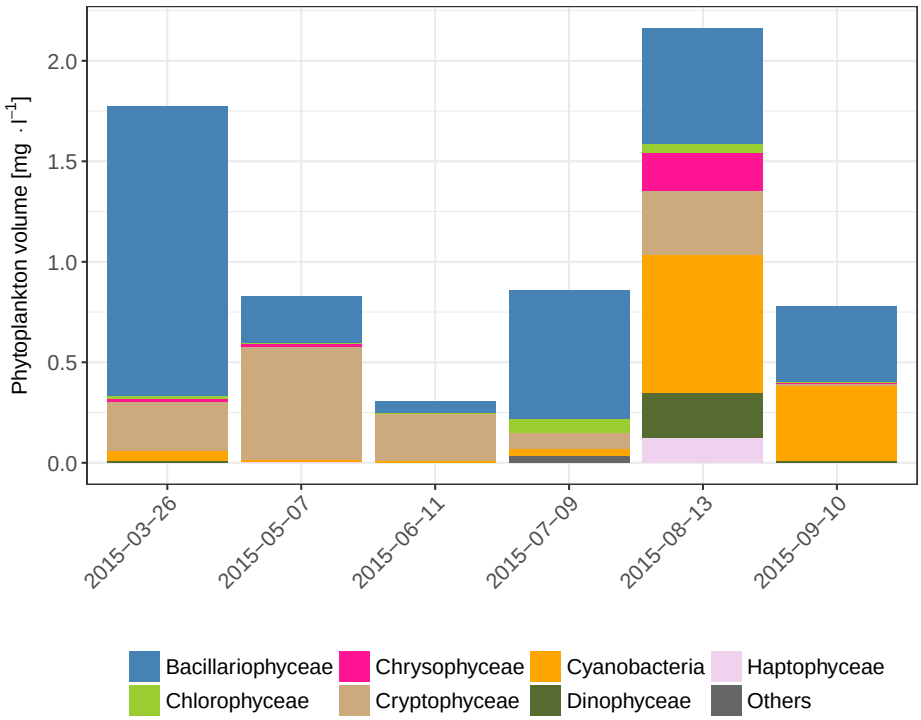

Figure 2.3: Phytoplankton biomass composition as measured from a mixed sample at the deepest point of Lake Kummerow during 2015 (data source: LU-MV, 2016). Modified from Dörnhöfer and Oppelt (2018).

Remote sensing validation measurements

The LU-MV measurements aim to fulfil the requirements of the WFD. Evaluations on the performance of new sensors and algorithms require further measurements relevant for remote sensing which are temporally proximate to satellite data acquisitions. Hitherto, Lake Kummerow lacked any published or available data related to remote sensing validation campaigns. From 2014-2016, several measurement campaigns were conducted to create a data basis for remote sensing analyses at Lake Kummerow as an example for eutrophic lake conditions. Most campaigns were organised between June and September 2015 on days with presumably clear sky conditions and satellite (Sentinel-2A, Landsat 8, RapidEye) or airborne hyperspectral (HySpex) data acquisitions (Fig 2.4).

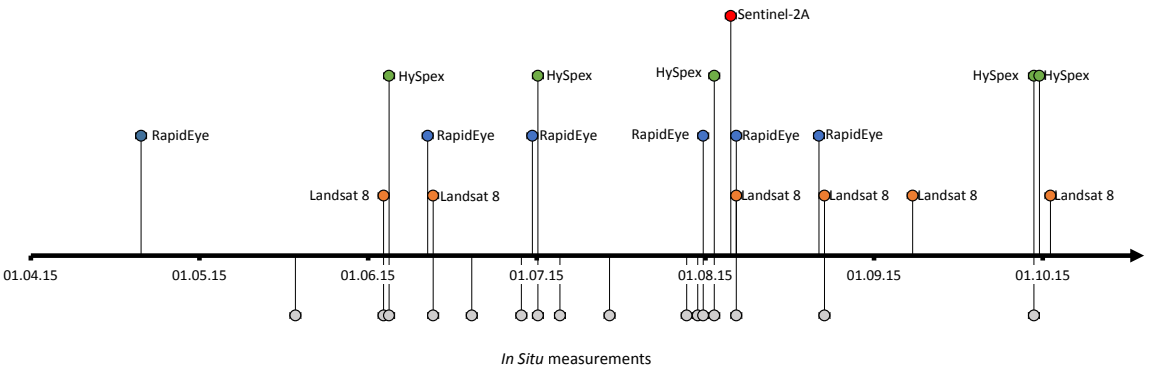

Figure 2.4: Overview of *in situ* measurement campaigns and (partially) cloud-free satellite and HySpex data acquisitions at Lake Kummerow during summer 2015. Modified from Dörnhöfer and Oppelt (2018).

During the measurement campaigns, students and colleagues from the EOM group helped to perform measurements and to take water samples. At each measurement date, 3-5 sites spread throughout the northern half of the lake were sampled; sampling site coordinates were tracked with a Trimble Juno SB GPS device having 2-5 m positional uncertainty. Measurements comprised radiometric light field assessments, weather conditions, limnological parameters and water sampling for subsequent laboratory analyses. Table 2.1 provides an overview on the measured parameters and used devices.

Table 2.1: List of *in situ* measured parameters and used devices.

Parameter	Device
Weather conditions	
air temperature [°C]	Ahlborn FHAD36RS
dew point temperature [°C]	Ahlborn FHAD36RS
air pressure [hPa]	Ahlborn FHAD36RS
relative humidity [%]	Ahlborn FHAD36RS
Limnological parameters	
pH [-]	WTW 330i
electric conductivity [$\mu S \cdot cm^{-1}$]	Ahlborn FYA641LFL1
visibility depth [m]	Secchi disk
water temperature [°C]	Ahlborn FYA641LFL1
Radiometric measurements	
upwelling radiance $L_u(\lambda)$ [$mW \cdot m^{-2} \cdot nm^{-1} \cdot sr^{-1}$]	TriOS RAMSES ARC-VIS
downwelling irradiance $E_d(\lambda)$ [$mW \cdot m^{-2} \cdot nm^{-1}$]	TriOS RAMSES ACC-VIS
land surface reflectance [%]	ASD LabSpec5000

Radiometric measurements

Radiometric measurements on the lake were conducted at each measurement site with two RAMSES sensors (Table 2.1) mounted on a flouting frame which could be lowered into different depths below the water surface (Fig. 2.5). Downwelling irradiance ($E_d(\lambda)$) measurements in different depths (z) below water surface were the basis to calculate the diffuse attenuation coefficient of downwelling irradiance ($K_d(\lambda)$) according to Eq. 2.1 (Kirk, 2011).

$$K_d(\lambda)[m^{-1}] = -\frac{1}{\Delta z} ln(\frac{E_d(z_1, \lambda)}{E_d(z_0, \lambda)}), with |z_1| > |z_0| \tag{2.1}$$

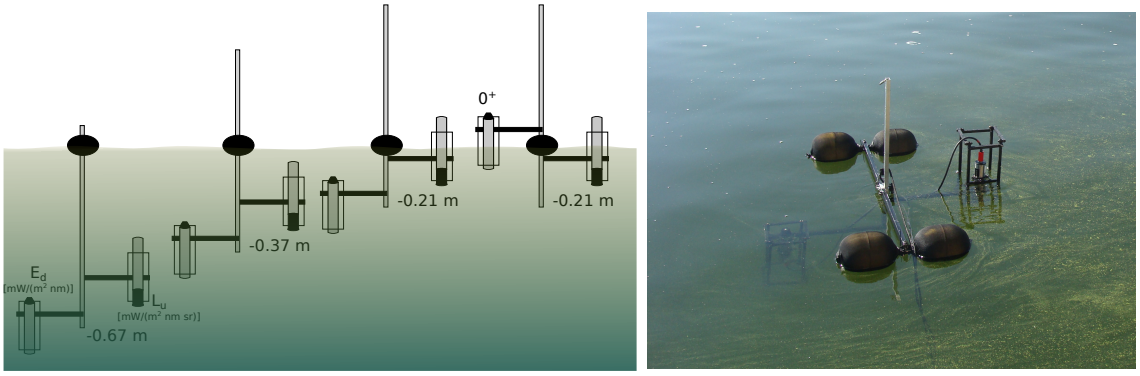

Figure 2.5: Schematic illustration of RAMSES measurement setup with a TriOS ARC-VIS (L_u) and ACC-VIS (E_d) measuring radiometric quantities in different water depths (a). RAMSES measurements during an algal bloom at Lake Kummerow (b). Adopted from Dörnhöfer and Oppelt (2018).

Dividing upwelling radiance ($L_u(\lambda)$) by $E_d(\lambda)$ yielded under water reflectance [sr^{-1}] for each measurement depth. remote sensing reflectance ($R_{rs}(\lambda)$) was derived according to Eq. 2.2 with $L_w(\lambda)$ being the water-leaving radiance.

$$R_{rs}(\lambda)[sr^{-1}] = \frac{L_w(\lambda)}{E_d(\lambda)} \tag{2.2}$$

Log-scaled $L_u(\lambda)$ measurements from different depths were linearly extrapolated to just beneath the water surface and adjusted for the air-water interface (Mobley, 1999) to obtain water-leaving radiance ($L_w(\lambda)$) as described in Fritz et al. (2017a). Fig. 2.6 shows exemplary $R_{rs}(\lambda)$ spectra and $K_d(\lambda)$ coefficients of Lake Kummerow acquired at different dates. At the beginning of June, the lake was relatively clear (clear water phase). High CDOM absorption leads to a low reflectance intensity, in particular in the blue wavelengths. During late summer and early autumn, strong presence of phytoplankton further decreases reflectance in the blue wavelengths; pronounced reflectance minima at $\sim$ 620 nm and $\sim$ 670 nm result from phycocyanin (pigment of cyanobacteria) and CHL absorption at these wavelengths (Matthews, 2011). The strong presence of highly absorbing constituents, i.e. CDOM and phytoplankton, leads to high $K_d(\lambda)$ coefficients.

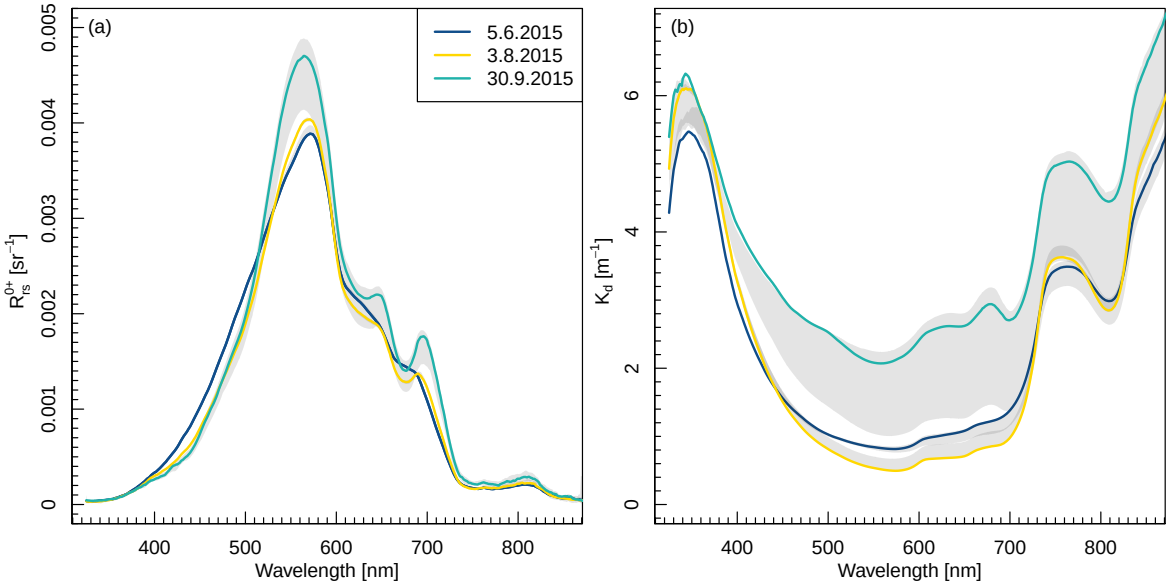

Figure 2.6: Median of exemplary measurements of $R_{rs}(\lambda)$ spectra (a) and $K_d(\lambda)$ coefficients (b) from a deep water measurement site at Lake Kummerow on different dates. The grey shaded area indicates 25 % and 75 % percentiles of measurements. Modified from Dörnhöfer and Oppelt (2018).

Water constituent analyses

At each measurement site, water samples were manually taken just below the water surface ($\sim$ 0.2 m), i.e. 3 x 1 L for CHL and 3 x 1 L for TSM. The transport to the laboratory followed under cool (cooling box) and dark conditions. Colleagues from TU Munich analysed CHL using a photometric approach (Lichtenthaler and Buschmann, 2000) and High Performance Liquid Chromatography (HPLC). Dörnhöfer et al. 2018a described the procedure of CHL analyses in detail.

Measuring TSM concentration followed similar to the descriptions in DIN 38 409-2: 1 L water sample was filtered through pre-weighted cellulose-acetate filters (pore size: 0.45 µm). The loaded filter was weighted (balance: Kern ABT 120-4M) after drying at 105 °C (1 hour) and cooling in a desiccator. Subtracting the filter's empty weight from the loaded weight and relating to the filtrated

volume yielded TSM concentration [g·m^{-3}]. Similar to CHL analyses (see Dörnhöfer et al., 2018a), an external laboratory (UCL Kiel) analysed an additional sample per measurement site for uncertainty purposes. Filtration of different water volumes according to Röttgers et al. (2014) with glass fibre filters (pore size: 0.7 µm) was applied during campaigns in 2016. This procedure allowed for the separation of the organic and inorganic parts of TSM through combustion at 550 °C (1 hour) (see DIN 38 409-2; Strömbeck and Pierson, 2001). To have a basis for comparison, the 2015 procedure was applied to one additional sample per measurement site.

CDOM is the visible light absorbing part of dissolved organic matter which is often quoted as an absorbing value [m^{-1}] at a reference wavelength, e.g. 440 nm (Brezonik et al., 2015). To remove any undissolved particles, 100 ml of three pre-filtered water samples (from CHL analyses) were filtered manually through 0.2 µm syringe filter holders. Previously, these filters have been cleaned with distilled Milli-Q water. Until further analyses, the samples were stored in dark and cool conditions in a refrigerator. To obtain CDOM absorption (similar to Bricaud et al., 1981; Sun et al., 2009), transmission (T) of the filtrate was measured in a 1 cm cuvette using a Perkin Elmer spectro-photometer (UV/VIS Spectromtere Lambda 2S, sampling interval: 1 nm, range: 200-900 nm) against Milli-Q water as a reference for pure water T. T was converted into optical density (OD) and subsequently absorption (a) (Eq. 2.3). Subtracting the arithmetic mean OD value between 710 and 720 nm corrected OD measurements for scattering (Bricaud et al., 1981, Eq. 2.4).

$$OD(\lambda) = -log10(\frac{T(\lambda)}{100}) \tag{2.3}$$

$$OD_{cor}(\lambda) = OD(\lambda) - \overline{OD_{710-720nm}} \tag{2.4}$$

Conversion from OD into absorption of CDOM ($a_{CDOM}(\lambda)$) followed Eq. 2.5 (Bricaud et al., 1981).

$$a_{CDOM}(\lambda)[m^{-1}] = \frac{2.303}{0.01} \cdot OD_{cor}(\lambda) \tag{2.5}$$

Fitting the measured curve exponentially using R (R Core Team, 2016) yielded a_{CDOM} at 440 nm and the exponential slope value, i.e. S_{CDOM}.

Table 2.2 summarises the measured water constituent concentrations during the summer months of 2015. According to these values, the lake is considered as an example for CDOM-rich waters with high summer CHL concentration and a strong seasonal phytoplankton variability.

Table 2.2: Summary of measured water constituent concentrations at Lake Kummerow during summer 2015.

Parameter	Min	Max	Mean	Standard deviation	Methodology
CHL [mg·m^{-3}]	0.1	143.8	9.3	16.5	HPLC
CHL [mg·m^{-3}]	0.7	57.5	9.0	7.7	photometric (Lichtenthaler and Buschmann, 2000)
TSM [mg·m^{-3}]	0.1	19.9	2.8	2.7	gravimetric (∼DIN 38 409-2)
a_{CDOM} [m^{-1}]	0.87	1.67	1.28	0.15	photometric and exponential fit
S_{CDOM}[nm^{-1}]	0.0150	0.0215	0.0172	0.0011	(∼ Bricaud et al., 1981; Sun et al., 2009)

2.2 Lake Starnberg

General information

Lake Starnberg's elongated form and size of about 56 km^2 also makes it suitable for remote sensing analyses. The lake is relatively deep with an average of 53.2 m and a maximum depth of 127.8 m (Fig. 2.1). Lake Starnberg has a monomictic character and regularly develops a thermal stratification between April and October (Wöbbecke et al., 2003, see also Section 4.2.1). Mean annual precipitation measured at DWD station Starnberg is about 959 mm with maxima ($\sim$ 120 mm) during summer months. The annual mean air temperature is 8 °C (Deutscher Wetterdienst, 2016a).

Water quality monitoring

The Bavarian Environmental Agency (BEA) regularly measures water quality indicators at the deepest point of Lake Starnberg throughout the year (GKD Bayern, 2013b). Lake Starnberg has an oligotrophic character with a long residence time since inflows mainly originate from groundwater. After a period of anthropogenically induced eutrophication, lake restoration programmes successfully reduced nutrient concentrations, in particular total phosphorous (P) (details in section 4.2.1). Thus, the lake offers optical characteristics typical for relatively clear waters low in nutrients (Fig. 2.7). Secchi disk depths range between 4 and 11 m. Reduced water clarity occurs along with higher phytoplankton biomass volume (Fig. 2.8) and CHL concentrations (Fig. 2.7) during summer. TOC is about 3 times lower at Lake Starnberg than at Lake Kummerow expecting a less absorbing water body. The low nutrient concentrations (nitrogen (N) < 0.4 $g \cdot m^{-3}$ and P < 0.008 $g \cdot m^{-3}$) cause low CHL concentrations (LfU, 2012). Nevertheless, CHL increases from spring to late summer whereas the maximum concentration remains on a low level (CHL < 4 $mg \cdot m^{-3}$; Fig. 2.7).

Diatoms predominate the phytoplankton character during most of the year. During autumn, however, the share of diatoms decreases and cyanobacteria have the highest share but a very low biomass level (Fig. 2.8). Warm water temperatures which cool down slowly during autumn favour cyanobacteria survival (LfU, 2012).

Remote sensing validation campaigns

Lake Starnberg was already part of previous remote sensing research. The focus was placed on spectral behaviour of SAV (Pinnel, 2006; Wolf, 2014; Wolf et al., 2013), mapping SAV with remote sensing data (Roessler et al., 2013; Rößler, 2014; Rößler et al., 2012, 2013) and bathymetry (Gege, 2014a). Thus, archived *in situ* data and hyperspectral imagery were available. To obtain data for new sensor validation, such as Sentinel-2A, colleagues from TU Munich and German Aeropace Center (DLR) conducted and provided *in situ* measurement data concurrently to Sentinel-2A and airborne hyperspectral data acquisitions. Furthermore, they offered seasonal reflectance measurements from different SAV species. Table 2.3 summarises water constituent concentrations analysed at Lake Starnberg during summer 2015. Dörnhöfer et al. (2016b), Fritz et al. (2017b) and Fritz and Schneider (2018) describe details about the measurements. According to these concentrations, Lake Starnberg is considered as an example for relatively clear waters with low concentrations of CHL, TSM and CDOM.

Due to the low concentrations of strongly absorbing water constituents, *in situ* $R_{rs}(\lambda)$ $R_{rs}(\lambda)$ measurements with RAMSES sensors were distinctly higher than at Lake Kummerow (Fig. 2.9a). Accordingly, the $K_d(\lambda)$ coefficient was lower (Fig. 2.9b).

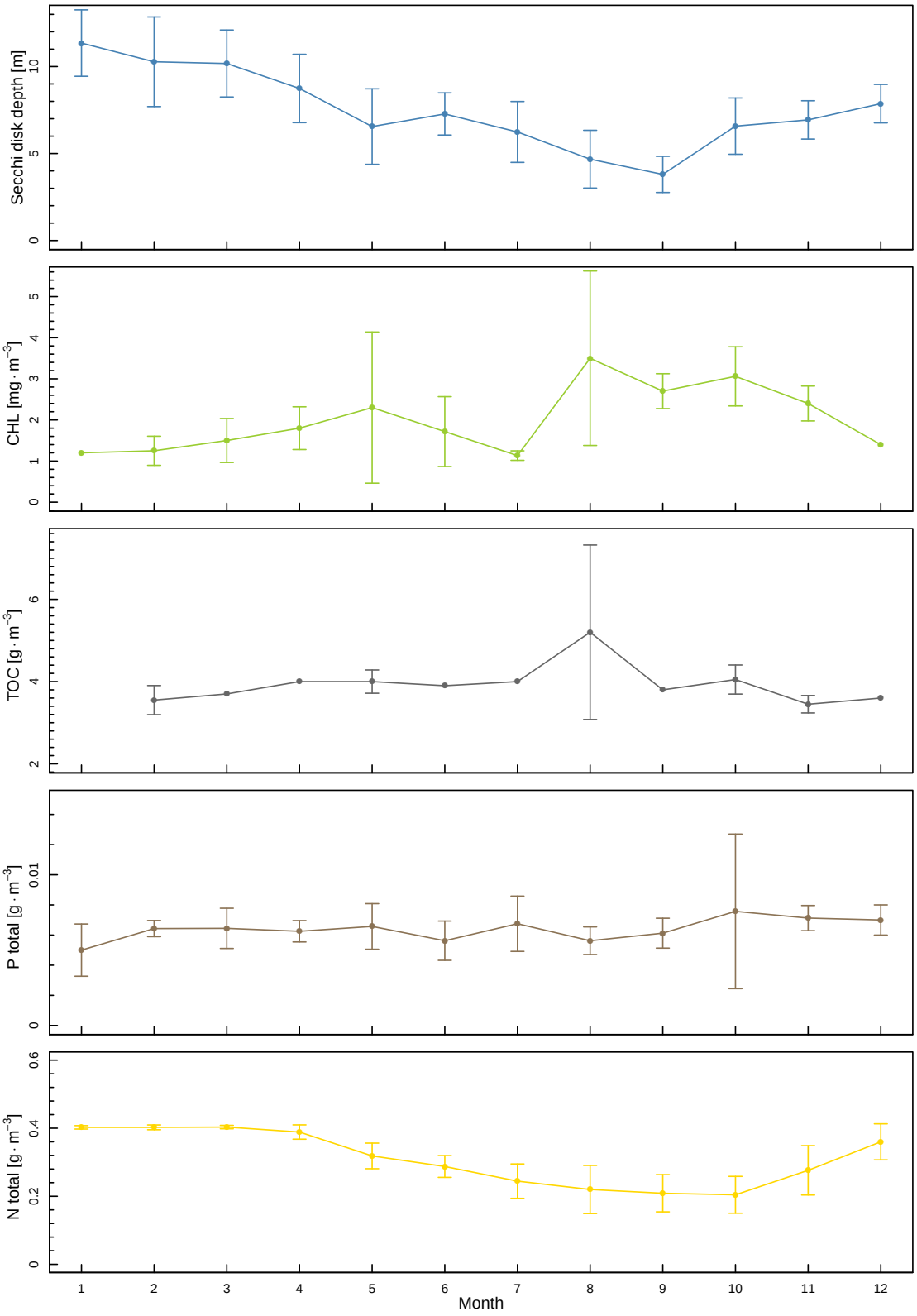

Figure 2.7: Monthly average values of Secchi disk depth (a), CHL (b), TOC (c), total phosphorous (d) and total nitrogen (e) at the sampling site 'deepest point' (solid line) at Lake Starnberg between 2004 and 2014. Vertical error bars depict the standard deviation (data source: GKD Bayern, 2013b). Modified from Dörnhöfer and Oppelt (2018).

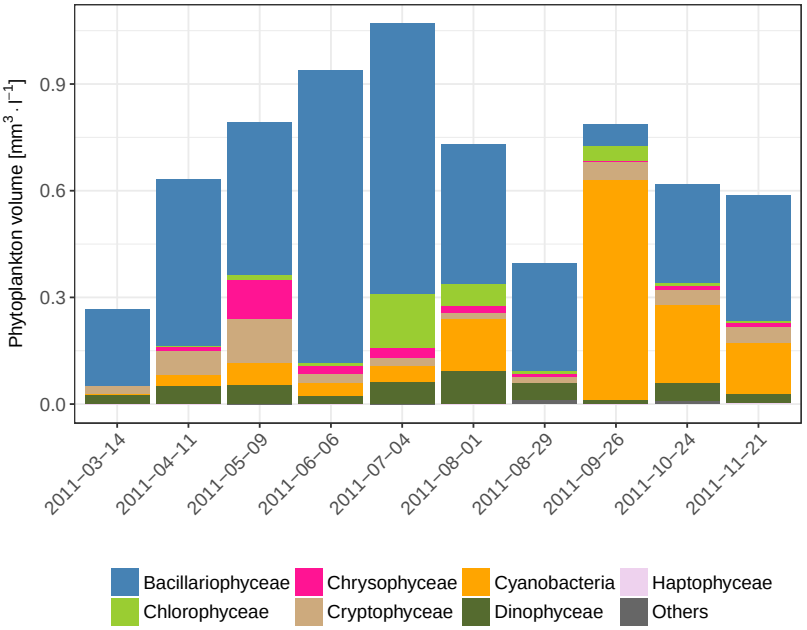

Figure 2.8: Phytoplankton biomass composition as measured from a mixed sample at the deepest point of Lake Starnberg during 2011 (data source: GKD Bayern, 2013a). Modified from Dörnhöfer and Oppelt (2018).

Table 2.3: Summary of measured water constituent concentrations at Lake Starnberg during summer 2015. TSM and CDOM values were only obtained during an airborne hyperspectral (HySpex) campaign on 12 Aug 2015.

Parameter	Min	Max	Mean	Standard deviation	Methodology
CHL [mg·m^{-3}]	0.2	1.1	0.5	0.2	HPLC
CHL [mg·m^{-3}]	0.8	1.9	1.2	0.4	photometric (Lichtenthaler and Buschmann, 2000)
TSM [mg·m^{-3}]	0.1	1.9	0.7	0.5	gravimetric (∼DIN 38 409-2)
a_{CDOM} [m^{-1}]	0.418	0.732	0.515	0.098	modelled from RAMSES
S_{CDOM}[nm^{-1}]	0.0125	0.0167	0.0151	0.0014	(Dörnhöfer et al., 2016b)

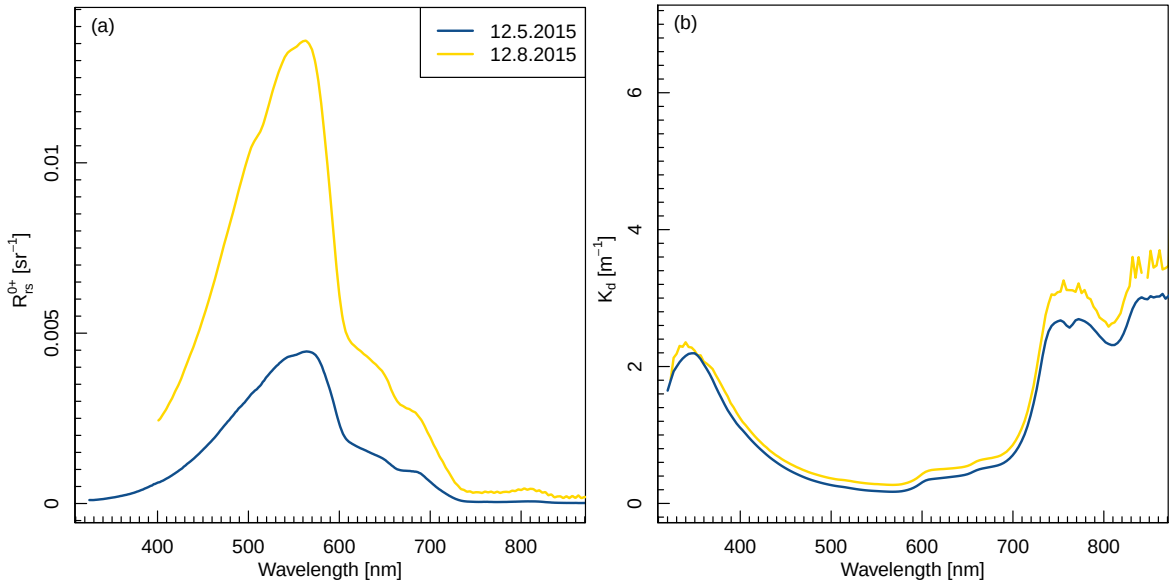

Figure 2.9: Median of exemplary measurements of $R_{rs}(\lambda)$ spectra (a) and $K_d(\lambda)$ coefficients (b) from a deep water measurement site at Lake Starnberg on different dates. On 12 May, location and RAMSES sensors are different in a and b. Modified from Dörnhöfer and Oppelt (2018).

Chapter 3

Remote sensing for lake research and monitoring - Recent advances

Katja Dörnhöfer and Natascha Oppelt
Ecological Indicators (2016), doi:10.1016/j.ecolind.2015.12.009
Received: 17 August 2015, Accepted: 9 December 2015

Changes made to the published version:
To harmonise the style of the entire thesis, chlorophyll-a is abbreviated as CHL instead of Chl-a.

Abstract

Lakes are important ecosystems providing various ecosystem services. Stressors such as eutrophication or climate change, however, threaten their ecological functions. National and international legislations address these threats and claim consistent, long-term monitoring schemes. Remote sensing data and products provide synoptic, spatio-temporal views and their integration can lead to a better understanding of lake ecology and water quality. Remote sensing therefore gains increasing awareness for analysing water bodies. Various empirical and semi-analytical algorithms exist to derive remote sensing indicators as proxies for climate change or ecological response variables. Nevertheless, most monitoring networks lack an integration of remote sensing data. This review article therefore provides a comprehensive overview how remote sensing can support lake research and monitoring. We focus on remote sensing indicators of lake properties, i.e. water transparency (suspended particulate matter, coloured dissolved organic matter, Secchi disk depth, diffuse attenuation coefficient, turbidity), biota (phytoplankton, cyanobacteria, submerged and emerged aquatic vegetation), bathymetry, water temperature (surface temperature) and ice phenology (ice cover, ice-on, ice-out). After a brief background introducing principles of lake remote sensing we give a review on available sensors and methods. We categorise case studies on remote sensing indicators with respect to lake properties and processes. We discuss existing challenges and benefits of integrating remote sensing into lake monitoring and ecological research including data availability, ready-to-use tools and accuracies.

Keywords

Water quality, Lake ecology, Accuracy, Monitoring, Remote sensing

3.1 Introduction

Inland waters, and especially lakes, have important functions in the environment. They provide habitat for a wide range of species and form essential components in hydrological, nutrient and carbon cycles (Moss, 2012). Humans benefit from various ecosystem services offered by inland waters, i.e. water bodies that are not directly connected to the sea (Carpenter et al., 2011). Water extraction serves for drinking water and irrigation; other usages encompass energy production, transportation, fishery and recreational purposes (Carvalho et al., 2013a; Stendera et al., 2012). Anthropogenic exploitation and multiple interacting stressors, however, threaten ecological functions of inland waters over the entire globe (Adrian et al., 2009). Prominent stressors include eutrophication, inorganic and organic contaminants, morphological alterations and climate change effects such as acidification or increasing water temperatures (Brönmark and Hansson, 2002; Dudgeon et al., 2006).
Several national and international directives address these problems and aim to improve the ecological state of inland waters. Examples are the US Clean Water Act (United States Congress House, 2002), South African National Water Act (Government of South Africa, 1998), National Water Management Strategy of Australia and New Zealand (Australian Government, 2000), the Canada Water Act (Government of Canada, 1985), and the Water Framework Directive in Europe (European Commission, 2000). A common target of these directives is to improve water quality by identifying stressors and by implementing sustainable management strategies supported by a more or less frequent monitoring (e.g. Birk et al., 2012; Gray and Shimshack, 2011; Warne, M. S. J. et al., 2014). Currently, most monitoring programmes are field based even if sampling and analysis are labour, cost and time intensive (Schaeffer et al., 2013). Although providing information on species level, single measurements or unevenly distributed sampling points are problematic and may result in erroneous water quality classifications (Bresciani et al., 2011c; van Puijenbroek et al., 2015). Moreover, *in situ* measurements hardly capture the temporal and spatial variability of phenomena such as short-living cyanobacterial or phytoplankton blooms (Reyjol et al., 2014).
For a comprehensive understanding of lake ecology and the role of lakes “as sentinels, integrators and regulators of climate change“ (Williamson et al., 2009) integrative, frequent and consistent long-term monitoring approaches are required globally (Hestir et al., 2015a; van Puijenbroek et al., 2015). Ecologists repeatedly proposed to integrate remote sensing into water quality research and monitoring to benefit from earth observation via satellite sensors (Birk and Ecke, 2014; Chen et al., 2004; Reyjol et al., 2014; Williamson et al., 2009). Remote sensing techniques have already been successfully integrated in terrestrial ecosystem service assessments (e.g. Andrew et al., 2014; de Araujo Barbosa, C.C. et al., 2015; Kandziora et al., 2014), for assessing indicators of terrestrial habitat quality (e.g. Spanhove et al., 2012) and for supporting management of marine and coastal protected areas (e.g. Kachelriess et al., 2014; Walshe et al., 2014). Until recently, remote sensing based studies of lake ecology and water quality were mainly carried out with airborne data or limited to large water bodies where ocean colour sensors with coarse spatial resolution such as MERIS or MODIS (spatial resolution represents the area on ground covered by an image element, which in the case of MERIS and MODIS is $\geq$ 300 m) have been used (e.g. Bresciani et al., 2011a). Maybe therefore the number of publications applying remote sensing in lake ecology or water quality lags far behind those without using remote sensing (Fig. 3.1) although various methods exist to derive proxies for water quality (e.g. Matthews, 2011; Odermatt et al., 2012).

Since 2010, the number of studies slightly increased (Fig. 3.1), which may also be due to several large projects funded by national authorities (e.g. Australia’s water for a healthy country flagship, Great Britain’s GloboLakes, North American Great Lakes Restoration Initiative, USA’s Harmful Algal Bloom early warning system project), space agencies (e.g. Diversity II, A Wealth of Water) and the European Commission (e.g. GLaSS, INFORM). Furthermore, recently launched sensors, such as NASA’s Landsat 8 and ESA’s Sentinel-2, offer spatial and radiometric resolutions which suit for inland water applications (Drusch et al., 2012; Pahlevan et al., 2014; Palmer et al., 2015b). The radiometric resolution defines how many brightness levels a sensor can perceive. A recently published special issue on inland water remote sensing of “Remote Sensing of Environment“ (Palmer et al., 2015b) supports the observation that remote sensing based lake monitoring is gaining importance. To further encourage integration of remote sensing for lake monitoring and research this review article

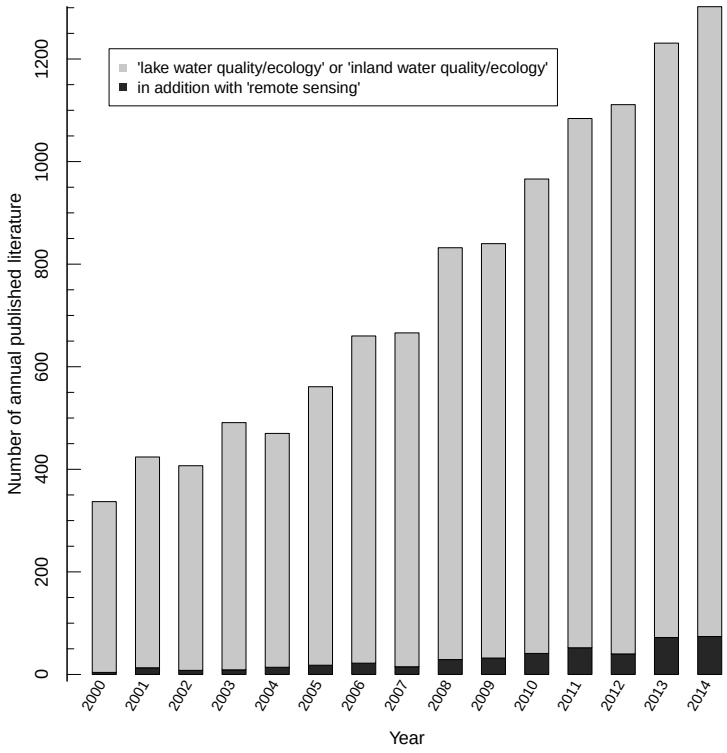

Figure 3.1: Number of published literature (2000-2014) listed in Web of Knowledge containing the terms “lake water quality/ecology“ or “inland water quality/ecology“ (light grey) and the former in addition with “remote sensing“ (dark grey).

gives an overview of methods currently available that provide a better understanding and a foundation for future innovation in this field. To this end, a brief background of inland water remote sensing is given, followed by a section reviewing studies on retrieving remote sensing indicators for lake ecology, in particular, water transparency, biota, hydrology, ice cover and surface water temperature. The last section discusses potential and limitations of remote sensing based methods to promote integrated lake research.

3.2 Remote sensing indicators of lake ecology

Climate change poses an increasingly apparent stressor for lakes (Hering et al., 2010) and influences lake water quality and ecology (Moss, 2012). In a comprehensive review Adrian et al. (2009) summarised lake properties and their key response variables to climate change. These response variables are related to both trophic states of lakes and catchment processes (Adrian et al., 2009) and therefore may be used as response variables of lake ecosystem health (Zhang et al., 2013a) and ecology (Poikane et al., 2015). Based on these response variables we selected indicators feasible to be achieved by remote sensors (remote sensing indicators); Table 3.1 therefore provides an overview how remote sensing can support lake research and monitoring. Recently published literature shows that case studies cover the entire globe; two agglomerations, however, exist in Europe and North America (Fig. 3.2). Fig. 3.2 also indicates that several lakes seem to be intensely investigated and have been analysed repeatedly, i.e. Lake Trasimeno and Garda (Italy), Lake Starnberg (Germany), Lake Balaton (Hungary) and the Laurentian Great Lakes (USA, Canada).

Table 3.1: List of lake properties, response variables (modified from Adrian et al., 2009) and related remote sensing indicators.

Lake properties	Response variables	Remote sensing indicator	Abbreviation
Transparency	Dissolved organic carbon (DOC)	Coloured dissolved organic matter	CDOM
	Turbidity	Suspended particulate matter	SPM
		Turbidity	Turb
		Diffuse attenuation coefficient	K_d
	Secchi disc depth	Secchi disc depth	Z_{SD}
		Euphotic depth	Z_{eu}
Biota	Algal blooms	Chlorophyll-a (phytoplankton)	CHL
		Phycocyanin (cyanobacteria)	Cyano
	Phenology	Time series analyses of CHL	
	Species composition	Submerged aquatic vegetation	SAV
		emerged vegetation	
		lake bottom sediment	
Hydrology	Water level	Bathymetry	z_B
Temperature	Epilimnic temperature	Surface temperature	T_{surf}
Ice phenology	Ice-out	Ice-out; time series analyses	Ice
	Ice duration	Ice-out; time series analyses	Ice

3.2.1 Background of inland waters remote sensing

Remote sensing, in general, analyses radiation measured by a distant sensor to derive information of a certain object or, in case of lakes, of the water body. To obtain information on lake properties such as water transparency, biota and hydrology, the water leaving radiance in the visible and near-infrared wavelengths, i.e. the wavelength region where water reflects and scatters most of the incoming solar radiation (400-900 nm) is of major interest (Dekker et al., 2002). Before the incident solar radiation interacts with the water body it has to pass the atmosphere where it is modified by absorption and scattering (see Fig. 3). At the water surface radiation is either reflected or it passes the water surface according to Snell's law and further propagates through the water body. In the water column, optically active constituents, e.g. SPM, CDOM and CHL, alter radiation by absorption and scattering characteristic for each constituent. The sum of these constituents represents the inherent optical properties of a water body (Odermatt et al., 2012). The apparent optical properties such as attenuation (represented by the diffuse attenuation coefficient K_d) or remote sensing reflectance (i.e. the ratio of water leaving radiance and downwelling irradiance) depend on the water itself and additionally on the radiation geometry (e.g. parameters such as solar angles or the angle incoming radiation hits the water surface, i.e. incidence angle) (Dekker et al., 2002). In optically deep water, water surface, water body and water constituents are the main sources of radiation from within a lake. In optically shallow water, the water leaving radiance partly includes radiation which has been reflected at the bottom. The water leaving radiance then contains, additionally to water constituents, information on bottom substrate and bathymetry (Mouw et al., 2015). By passing the water surface the water leaving radiation is again refracted and, through its way towards an airborne or satellite sensor, is affected once more by atmospheric absorption and scattering. Altogether, about 90-98 % of the signal obtained by a remote sensor originates from contributions of the water surface and the atmosphere (Gitelson and Kondratyev, 1991). The remaining 2-10 % include the signal interesting for water remote sensing, i.e. the water leaving radiance. For that reason, an accurate removal of effects due to the atmosphere and water surface is essential (Mouw et al., 2015).

Separation of the various contributors from the water leaving radiance allows to obtain quantitative information on water constituents (e.g. SPM, CDOM, phytoplankton or cyanobacteria) and, for shallow water, bathymetry and bottom substrate (e.g. benthic vegetation, sediment). To this end, various empirical and semi-analytical algorithms exist. Empirical approaches require *in situ* measurements of the variable of interest which

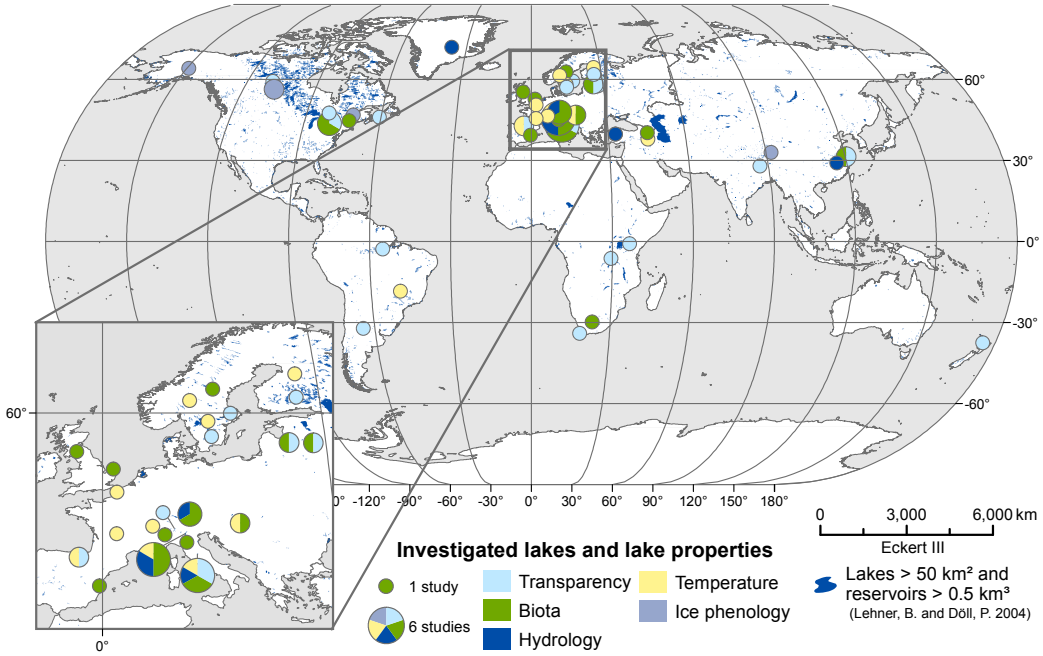

Figure 3.2: Location of lakes included in case studies and investigated lake properties. Size of circle indicates the number of times a lake appeared in literature (lakes and reservoirs shape file source: Lehner and Döll (2004)).

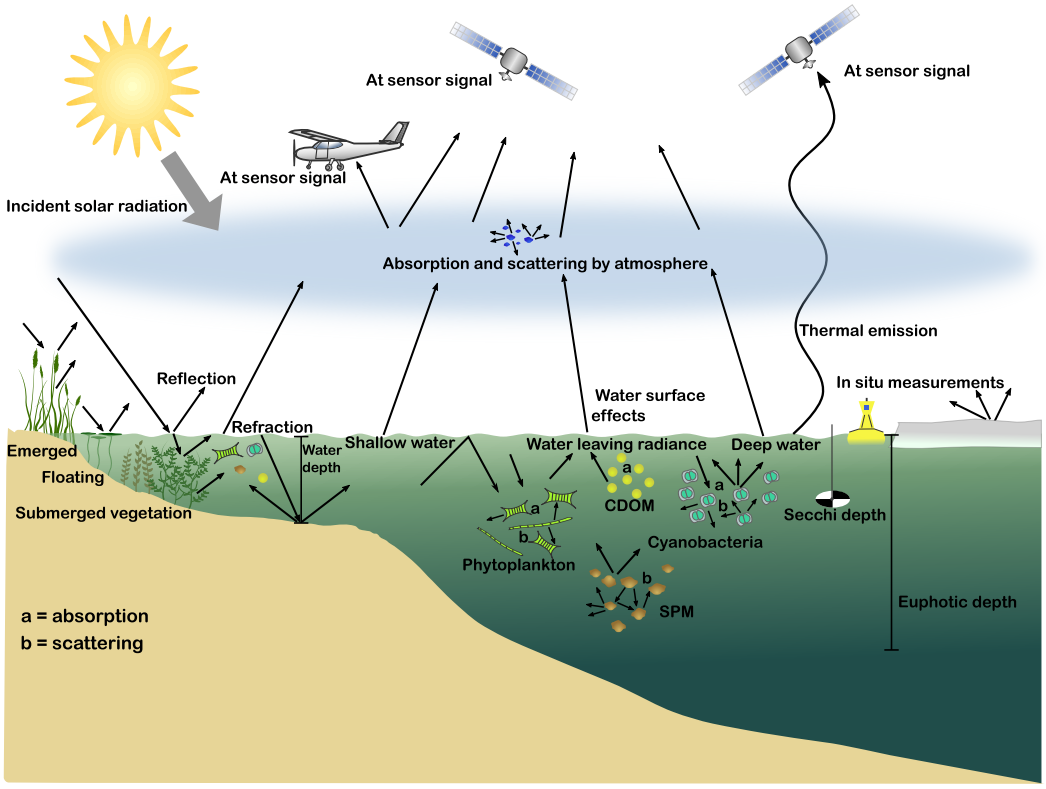

Figure 3.3: Interaction between radiation, remote sensing indicators of lake ecology and sensors.

serve as a basis for establishing an empirical relationship (e.g. linear or non-linear regression) with the water leaving radiance measured in one or multiple sensor bands. The regression equation is then applied to every image element (i.e. pixel) providing a spatial depiction of the respective indicator. The setup of empirical

models is relatively easy; their application, however, is often limited to a specific study site and/or a particular sensor (Giardino et al., 2010b). Advanced, semi-empirical algorithms such as artificial neural networks rely on large data sets of remote sensing and accompanying *in situ* data (e.g. Ceyhun and Yalçın, 2010; Doerffer and Schiller, 2007). Using large parts of this database the artificial neural network is trained to derive a statistical relationship between remote sensing data and one or multiple optical constituent(s). Similar to empirical approaches the remaining data serve as a validation basis to derive performance criteria. Matthews (2011) provides a systematic overview of empirical and semi-empirical algorithms.
Owing to the complex optical behaviour of lakes various scientists developed semi-analytical algorithms based on radiative transfer in the water column (e.g. Gege, 2014b; Giardino et al., 2012; Mobley, 1989). Applying the radiative transfer equation enables to separate optically active constituents from the water leaving radiance. Semi-analytical models, however, require detailed spectral information of optically active water constituents in a lake. Nevertheless, due to their physical basis these models are broadly applicable (Giardino et al., 2010b). Solving the radiative transfer equation mainly follows two approaches, i.e. via look-up tables and inversion methods. Look-up tables consist of a large spectral database containing water leaving radiance spectra with known constituent concentrations, inherent optical properties, bathymetry and bottom properties. Image spectral signatures and data base records are compared until the closest match for all variables is found. Dekker et al. (2011) provide a comparison of different look-up table approaches in coastal waters. Inversion approaches simulate spectral signatures according to the radiative transfer and a set of constant and variable model parameters characterising lake inherent and apparent optical properties. For each pixel, variable parameters are modified iteratively until deviations between simulated and image spectral signatures reach a minimum. The resulting maps provide spatial distributions of water constituents, bathymetry or bottom substrates.
Empirical classification approaches (supervised and unsupervised) are another possibility to derive bottom substrates such as submerged aquatic vegetation and sediment types. Unsupervised classifiers assign image pixels to classes according to statistical similarities in their spectral signatures. Afterwards the user defines thematic attributes for each class (e.g. Dogan et al., 2009; Oppelt et al., 2012). In a supervised classification the user defines training pixels with known class properties prior to classification. Using the spectral signatures of the training pixels the classifier then allocates each image pixel to one of the predefined classes (e.g. Hunter et al., 2010a; Oppelt et al., 2012).
Table 3.2 summarises key points of methodologies to assess remote sensing indicators. The aforementioned methods mainly use the visible and to some extend near-infrared wavelengths; to obtain water surface temperatures we need sensors measuring radiation in the thermal infrared (7-13 µm). The earth emits radiation depending on the temperature (Stefan-Boltzmann law) and the emissivity of a surface (Kuenzer and Dech, 2013). To retrieve surface temperatures several approaches exist including semi-empirical and physically based algorithms (Hulley et al., 2011). Several authors developed semi-empirical, mono-window (i.e. one thermal band located in one atmospheric window) algorithms which are mainly applicable for Landsat imagery (1972-2011). They use approximations of he radiative transfer equation relying on estimates of atmospheric water vapour to specify the atmospheric transmissivity (Jimenez-Munoz et al., 2009). Semi-empirical, split-window (i.e. thermal bands in two different atmospheric windows) algorithms have been developed for sensors with more than one thermal band. The differences in two neighbouring bands enable an enhanced estimate of the atmospheric transmissivity which increases retrieval accuracy (Rozenstein et al., 2014).

Assessing accuracies of obtained remote sensing indicators requires *in situ* measurements of related parameters contemporary to image acquisition since lake conditions may change rapidly. Retrieved water constituent concentrations often are compared with water samples from the upper water column which are analysed in laboratory (Odermatt et al., 2012). The validation of bottom substrates is challenging since it requires mappings from boat or by divers (e.g. Hunter et al., 2010a). The same applies for shallow water bathymetry which may be validated using, rarely existing, echo sounding data (e.g. Gege, 2014a). *In situ* measurements of water temperature near the surface enable a comparison with remote sensing based temperature measurements. Visual observations are the basis to validate remote sensing indicators of ice phenology (Latifovic and Pouliot,

Table 3.2: Methodical key points of remote sensing indicators of water transparency, biota and lake hydrology.

Method	Algorithms	Key points	Remote sensing indicators
Empirical	Statistical regressions with band ratios, single/multiple bands algebra	Easy to apply, *in situ* data required, difficult to transfer	CDOM, SPM, Z_{SD}, CHL, z_B,T_{surf}
	Artificial neural networks	Advanced algorithms with huge data bases; tools already available; improves with study area specific adaptation	CDOM, SPM, Z_{SD},Z_{90}, K_d,CHL, Cyano
	Unsupervised/ supervised classification	Assigns pixels to semantic classes based on statistic measures (acc. to pre-defined spectral signatures)	SAV
Semi-analytical	Look-up tables	Based on radiative transfer in the water column; need large data bases	CDOM, SPM, CHL, SAV, z_B
	Inversion models/ bio-optical models	Apply radiative transfer equation to obtain the spectral signature and inherent optical properties for each pixel; relate inherent optical properties to constituent concentrations	CDOM, SPM, CHL, SAV, z_B

2007). In most cases, coefficients such as the coefficient of determination (R^2) or the root mean square error (RMSE) serve as accuracy measures, while only a few approaches include simulated data sets (Odermatt et al., 2012).

Satellite sensors suitable for retrieving remote sensing indicators (Table 3.3) are mainly multispectral (e.g. Landsat, RapidEye), i.e. they record reflected or emitted radiation in a few spectral bands that cover a relatively broad range of the electromagnetic spectrum. Hyperspectral sensors measure “contiguously across the electromagnetic spectrum in numerous narrow bands“ (Oppelt et al., 2015). Hyperspectral systems are available for airborne platforms; planned satellites are e.g. EnMAP, HySpIRI and PRISMA. The high spectral resolution of these sensors allows analysis of narrow spectral features such as CHL absorption at $\sim$670 nm.

Table 3.3: Archived and operating satellite sensors used and upcoming sensor suitable for lake monitoring (Sources: Dekker and Hestir, 2012; Drusch et al., 2012; Hestir et al., 2015a; Lee et al., 2015a). Spatial resolution = area on ground covered by one pixel; temporal resolution = time period between a sensor can image the same area on ground.

Sensor	Spectral bands (400-1000 nm)	Spatial resolution [m]	Temporal resolution	Availability	Operating time	Indicators Sections x - Y)										
						CDOM	SPM	Z_{SD}	Turb	K_d	CHL	Cyano	SAV	z_B	T_{surf}	Ice
Archived imagery																
AATSR	3/Thermal	1000	2-3 days	Web-enabled, free	2002-2012										x	
AVNIR-2	4	10	46 days	Web-enabled, free	2006-2011		x						x			
Landsat-TIR	Thermal	60	16 days	Web-enabled, free	1982-2011		x								x	
Landsat-TM	4	30	16 days	Web-enabled, free	1982-2011	x	x	x			x		x			
MERIS	15	300	2-3 days	Web-enabled, free	2002-2012	x	x	x		x	x	x	x			
Operating sensors																
ASTER	3	15	Daily	Web-enabled, free	since 1999								x			
AVHRR	Thermal	1000	Daily	Web-enabled, free	since 2005										x	x
Landsat ETM	4	30	16 days	Web-enabled, free	since 1999	x	x	x			x		x		x	
Landsat OLI	5	30	16 days	Web-enabled, free	since 2013		x							x		
Landsat TIRS	Thermal	100	16 days	Web-enabled, free	since 2013										x	
MODIS	2-9	250-1000	daily	Web-enabled, free	since 1999	x		x		x		x			x	x
Proba-1 CHRIS	18-63	18-36	On-demand	Scientific use	since 2001						x			x		
Quickbird	4	2.6	On-demand	Commercial, at a cost	since 2001								x			
RapidEye	5	6.5	On-demand	Commercial, at a cost	since 2008								x	x		
Sentinel-2	9	10-60	5-10 days	Web-enabled, free	since 2015	x	x	x		x	x	x	x	x		
WorldView-2	8	2	On-demand	Commercial, at a cost	since 2009								x	x		
Upcoming sensors																
EnMAP	90	30	On-demand	Free for scientific users	planned 2018	x	x	x		x	x	x	x	x		
HySpIRI VSWIR	60	30	16 days	Web-enabled, free	planned	x	x	x		x	x	x	x	x		
HySpIRI TIR	Thermal	30	5 days	Web-enabled, free	planned										x	
PRISMA	60	20	On-demand	Free for scientific users	planned 2018	x	x	x		x	x	x	x	x		
Sentinel-3	21/Thermal	300	daily	Web-enabled, free	planned 2015	x	x	x		x	x	x	(x)	x		x

3.2.2 Indicators of transparency

Water transparency is an essential lake property influencing light availability (Peeters et al., 2009). Light availability is important for biological, chemical and physical processes such as primary production and formation of macrophytes and is therefore a physical sentinel of climate change and water quality (Peeters et al., 2009; Williamson et al., 2009). Inherent optical properties influence water transparency and therefore light availability due to absorption and scattering (Kirk, 2011). Secchi disc depth (i.e. the depth where a white Secchi disc is no longer visible for human eye (Kirk, 2011)), euphotic depth (i.e. the depth where the radiation available for photosynthesis is 1 % of its value at surface (Kirk, 2011)), Z_{90} (i.e. the zone from which 90 % of water-leaving radiance originates (Doerffer and Schiller, 2007)) and the diffuse attenuation coefficient of downwelling irradiance K_d represent widely used remote sensing indicators for transparency. Using semi-analytical or advanced empirical approaches indicators are often derived together (Table 3.4).

Table 3.4: Studies deducing indicators of lake transparency. When several algorithms have been tested, the table indicates the approach with the highest accuracy. rRMSE = relative root mean square error, R^2 = determination coefficient, WFD = Water Framework Directive. *Airborne, hyperspectral sensor.

Authors	Techniques	Sensor	Parameter	Range	Accuracy	Study area	Time	Process
Binding et al. (2010)	Empirical band ratios	MODIS	Surface SPM	0-20 g·m^{-3}	rRMSE: 40%	Lake Erie (Canada/ USA)	2003-2007	Time series analyses; seasonal and event-driven cycles of SPM
	Semi-analytical model		Water column SPM	0-200 g·m^{-3}	-			Calculation of water column SPM
Bonansea et al. (2015)	Linear empirical models	Landsat TM, ETM	CHL	0-133 mg·m^{-3}	rRMSE: 7.25%	Río Tercero reservoir (Argentina)	2003-2010	Time series analyses; Interaction of ST, rainfall, transparency and phytoplankton
			z_{SD}	0.3-6 m	rRMSE: 30.8%			
			T_{surf}	10-31 °C	-			
Chao Rodríguez et al. (2014)	Emprirical band ratios	Landsat TM	CHL	0.4-20 mg·m^{-3}	-	Lake Arreo (Spain)	2000-2012	Temporal dynamics of water quality parameters; development of model
			z_{SD}	1.33-7.53 m	RMSE: 0.48 m			
			T_{surf}	5-25 °C	RMSE: 4.18 °C			
Giardino et al. (2015)	Bio-optical inversion BOMBER (Giardino et al., 2012)	MIVIS*	SPM	2.3-5.75 g·m^{-3}	R^2: 0.91	Lake Trasimeno (Italy)	September 2009	Interaction of SPM and SAV and water depth
			CHL	0.25-4.45 mg·m^{-3}	R^2: 0.71			
			CDOM	0.3-0.72 m^{-1}	R^2: 0.78			
			SAV	0-100 %	Qualitative			
			Water depth	0-4 m	R^2: 0.84			
Giardino et al. (2014b)	Neural network MERIS C2R	MERIS	CHL	0-12 mg·m^{-3}	Qualitative; referring to reference studies	Lake Maggiore (Italy)	2003-2011	Spatiotemporal dynamics and trend analyses; WFD monitoring
			CDOM	0.03-0.2 m^{-1}				
			SPM	0-2.8 g·m^{-3}				
			Z_{90}	4-25 m				
		Landsat 8	T_{surf}	10-16 °C				
Giardino et al. (2010a)	Neural Network MERIS C2R	MERIS	CHL	0-20 mg·m^{-3}	Qualitative; temporal and spatial mismatch of sensor and *in situ* data	Lake Trasimeno (Italy)	2005-2008	Relation between land use and water transparency;
			SPM	3-21 g·m^{-3}				

Continued on next page

Table 3.4 – *Continued from previous page*

Authors	Techniques	Sensor	Parameter	Range	Accuracy	Study area	Time	Process
			Z_{90}	0.5-5 m				
	MODIS product	MODIS	T_{surf}	4-30 °C			2003-2008	Improvement of
	Decision tree classification, Maximum Likelihood classification	Landsat TM, MSS, AVNIR-2, ASTER	Land use/ cover, SAV		Qualitative		1978-2008	environmental knowledge; WFD reference conditions
Giardino et al. (2010b)	Empirical regression	AVNIR-2	SPM	0-250 g·m^{-3}	R^2:0.924	Lakes in Mount Everest region	October 2008	Information on remote, hardly accessible lakes; glacier-lakeinteractions
Hicks et al. (2013)	Empirical regression	Landsat ETM	SPM	3.9-145 g·m^{-3}	R^2:0.939	34 lakes in New Zealand	2000-2009	Filling information gaps on water clarity for unmonitored lakes;
Horion et al. (2010)	Regionally adjusted bio-optical algorithms	MODIS	CHL	0-5 mg·m^{-3} Blooms: 10-20 mg·m^{-3}	R^2: 0.66	Lake Tanganyika (Burundi, Congo, Tanzania, Zambia)	2002-2006	Phytoplankton and primary productivity dynamics; Bloom detection
			K_d(490 nm)	0.07-0.23 m^{-1}	R^2:0.56			
Kutser et al. (2009)	Empirical band ratios	ALI, Landsat ETM, IKONOS	CDOM	0-20 m^{-1}	-	Boreal lakes in Sweden, Finland, USA, Canada	July 2003 July-August 2002	Large scale CDOM assessment; regional differences
Kutser (2012)	Empirical band ratio regression	Landsat TM, ETM	CDOM	0.5-6 m^{-1}	R^2: 0.62	Lake Malären (Sweden)	1984-2011	Long-term trend information on lake carbon content; climate change
Lobo et al. (2015)	Non-linear empirical regression	Landsat TM, ETM, OLI	SPM	2.5-301 g·m^{-3}	R^2: 0.94	Tapajós River Basin (Brasil)	1973-2013	Relation to gold-mining activities; spatiotemporal information on water quality
Long and Pavelsky (2013)	Empirical band ratio regression	MERIS	SPM	0-2500 g·m^{-3}	Spearman's p: 0.97	Lake Athabasca (Canada)	2000-2011	Relation of river discharge and SPM
Majozi et al. (2014)	Neural network MERIS C2R;	MERIS	K_d(490 nm)	1.7-11.9 m^{-1}	RMSE: 0.26 m^{-1}	Lake Naivasha (Kenya)	September 2010	Relation between K_d, Z_{eu} and CHL, CDOM,
	MERIS EL		Z_{eu}	0.7-1.1 m	RMSE: 0.17 m			SPM

Continued on next page

Table 3.4 – *Continued from previous page*

Authors	Techniques	Sensor	Parameter	Range	Accuracy	Study area	Time	Process
Matthews et al. (2010)	Neural network MERIS EL; MERIS C2R; empirical regression	MERIS	CHL	50-240 $mg \cdot m^{-3}$	RMSE: 9.8 %	Lake Zeeklovei (Africa)	April 2008	Spatio-temporal dynamics; Integration into monitoring
			SPM	46-55 $g \cdot m^{-3}$	RMSE: 14.1 %			
			CDOM	1.9-2.8 m^{-1}	RMSE:13 %			
			z_{SD}	0.23-0.3 m	RMSE: 8.0 %			
Shi et al. (2014)	Empirical regression	MERIS	K_d(PAR)	0-24 m^{-1}	R^2:0.74	Lake Taihu (China)	2003-2010	Seasonal and spatial variations in K_d; relation to wind speed and other constituents

3.2.2.1 Coloured dissolved organic matter

CDOM is a quantifiable remote sensing indicator calculated as absorption in m^{-1} at a specific wavelength λ ($a_{CDOM}(\lambda)$), often 440 nm. CDOM is used as a proxy for the lake carbon content indicator DOC (Kutser et al., 2015). This relationship is well established for boreal lakes but varies depending on the CDOM source which may be allochthonous (e.g. decaying wooden plants in the catchment) or autochthonous (e.g. decaying aquatic plants within the lake) (Brezonik et al., 2015; Kutser, 2012). Showing an exponential decrease of absorption with increasing wavelengths CDOM strongly absorbs radiation in the ultraviolet and blue wavelengths (Nguy-Robertson et al., 2013). Absorption by CDOM thus influences the spectral distribution of radiation available in water bodies; high amounts reduce penetration depth of light. Since CDOM is a main absorber, CDOM-rich waters offer very low water leaving radiances which complicates remote CDOM derivation (Brezonik et al., 2015).Valid sensors offer bands in the visible wavelength with high radio-metric resolution and signal-to-noise ratio (Kutser et al., 2009).The hyperspectral sensor MIVIS offers these characteristics so that Giardino et al. (2015) obtained $a_{CDOM}(440)$ with high accuracy (R^2= 0.78) in a relatively low concentration range (0.30-0.72 m^{-1}) at Lake Trasimeno (Italy). Higher CDOM concentrations in boreal lakes enabled Kutser (2012) and Kutser et al. (2009) to empirically retrieve $a_{CDOM}(440)$ from multispectral data. Although being less accurate (R^2= 0.62, Table 3.4) these data allow gathering information from the past to derive, e.g. seasonal trends of CDOM (e.g. Kutser, 2012) or spatially large scale assessments (e.g. Kutser et al., 2009).Temporal and spatial distribution of CDOM, indicating DOC concentrations over wide geographic scales, is essential to fully understand the role of lakes in carbon cycling and climate change (Kutser, 2012)(Williamson et al., 2009). Accurate atmospheric correction remains challenging for CDOM retrieval (e.g. Matthews et al., 2010) but also is necessary for generating time series.

3.2.2.2 Suspended particulate matter

SPM enters a lake through tributaries and originates from soil and bedrock erosion in its hinterland (Lindström et al., 1999) or from internal resuspension (Madsen et al., 2001). Thus, SPM is an important carrier of nutrients and contaminants. SPM attenuates light which leads to decreasing transparency with increasing SPM concentrations ($g{\cdot}m^{-3}$ or $mg{\cdot}l^{-1}$), yet it also scatters light which results in increased water leaving radiances (Giardino et al., 2015). Using hyperspectral data Giardino et al. (2015) distinguished small increments of SPM with high accuracies. Case studies retrieving SPM from multispectral sensors showed similar high accuracies ($R^2 \geq 0.9$); depending on the study area SPM varied between medium (0-20 $g{\cdot}m^{-3}$) and high concentrations (up to 2500 $g{\cdot}m^{-3}$). Most studies focused on time series of archived MERIS and Land-sat data to analyse spatio-temporal dynamics of SPM and its drivers (e.g. Binding et al., 2010; Giardino et al., 2014b, 2010b; Lobo et al., 2015). Binding et al. (2010) detected storm driven resuspension events and seasonal SPM cycles at Lake Erie (USA/Canada) by combining remote sensing SPM and wind speed data. Lobo et al. (2015) investigated water siltation effects by gold mining activities in Brazil and defined reference conditions for SPM concentrations before the mining activities. Long and Pavelsky (2013) combined measured river discharge and SPM distribution to determine threshold values for the discharge required to replenish periodic lakes at Peace-Athabasca Delta (Canada). Remote sensing further provides monitoring options for lakes with difficult access or which lack regular *in situ* monitoring (Giardino et al., 2010a,b; Hicks et al., 2013; Matthews et al., 2010).

3.2.2.3 Further indicators of transparency

Water transparency in terms of the diffuse attenuation coefficient of downwelling irradiance K_d describes the exponential decline of irradiance with increasing water depth (Kirk, 2011) and is often measured at 490 nm. Absorption by pure water, CDOM, phytoplankton and scattering by SPM influence K_d. K_d of the photosynthetically active radiation (PAR) determines the availability of light for phytoplankton and macrophytes, which makes it an important descriptor of lake transparency also used for primary production estimates (see Section 3.2.3.1). Several case studies revealed that remote sensing data allow retrieval of a wide range from low K_d

(0.07-0.23 m^{-1} indicating high transparency, Horion et al., 2010) to high K_d values (up to 24 m^{-1}, Shi et al., 2014) from MERIS and MODIS data which offer bands at 490 nm. Detected seasonal and spatial variations assist investigating lake primary production (Horion et al., 2010; Majozi et al., 2014; Shi et al., 2014). Analysing K_d time series also revealed strong correlations between K_d and wind speed (Shi et al., 2014). Various studies obtained Secchi disc depth and Z_{90} as proxy for water transparency using MERIS and Landsat imagery (Table 3.4). Retrieved values ranged from 0.3 m (Matthews et al., 2010) up to 25 m (Z_{90} Giardino et al., 2014b). Majozi et al. (2014) calculated the euphotic depth using MERIS K_d. The broad majority of studies, however, focused on analysing spatio-temporal dynamics of Secchi disc depth or Z_{90} proving the additional value for lakes which lack regular *in situ* monitoring (Hicks et al., 2013) and the suitability for integration into existing water quality monitoring (e.g. Giardino et al., 2014b; Matthews et al., 2010).

3.2.3 Indicators of biota

Indicators of biota play a key role in lake ecology (Birk et al., 2012; Brucet et al., 2013; Reyjol et al., 2014). Some biological indicators such as phytoplankton, submerged macrophytes and riparian vegetation can be retrieved directly by remote sensing (Table 3.5).

Table 3.5: Studies deducing indicators of lake biota. When several algorithms have been tested, the table indicates the approach with the highest accuracy. k = Kappa coefficient, OA = overall accuracy, r = correlation coefficient, RMSE = root mean square error, R^2 = determination coefficient, WFD = Water Framework Directive. *Airborne, hyperspectral sensor.

Authors	Techniques	Sensor	Parameter	Range	Accuracy	Study area	Time	Process
Phytoplankton and Cyanobacteria								
Bresciani et al. (2011c)	Neural Network MERIS C2R (Doerffer and Schiller, 2008)	MERIS	CHL	0-20 mg·m^{-3}	-	Perialpine lakes	2003-2009	WFD monitoring
Gómez et al. (2011)	Empirical band regression	CHRIS MERIS	CHL Cyano	0-250 mg·m^{-3} 0-250 mg·m^{-3}	RMSE: 8.6 mg·m^{-3} RMSE: 12.92 mg·m^{-3}	Albufera of Valencia (Spain)	2001-2005	WFD monitoring
Hunter et al. (2010b)	Empirical band ratio regressions, semi-analytical	CASI-2* AISA*	CHL Cyano	0 - >150 mg·m^{-3}	R^2: 0.832 R^2: 0.984	Loch Leven, Esthwaite Water (UK)	13, 26 Apr, 22 Aug 2007	Monitoring cyanobacterial blooms
Kauer et al. (2015)	MERIS NN C2R MERIS FUB	MERIS	CHL K_d(PAR)	0-100 mg·m^{-3} 0-3 m^{-1}	R^2: 0.92 R^2: 0.82	Lake Peipsi, Lake Võrtsjärv (Estonia)	2005-2009	Phytoplankton primary production model
Keith et al. (2012)	Empirical band ratio regression	Hyper-OCR*	CHL	2-90 mg·m^{-3}	R^2: 0.97	49 lakes in New England (USA)	15-17 Sep 2009	Trophic status assessment, CWA monitoring
Matthews (2014)	Maximum Peak Height algorithm (Matthews and Odermatt, 2015)	MERIS	CHL Cyano Surface scum area	1-500 mg·m^{-3} 1-50 % 0.01-10 %	r: 0.72 - -	50 lakes in South Africa	2002-2012	Time series analyses, trends, monitoring blooms
Palmer et al. (2015c)	MERIS FLH algorithm (Gower et al., 2004)	MERIS	CHL Phenology features	0->60 mg·m^{-3} Days, rates	R^2: 0.87 0.58 <R^2< 0.84	Lake Balaton (Hungary)	2002-2012	Phytoplankton phenology, spatio-temporal trends and changes
Wu et al. (2015)	Empirical (Floating Algal Index)	MODIS	Cyano bloom areas	100-800 km^2	-	Lake Taihu (China)	2000-2011	Cyanobacterial blooms and wind speed
Submerged aquatic vegetation and littoral vegetation								
Birk and Ecke (2014)	Manual detection	UAV RGB camera	31 macrophyte taxa	-	Evaluation of trophic metrics	72 Swedish lakes	2007-2010	Implementation for WFD monitoring

Continued on next page

Table 3.5 – *Continued from previous page*

Authors	Techniques	Sensor	Parameter	Range	Accuracy	Study area	Time	Process
Bolpagni et al. (2014)	Supervised classification	APEX*	Floating, submerged, emergent, littoral macrophytes	Discrete classes	k: 0.83	Mantua lakes (Italy)	21 Sep 2011	Interaction of phytoplankton and macrophytes
	Empirical band ratio regression		CHL	0-60 $mg \cdot m^{-3}$	r: 0.92			
Bresciani et al. (2011b)	Empirical band regression	GeoEye-1	Emergent reed beds	Leaf area index $m^2 \cdot m^{-2}$	R^2: 0.84	Lake Garda (Italy)	2009, 2010	Management effects on physiological status of reed beds
Brooks et al. (2015)	SAVMA (Shuchman et al., 2013b)	Landsat TM	Bottom substrate: sand, dense SAV, less dense SAV	Discrete classes	OA: 83%	Laurentian Great Lakes (USA, Canada)	2008-2011	Baseline map, trends in SAV coverage
			Biomass	129 kt				
Dogan et al. (2009)	Unsupervised classification	Quickbird	4 SAV classes; SAV coverage	Discrete classes	k: 86.5% k: 65.95%	Lake Mogan (Turkey)	6 Aug 2005	Monitoring macrophytes
Giardino et al. (2007)	Bio-optical inversion	MIVIS*	Sand, SAV (Bathymetry) (CHL, CDOM, SPM)	0-100%; 1-7 m	qualitative	Lake Garda (Italy)	1997, 2005	Changes in macrophyte patterns
Giardino et al. (2015)	Bio-optical inversion	MIVIS*	SAV	0-100%	qualitative	Lake Trasimeno (Italy)	12 May 2009	Relation between SPM and SAV colonisation
			SPM	0-10 $g \cdot m^{-3}$	$R^2 > 0.7$			
			Bottom depth	0.1-3.8 m	-			
Heblinski et al. (2011)	Bio-optical model	QuickBird	Bottom coverage	%	Qualitative	Lake Sevan (Armenia)	2006-2008	Effects of water level changes on aquatic vegetation structure
	Supervised classification		Vegetation types	Discrete classes				
Hunter et al. (2010a)	Supervised classification	CASI*	Growth-habitats (submerged, floating, partially-emergent, emergent); SAV species	Discrete classes	k: 0.72; k: 0.84	Upper Thurne region (UK)	22 June, 28 Aug 2005	WFD monitoring

Continued on next page

Table 3.5 – *Continued from previous page*

Authors	Techniques	Sensor	Parameter	Range	Accuracy	Study area	Time	Process
Shuchman et al. (2013b)	Semi-analytical classification (SAVMA)	Landsat TM, Quick-bird, World-View-2, MODIS, MERIS	Bottom substrate: sand, dense SAV, less dense SAV	Discrete classes	OA: 87 %	Laurentian Great Lakes (USA, Canada)	2009, 2010	SAV monitoring (Cladophora), biomass estimates
Roessler et al. (2013)	Spectral unmixing of depth invariant index	RapidEye	Bottom coverage (bare soil, *Najas marina*, *Elodea nuttallii*)	0-100 %	Qualitative	Lake Starnberg (Germany)	6 May, 3 Sep 2011	Monitoring invasive macrophytes
Rößler et al. (2013)	Bio-optical inversion	APEX*	Bottom coverage (sediment, *Najas marina*, *Chara spec.*)	0-100 %	Qualitative	Lake Starnberg (Germany)	2011	Monitoring invasive macrophytes

3.2.3.1 Algal blooms and phenology

Being closely related to nutrient availability phytoplankton represents a prominent indicator of the trophic state of fresh water ecosystems (Solheim et al., 2013). CHL is a proxy for phytoplankton (Carvalho et al., 2013b), and assessment via remote sensing uses its characteristic absorption features between 440 and 560 nm and at $\sim$ 670 nm (Matthews, 2011). In recent times, public media reported an increasing number of cyanobacteria blooms (Bojanowski, 2014; Zimmer, 2014) as they affect water usage for drinking, irrigation and recreational purposes (Carvalho et al., 2011). Due to their toxicity monitoring of cyanobacterial blooms requires rapid response and forecast tools that assist local authorities to swing into action timely. Just as for CHL, various empirical and semi-analytical algorithms exist for cyanobacteria retrieval (Table 3.5). To assess cyanobacteria concentrations, however, most authors use the absorbing feature of phycocyanin at $\sim$ 620 nm (Matthews, 2011).Various remote sensing algorithms are available to assist monitoring of algal phenology and blooms (Table 3.5). Using airborne hyperspectral and MERIS data case studies retrieved CHL and cyanobacteria concentrations in broad ranges (0-500 mg·m^{-3}) with high accuracies ($R^2 \geq 0.83$). Bresciani et al. (2011c) and Gómez et al. (2011) focused on analysing CHL with respect to Water Framework Directive monitoring. Keith et al. (2012) classified the trophic state from remotely sensed CHL to support lake monitoring with in the Clean Water Act. Several studies assisted cyanobacterial monitoring and risk assessment (e.g. Gómez et al., 2011; Hunter et al., 2010b; Matthews, 2014; Wu et al., 2015). Some authors used times series to support understanding of phytoplankton phenology (e.g. Palmer et al., 2015c). Kauer et al. (2015) integrated algal phenology into a lake primary production model.

3.2.3.2 Submerged aquatic vegetation and emerged vegetation

Benthic vegetation plays an important role in lake ecosystems and therefore serves as a widely used indicator for lake ecology (Søndergaard et al., 2010). SAV is sensitive to changes in water temperature, water level and transparency; as a result SAV is a valuable indicator for trophic state assessment (Penning et al., 2008; Poikane et al., 2015; Søndergaard et al., 2010). The species composition further indicates habitat persistency or presence of invasive species (Ginn, 2011). Mapping approaches include empirical classifications (e.g. Hunter et al., 2010a; Oppelt et al., 2012) and semi-analytical, spectral unmixing algorithms (e.g. Dörnhöfer and Oppelt, 2014; Giardino et al., 2015). Emerged vegetation is often assessed through classification approaches and band ratios (e.g. Bresciani et al., 2011b; Villa et al., 2013).
Case studies (Table 3.5) mainly use multispectral sensors with high spatial resolution or airborne, hyperspectral data. Accuracy assessments often are qualitative; in case of quantitative assessments accuracy measure showed good to very good performance ($k \geq 0.7$). Most studies retrieved percentage coverages of few single species or discrete growth habitat classes. Birk and Ecke (2014) identified 31 macrophyte species via visual image interpretation and integrated their results into a trophic metric of the Water Framework Directive. Semi-automated classification approaches distinguished less species. Macrophytes on growth habitat level,however, improved understanding of interactions with phytoplankton (e.g. Bolpagni et al., 2014) and supported field mappings (e.g. Dogan et al., 2009; Hunter et al., 2010a).
To minimise the influence of the water overlying SAV several authors developed depth-invariant indices (e.g. Brooks et al., 2015; Roessler et al., 2013; Shuchman et al., 2013b). By analysing a 30-year time series Brooks et al. (2015) demonstrated that SAV distribution maps can reproduce impacts of previous water management strategies, e.g. to reduce phosphorous inputs. Roessler et al. (2013) also created depth invariant indices, which allowed distinguishing two invasive macrophyte species (*Najas marina*, *Elodea nuttallii*) and uncovered sediment. Semi-analytical models such as BOMBER (Giardino et al., 2012) integrate the influence of water, water depth and water constituents in a radiative transfer model. For optically shallow water, BOMBER also includes a linear unmixing approach of up to three bottom substrates. Comparing obtained SAV distribution maps from different dates thus allowed to detect changes in SAV patterns (e.g. Giardino et al., 2007). Furthermore, the spatial information helped to analyse interactions of SAV and SPM concentrations (e.g. Giardino et al., 2015) or to detect distribution of invasive macrophytes (e.g. Roessler et al., 2013). Further studies monitored effects of

management strategies (Bresciani et al., 2011b) and changing water levels (Heblinski et al., 2011) on benthic vegetation structure.

3.2.4 Indicators of lake hydrology

Concerning hydrological properties of lakes Adrian et al. (2009) placed the water level to the list of key response variables. In shallow waters remote sensing is a valuable method to derive water levels (also referred to as water depths or bathymetry). Gao (2009) presented a review on empirical and analytical methods for bathymetry retrieval. While various studies exist for coastal bathymetry (e.g. Dekker et al., 2011; Garcia et al., 2014) less attention was paid to inland waters. Instead, shallow water areas have often been ignored or masked, especially when using ocean colour sensors. With airborne imagery and the advent of sensors with high spatial resolutions retrieval of lake or river bathymetry became feasible (Table 3.6, e.g. Flener et al., 2012; Legleiter et al., 2009). Recent bathymetric studies, however, focused on developing algorithms rather than using existing products (Table 3.6). Empirical derivation of bathymetry using multispectral satellite data with high spatial resolution showed high accuracies (R^2 > 0.9) in areas with homoge-nous substrate and water column properties (e.g. Legleiter et al.,2014; Yuzugullu and Aksoy, 2014).
As mentioned previously, bio-optical models account for different substrates and water constituent concentrations. Gege (2014a) presented a study at Lake Starnberg (Germany) which focused on improved model parameterisation and bathymetry retrieval. He used airborne, hyperspectral data and the recently published bio-optical tool WASI-2D (Water Colour Simulator, Gege, 2014b); resulting bathymetry values ranged between 0 and 8 m and showed high accuracy (RMSE = 0.37 m). To obtain information on substrates in optically shallow water Giardino et al. (2007, 2015) applied BOMBER to airborne, hyperspectral data at Lake Garda (Italy) and Lake Trasimeno (Italy). Focusing on satellite imagery for bottom substrate mapping, Giardino et al. (2014a) applied BOMBER to RapidEye and Landsat 8 data retrieving promising results.

Table 3.6: Studies deducing indicators of lake hydrology, in particular water depth. When several algorithms have been tested the table indicates the approach with the highest accuracy. RMSE = root mean square error, R^2 = determination coefficient. *Airborne, hyperspectral sensor.

Authors	Techniques	Sensor	Parameter	Range [m]	Accuracy	Study area	Time	Process
Gege (2014a)	Bio-optical inversion	HySpex*	water depth	0-8	RMSE: 0.37 m	Lake Starnberg (Germany)	14 May 2012	Model paper
Giardino et al. (2007)	Bio-optical inversion	MIVIS*	Sand, SAV, water depth	1-7	Avg. deviation from official map 1.3 % (1997), 4.7 % (2007)	Lake Garda (Italy)	1997, 2005	Changes in macrophytes patterns
Giardino et al. (2014a)	Bio-optical inversion	Rapid Eye, Landsat 8	water depth	0-7	Qualitative	Lake Garda (Italy)	10 June 2014	Model paper
Giardino et al. (2015)	Bio-optical inversion	MIVIS*	SPM, CHL, CDOM, SAV, water depth	0.1-3.8	R^2: 0.84	Lake Trasimeno (Italy)	12 May 2009	Relation between SPM and SAV colonisation
Legleiter et al. (2014)	Empirical band regression	WorldView-2	water depth	0-10.45	0.87< R^2< 0.92	Supraglacial lakes (Greenland)	18 and 23 July 2012	Water storage volume

Yuzugullu and Aksoy (2014)	Empirical band regression	WorldView-2	water depth	0-6	R^2: 0.9	Lake Eymir	28 July 2010	Outlook for water quality

3.2.5 Indicators of temperature

Water temperature in general is linked to heat and energy fluxes and regulates thermal stratification (Politi et al., 2012). Changes in water temperature thus affect ecosystem functions of lakes and result in changes of species composition and oxygen concentration (Williamson et al., 2009). Epilimnic temperature is regarded as a lake property directly affected by climate change (Adrian et al., 2009). Remote sensing provides spatial information on the radiometric skin surface temperature which may indicate epilimnic temperature; depending on wind speed, however, skin surface temperature tends to be cooler than the upper 50 cm bulk layer of the water column (Crosman and Horel, 2009).

A variety of studies showed that thermal remote sensing data can obtain surface temperature. Table 3.7 presents literature that used surface temperature products and retrieval algorithms for lake monitoring. Most studies applied sensors with coarse spatial resolution (MODIS, AVHRR and AATSR, Table 3.7) which provide images on a daily basis (e.g. Alcântara et al., 2010; Politi et al., 2012). Authors generally referred to generic product accuracies; if *in situ* measurements were available, high accuracies were achieved ($R^2 \geq 0.9$). Sima et al. (2013) benefited from the high temporal resolution to monitor diurnal, monthly, seasonal and inter-annual variations of surface temperature and to calculate lake water budgets. Analysing time series further enabled to detect global trends in lake surface temperature with respect to climate warming (Schneider and Hook, 2010), to complement data gaps of *in situ* archives (Politi et al., 2012), to investigate interactions with CHL patterns (Bresciani et al., 2011a), to indicate periods of lake mixing or thermal stratification (Alcântara et al., 2010) or to improve numerical weather prediction models (Pour Kheyrollah et al., 2014). Simon et al. (2014) recommended the Landsat archive with higher spatial but lower temporal resolution for obtaining spatially explicit, historical surface temperature. Chao Rodríguez et al. (2014) used the Landsat archive to develop a model which enables analysis of lake temperature cycles from 2002 to 2012.

Table 3.7: Studies deducing surface temperature as indicator of lake water temperature. When several algorithms have been tested, the table indicates the approach with the highest accuracy. RMSE = root mean square error, R^2 = determination coefficient.

Authors	Techniques	Sensor	Range [°C]	Accuracy	Study area	Time	Process
Alcântara et al. (2010)	T_{surf} product (diurnal, nocturnal)	MODIS	12-35	-	Itumbiara hydroelectric reservoir (Brazil)	2003-2008	Time series of T_{surf}, analyses of heat fluxes and influence of meteorological variables, calculation of surface energy budget
Bresciani et al. (2011a)	T_{surf} product	MODIS	0-30	-	Lake Trasimeno, Lake Garda (Italy)	2005-2008, 2004-2009	Relationship between T_{surf} and CHL
Chao Rodríguez et al. (2014)	Empirical band ratios	Landsat TM	5-25	RMSE: 4.18 °C	Arreo lake (Spain)	2000-2012	Temporal dynamics of water quality parameters; Development of model

Continued on next page

Table 3.7 – *Continued from previous page*

Authors	Techniques	Sensor	Range [°C]	Accuracy	Study area	Time	Process
Politi et al. (2012)	Split-window algorithm	AVHRR	0-30	R^2>0.9	Lake Geneva (Switzerland), Balaton (Hungary), Vattern (Sweden), Oulujarvi (Finland)	1993-1996; 2001-2005	Temporal and spatial trends in T_{surf} of European lakes
Pour Kheyrollah et al. (2014)	T_{surf} product	MODIS AATSR	-2->0	-	Lakes > 6 km^2 in northern Europe	Winter 2010/11; 2011/12	Improvement of lake description in numerical weather prediction model
Schneider and Hook (2010)	Split-window algorithm	AATSR AVHRR Nighttime	-	RMSE: 0.013 °C y^{-1}	167 large inland water bodies globally	1985-2009 (Jul-Sep; Jan-Mar)	Trends in lake T_{surf} related to climate change
Sima et al. (2013)	T_{surf} product	MODIS	5-30	R^2: 0.92	Urmia Lake (Iran)	2007-2010	Spatial and temporal T_{surf} variation; relation to lake evaporation
Simon et al. (2014)	Mono-window algorithm	Landsat TM	4-25	R^2>0.9, RMSE: 1-2 °C	Lake Bariousses, Lake Bimont (France)	2009-2013	Suitability of Landsat archive for information on historical lake T_{surf}

3.2.6 Indicators of ice phenology

For lakes with periodic ice cover ice phenology is an essential lake property influencing the underwater light climate, energy balance and biogeochemical processes. Brown and Duguay (2010) as well as Kirillin et al. (2012) defined two parameters most important for analysing the interplay between lake ice and climate: ice-on when ice occurs on a lake for the first time in a season, ice-out on a lake due to thawing. Apart from air temperature ice-on depends on parameters such as lake depth, heat storage, inflows and internal currents; for ice-out air temperature is the major driver (Brown and Duguay, 2010). Compared to water the albedo of ice and snow is high (Kirillin et al., 2012) which is important for detecting ice cover with optical sensors. Most ice phenology studies are based on point data records dating back to the 19th century (Brown and Duguay, 2010). A long-term trend analysis of lake ice records (1855-2004) in the northern hemisphere revealed that ice-on occurred 0.3-1.6 days/decade later, while ice-out now happens 0.5-1.9 days/decade earlier; lake-ice duration therefore decreased between 0.7 and 4.3 days/decade depending on the investigated time period (Benson et al., 2012).

In general, satellite monitoring of lake ice is amenable to operational monitoring on a regional to global scale. Using passive optical remote sensing, major limitations are cloud cover (e.g. Arp et al., 2013) and low sun angles during ice-on periods (Latifovic and Pouliot, 2007) which aggravate image acquisition and processing. Being less affected by cloud cover and illumination passive and active microwave remote sensing therefore are primarily used for ice phenology studies, but are beyond the scope of this paper. Passive remote sensing, however, also serves as a valid tool for lake-ice monitoring. Case studies mainly used large scale sensors with low spatial resolution. Comparing *in situ* observations with satellite derived phenological parameters showed reasonable accuracies (Table 3.8). Remote sensing supported filling data gaps in *in situ* records (Latifovic and

Pouliot, 2007) and further enabled a spatially more explicit monitoring of ice phenology and its drivers (e.g. Arp et al., 2013; Kropáček et al., 2013). Combining lake ice phenology and its main drivers Brown and Duguay (2012) as well as Shuter et al. (2013) simulated effects of climate change scenarios on lake ice phenology.

Table 3.8: Studies deducing indicators of lake ice phenology. When several algorithms have been tested, the table indicates the approach with the highest accuracy. RMSE= root mean square error, MAE = mean absolute error.

Authors	Techniques	Sensor	Parameter	Accuracy	Study area	Time	Process
Arp et al. (2013)	Visual interpretation	MODIS	Ice-out	RMSE: 7.1 days	55 large lakes in Alaska (USA)	2007-2012 (1.4.-1.7.)	Spatial and temporal variation among lakes; Baseline of ice-out for change analyses
Brown and Duguay (2012)	MODIS snow product	MODIS IMS product	Ice phenology	Average product accuracy 93 %	Lakes in Québec (Canada)	2000-2001 2004-2011	Model for ice phenology; Climate change projection
Kropáček et al. (2013)	MODIS 8-days composite	MODIS	Ice phenology	RMSE: 9.6 days	59 large lakes in Tibetan Plateau	2001-2010	Drivers of ice phenology
Latifovic and Pouliot (2007)	Temporal reflectance profiles	AVHRR	Ice-on start	MAE: 9.8 days	42 Canadian lakes	1985-2004	Trends in ice phenology; Filling *in situ* data gaps
			Ice-on end	MAE: 7.4 days			
			Ice-out start	MAE: 11.9 days			
			Ice-out end	MAE: 4.2 days			
Shuter et al. (2013)	Data from Latifovic and Pouliot (2007)	AVHRR	Ice phenology	See Latifovic and Pouliot (2007)	42 Canadian lakes	2055	Model linking ice phenology and climate; Climate change projection

Continued on next page

3.2.7 Synthesis

The great variety of case studies emphasises that valid remote sensing approaches are available to assist lake monitoring and ecological research. Furthermore, recent remote sensing technology and data archives pose an invaluable asset for retrieving historical information on indicators of lake ecology in non-investigated lakes. Especially in regions where information is scarce and which lack monitoring *in situ* networks integrating remote sensing would add value significantly.

Remote sensing, however, still needs to be integrated in monitoring frameworks such as the Water Framework Directive (Reyjol et al., 2014) or Clean Water Act (Schaeffer et al., 2013). Keith et al. (2012) performed an attempt to support the Clean Water Act with airborne remote sensing since *in situ* monitoring captured only 39 % of US inland waters during the 2004 reporting cycle. Looking beyond established monitoring networks large data gaps exist fora great variety of lakes. Fig. 3.4 highlights that, on a global level, the share of studies using remote sensing is similarly low.

To figure out reasons impeding a broader use of remote sensing in water quality management, Schaeffer et al. (2013) conducted a survey among staff of the US Environmental Protection Agency and revealed costs, data continuity, product accuracy and programmatic support as the four main aspects mentioned.

Nowadays, imagery of many archived, operating and future satellite missions are available free of charge (see Table 3.3). The US missions, the European Copernicus programme with its Sentinel missions and national contributing missions have a free and open data policy (Oppelt et al., 2015). The high temporal resolution of freely available ocean colour sensors alleviates interferences with clouds; their medium to coarse spatial resolution, however, impedes the analysis of small lakes (< 1 km^2) (Matthews et al., 2010). The Landsat sensors as well as Sentinel-2 data offer data with improved spectral and spatial characteristics that serve as valuable basis for a wide range of applications. If required, commercial missions such as WorldView-2 or Quickbird provide data with very high spatial resolution ($<$1 m) on a regular basis (Table 3.3).

As expected, users prefer ready products and algorithms which are integrated into software or toolboxes going along with technical assistance (Gómez et al., 2011; Odermatt et al., 2012). Nowadays, several open-source tools are available; the European Space Agency (ESA) as well as the National Aeronautics and Space Administration (NASA) developed toolboxes including algorithms especially designed for their missions (ESA, 2014a,b; NASA, 2015). These tools provide easily calculable estimates of lake variables. Additionally, ESA and NASA provide thematic products which may be downloaded via their websites. Current and near future earth observation missions also consider data continuity for the next decades (Berger et al., 2012; Oppelt et al., 2015). For advanced users bio-optical models are also available free of charge (e.g. Gege, 2014b; Giardino et al., 2012). They enable the assessment of water constituent concentrations, bathymetry and bottom substrate composition (cf. Section 3.2.1). Training and a fundamental understanding of remote sensing principles, however, are indispensable to use the models adequately.

Along with the availability and continuity of multi-sensor algorithms and products, accuracies are critical to end users. Water managers demand product accuracies specific for “their“ water body (Schaeffer et al., 2013); remote sensing algorithms and global products, however, are validated at specific study areas and sensors. Therefore adaptation of existing algorithms is often required. Required *in situ* measurements are costly, time-consuming and must be taken contemporary to image acquisition. These factors may explain why the majority of lakes intensely investigated by remote sensing is concentrated in the vicinity of research institutions/groups focusing on inland water remote sensing (cf. Fig. 3.2). Collaboration of disciplines may further improve both combination of *in situ* and remote sensing data and the global coverage of lakes investigated using valid remote sensing approaches.

For remote sensing products accuracy measures indicate measurement uncertainties, i.e. (relative) root mean squared error,mean absolute percentage error, coefficient of determination, overall accuracy (OA) or Cohen's kappa (k) (cf. tables in Section 3.2.1). An essential problem in validating remote sensing indicators, however, is the upscaling of discrete *in situ* measurements to the spatial measurement of a sensor (Dörnhöfer and Oppelt, 2014; Giardino et al., 2010a; Yang et al., 2013). Moreover, uncertainty assessments require field observations or water samples with given accuracies. In spite of that, uncertainty assessments of *in situ* measurements are rare even in monitoring frameworks (Hering et al., 2010). Only few studies mentioned accuracies of *in situ* measurements such as GPS positional accuracies (Dörnhöfer and Oppelt, 2014; Hunter et al., 2010a), temperature measurements (Alcântara et al., 2010) or echo soundings (Legleiter et al., 2014). High accuracies are demanded for remote sensing products whereas *in situ* measurements intrinsically are accepted as correct (e.g. Schaeffer et al., 2013). A round robin test among different laboratories in Germany (CHL and phaeophytin) showed that uncertainty assessments of current methods still are insufficient (AQS, 2008). In this vein, standardised uncertainty assessments are necessary for remote sensing indicators and *in situ* data, whereas both sides would clearly benefit from collaboration.

A major uncertainty in remote sensing of lakes remains atmospheric correction. High reflectance from nearby land or clouds affecting the reflectance of water bodies (adjacency effect) and difficult parameterisation of aerosols complicate atmospheric correction (Matthews et al., 2010; Mouw et al., 2015). First approaches designed for inland waters were recently developed (Sterckx et al., 2015b; Vanhellemont and Ruddick, 2015); due to the lack of operationally available algorithms, authors adopted correction methods developed for land or used *in situ* measurements.

Furthermore, radiometric and spectral resolution of a sensor determine the detail at which values of remote

sensing indicators can be differentiated. Sensors with high radiometric and spectral resolution, such as airborne hyperspectral or ocean colour sensors, detected even small variations at low concentration ranges (Giardino et al., 2014b, 2015). Multispectral sensors with lower radiometric resolution enabled assessments of high concentrations of CDOM (Kutser, 2012) and SPM (Lobo et al., 2015). *in situ* measurements can resolve response variables at finer detail than remote sensing. Moreover, water constituent concentrations retrieved from *in situ* samples show higher variability than remote sensing measurements (e.g. Matthews et al., 2010); phytoplankton communities and macrophytes can be differentiated at species level whereas most remote sensing studies focused on growth habitats. Nonetheless, remote sensing indicators provide information at higher temporal frequency and a larger spatial extent than *in situ* based monitorings. Spatial assessments can better characterise average properties of an entire lake than point-based *in situ* measurements. According to Matthews et al. (2010) the large sample size in remote sensing images results in smaller standard errors when calculating average water constituent concentrations. Giardino et al. (2010a) reported that *in situ* sampling may not be able to capture reoccurring events of high SPM concentrations due to a ferry route, where dredging hinders SAV colonisation and induces resuspension, and SPM entering a lake at stream inlets. Sima et al. (2013) modelled lake evaporation in Iran using point-based *in situ* and spatially explicit remote sensing temperatures.They revealed a difference in evaporation of 147 mm/year which is essential for water management in a semi-arid region.

The majority of authors used remote sensing data to analyse time series. Remote sensing data may provide timely information on rapidly occurring changes in a lake during, for instance, algalblooms, heavy rains or droughts. Thus, analysing time series of lakeremote sensing indicators and environmental factors improved understanding of processes in lakes. To further investigate interactions between drivers and response variables, spatio-temporally explicit remote sensing data also represent a valuable source for lake ecological models (e.g. Jørgensen, 2010; Kauer et al., 2015).

At present, efforts increase in both lake remote sensing and water management communities (Fig. 3.1), and combining existing know-how will certainly improve knowledge of lake ecology. Moreover, large scale, multitemporal monitoring supports the analysis of spatio-temporal patterns of ecological indicators. It is therefore not a question of replacing discrete *in situ* measurements and observations; it is a question of combining different specialist fields to complete the puzzle of inland water ecology and the role of lakes in climate change and water quality aspects.

3.3 Conclusions

This review presents how remote sensing can assist lake research and monitoring including the most important remote sensing indicators of lake properties, i.e. water transparency, biota, lake hydrology, temperature and ice phenology. Published literature shows that various products, algorithms and ready-to-use tools are available to support lake research and management.

Operational algorithms and products already exist for indicators such as CHL and SPM. Moreover, data and product archives promote a deeper understanding of trends in lake properties and their external drivers. Time series of phytoplankton and cyanobacteria, for instance, revealed new insights into algae phenology and enabled identification of critical lake areas. Furthermore, remote sensing based assessments of CHL were evaluated for integration into monitoring frameworks such as Clean Water Act and Water Framework Directive. Remote sensing of CDOM, SPM, K_d and Secchi disc depth focused on analysing time series to investigate correlations with environmental drivers or other lake response variables. Studies on submerged aquatic vegetation considered detection of invasive species and supported *in situ* monitoring by identifying growth habitats.

Unless being unable to retrieve temperature depth profiles, thermal data provide a valuable indicator of epilimnic temperature and its spatial patterns. Present studies also show that remote sensing supports lake-ice monitoring and is useful to overcome existing limitations of local observations. Then again, remotely sensed bathymetry is an indicator which has not yet been used to its possible extent.

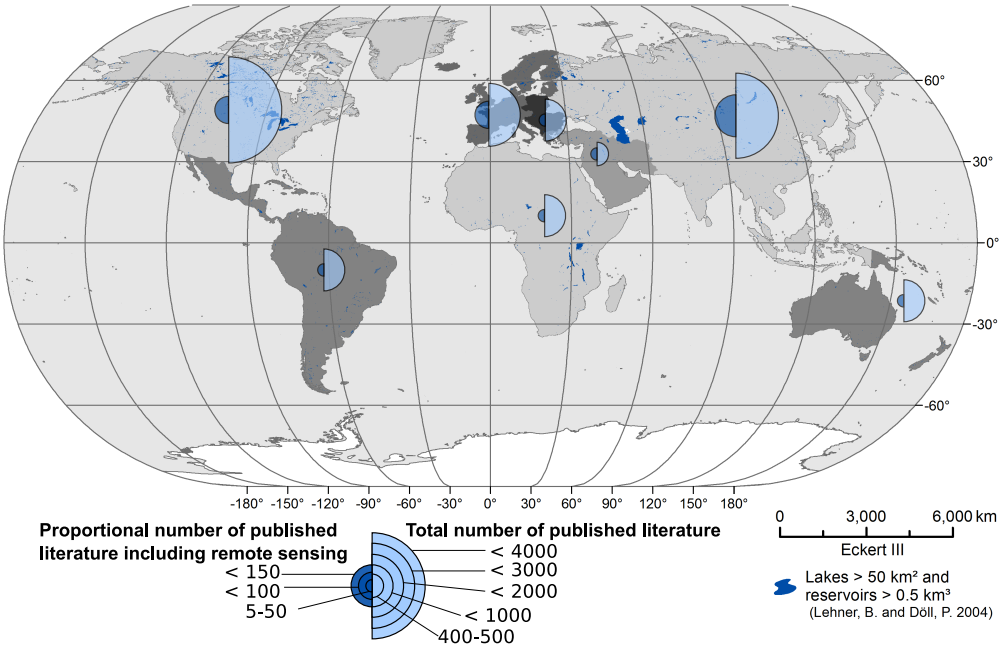

Figure 3.4: Number of published literature (Web of Knowledge data base 2000-2015) which contains the search terms “inland water quality/ecology“ or “lake water quality/ecology“ (light blue) and “remote sensing“ (dark blue) grouped by regions (grey levels). Study area location was filtered by searching for state names. Thus, studies which lack state information in the abstract were not considered (lakes and reservoir shape file source: Lehner and Döll (2004)). (For interpretation of the references to colour in this legend, the reader is referred to the web version of the article.)

A synergetic use of *in situ* measurements and earth observation data can fill data gaps and support water resource management. We invite lake ecologists, water managers and authorities to benefit from integrating remote sensing and its synoptic view of lake properties. Remote sensing is certainly unable to capture all indicators used in lake ecology or to identify the same levels of detail as *in situ* measurements. Remote sensing data, however, may well support sparsely distributed *in situ* measurements with spatially and temporally more frequent data. Furthermore, lake ecological models may also benefit from spatio-temporally explicit information derived from remote sensing data. Synergetic use of sensors with different temporal, spatial and spectral resolution such as Landsat 8, Sentinel-2 and Sentinel-3 may overcome limitations of single systems. The complementary use of conventional measures and remote sensing data/products maximises strengths and minimises existing weaknesses in lake monitoring. Moreover, currently available and upcoming sensors, open access and free data policies, operational algorithms and open source tools will certainly further promote remote sensing applications in lake research.

Acknowledgments

The authors thank the anonymous reviewers whose comments helped to improve the manuscript. The Federal Ministry for Economy Affairs and Energy supported our work on the basis of a decision by the German Bundestag (funding code: 50EE1340).

Chapter 4

Water Constituents and Water Depth Retrieval from Sentinel-2A – A First Evaluation in an Oligotrophic Lake

Katja Dörnhöfer, Anna Göritz, Peter Gege, Bringfried Pflug and Natascha Oppelt
Remote Sensing (2016), doi:10.3390/rs8110941
Received: 30 August 2015, Accepted: 3 November 2015

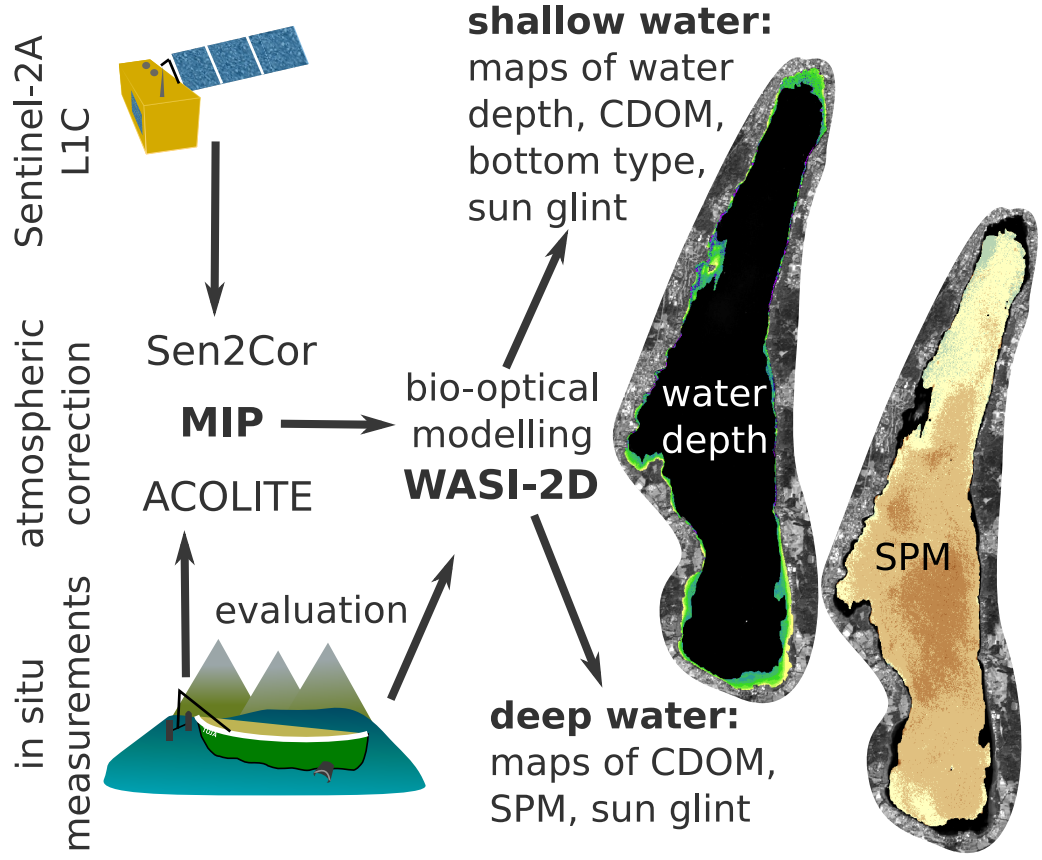

Changes made to the published version:
To harmonise the style of the entire thesis, chlorophyll-a is abbreviated as CHL instead of Chl-a and Senitnel-2A as S2A instead of S2A.

Abstract

Satellite remote sensing may assist in meeting the needs of lake monitoring. In this study, we aim to evaluate the potential of Sentinel-2 to assess and monitor water constituents and bottom characteristics of lakes at spatio-temporal synoptic scales. In a field campaign at Lake Starnberg, Germany, we collected validation data concurrently to a Sentinel-2A (S2A) overpass. We compared the results of three different atmospheric corrections, i.e., Sen2Cor, ACOLITE and MIP, with *in situ* reflectance measurements, whereof MIP performed best (r = 0.987, RMSE = 0.002 sr^{-1}). Using the bio-optical modelling tool WASI-2D, we retrieved absorption by coloured dissolved organic matter ($a_{CDOM}(440)$), backscattering and concentration of suspended particulate matter (SPM) in optically deep water; water depths, bottom substrates and $a_{CDOM}(440)$ were modelled in optically shallow water. In deep water, SPM and $a_{CDOM}(440)$ showed reasonable spatial patterns. Comparisons with *in situ* data (mean: 0.43 m^{-1}) showed an underestimation of S2A derived $a_{CDOM}(440)$ (mean: 0.14 m^{-1}); S2A backscattering of SPM was slightly higher than backscattering from *in situ* data (mean: 0.027 m^{-1} vs. 0.019 m^{-1}). Chlorophyll-a concentrations ($\sim$1 mg·m^{-3}) of the lake were too low for a retrieval. In shallow water, retrieved water depths exhibited a high correlation with echo sounding data (r = 0.95, residual standard deviation = 0.12 m) up to 2.5 m (Secchi disk depth: 4.2 m), though water depths were slightly underestimated (RMSE = 0.56 m). In deeper water, Sentinel-2A bands were incapable of allowing a WASI-2D based separation of macrophytes and sediment which led to erroneous water depths. Overall, the results encourage further research on lakes with varying optical properties and trophic states with Sentinel-2A.

Keywords

WASI, atmospheric correction, bathymetry, submerged aquatic vegetation, sun glint, water quality, validation, inland waters, inverse modelling

4.1 Introduction

The monitoring of lake water quality is gaining increasing importance due to an increase in stressors such as climate change, eutrophication, contamination of organic and inorganic substances, and anthropogenic influences which threaten ecological functions (Adrian et al., 2009; Stendera et al., 2012). Humans both benefit from and depend on a variety of ecosystem services provided by lakes, e.g., drinking water, irrigation, energy production, fisheries, and recreation (Millennium Ecosystem Assessment, 2005). Therefore, healthy lake ecosystems are of great importance. International and national legislations such as the European Water Framework Directive (European Commission, 2000) or the US Clean Water Act (United States Congress House, 2002) include regular monitoring schemes that observe the ecological states of lakes and detect changes which may influence lake ecology and water quality (Hering et al., 2010). Most monitoring schemes are based on selective sampling during summer or installation of measurement buoys (Birk et al., 2012). Deploying these sampling strategies is labour, time and cost intensive (Schaeffer et al., 2013); yet, it may not allow for the detection of changes which occur on varying temporal and spatial scales (Reyjol et al., 2014).

To overcome spatio-temporal limitations, remote sensing may assist *in situ* monitoring since it can extract indicators on water transparency, biota, bathymetry, water surface temperature and ice phenology (Dörnhöfer and Oppelt, 2016). Empirical and physical-based algorithms can be used to retrieve water constituents, water depths and bottom substrates. Several publications provide reviews of existing approaches (Dekker et al., 2011; Dörnhöfer and Oppelt, 2016; Gao, 2009; Matthews, 2011; Odermatt et al., 2012). Compared to empirical algorithms, physically-based approaches are broadly applicable and transferable among lakes and sensors. Suitable sensors must deploy bands in the visible and near-infrared (VNIR) wavelengths with high radiometric

sensitivity such as ocean colour sensors (e.g., MODIS and MERIS). Owing to their spatial resolution (∼300 m), studies conducted with these sensors focus mainly on large lakes such as Lake Balaton (Palmer et al., 2015c), Lake Geneva (Kiefer et al., 2015), Lake Taihu (Jiang et al., 2015)(Luo et al., 2016)(Shi et al., 2015), or Great Lakes (Binding et al., 2015), but rarely on small lakes (Matthews, 2014; Matthews et al., 2010). Studies on smaller lakes refer to less sensitive Landsat data (Chao Rodríguez et al., 2014) or to high spatial resolutions from commercial sensors such as WorldView (Yuzugullu and Aksoy, 2014) or Quickbird (Heblinski et al., 2011). Moreover, airborne hyperspectral data often are used for mapping bottom substrates or water depths (e.g., Bolpagni et al., 2014; Giardino et al., 2015; Hunter et al., 2010a). Though designed primarily for land applications, the new generation of multispectral sensors such as Landsat 8 and Sentinel-2 offers unprecedented opportunities for lake remote sensing (Dörnhöfer and Oppelt, 2016; Palmer et al., 2015b). Additional bands in the VNIR wavelengths, higher radiometric sensitivity, signal-to-noise ratios and, in the case of Sentinel-2 – the spatial resolution of up to 10 m, enables detailed lake analyses. Synergetic multi-sensor use may increase temporal coverage and allow for cloud-free data (Dörnhöfer and Oppelt, 2016). Landsat 8 has the capabilities for retrieving water constituents (Eder et al., 2016; Giardino et al., 2014a; Lobo et al., 2015; Slonecker et al., 2016), water depths (Giardino et al., 2014a, 2016), Secchi disk depth (Lee et al., 2016) and bottom substrates (Giardino et al., 2016). Model based sensitivity and field data analyses have revealed a high potential of Sentinel-2 for water constituent retrieval (Kutser et al., 2016; Manzo et al., 2015) and bottom substrate mapping such as coral reefs (Hedley et al., 2012). A study by Toming et al. (Toming et al., 2016a, this special issue) focused on transferring empirical algorithms to S2A for retrieving water quality parameters in optically deep water.

This study was conducted at Lake Starnberg, a clear, deep lake located in the peri-alpine region; its current trophic state is oligotrophic (Arle et al., 2013). The shallow waters along the shoreline are partially covered by submerged macrophytes, sand or stony ground. Earlier studies at Lake Starnberg analysed multi-temporal RapidEye data with a depth-invariant index to track the development of submerged native and invasive macrophytes (Roessler et al., 2013; Rößler et al., 2012). Rößler et al. 2013 applied the bio-optical modelling tool BOMBER (Giardino et al., 2012) in order to retrieve water constituents and submerged macrophytes from airborne hyperspectral imagery. Gege 2014a also used a physical based bio-optical modelling tool, i.e., WASI-2D (Gege, 2014b), and focused on deriving water depths from airborne hyperspectral imagery.

In this study, we assess the suitability of S2A for retrieving water constituents, water depths and bottom substrates using the physically-based model, WASI-2D. The study is based on the results by Dörnhöfer et al. 2016a who demonstrated the potential of S2A data for retrieving SPM, $a_{CDOM}(440)$ and water depths. We aim (1) to compare the performance of three different atmospheric corrections over water surfaces (2) to evaluate the capability of S2A to retrieve absorption by coloured dissolved organic matter (a_{CDOM}), backscattering and concentration of suspended particulate matter (SPM) in optically deep water; (3) to derive water depths and bottom substrates in optically shallow waters. For validation, we use *in situ* data acquired during a measurement campaign concurrently with a S2A image acquisition from August 2015.

4.2 Materials and Methods

4.2.1 Study area and Field Data

Located in the pre-alpine region, Lake Starnberg (11°19'14"E, 47°49'34"N) formed during the last ice age. With an area of 56.4 km^2, it is the fifth largest lake in Germany reaching a maximum depth of 127.8 m (average depth: 53.2 m) (Wöbbecke et al., 2003). In comparison to the lake's total volume (2.999 Mio. m^3), the catchment area, made up primarily of forest and cultivated grassland, is relatively small (315 km^2). Inflows are slow, and consist of groundwater flows, small creeks and streams. Outflows include the river Würm, located at the northern end of the lake which also has a slow discharge. Low inflow (3.6 $m^3 \cdot s^{-1}$ Melzer et al., 2003) and low discharge (4.5 $m^3 \cdot s^{-1}$ Melzer et al., 2003) result in a long residence time of water (21 years) (Wöbbecke et al., 2003). After showing rising levels of eutrophication, a drainage system was introduced in the 1970s.

Since then, the water quality steadily increased and the lake turned into a popular recreation area. Between 2004 and 2014, the average total phosphorous concentration was around 6 $\pm$ 2 mg·m^{-3}, nitrogen concentration around 0.3 $\pm$ 0.1 g·m^{-3}, average chlorophyll-a (CHL) concentration in 2 m water depth was 2.3 $\pm$ 1.0 mg·m^{-3}; Secchi disk depth was on average 9 $\pm$ 2 m during winter and 6 $\pm$ 2 m during summer season (Bayern, 2013). Sandy sediments are the predominating substrate, gravel forms the substrate in the very shallow water (<0.5 m water depth). A variety of submerged macrophytes colonise shallow waters; Chara sp. are the predominating macrophyte species with interspersed patches of Potamogeton sp. In the northern and western parts of the lake (*Elodea nuttallii*, *Elodea canadensis*) and south-western parts (*Najas marina*), invasive macrophyte species are present. Recently, the monomictic lake has been classified as oligotrophic-equal to its natural state (Arle et al., 2013).

To evaluate S2A ability to retrieve information on lake ecology indicators, such as SPM, $a_{CDOM}(440)$ or bottom substrates (Dörnhöfer and Oppelt, 2016), we conducted a measurement campaign on 12-13 August 2015. We compiled field data which allow us to assess performance of atmospheric correction procedures, to adapt and regionalise a bio-optical model, and to validate resulting S2A derived products. We focused on the southern lake area with moderately sloping regions (Fig. 4.1). At the end of the text, a list of all used abbreviations is provided. Fig. 4.2 provides a schematic illustration of the methodological workflow.

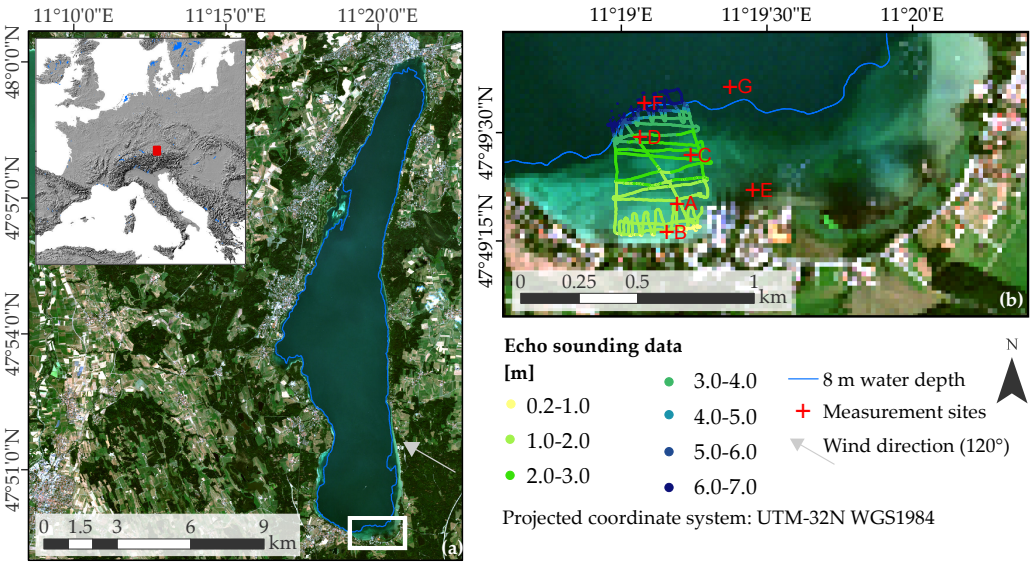

Figure 4.1: S2A true-colour composite (R-G-B: 665 nm-560 nm-490 nm, 13 August 2015, 10 m) of Lake Starnberg, Germany (a) and location of measurement sites (b).

Close to the satellite overpass, we measured aerosol optical thickness (AOT) with Microtops sun photometers (AOT = 0.151 at 550 nm, 12:17 UTC + 2). AOT data from a nearby (23 km) Aeronet station "Hohenpeißenberg" (989 m AMSL, AOT = 0.168 at 550 nm, 12:22 UTC + 2) were extrapolated to lake elevation (AOT = 0.179 at 550 nm) (Riedel et al., 2016). Using an Ibsen FREEDOM VIS FSV-305 spectroradiometer (390-850 nm, 0.5 nm sampling interval) and a Labsphere reflectance standard with ~10 % diffuse reflectance (Labsphere, ated), we measured radiance reflectance spectra nadir-looking approx. 0.5 m above the water surface $R^{BOA}_{rs-FREEDOM}(0^+, \lambda)$ at all seven measurement sites concurrently (-1 to +2 h) to the S2A overpass on 13 August 2015 (12:16 UTC + 2). The location and number of measurement sites was a trade-off between covering different water depths, bottom substrates, deep and shallow water within a narrow time window. Measurement sites A to E were located in optically shallow water where the ground was visible; F and G were located in optically deep water with a measured mean Secchi disk depth of 4.2 $\pm$ 0.3 m. Sediment samples were collected with a Ekman-Birge type bottom sampler at each measurement site and $R^{BOA}_{rs-FREEDOM}(0^+, \lambda)$ recorded ex situ

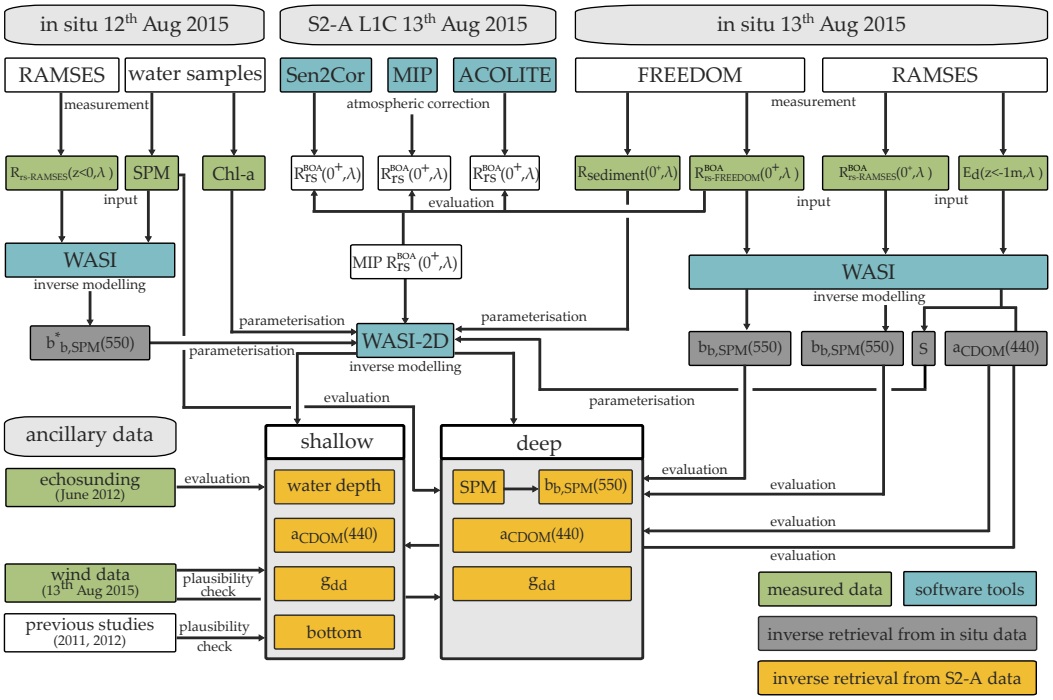

Figure 4.2: Simplified methodological workflow of the study.

using the FREEDOM spectroradiometer. We measured downwelling spectral irradiance $E_d(z, \lambda)$ using a TriOS RAMSES ACC-VIS sensor, and upwelling spectral radiance $L_u(z, \lambda)$ with a TriOS RAMSES ARC-VIS sensor (320-950 nm, 3.3 nm sampling interval). These radiometers and a Tritech PA500 altimeter were mounted on a custom built frame ensuring that the entrance optics of each instrument were at the same depth (z). This setup allowed for simultaneous measurements of all instruments at varying sensor depths (z) below (z < 0, measurement site A-E, G) and above water (z = 0^+ F and G). The depth of the sensor level was determined using a step counter for measuring the cable length (uncertainty for levelling the sensor: Approx. $\pm$ 2 cm at calm conditions); the distance to the ground was measured in a range from 0 to 10 m at a resolution of 1 mm with the Tritech PA500 altimeter. Radiance reflectance was calculated simultaneously for each recorded pair of measurements as $R_{rs-RAMSES}(z, \lambda) = L_u(z, \lambda / E_d(z, \lambda)$. To account for the spectral differences of the $L_u$and E_d sensors, we resampled the spectra to a uniform 1 nm grid using cubic interpolation.

A second data set was collected on the previous day at the same seven locations. Geolocation uncertainties (5-20 m, at D: 50m) due to boat drift and GPS positional inaccuracies were considered in the validation process as described in Section 4.2.2. During this campaign, we measured $E_d(z, \lambda)$ and $L_u(z, \lambda)$ in several depths with a second set of identical RAMSES radiometers (TriOS, 2015). Furthermore, we collected water samples from the top (0.3 m) water layer for further laboratory analysis. The temporal offset between water sampling and S2A overpass is noticeable. Lakes are dynamic systems requiring sampling temporally close to image acquisition. Water body conditions can change between sampling dates, causing discrepancies and incorrect validation. The weather conditions were stable and did not indicate changing water constituent concentrations between both days (Deutscher Wetterdienst, 2016a). RAMSES data of both campaign dates showed similar reflectances and indicated stable water conditions. Therefore, the water samples taken the day before seem to be comparable. We determined SPM concentration gravimetrically according to Strömbeck and Pierson 2001; a 1 L water sample was filtered through pre-weighed cellulose-acetate filters (pore size: 0.45 µm). The filters were then dried at 105 °C and weighed again. To retrieve concentration of CHL, we filtered a 1 L water sample through a GF/F filter (pore size: 0.7 µm). Pigments were removed from filter using 99.9 % acetone. Pigment concentration was measured using high performance liquid chromatography.

For assessing the accuracy of retrieved water depths, we used echo sounding data (BioSonics MX aquatic habitat echosounder) acquired in June 2012 in the southern part of the lake (near Seeshaupt). Water level measurements on 13 August (584.3 m AMSL, Bavarian Environmental Agency, 2016) were close to mean water level measured during June 2012 (584.4 m AMSL, Bavarian Environmental Agency, 2016). The data therefore seem to be comparable. We distinguished optically deep and shallow water with the 8 m water depth line in reference to the official bathymetry map (Fig. 4.1 Bavarian Environmental Agency, 2000).

4.2.2 Preprocessing of S2A Data

S2A acquired an image over Lake Starnberg on 13 August at 12:16 (UTC+2). We conducted atmospheric correction procedures on reprocessed L1C data (processing baseline: 02.01) using three different algorithms, i.e., Sen2Cor (Version 2.2.1, Müller-Wilm, 2016), ACOLITE (Version 20160520.1, Vanhellemont and Ruddick, 2015, 2016) and MIP (Modular Inversion and Processing System, Heege, 2000; Heege and Fischer, 2004; Heege et al., 2014).

Prior to atmospheric correction, Sen2Cor classifies the scene roughly into cloud and land cover classes. The atmospheric correction is based on 24 look-up table sets modelled with libRadtran (Müller-Wilm, 2016). Sen2Cor applied a dense, dark vegetation approach to determine AOT using bands B12 (2190 nm), B04 (665 nm) and B03 (560 nm). For assessing water vapour column height, the bands B8A (865 nm) and B09 (945 nm) were used (Müller-Wilm, 2016). We configured Sen2Cor for processing with default settings including correction for adjacency effects with an adjacency range of 1000 m. We used the rural aerosol model, a SRTM-digital elevation model and selected ozone concentration calculation based on the value provided in the metadata. We calculated Sen2Cor products on the 10 m pixel size; bands with a spatially lower resolution were only resampled rather than interpolated. Since Sen2Cor has been developed for land surfaces it lacks a correction of water surface effects and provides the corrected data in units of bottom of atmosphere irradiance reflectance $R^{BOA}(0^+, \lambda)$. For analysing the water body, we used bottom of atmosphere radiance reflectance $R_{rs}^{BOA}(0^+, \lambda)$ as the sum of remote sensing reflectance and water surface reflectance; we therefore converted $R^{BOA}(0^+, \lambda)$ to $R_{rs}^{BOA}(0^+, \lambda)$ according to Eq. 4.1 (Mobley et al., 2015):

$$R_{rs}^{BOA}(0^+, \lambda)[sr^{-1}] = \frac{R^{BOA}(0^+, \lambda)}{\pi} \tag{4.1}$$

ACOLITE is an atmospheric correction tool specifically developed for water bodies, currently available for Landsat 8 and Sentinel-2 (Vanhellemont and Ruddick, 2014, 2015, 2016). ACOLITE amended atmospheric Rayleigh reflectance using a Second Simulation of the Satellite Signal in the Solar Spectrum (6S)-V look-up table which considers sensor and sun geometry as well as sun and sky glint (modelled for a wind speed of 1 m·s^{-1}) (Vanhellemont and Ruddick, 2014). Atmospheric pressure correction was conducted for the site elevation of 595 m AMSL. Pixels having a Rayleigh corrected irradiance reflectance above 0.03 (0.0215 by default) in band B09 (1610 nm) were masked as non-water. Using the ratio between shortwave infrared (SWIR) bands B09 (1610 nm) and B10 (2190 nm) ACOLITE estimated the aerosol type over water pixels. The reflectance in SWIR bands above water bodies was assumed to be zero, observed reflectance was assumed to result solely from aerosol. Aerosol reflectance was then extrapolated exponentially to VNIR wavelengths (Vanhellemont and Ruddick, 2015). We chose the option “estimating aerosol type on a per pixel basis“, but also followed the suggestion by Vanhellemont and Ruddick 2016 to conduct the estimation on spatially binned ($320 \cdot 320$ m^2) SWIR bands to reduce noise effects from low signal-to-noise ratio and low reflectances in these bands. The resulting $R_{rs}^{BOA}(0^+, \lambda)$ dataset was resampled to 10 m pixel size, whereas bands with 20 m and 60 m spatial resolution were replicated.

MIP is a physics-based, sensor-independent, atmospheric correction software developed for coastal and inland waters (Heege, 2000; Heege and Fischer, 2004; Heege et al., 2014). Atmospheric scattering and absorption is calculated based on radiative transfer modelling considering bidirectional properties. Vertical characterisation of atmospheric layers follows MODTRAN, and considers different seasons, aerosol types and AOT. Furthermore, MIP analytically calculates, and subtracts the contribution of adjacent pixels on the reflectance (Heege

et al., 2014). Currently, MIP does not correct sun glint for sensors such as S2A. Land and cloud masking is conducted automatically during processing. The resulting $R_{rs}^{BOA}(0^+, \lambda)$ dataset was interpolated to 10 m pixel size using a regression based filtering approach. Additionally, MIP calculated a quality indicator for each pixel which documents fit performance and sun glint (Heege et al., 2014). EOMAP GmbH & Co.KG holds MIP, distributes atmospherically corrected products and conducted data processing.

For evaluating the performance of the three different atmospheric correction algorithms, we resampled the FREEDOM $R_{rs-FREEDOM}^{BOA}(0^+, \lambda)$ measurements to the S2A spectral response curves (ESA, 2015) according to Eq. 4.2:

$$R_{rs-FREEDOM}^{BOA}(0^+, \lambda_X) = \frac{\sum_{i=\lambda_{min}}^{\lambda_{max}} r(\lambda_i) \cdot R_{rs-FREEDOM}^{BOA}(0^+, \lambda_i)}{\sum_{i=\lambda_{min}}^{\lambda_{max}} r(\lambda_i)} \tag{4.2}$$

where $R_{rs-FREEDOM}^{BOA}(0^+, \lambda_X)$ is the band equivalent reflectance for band X, λ_{min} and λ_{max} represent start and end wavelengths of the filter function for band X, $r(\lambda_{min})$ is the relative response for band X at wavelength λ_i, $R_{rs-FREEDOM}^{BOA}(0^+, \lambda_i)$ is the reflectance measured by the FREEDOM spectroradiometer at band i centred at wavelength λ_i.

In cases with more than 1 resp. 2 measurements at a measurement site, we calculated the mean and standard deviation of *in situ* measured reflectance. In the 10x10 m² pixel size S2A data, we located the pixel corresponding to the GPS location of a measurement site. To address GPS positional inaccuracies, potential boat drifting and water masses, we calculated the mean spectrum and standard deviation of the S2A $R_{rs-S2A}^{BOA}(0^+, \lambda)$ spectra based on a 7x7 pixel environment for deep water measurement sites (F and G). To reduce the effect of bottom heterogeneity we chose a 3x3 pixel environment in shallow water (site A to E). We then compared resampled mean *in situ* $R_{rs-FREEDOM}^{BOA}(0^+, \lambda)$ and mean S2A $R_{rs-S2A}^{BOA}(0^+, \lambda)$ spectra, and calculated Pearson's correlation coefficient (r, Equation 4.3) to evaluate the correspondence in shape.

$$r = \frac{\sum_{X=1}^{n}(R_{rs-FREEDOM}^{BOA}(0^+, \lambda_X) - \overline{R_{rs-FREEDOM}^{BOA}(0^+)}) \cdot (R_{rs-S2A}^{BOA}(0^+, \lambda_X) - \overline{R_{rs-S2A}^{BOA}(0^+)})}{\sqrt{\sum_{X=1}^{n}(R_{rs-FREEDOM}^{BOA}(0^+, \lambda_X) - \overline{R_{rs-FREEDOM}^{BOA}(0^+)})^2} \cdot \sqrt{\sum_{i=1}^{7}(R_{rs-S2A}^{BOA}(0^+, \lambda_X) - \overline{R_{rs-S2A}^{BOA}(0^+)})^2}} \tag{4.3}$$

with $R_{rs-FREEDOM}^{BOA}(0^+, \lambda_X$ and $R_{rs-S2A}^{BOA}(0^+, \lambda_X)$ being the reflectance at band λ_X (band B01- B07) of resampled *in situ* respectively S2A data; $\overline{R_{rs-FREEDOM}^{BOA}(0^+)}$ respectively $\overline{R_{rs-S2A}^{BOA}(0^+)}$ are the mean reflectance values calculated from band B01-B07 (n = 7).

The second calculated performance indicator was Root Mean Square Error (RMSE, Equation 4.4) which expressed the absolute difference between both reflectance spectra (Sterckx et al., 2015b).

$$RMSE = \sqrt{\frac{\sum_{X=1}^{n}(R_{rs-FREEDOM}^{BOA}(0^+, \lambda_X) - R_{rs-S2A}^{BOA}(0^+, \lambda_X))^2}{n}} \tag{4.4}$$

We further calculated the Chi-square (X^2 , Equation 4.5) which incorporates both shape and intensity of spectra, and the mean absolute percentage error (MAPE, Equation 4.6) which usually is easier to comprehend due to the percentage statement.

$$X^2 = \sum_{X=1}^{n} \frac{(R_{rs-S2A}^{BOA}(0^+, \lambda_X) - R_{rs-FREEDOM}^{BOA}(0^+, \lambda_X))^2}{R_{rs-FREEDOM}^{BOA}(0^+, \lambda_X)} \tag{4.5}$$

$$MAPE = \frac{1}{n} \cdot \sum_{X=1}^{n} \left| \frac{R_{rs-FREEDOM}^{BOA}(0^+, \lambda_X) - R_{rs-S2A}^{BOA}(0^+, \lambda_X)}{R_{rs-FREEDOM}^{BOA}(0^+, \lambda_X)} \right| \cdot 100 \tag{4.6}$$

MIP showed best performance (cf. Section 4.3.1); we therefore used the MIP corrected dataset for further processing and analysis. The MIP $R_{rs}^{BOA}(0^+, \lambda)$ product with 10 m pixel size was resampled to 20 m and 60 m using nearest neighbour approach. For each data set (10 m, 20 m, and 60 m), we calculated the noise-equivalent remote sensing reflectance difference, NEΔR$_{rs}$E, as the standard deviation of MIP $R_{rs}^{BOA}(0^+, \lambda)$ spectra within a relatively homogenous area in optically deep water (Brando and Dekker, 2003). It is an indicator

for the suitability of the data for analysing water constituents concerning random noise. We chose an area of 320 x 320 m^2 which corresponds to 32 x 32 pixels in the 10 m product, 9 x 9 in the 20 m, and 3 x 3 in the 60 m product. Apart from the signal-to-noise ratio, the applied atmospheric correction and environmental conditions during image acquisition, such as water surface or downwelling irradiance, influence the $NE\Delta R_{rs}E$. For analysing water constituents from remote sensing data, $NE\Delta R_{rs}E$ < 0.00025 sr^{-1} is optimal (Giardino et al., 2015, see black line in Fig. 4.3). Fig. 4.3 shows the resulting band and pixel size dependence of $NE\Delta R_{rs}E$. Mean values of bands B01-B07 were 0.00014 sr^{-1}, 0.00014 sr^{-1} and 0.00012 sr^{-1} for 10 m, 20 m and 60 m pixel size, respectively. Referring to Fig. 4.3 and mean values, spatial binning from 10 m to 20 m barely improved $NE\Delta R_{rs}E$; spatial binning to 60 m reduced $NE\Delta R_{rs}E$ in bands B01-B04, but slightly increased it in bands B05-B07. Except for band B01 (10 m and 20 m), all bands achieved values <0.00025 sr^{-1}; concerning noise, we therefore considered the MIP corrected scene appropriate for further analyses.

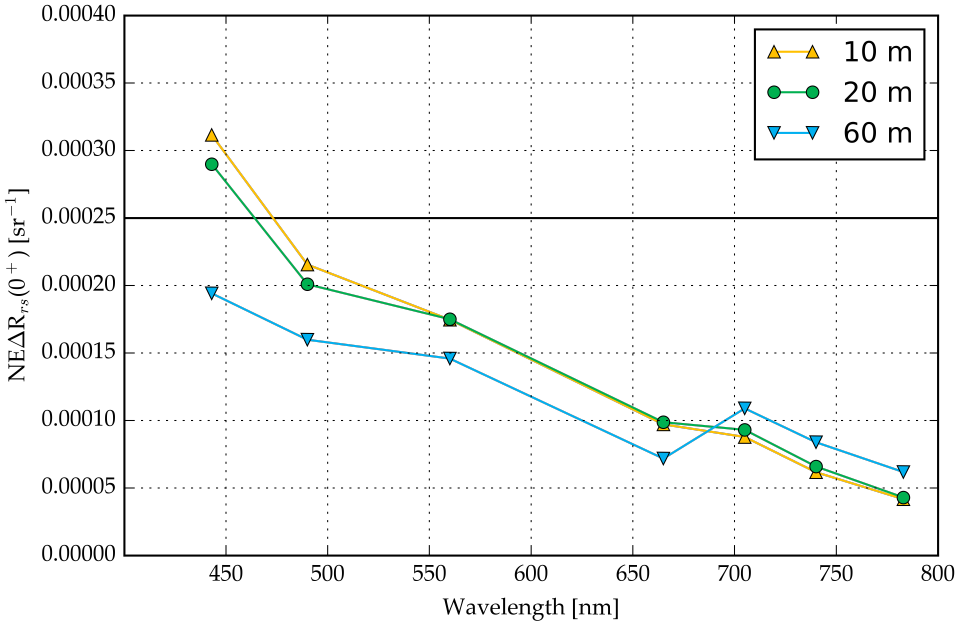

Figure 4.3: $NE\Delta R_{rs}E$ for each band calculated for the MIP atmospherically corrected dataset.

4.2.3 Inverse Modelling with WASI-2D

WASI-2D is a freely available software tool (http://www.ioccg.org/data/software.html) for analysing atmospherically corrected multispectral and hyperspectral imagery in both optically deep and shallow water (Gege, 2014b). In optically deep water, absorption and scattering by optically active water constituents such as CHL, SPM, CDOM and water itself, shape water reflectance. In optically shallow water, bottom reflectance and water depth additionally influence reflectance (Dörnhöfer and Oppelt, 2016; Odermatt et al., 2012). Satellite sensors, such as S2A, measure top-of-atmosphere spectral radiances; the atmospheric correction algorithm then converts them to bottom-of-atmosphere reflectances. Such algorithms often lack a correction of specular reflectance of sun and sky at the surface, which can be quite significant for water. WASI-2D therefore includes a sky radiance model for correcting sun and sky glint.

To derive information on water constituents, bottom substrate and water depth from $R_{rs}^{BOA}(0^+, \lambda)$ spectra, WASI-2D includes several analytic models to analyse measured spectra using an optimisation approach. The optimisation procedure inversely models the $R_{rs}^{BOA}(0^+, \lambda)$ spectrum of each pixel adjusting a number of model parameters, called fit parameters, until the calculated spectrum matches $R_{rs}^{BOA}(0^+, \lambda)$ as close as possible. Fit

parameters vary within a pre-defined range, depending on the study area's characteristics. Curve fitting terminates when measured and inversely modelled spectra correspond best (residuum < 1.0 x 10^{-4}, least squares). If the residuum criterion is not met, the fit routine stops after a pre-defined number of iterations. WASI-2D writes the final values of fit parameters for each pixel to file, resulting in a multi-band raster image where each band corresponds to a fit parameter. For modelling $R_{rs}^{BOA}(0^+, \lambda)$ in optically deep and shallow water, we applied the analytic equation of Albert and Mobley 2003. In the WASI implementation of this model, SPM and water comprise the backscattering properties; water, different classes of phytoplankton, CDOM and detritus can be selected as the absorbing components. In optically shallow water, water depth is additionally included in calculating reflectance of water; WASI-2D further considers contributions of up to six linearly mixed bottom types. To address surface reflectance, we applied the implemented model of sky radiance which is based on the downwelling irradiance model by Gregg and Carder 1990. In our data processing, WASI-2D accounted for reflected solar irradiance (sun glint) during inverse modelling. We omitted considerations to diffuse reflectance (sky glint) as it was included in MIP. A detailed description of the models can be found in Gege 2014b.
Inverse modelling was conducted using the MIP atmospherically corrected $R_{rs}^{BOA}(0^+, \lambda)$ dataset and bands B01 (443 nm) to B07 (783 nm). We therefore resampled the WASI-2D spectral database to the S2A spectral response curves (ESA, 2015) adopting Equation 4.2. According to a previous study at Lake Starnberg dinoflagellates were chosen as phytoplankton type (Gege, 2014a). Based on results of the water sample analysis, the CHL concentration was fixed to 1 mg·m^{-3}. The CDOM absorption coefficient was modelled according to Equation 4.7,

$$a_{CDOM}(\lambda) = a_{CDOM}(440) \cdot e^{-S_{CDOM} \cdot (\lambda - 440)} \tag{4.7}$$

where $a_{CDOM}(440)(m^{-1})$ was treated as fit parameter while the slope factor S_{CDOM} was set as constant (0.0155 nm^{-1}, mean of *in situ* S). Backscattering of suspended matter was calculated according to Equation 4.8,

$$b_{b,SPM}(550) = SPM \cdot b^*_{b,SPM}(550) \tag{4.8}$$

with SPM (g·m^{-3}) treated as fit parameter in optically deep water, and set constant in shallow water (1.8 g·m^{-3}, mean SPM of deep water result). When considering bottom reflectance in modelling shallow water, WASI-2D requires irradiance reflectance spectra representing the bottom types at the test site. WASI-2D allows for up to six different bottom types. Giardino et al. 2016 advised using not more than two bottom types for multispectral imagery. We used a sandy sediment spectrum acquired ex situ with the FREEDOM radiometer on 13 August 2015 (Section 4.2.1), and a macrophyte spectrum of the predominating species (*Chara* sp., WASI-2D database) growing at the southern part of Lake Starnberg (Fig. 4.4). The sum of fractional area (fA[sediment] and fA[macrophyte]) was allowed to range between 1.0 and 1.2. Since MIP lacked a correction of sun glint, the fraction of sun glint per pixel area (g_{dd}) was chosen as a fit parameter in both optically shallow and deep water.

4.2.4 Retrieval of Inherent Optical Properties from *in situ* Measurements

The downwelling irradiance in water, $E_d(z < 0,\lambda)$, can be used for determining the concentration of phytoplankton (Gege, 2012) and CDOM (Linnemann et al., 2013) if sensor depth z is large enough to capture the impact of absorption by water constituents on the spectral signature of $E_d(z < 0,\lambda)$. For lakes with CHL and CDOM concentrations similar to Lake Starnberg, this critical depth is in the order of 1.0-1.5 m (Gege, 2012; Linnemann et al., 2013). Following this principle, we estimated the CDOM parameters $a_{CDOM}(440)$ and S from RAMSES $E_d(z < 0,\lambda)$ measurements in water.
First, we fitted the above water RAMSES measurements of downwelling irradiance $E_d(z=0^+,\lambda)$ in WASI-2D using the Gregg and Carder model 1990 to derive the atmospheric parameters required as input for modelling the under-water $E_d(z < 0,\lambda)$ spectra. The turbidity coefficient and water vapour concentration were treated as fit parameters, the Angström exponent of aerosol scattering (1.32) and the scale height of ozone (0.45 cm)

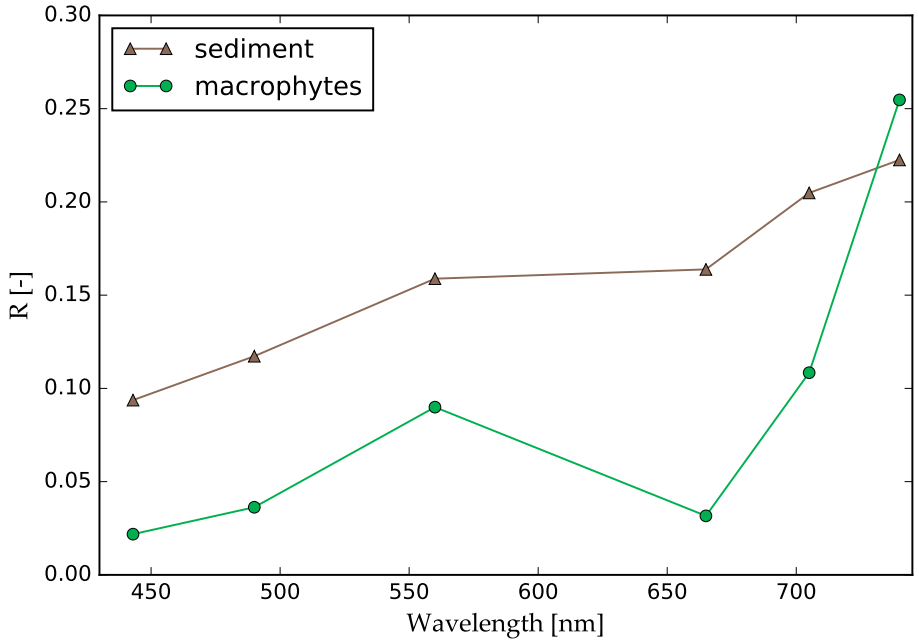

Figure 4.4: S2A resampled irradiance reflectance spectra of the two considered bottom types. The sediment spectrum is the average of reflectance measurements on 13 August 2015, the macrophyte spectrum originates from the WASI-2D database.

were kept constant. Second, we retrieved $a_{CDOM}(440)$ and S from $E_d(z < 0,\lambda)$ measurements with z < -1 m by inverse modelling. The atmospheric parameters were kept constant at the results of step 1 for the actual site; phytoplankton was kept constant at 1 mg·m^{-3}. The fractions of the direct and diffuse components of $E_d(\lambda)$ and sensor depth were fitted along with $a_{CDOM}(440)$ and S.
Above water measurements of $R_{rs}^{BOA}(0^+,\lambda)$ from the RAMSES and FREEDOM sensors were used to estimate the backscattering coefficient of SPM, $b_{b,SPM}(550)$. Using WASI, we inversely modelled $R_{rs-FREEDOM}^{BOA}(0^+,\lambda)$ and $R_{rs-RAMSES}^{BOA}(0^+,\lambda)$ spectra which were measured at the optically deep sites F and G.

4.3 Results and Discussion

4.3.1 Comparison of Atmospheric Correction Approaches

We compared three approaches for atmospheric correction from which two were specifically developed for water surfaces. Fig. 4.5a-g show resampled *in situ* spectra and atmospherically corrected spectra of the corresponding pixel environment. The common feature of the seven measurement sites is that all approaches retrieved different $R_{rs}^{BOA}(0^+,\lambda)$ spectra. Table 4.1 summarises performance indicators for evaluating the results of the three different atmospheric correction algorithms. MIP outperformed Sen2Cor and ACOLITE at most measurement sites (Table 4.1).

Table 4.1: Performance indicators of resampled *in situ* and atmospherically corrected spectra at measurement sites in optically shallow (A-E) and deep (F-G) water. Green colour highlights the atmospheric correction algorithm with the best performance.

	A	B	C	D	E	F	G	Mean
	Shallow water					Deep water		
Measurement time (UTC)	11:54	11:44	11:20	11:07	12:23	10:50	09:52	
MIP (r)	0.990	0.993	0.993	0.985	0.976	0.986	0.984	0.987
RMSE (sr^{-1})	0.002	0.002	0.001	0.004	0.003	0.002	0.003	0.002
MAPE (%)	46.8	17.7	45.0	98.9	83.6	60.8	72.4	60.7
$X^2(sr^{-1})$	0.005	0.001	0.004	0.021	0.016	0.007	0.010	0.009
Sen2Cor (r)	0.953	0.953	0.940	0.846	0.757	0.795	0.838	0.869
RMSE (sr^{-1})	0.002	0.005	0.003	0.002	0.002	0.003	0.002	0.003
MAPE (%)	120.1	96.5	61.6	83.9	95.4	78.6	83.8	88.6
$X^2(sr^{-1})$	0.021	0.023	0.010	0.010	0.015	0.012	0.012	0.015
ACOLITE (r)	0.979	0.980	0.978	0.960	0.853	0.953	0.953	0.951
RMSE (sr^{-1})	0.003	0.006	0.003	0.001	0.002	0.002	0.002	0.003
MAPE (%)	131.4	110.2	67.4	76.4	97.4	73.8	77.3	90.6
$X^2(sr^{-1})$	0.026	0.032	0.011	0.010	0.017	0.011	0.011	0.017

At all measurement sites, Sen2Cor obtained $R_{rs}^{BOA}(0^+, \lambda)$ values at band B01 (443 nm) and B02 (490 nm) significantly lower than the *in situ* data. This observation presumably resulted from an erroneous aerosol parameterisation. Sen2Cor obtained an AOT value of 0.185 $\pm$ 0.002 (550 nm) for southern Lake Starnberg pixels which was higher compared to measurements with sun photometers (0.151) and at the Aeronet Station (0.179). Thus, Sen2Cor overestimated aerosol reflectance resulting in overcorrected $R_{rs}^{BOA}(0^+, \lambda)$ spectra. Both, ACOLITE and Sen2Cor calculated $R_{rs}^{BOA}(0^+, \lambda)$ values in bands B06 (740 nm) and B07 (783 nm) higher than *in situ* measurements. ACOLITE lacks a correction of adjacency effects, and reflectance from neighbouring land pixels therefore contributes to the signal and accounted for higher reflectance values above 705 nm. Extrapolating aerosol reflectance from the SWIR bands to the shorter wavelengths thus may result in overcorrected spectra. Similar to Sen2Cor, ACOLITE tended to lower reflectance values compared to *in situ* measurements, though inconsistently. Sen2Cor includes a correction for adjacency effects based on a range-independent reflectance in a large neighbourhood of each pixel, which performs insufficiently for water pixels close to the shoreline. At wavelengths above 700 nm, the impact of adjacency effects is particularly strong since neighbouring land pixels show distinctly higher reflectance (Sterckx et al., 2015b). The distance between measurement sites and land varied between 40 m (B) and 600 m (F); consequently, adjacency effects altered all pixel environments (Fig. 4.5). The same applies for all lake pixels due to the lake's width ranging from 1 km to 4.5 km. Sterckx et al. 2011 illustrated that adjacency effects occur even for pixels several hundred metres away from the shoreline. Santer and Schmechting 2000 indicated that for similar solar elevation, adjacency effects become negligible (less than 0.1%) only for a distance greater than 5 km from the shoreline. Thus, a correction of adjacency effects appropriate for the water/land environment is essential for reliable spectra. At all measurement sites, MIP retrieved reflectances in bands B06 and B07 slightly above zero, similar to the *in situ* measurements. MIP calculated zero values for 1.2% of lake pixels in B06 (740 nm) and for 19.0% in B07 (783 nm), which may result from sky glint overcorrection. At A-C, MIP performed well in retrieving both shape and intensity (high r, low RMSE, low X^2, cf. Table 4.1); at other sites, MIP obtained comparable shapes, but showed higher intensities compared to *in situ* measurements and spectra from ACOLITE and Sen2Cor. In the validation area, MIP calculated an AOT of 0.160 (550 nm) which was close to Microtops measurement values; MIP AOT was lower than AOT calculated by Sen2Cor which partly explains the significantly higher spectra compared to Sen2Cor. Different treatment of adjacency effects, sky glint correction and the used aerosol model for calculating atmospheric scattering may further account for differences in spectral shape.

Apart from temporal differences, one has to bear in mind the problem of upscaling while comparing *in situ* measured reflectance over a small area of water (<1 m) compared to the spatial measurement of S2A (10 m,

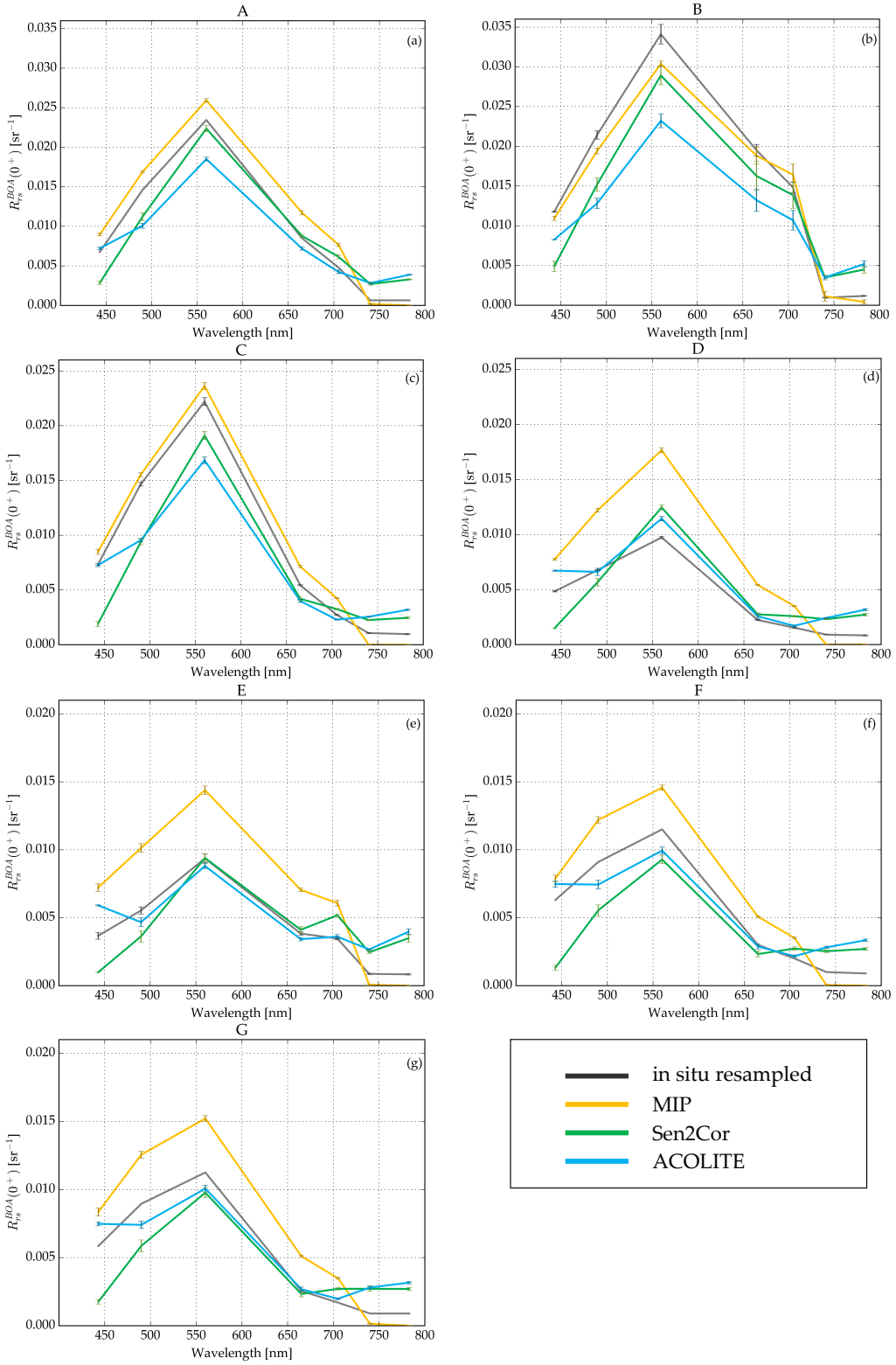

Figure 4.5: Comparisons of resampled *in situ* and mean atmospherically corrected $R_{rs}^{BOA}(0^+, \lambda)$ spectra. Error bars represent the standard deviation within a 3 x 3 ((a-e) shallow water) and 7 x 7 ((f-g) deep water) pixel environment and standard deviation of *in situ* spectra. Note different scaling of ordinate axis.

20 m and 60 m). Measurement sites A-E were located in optically shallow water, where varying bottom characteristics (i.e., different macrophytes or sediments), and water depths, influence water reflectance. The satellite sensor records a mixed signal from this variance. Statistical approaches to overcome upscaling problems from point to pixel scale were developed for ocean-colour sensors (Salama and Su, 2011). Furthermore, *in situ* measurements also underlie a number of uncertainties such as shading by instrument, boat and changes in incident radiation due to atmospheric variability (Mueller et al., 2003). Larger error bars (standard deviation) of both *in situ* and atmospherically corrected spectra in Fig. 4.5b indicate the resulting higher standard deviations. For case-1 open ocean water algorithms, the required accuracy of water-leaving radiances is 5% to achieve a Chl-a product with 30 % accuracy, for instance (International Ocean-Colour Coordinating Group, 2012). To our knowledge, a comparable accuracy target is not yet defined for atmospheric correction algorithms over inland waters. The evaluated atmospheric corrections showed MAPE values between 61% and 91% on average and underpin that atmospheric correction over inland waters still is an unresolved problem. The large differences of atmospheric corrections are another critical point. Each atmospheric correction model resulted in a different $R_{rs}^{BOA}(0^+, \lambda)$ spectrum from the same S2A at-sensor radiance. An EU-FP7 GLaSS project report also compared different atmospheric correction algorithms retrieving highly varying results (GLaSS, 2014). Caused by the low reflectance of water, small absolute differences in reflectance rapidly result in large relative differences. These differences may propagate to the subsequent retrieval of lake ecology indicators when using (analytic) approaches that rely on both shape and intensity of spectra. Assessing this issue, however, is beyond the scope of this study and may be expanded to other sensors as well.

4.3.2 Optically deep water

Fit parameters in optically deep water were $a_{CDOM}(440)$ and SPM concentration. Since the $R_{rs}^{BOA}(0^+, \lambda)$ data used during inverse modelling (bands B01-B07) were not corrected for sun glint, we also selected the fraction of sun glint per pixel area, g_{dd}, as a fit parameter. Table 4.2 summarises *in situ* and S2A derived values at the measurement sites. Variations due to spatial resampling were minor. Absence of processing artefacts, such as stripping, in the resulting parameter maps (Fig. 4.6) shows that processing performed well. Low residuals (mean: 3.96 x 10^{-4} $\pm$ 3.82 x 10^{-5}) between S2A and inversely modelled spectra underpinned a good modelling performance. The g_{dd} map (Fig.4.6c) indicates higher sun glint in the northern part of the lake, while the southern region including our measurement sites was only slightly affected. Retrieved $a_{CDOM}(440)$ ranged between 0.10 and 0.74 m^{-1} (mean: 0.14 $\pm$ 0.02 m^{-1}), SPM between 1.1 and 5.1 $g{\cdot}m^{-3}$(mean: 1.8 $\pm$ 0.2 $g{\cdot}m^{-3}$). These ranges correspond well with concentrations obtained from hyperspectral imagery in other studies at Lake Starnberg (Gege, 2014a; Rößler et al., 2013). Referring to the different spatial resolutions, WASI-2D retrieved similar concentration values (Table 2). Reducing the pixel size of S2A data must not necessarily result in a significant improvement which might be interesting for analysing small lakes.

Both SPM concentrations and $a_{CDOM}(440)$ showed little variations indicating homogenous and clear lake conditions (Fig. 4.6). SPM in the water column may result from resuspension (Madsen et al., 2001) or from catchment erosion (Lindström et al., 1999). The lowest SPM concentrations around 1.4 $g{\cdot}m^{-3}$ occurred in the northern part of the lake; slightly higher concentrations around 2.0 $g{\cdot}m^{-3}$ were retrieved in the southern part. CDOM originates from allochthonous sources from rotting plants in the catchment, or from autochthonous sources such as decomposing phytoplankton or macrophytes (Brezonik et al., 2015). In the S2A data, $a_{CDOM}(440)$ values were slightly higher in the southern regions compared to the northern part. External input from catchment of both SPM and $a_{CDOM}(440)$ was presumably low since no rainfall occurred the week prior to image acquisition (Deutscher Wetterdienst, 2016a). Furthermore, Lake Starnberg receives mainly groundwater inflows (Wöbbecke et al., 2003), thus, the low values of both SPM concentration and $a_{CDOM}(440)$ are reasonable. Chl-a was considered as a constant parameter during inverse modelling.

Water sample analyses also revealed low concentrations of CHL ($\sim$1 $mg{\cdot}m^{-3}$) causing water absorption to be predominated by CDOM. Both CHL and CDOM absorb in the blue wavelength region (Matthews, 2011). Compared to Landsat 8 OLI, S2A offers an additional band at 705 nm (B06) which may support CHL assessment

(Vanhellemont and Ruddick, 2016). Under low CHL concentrations, however, other optically active constituents may superimpose the absorption feature. Empirical NIR-red algorithms based on the feature, for instance, perform more reliable at CHL concentrations >10 mg·m^{-3} (Gitelson et al., 2008; Odermatt et al., 2012). At Lake Starnberg, CHL concentrations were too low for a retrieval along with $a_{CDOM}(440)$ and SPM.

Table 4.2: Comparison of *in situ* and S2A (WASI-2D) results in optically deep water. Term in parentheses indicates *in situ* data source. SPM values originate from water samples taken the day before image acquisition. Mean and standard deviation of 5 x 5 respectively 3 x 3 pixel environment were calculated for 10 m and 20 m pixel size, respectively, and reflect spatial variability. The values of the 60 m pixels correspond to GPS coordinates. Errors for *in situ* (RAMSES) are derived from inversion and reflect variability during a measurements series.

Point	Pixel Size	SPM [g·m^{-3}]		$b_{b,SPM}(550)$ [m^{-1}]		$a_{CDOM}(440)$ [m^{-1}]	
		in situ (Sample)	S2A (WASI-2D)	*in situ* (RAMSES)	*in situ* (FREEDOM)	S2A (WASI-2D)	*in situ* (RAMSES)	S2A (WASI-2D)
F	10	1.9	1.44±0.65	no measurement	0.015; 0.020*	0.0216± 0.0098	0.436±0.003	0.14±0.06
	20		1.72±0.04			0.0258±0.0006		0.16±0.01
	60		1.71			0.0257		0.16
G	10	0.4	1.80± 0.04	0.021±0.01	0.021*	0.0270±0.0006	0.418±0.003	0.17±0.04
	20		1.77±0.03			0.0266±0.0005		0.16±0.01
	60		1.76			0.0264		0.16

*only two measurements.

Spatial patterns of g_{dd} (Fig. 4.6c) revealed high sun glint influence in the northern and western lake regions, whereas the southern and eastern regions were only slightly affected by sun glint. Sun glint occurs on water surfaces where radiation is directly reflected to the sensor as a combination of surface roughness, sun position and sensor viewing angle (Kay et al., 2009). The statistical model for predicting sun glint probability by Cox and Munk 1954 is widely used in ocean colour remote sensing; it shows that increasing wind speed increases the probability of the water surface being oriented to cause sun glint. Wind direction was from east-southeast (120°, wind speed: 3.0 m·s^{-1} Deutscher Wetterdienst, 2016a) close to image acquisition (12:00 UTC+2). Due to a lateral moraine extending from north to south the eastern parts of the lake were less exposed to wind. The southern part was even more sheltered since the ridge becomes broader and is covered by forest. Thus, the smoother water surface resulted in less sun glint in sheltered regions; the probably roughened surface caused higher sun glint in the more wind exposed northern part. Integrating wind maps, if available, into remote sensing analyses of lakes may further help to understand these patterns. The spatial variability of retrieved sun glint underpins the need for considering the spatial variability of these parameters. Kay et al. 2009 reviewed existing correction approaches: the statistical model by Cox and Munk performed insufficiently for sensors with spatial resolutions <100 m; furthermore, at inland waters local wind fields can hardly be predicted. Approaches based on zero water reflectance in the NIR often assume spatially constant sun glint and are inapplicable in shallow or turbid waters (Kay et al., 2009). The spectral model of sun glint implemented in WASI-2D addresses both spatial variability and spectral dependency. Gege and Groetsch 2016 provide a detailed description and analysis of this topic.

To assess the performance of SPM and $a_{CDOM}(440)$ retrieval, we compared WASI-2D values with concentrations and backscattering or absorption coefficients from *in situ* measurements (Table 4.2). A common approach is to compare SPM mass concentrations derived from water samples with concentrations derived from remote sensing algorithms (Dörnhöfer and Oppelt, 2016). WASI-2D derived SPM concentrations fell within the range of measured concentrations; on average, they were slightly higher than measured SPM. Arriving at an identical match, however, would be credited to mere coincidence rather than a flawless model. We compared two different methods of SPM estimation: *in situ* data from a gravimetric measurement of a 1 L water sample, and SPM from S2A radiance values of selected pixels at varying spatial resolutions, i.e., 10-60 m. Gravimetric

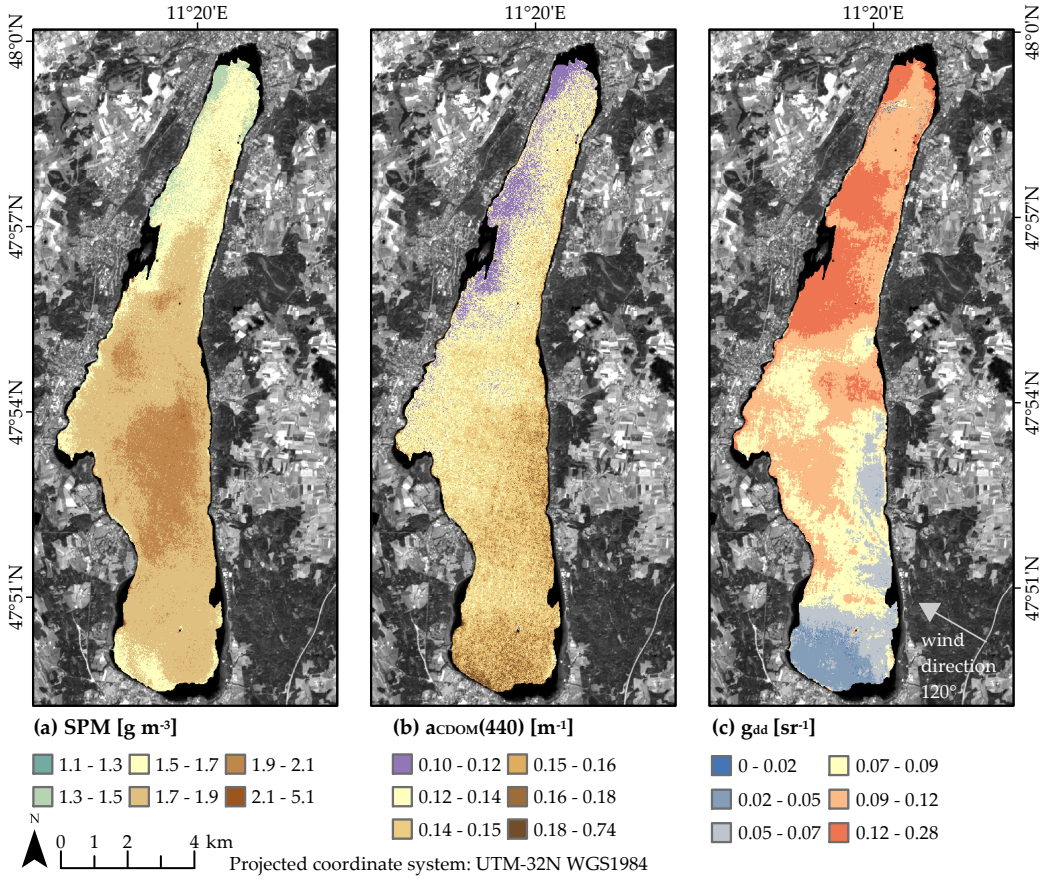

Figure 4.6: Results of deep water inversion using the MIP 20 m pixel size dataset. Background is gray scaled S2A band B05 (705 nm).

analyses of SPM contain a variety of uncertainties, such as loss of filter or sample material (Röttgers et al., 2014). Thus, SPM concentrations retrieved from water samples should not be considered absolute. Moreover, the term $b^*_{b,SPM}(550)$ (Equation 4.8) introduces additional uncertainties while comparing SPM concentrations retrieved from water samples and S2A data. $b^*_{b,SPM}(550)$ is used to convert $b_{b,SPM}(\lambda)$ to SPM concentrations (Equation 4.8). $b^*_{b,SPM}(550)$ depends on mineral composition, size, and shape of particles (Effler et al., 2013; Peng and Effler, 2012) and therefore is lake specific, but also temporally and spatially variable within a particular lake. We adapted $b^*_{b,SPM}(550)$ to the study area by inverse modelling of *in situ* measured RAMSES reflectance data considering SPM concentrations from water samples as correct. To further assess the suitability of S2A for analysing water bodies, we considered an evaluation of a parameter directly retrieved from S2A $R^{BOA}_{rs}(0^+, \lambda)$, i.e., $b_{b,SPM}(550)$. At measurement site F and G, we retrieved $b_{b,SPM}(550)$ from *in situ* measured $R^{BOA}_{rs-FREEDOM}(0^+, \lambda)$ and $R^{BOA}_{rs-RAMSES}(0^+, \lambda)$ using FREEDOM and RAMSES (only G) radiometers. Values of $b_{b,SPM}(550)$ from *in situ* and S2A data matched well; on the contrary, modelled and *in situ* SPM concentrations differed notably. SPM concentration is often measured in lake ecology or hydrology and is easier to grasp than $b_{b,SPM}(550)$; retrieval of the latter, however, is more accurate since it is directly assessed from remote sensing data. Thus, $b_{b,SPM}(550)$ represents the parameter most relevant for assessing quality of remote sensing products.

Table 4.2 compares the S2A derived $a_{CDOM}(440)$ values with $a_{CDOM}(440)$ obtained from under-water RAMSES $E_d(z < 0, \lambda)$ measurements. The S2A derived $a_{CDOM}(440)$ values were lower compared to the values retrieved from $E_d(z < 0, \lambda)$ measurements.

Bearing in mind that we only have two measurement sites in optically deep water, our results are a first evaluation. Further assessments are required. Our results show that it was possible to distinguish small differences

in water constituents even for low concentrations – at least for SPM and CDOM. The spatially synoptic view of S2A across the entire lake showed a relatively clear and homogenous water surface of optically deep water during image acquisition.

4.3.3 Optically Shallow Water

In optically shallow water, we conducted inverse modelling on the datasets with pixel sizes of 10 m and 20 m. In some parts of the lake, the shallow zone has a width of less than 100 m; water depth and bottom substrates may also change, even within 10 m pixels. g_{dd}, $a_{CDOM}(440)$, water depth and the aerial fraction (fA) of two bottom types (macrophyte and sandy sediment) were chosen as fit parameters. SPM was kept constant (SPM = 1.8 g·m^{-3}) to avoid excess fit parameters. Fig. 4.7 illustrates the resulting maps of $a_{CDOM}(440)$ and g_{dd}. Fig. 4.8 presents the retrieved bottom types and Fig. 4.9 the water depth map. Higher reflectances caused slightly higher residuals on average (4.0 x 10^{-4} $\pm$ 2.8 x 10^{-4}) compared to optically deep water. Similar to deep water, no processing artefacts such as striping occurred.

The parameter $a_{CDOM}(440)$ varied between 0.1 and 1.5 m^{-1} (mean: 0.15 $\pm$ 0.11 m^{-1}) in calculated water depths above 1 m. Table 4.3 summarises modelled and $a_{CDOM}(440)$ values derived from $E_d(z < 0, \lambda)$ and water depths. As in deep water, S2A derived $a_{CDOM}(440)$ was lower compared to $a_{CDOM}(440)$ values from *in situ* measurements. The parameter g_{dd} showed a consistent spatial distribution as in deep water: higher values in the northern lake area than in the southern part. The speckled results (zoomed parts in Fig. 4.7b,c) indicate that g_{dd} alleviates sun glint induced irregularities; thus, the other parameters retrieved in optically shallow water appeared less noisy.

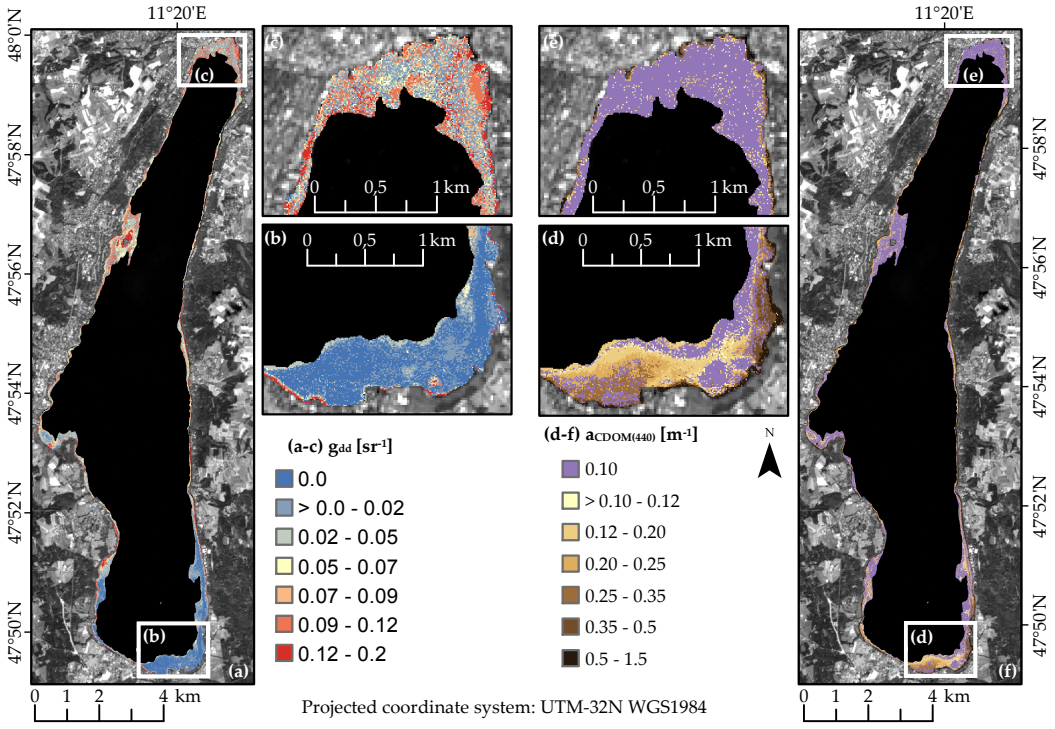

Figure 4.7: Results of g_{dd} (a-c) and $a_{CDOM}(440)$ (d-f) of shallow water inversion using the MIP 10 m pixel size dataset. Background is gray scaled S2A band B05 (705 nm).

Table 4.3: Comparison between *in situ* measured and S2A (WASI-2D) results in optically shallow water. Term in parentheses indicates *in situ* data source. Mean and standard deviation of 5 x 5 respectively 3 x 3 pixel environment were calculated for 10 m respectively 20 m pixel size and reflect spatial variability. Errors for *in situ* data (RAMSES) are derived from inversion and reflect variability during a measurement series.

Point	Pixel Size	$a_{CDOM}(440)$ [m^{-1}] *in situ* (RAMSES)	$a_{CDOM}(440)$ [m^{-1}] S2A (WASI-2D)	Water depth [m] *in situ* (measured)	Water depth [m] S2A (WASI-2D)
A	10	0.46±0.06	0.28±0.06	1.65	1.11±0.07
	20		0.25±0.07		1.11±0.08
B	10	0.73±0.18	0.17±0.12	0.86	0.58±0.07
	20		0.16±0.11		0.65±0.09
C	10	0.52±0.09	0.19±0.07	2.75	1.58±0.18
	20		0.17±0.07		1.50±0.16
D	10	0.49±0.06	0.15±0.01	3.85	1.59±0.05
	20		0.14±0.02		1.59±0.04
E	10	no measurements	0.13±0.03	1.59	0.92±0.05
	20		0.14±0.03		0.96±0.04

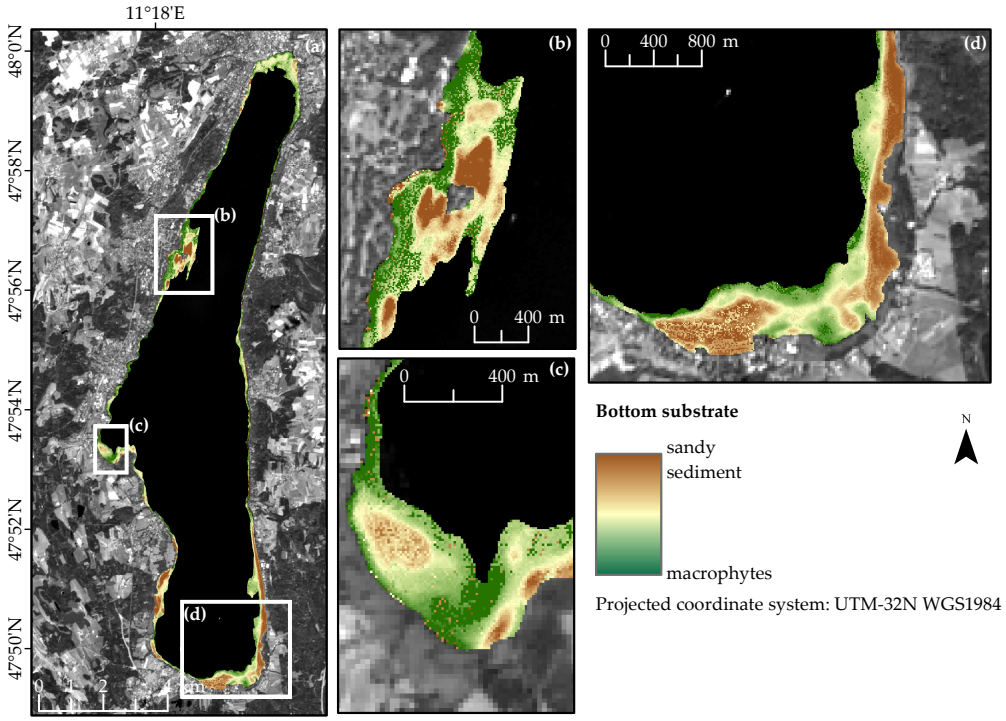

Figure 4.8: Results of bottom substrate unmixing using the MIP 10 m dataset (a); Zoomed areas are Roseninsel (b); Karpfenwinkel (c) and Seeshaupt (d). Low shares of sediment are illustrated as high macrophyte coverage. Background is gray scaled S2A band B05 (705 nm).

Accurate information of bottom substrate and water depths is crucial in optically shallow water. Following the suggestions in Giardino et al. 2016, we differentiated only two substrate types, i.e., macrophytes and sandy sediment. The resulting map revealed reasonable spatial patterns with sandy sediment predominating along the south-eastern shoreline close to “Seeshaup“ (Fig. 4.8d). High macrophytes coverage towards deeper water at Seeshaupt, however, appears unreasonable. Unfortunately, no bottom substrate mappings exist for 2015. Nevertheless, to check the plausibility, we compared our results with those of previous studies at Lake Starnberg conducted in 2011. In accordance to Rößler et al. 2013, the bottom north of the “Roseninsel“ (Fig. 4.8b) was identified as sandy sediment. At “Karpfenwinkel“ (Fig. 4.8c), WASI-2D retrieved an oval shaped structure

of sediment; dense macrophytes occurred south-east of it. Rößler et al. 2013 also described these patterns using airborne hyperspectral data. Nevertheless, bottom characteristics are highly variable at Lake Starnberg; a variety of macrophyte species are present and also bare substrate varies between stony, sandy and dark or light coloured. Neither the *in situ* measured sandy sediment spectrum nor the spectrum of one single macrophyte species is able to cover the spectral variability of the entire lake's bottom. Parameterising classification algorithms or bio-optical models with appropriate spectra therefore remains challenging. Currently, several approaches are available such as ex situ measurements (Giardino et al., 2016, 2015, this study), image based derivation (Gege, 2014a) or seasonal dependent reflectance models based on empiric measurements (Wolf et al., 2013). Assessing the suitability of S2A for distinguishing bottom types in detail may therefore be of interest for subsequent studies.

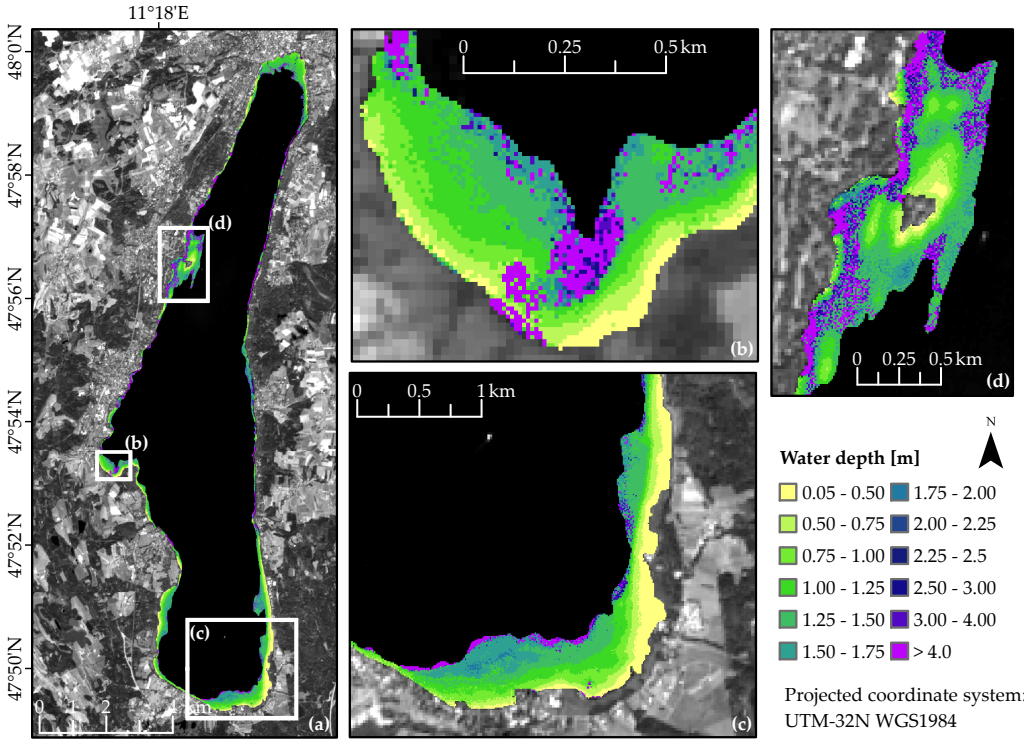

Figure 4.9: Results of water depths retrieval during shallow water inversion using the MIP 10 m pixel size dataset (a); Zoomed areas are Karpfenwinkel (b); validation area Seeshaupt (c) and Roseninsel (d). Background is gray scaled S2A band B05 (705 nm).

Bottom substrate unmixing is accompanied by fitting water depths. Fig. 4.9a depicts water depths around the entire lake and for regions with extensive shallow water areas. Water depths reasonably increased from the shore line towards the deep water mask, remained, however, in most parts of the lake below 2.0 m. At the northern end of the lake, calculated water depths rarely exceeded 1.5 m which is a clear underestimation of the actual water depths. The shallow water mask was oriented at the 8 m depth line (Fig. 4.1) of the official bathymetry map. A reason could be that bottom type spectra were inappropriate for this area. *in situ* measurements were conducted at the southern end. At measurement sites, S2A-derived water depths underestimated measured water depths about 0.5 m (Table 4.3). At measurement site D, water depths differed more than 2.5 m. This measurement site is located close to a ledge; minor GPS variations and positioning inaccuracy may therefore result in contradicting values; nevertheless, geolocation uncertainties exclusively hardly explain such a strong deviation (next paragraph).

To quantitatively evaluate the capability of S2A 10 m data for water depth retrieval, we used echo sounding

data (Fig. 4.1b, Gege, 2014a) as a validation source (Fig. 4.10). Echo sounding and S2A derived water depths are highly correlated (r = 0.95, residual standard deviation = 0.12 m) up to 2.5 m (echo sounding). Nevertheless, the RMSE (0.56 m) and offset from the 1:1 line (Fig. 4.10a) indicate that WASI-2D underestimated water depths. In water depths ranging between 0 and 4 m (measured Secchi disk depth), RMSE was 0.95 m which was higher than RMSE values obtained by Gege 2014a (mean (0-4 m) = 0.29 m) using airborne hyperspectral data. In water depths deeper than 2.5 m, WASI-2D modelled water depths at around 1.8 m (Fig. 4.10a). For these pixels, WASI-2D retrieved lower shares of sediment, and consequently higher macrophyte coverages, which is also indicated by a greenish colour in Fig. 4.10a; WASI-2D therefore considered a dark bottom type (low reflectance values due to high macrophytes coverage) accompanied by lower water depths instead of a bottom covered by sediment (high reflectance) and high water depths. Thus, WASI-2D achieved a low residuum between S2A and modelled spectrum, correct spectral unmixing, however, failed; at water depths deeper than 2.5 m, the spectral signatures of both bottom types were too similar for a correct differentation. At the points which scattered around the 1:1 line above 4 m, WASI-2D correctly fitted pure macrophyte coverage (dark green colour) and consequently retrieved correct water depths. To check these presumptions, we repeated modelling in shallow water and fixed the bottom type as sediment (fA[Sediment] = 1). Indeed, WASI-2D retrieved higher water depths, though still underestimating absolute values, with a high correlation up to 4 m (r = 0.96, residual standard deviation = 0.15 m) which was slightly below Secchi disk depth measured on 13 August (4.2 m $\pm$ 0.3 m). The MIP retrieved $R_{rs}^{BOA}(0^+, \lambda)$ spectra in shallow water were higher (except B) compared to *in situ* measured spectra. Assuming the same bottom type, higher reflectance means lower water depth which may partly explain the systematic underestimation of around 0.6 m. Furthermore, sedimentation processes may have altered bottom conditions slightly within the time difference being four years between echo sounding and image acquisition. Using sediment as fixed bottom type, WASI-2D overestimated or reached maximum value for water depths above 4 m (Fig. 4.10b). The previous setting indicated pure macrophyte coverage at these echo sounding points. Modelling with fixed sediment coverage, consequently, caused miscalculations.

Small scale variance, however, may not be captured even with using the 10 m data set. Furthermore, echo sounding data also may include measurement uncertainties, especially at ledges. S2A geolocation uncertainty, which was 12.36 m for processing baseline 02.01 (European Space Agency, 2016), may also result in misalignments between echo sounding and satellite data.

Overall, the water depths retrieval performed better with fixed bottom coverage. We therefore conclude that S2A spectral information was insufficient to accurately separate mixed coverages of macrophytes and sediment in water depths deeper than 2.5 m. This conclusion certainly is restricted to the specific lake conditions during image acquisition date, atmospheric correction algorithm (MIP) and bio-optical model applied (WASI-2D). The atmospheric correction algorithm is crucial, in particular for the application of bio-optical models which need high accuracies of both shape and intensity of $R_{rs}^{BOA}(0^+, \lambda)$ spectra. MIP retrieved the best $R_{rs}^{BOA}(0^+, \lambda)$ spectra compared to the available *in situ* spectra; however, they also showed deviations. Furthermore, MIP lacks a sun glint correction for S2A data. For this reason, we included sun glint assessment in the bio-optical modelling process. Improvements towards sun glint correction during atmospheric correction procedures may therefore also improve bio-optical analyses of lakes.

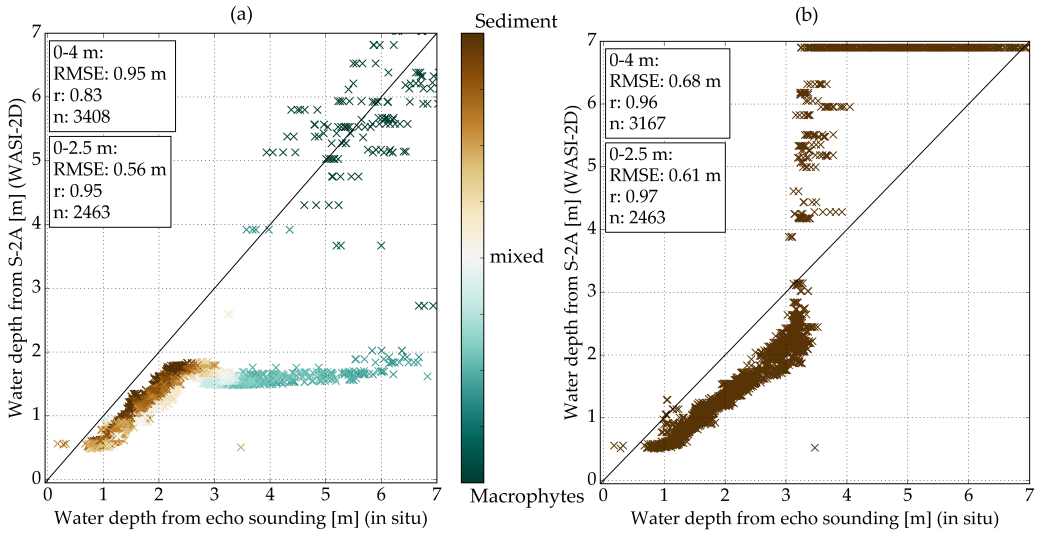

Figure 4.10: Scatterplots comparing echo sounding data (acquisition June 2012) and S2A (WASI-2D) derived water depths (10 m) while unmixing two bottom types; the colour gradient highlights bottom type (a). Scatterplot (b) results from modelling water depths with fixed sediment coverage (fA[Sediment] = 1.0).

4.4 Conclusions

This study used a physically based processing chain to test the suitability of S2A for retrieving lake ecology indicators, i.e., SPM, $a_{CDOM}(440)$, water depths and bottom substrates. To this end, we conducted a measurement campaign at Lake Starnberg (Germany) concurrently to a S2A overpass. Analysing the results of three different atmospheric correction algorithms (Sen2Cor (Müller-Wilm, 2016), ACOLITE (Vanhellemont and Ruddick, 2016) and MIP (Heege et al., 2014)) revealed different spectra for each algorithm. By comparing $R_{rs}^{BOA}(0^+, \lambda)$ spectra with in situ measured reflectance, MIP performed best and therefore was used for further processing. We then applied the bio-optical modelling software WASI-2D (Gege, 2014b). S2A band positions and calibration as well as low $NE\Delta R_{rs}E$ of the scene (mean: 0.00014 sr^{-1} for the 10 m data set) allowed retrieval of SPM and $a_{CDOM}(440)$, even at low concentrations. Absorption by CHL, however, was too low for assessment along with the other constituents. Modelled $a_{CDOM}(440)$ was lower than *in situ* values (*in situ*: 0.42-0.44 m^{-1}, S2A: 0.1-0.74 m^{-1}, mean: 0.14 $\pm$ 0.02 m^{-1}). Resulting SPM concentrations (*in situ*: 0.4-1.9 $g{\cdot}m^{-3}$, S2A: 1.1-5.1 $g{\cdot}m^{-3}$, mean: 1.8 $\pm$ 0.2 $g{\cdot}m^{-3}$) were within the range of analysed water samples. A comparison with backscattering coefficients of SPM (*in situ*: 0.015-0.021 m^{-1}, S2A: 0.018-0.077 m^{-1}) approved even better performance. Spatial resampling of the S2A data to 20 m or 60 m showed negligibly different results. In optically shallow water, parameters of interest were bottom substrate and water depths. We obtained reasonable patterns of macrophytes and sandy sediment in most parts of the lake. Modelled water depths also showed reasonable patterns. Quantitative evaluation approved a good correlation, but underestimation occurred between 0 and 2.5 m (RMSE: 0.56 m, r: 0.95). With water deeper than 2.5 m, S2A spectral information was inadequate to differentiate mixed coverages of macrophytes and sediment. Furthermore, the time difference between echo sounding and image acquisition and the challenging measurement of representative bottom spectra contributes to inaccurate bottom coverage and water depth retrieval.

This study points out that S2A has great potential to assist lake ecology in retrieving indicators on a spatially synoptic scale. The study was conducted under conditions with low water constituent concentrations and low spatial variability. Studies of lakes with different optical properties and trophic characteristics may further advance knowledge of S2A's suitability for lake monitoring. Shape and intensity of spectra strongly depend on the applied atmospheric correction algorithm; further research and improvements in this field are required.

Acknowledgments: This work was conducted within the project LAKESAT (grant No.: 50EE1340) funded by the Federal Ministry for Economic Affairs and Energy, Germany. We acknowledge financial support for publications costs by Land Schleswig-Holstein within the funding programme Open Access Publikationsfonds. A. Göritz would like to thank for support by Deutsche Forschungsgemeinschaft (DFG) through the TUM International Graduate School of Science and Engineering (IGSSE). We further thank ESA for providing Sentinel-2A data. We thank Philip Klinger of EOMAP GmbH & Co. KG for processing Sentinel-2A data with MIP. We are very grateful to Christine Fritz (TUM), Markus Hoffmann (TUM), Sebastian Riedel (CAU Kiel/DLR) and Thomas Schneider (TUM) for assistance in fieldwork and laboratory analyses. We further thank Austin Saly (CAU Kiel) for English language editing. We thank five anonymous reviewers for their effort and helpful comments.

Chapter 5

Multi-sensor satellite and *in situ* monitoring of phytoplankton development in a eutrophic-mesotrophic lake

Katja Dörnhöfer, Philip Klinger, Thomas Heege and Natascha Oppelt
Science of the Total Environment (2018), doi:10.3390/rs8110941
Received: 1 June 2017, Accepted: 21 August 2017

Highlights

- We analysed the potential of monitoring chlorophyll-a with multiple satellites.
- *in situ* and satellite results show similar and different developments.
- *in situ* and satellite chlorophyll-a lead to different trophic class assessment.
- Uncertainties of *in situ* data have to be accounted.
- Combined use of multi-sensor and *in situ* data enhance phytoplankton monitoring.

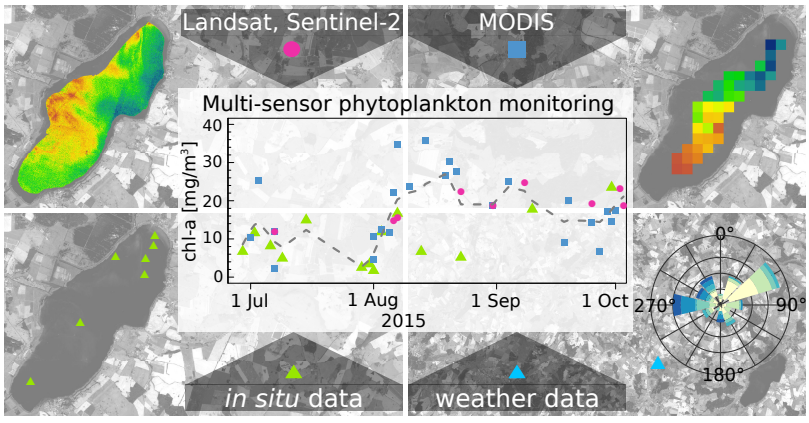

Changes made to the published version:
To harmonise the style of the entire thesis, chlorophyll-a is abbreviated as CHL instead of Chl-a.

Abstract
Phytoplankton indicated by its photosynthetic pigment chlorophyll-a is an important pointer on lake ecology and a regularly monitored parameter within the European Water Framework Directive. Along with eutrophication and global warming cyanobacteria gain increasing importance concerning human health aspects. Optical remote sensing may support both the monitoring of horizontal distribution of phytoplankton and cyanobacteria at the lake surface and the reduction of spatial uncertainties associated with limited water sample analyses. Temporal and spatial resolution of using only one satellite sensor, however, may constrain its information value. To discuss the advantages of a multi-sensor approach the sensor-independent, physically based model MIP (Modular Inversion and Processing System) was applied at Lake Kummerow, Germany, and lake surface chlorophyll-a was derived from 33 images of five different sensors (MODIS-Terra, MODIS-Aqua, Landsat 8, Landsat 7 and Sentinel-2A). Remotely sensed lake average chlorophyll-a concentration showed a reasonable development and varied between 2.3 $\pm$ 0.4 and 35.8 $\pm$ 2.0 mg·m^{-3} from July to October 2015. Match-ups between *in situ* and satellite chlorophyll-a revealed varying performances of Landsat 8 (RMSE: 3.6 and 19.7 mg·m^{-3}), Landsat 7 (RMSE: 6.2mg·m^{-3}), Sentinel-2A (RMSE: 5.1 mg·m^{-3}) and MODIS (RMSE: 12.8 mmg·m^{-3}), whereas an *in situ* data uncertainty of 48 % needs to be respected. The temporal development of an index on harmful algal blooms corresponded well with the cyanobacteria biomass development during summer months. Satellite chlorophyll-a maps allowed to follows patial patterns of chlorophyll-a distribution during a phytoplankton bloom event. Wind conditions mainly explained spatial patterns. Integrating satellite chlorophyll-a into trophic state assessment resulted in different trophic classes. Our study endorsed a combined use of satellite and *in situ* chlorophyll-a data to alleviate weaknesses of both approaches and to better characterise and understand phytoplankton development in lakes.

Keywords
Phytoplankton, Remote sensing, Validation, Bio-optical modelling, Time series

5.1 Introduction

A variety of interacting stressors, such as eutrophication, climate change, anthropogenic exploitation and pollution, affect the ecological integrity of lakes (e.g. Adrian et al., 2009; Dudgeon et al., 2006). Detecting indicators of ecological integrity and their changes therefore is vital for lake management to mitigate stressors and minimise negative influences on ecology and ecosystem services. Phytoplankton is a common indicator in lake ecology and a key biological quality element for assessing the ecological status of lakes within the European Union's Water Framework Directive (WFD, Carvalho et al., 2013b; European Commission, 2000; Kelly et al., 2016; Solheim et al., 2013). Along with climate change and eutrophication, cyanobacteria receive special awareness (Kosten et al., 2012; Paerl et al., 2016) because they produce toxins which may directly affect human and animal health; moreover scum forming blooms affect light conditions in water (Carvalho et al., 2013a; Rastogi et al., 2014; Sukenik et al., 2015). Phytoplankton itself cannot be monitored from space. Phytoplankton biomass and chlorophyll-a concentration (CHL), however, are highly correlated; therefore CHL often serves as a proxy for phytoplankton biomass (Birk and Ecke, 2014; Poikane et al., 2015). Whereas CHL is present in all phytoplankton species, pigments from the phycobilins group, such as phycocyanin and phycoerythrin, are highly correlated with cyanobacteria biomass. These pigments therefore serve as proxies for a remote sensing based estimation of cyanobacteria (Srivastava et al., 2013).
Sampling and mapping strategies should generally address the temporal and spatial variation of CHL and cyanobacteria to minimise uncertainties in ecological status assessment and health issues (Chorus et al., 2000; Søndergaard et al., 2016). For monitoring massive blooms of cyanobacteria, the World Health Organisation recommends fortnightly inspections (Chorus et al., 2000). *In situ* based sampling and laboratory analyses, how-

ever, are time-consuming and cost intensive (Schaeffer et al., 2013). For this reason, monitoring approaches are often a trade-off between an ideal sampling strategy, financial possibilities and logistics; within the scope of WFD, the broad majority of European states decided to collect water samples from the euphotic layer at the deepest or mid-lake point throughout the year (e.g. one to nine times per year or monthly during summer; Pasztaleniec, 2016). This strategy, however, may not capture the spatial and temporal variability of phytoplankton. A more frequent, spatial monitoring therefore is required, especially ith regard to short-living cyanobacteria blooms with their potential negative effects on human health (Bertani et al., 2017; Reyjol et al., 2014).

Remote sensing techniques may assist traditional sampling strategies to increase information on CHL and cyanobacteria spatial variability and temporal frequency (Dörnhöfer and Oppelt, 2016). Various empirical and physical algorithms can obtain CHL from remote sensing data by using its specific absorption features between 440 and 560 and at around 670 nm; for retrieving information on cyanobacteria, remote sensing approaches employ the absorption features of phycocyanin at around 620 nm (Dörnhöfer and Oppelt, 2016; Kutser, 2009; Matthews, 2011; Odermatt et al., 2012). Retrieving CHL and phycocyanin absorption from satellite data therefore requires sensors with high radiometric resolution, and a spectral resolution that can capture the CHL and phycocyanin specific absorption features (Stumpf et al., 2016). For this reason, studies analysing CHL and cyanobacteria often use time series of ocean colour sensors with coarse spatial resolutions (300 m x 300 m - 1 km x 1 km), such as MERIS or MODIS. Moreover, they tend to focus on large lakes (> 500 km^2; Bresciani et al., 2011c; Palmer et al., 2015c; Wu et al., 2015; Zhang et al., 2015) rather than on smaller lakes (Bresciani et al., 2011a; Matthews, 2014).

The monitoring of lakes requires sensors with high radiometric and spectral resolution, especially in the visible wavelength domain (Oppelt et al., 2015). Nevertheless, Landsat 7 (L7) and Landsat 5 showed sufficiently high accuracy for observing general trends in organic substances (Kutser, 2012) and mineral particles (Lymburner et al., 2016). The new generation of land observation satellites, such as Landsat 8 (L8) and Sentinel-2A (S2A), offer improved spectral and radiometric characteristics for inland water remote sensing (Pahlevan et al., 2014; Palmer et al., 2015b). Bresciani et al. 2016, Concha & Scott 2016 and Giardino et al. 2014a concluded that L8 was suitable for retrieving CHL at low ($\sim$ 1 $mg{\cdot}m^{-3}$) and high ($\sim$ 100 $mg{\cdot}m^{-3}$) concentrations. Recent studies highlighted S2A's capability for retrieving CHL, organic substances and water colour (Toming et al., 2016a); Dörnhöfer et al. 2016b successfully derived mineral particles, organic substances and, in shallow water, water depths and bottom substrates. L8 and S2A therefore seem promising sensors for inland water monitoring. The enhanced spatial resolution, however, implies a lower revisit time (5-16 days) compared to the ocean colour sensors (1-2 times per day). Using only one satellite system, cloud coverage can further reduce image availability and hamper a regular monitoring. Daily or even multiple data acquisitions per day may improve observing spatio-temporally highly dynamic processes, such as phytoplankton or cyanobacteria blooms (Hestir et al., 2015a). A synergistic use of sensors with different spatial resolutions may overcome the limitations of a single sensor application, which would increase availability and continuity of suitable remote sensing data for CHL monitoring. This, however, raises the question of inter-comparability of measurements while considering each sensor's limitations and capabilities.

To address this, the present study was conducted at Lake Kummerow, Germany, between July and October 2015; it includes a series of remote sensing data (MODIS-Aqua (MODAQ), MODIS-Terra (MODTE), L7, L8 and S2A) and *in situ* measurements. The specific objectives of this study were (1) to analyse the mutual inter-comparability of satellite products and *in situ* data, (2) to relate the spatial development of a phytoplankton bloom to meteorological data and (3) to integrate remotely sensed CHL into WFD trophic state assessment.

5.2 Materials and methods

5.2.1 Study area description

Located in the northern German lowlands, Lake Kummerow (53.808° N, 12.856° E) formed as a proglacial lake during last glacial period. With a size of 32.55 km^2 and an average depth of 8.1 m (maximum: 23.3 m), the lake is relatively shallow. Agriculture fields predominate the land use in the catchment (total size: 1,150 km^2, Fig. 5.1). The lake is an important resting area for migrating birds and a place for manifold recreational activities in a popular tourist area. The wind-exposed location leads to prevailing mixing conditions with a polymictic character. Table 5.1 summarises measurement values of limnological parameters describing chemical conditions at Lake Kummerow.

Table 5.1: Limnological parameters measured at Lake Kummerow between 2004 and 2015 (March-October) (data source: LU-MV, 2015b).

	CHL [$mg \cdot m^{-3}$]	Secchi disk depth [m]	Total phosphorous [$mg \cdot m^{-3}$]	Total nitrogen [$g \cdot m^{-3}$]	Total organic carbon [$g \cdot m^{-3}$]
Arithmetic mean	12.9	1.8	89.8	1.6	10.7
Standard deviation	8.8	0.8	100.4	0.6	1.1
Minimum	1.1	0.6	16.0	0.5	8.7
Maximum	45.4	5.6	1060.0	4.9	14.3

The trophic classification according to the WFD varied between eutrophic 1 and 2; in 2015, the lake was classified as mesotrophic 2 for the first time which resembles its reference state (LU-MV, 2015b). Phytoplankton analyses (2004-2015) revealed predominating diatoms (*Bacillariophyceae*) in spring whereas cyanobacteria accumulations occurred in summer and autumn, i.e. toxin producing *Microcystis spp.*, (LU-MV, 2016). In 2014 and 2015, cyanobacterial blooms occurred after a few calm days with high air temperatures. These blooms also entailed public interest (e.g. Plath, 2014, 2015) since they affected popular beaches and piers.

5.2.2 *In situ* sampling and laboratory analyses

The department of lakes (LU-MV) monitors Lake Kummerow related to WFD assessment within the lake monitoring programme of the federal state Mecklenburg-Western Pomerania (LU-MV, 2015b). Sampling occurs, independent from any satellite overpasses, once a month between March and September. LU-MV staff collects mixed water samples from the euphotic layer at two sampling sites, i.e. the deepest point (approx. middle of lake, Fig. 5.1) and "Gorschendorf" (southern end of lake, Fig. 5.1). CHL is measured in a laboratory with a spectrophotometer according to DIN 38412-L16. For the central lake samples, LU-MV also measures phytoplankton biomass and species composition.

To provide *in situ* data concurrently to satellite data acquisition, we conducted several field campaigns on days of satellite overpasses, and clear weather conditions. We took water samples (3 x 1 L per sampling site) just below the water surface (approx. 0.2 m) in the northern part of the lake. At days with wind conditions unsuitable for boat transport, water sampling has been conducted from a pier. At each sampling site, we measured water temperature just below the water surface with an Ahlborn instrument (FYA641LFL1). A Trimble Juno SB GPS device (2-5 m positional uncertainty, Trimble, 2012) recorded sampling positions. We transported water samples in a cooling box to the laboratory. Here, we filtered the samples through glass fibre filters (pore size: 0.7 µm) resulting in three separate filters for each sampling site. Filters were frozen before we extracted pigments using 99.9 % acetone. CHL was analysed photometrically with a Perkin Elmer Lambda 1050 spectrophotometer in a laboratory of the Limnological Station Iffeldorf (TU Munich) according to Lichtenthaler and Buschmann 2000. For each sampling site, we calculated the arithmetic mean and standard deviation of the three samples.

For three sampling dates, we sent water samples (4-5 per sampling day, one per sampling site, Table 5.2) to an accredited laboratory (Umwelt Control Labor - UCL, Kiel) which determined CHL photometrically according to

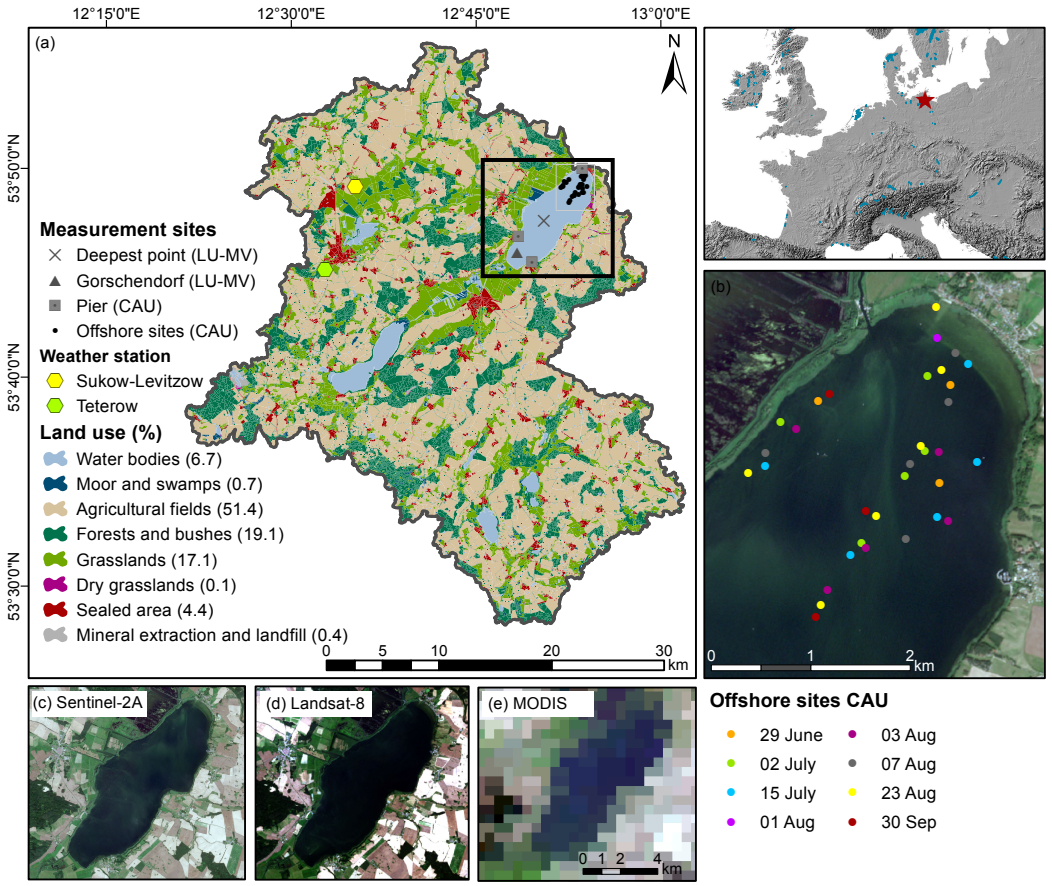

Figure 5.1: Location of Lake Kummerow and land use in its catchment (a, data source: LU-MV, 2002a) and location of offshore measurements sites (CAU) depending on the date (b). True-colour-composites emphasize different spatial scales of used satellite data Sentinel-2A (10 m spatial resolution, c), Landsat 8/7 (30 m, d) and MODAQ/MODTE (500 m, e). Coordinate system: UTM zone 33N, WGS 84.

DIN 38412-L16. Using these samples, we assessed an error margin of CHL retrieved from *in situ* collected water samples (CAU/TUM). Applying the approach by Claustre et al. 2004, we calculated the relative percentage differences (RPD) according to Eq. 5.1.

$$RPD = 100 \cdot \frac{CHL_i(S_k) - \overline{CHL_i(S_k)}}{\overline{CHL_{i,j}(S_k)}} \tag{5.1}$$

where $CHL_i(S_k)$ is the CHL of laboratory i (i = [CAU/TUM, UCL]) at sampling site S_k and $\overline{CHL_{i,j}(S_k)}$ is the arithmetic mean of CHL of both laboratories at sampling site S_k. According to McKee et al. 2014, the 95 % prediction interval of all RPD values represents the uncertainty measure.
Table 5.2 lists all sampling dates, number of samples and corresponding weather conditions.

Table 5.2: Summary of sampling dates and prevailing weather conditions. Data from weather station Sukow-Levitzow (Fig. 5.1; Deutscher Wetterdienst, 2016b).

Sampling Date	Time (UTC)	Source	No. of sites	No. of samples	No. of samples to UCL	Match-up (± day of satellite acquisition)	Wind speed [$m \cdot s^{-1}$]	Wind direction [°]
05 June	08:10-11:55	CAU/TUM	5	14	4	-	5.2-6.0	130-140
29 June	9:00-10:30	CAU/TUM	3	9	0	-	2.7-4.6	210-230
02 July	8:00-13:45	CAU/TUM	5	15	5	MODTE (-1) MODTE (+1)	5.1-6.3	90-100
06 July	10:00-14:00	CAU/TUM	3 (pier)	9	0	MODTE (+1) MODAQ (+1)	7.5-7.7	270-300
09 July	7:50-8:50	LU-MV	2	2	0	L7 (-2)	8.9-9.6	270
15 July	8:15-11:00	CAU/TUM	5	15	0	-	4.6-5.5	290-300
29 July	13:00	CAU/TUM	1 (pier)	3	0	-	8.8	230
31 July	11:00-11:15	CAU/TUM	2 (pier)	6	0	-	6.5	270
01 Aug	13:35	CAU/TUM	1	3	0	MODTE (0) MODAQ (0)	1.7-1.9	50-80
03 Aug	9:40-13:25	CAU/TUM	6	16	4	MODAQ (0)	2.4-2.9	90-130
07 Aug	8:30-11:00	CAU/TUM	5	15	0	MODTE (-1) MODAQ (0) S2A (-1) L8 (0)	1.1-5.3 (increasing)	190-330
13 Aug	9:25-10:15	LU-MV	2	2	0	MODAQ (+1)	4.2-4.6	50-60
23 Aug	8:15-12:00	CAU/TUM	6	18	0	MODTE (-1) L8 (0)	3.9-7.3(increasing)	90-120
10 Sep	10:25-12:00	LU-MV	2	2	0	-	3.7-4.6	90-100
30 Sep	9:15-11:15	CAU/TUM	3	9	0	MODTE (0) MODAQ (-1)	0.7-2.2	70-160

5.2.3 Algorithm for retrieving CHL and eoHAB

The study focused on the period between 1st July and 3rd October. We used data from five different sensors, i.e. MODTE, MODAQ, L7, L8 and S2A, which differ in spatial, radiometric and spectral resolution (Table 5.3). Retrieval of CHL using sensors with different spectral characteristics requires a sensor independent model. The methodology of this study bases on an established multi-sensor processing system, i.e. the Modular Inversion and Processing System (MIP; Heege and Fischer, 2004; Heege et al., 2003, 2014, 2015).

Table 5.3: Central wavelength (bandwidth), radiometric and spatial resolution of satellite sensors used in the study.

	MODIS (Terra & Aqua)	Landsat 8	Landsat 7	Sentinel-2A
Spatial resolution [m]	250-500 (resampled to 500)	30	30	10-60 (interpolated to 10)
Radiometric resolution [bit]	12	12	8	12
Central wavelength (bandwidth) [nm]	469 (20)	440 (20)	485 (70)	443 (20)
	555 (20)	480 (60)	570 (80)	490 (65)
	645 (50)	560 (60)	660 (60)	560 (35)
	858.5 (35)	655 (30)	840 (120)	665 (30)
	1240 (20)	865 (30)	1650 (200)	705 (15)
	1640 (12)	1370 (20)	2220 (260)	740 (15)
	2130 (50)	1610 (80)		783 (20)
		2200 (180)		842 (115)
				865 (20)
				945 (20)
				1375 (30)
				1610 (90)
				2190 (180)

5.2.3.1 The MIP model

MIP includes physics-based retrieval algorithms for optically shallow and deep waters, based on calculations of a radiative transfer solver Finite Element Model (FEM; Bulgarelli et al., 1999; Kiselev et al., 1995). FEM forward calculations cover the full bi-directional properties of the atmosphere, the air-water interface, and the

water body itself. Focusing on wavelengths between 350 and 2800 nm, FEM calculations generate a large database, which relates sensor radiances directly with in-water absorption and backscattering properties in 1 nm steps. The model addresses the entire range of possible geometric conditions between sensor, sun and target for all dependencies of scattering and absorption in a multi-layer atmosphere-system, the water body, as well as bidirectional reflection/ transmission at the water surface. Further variables consider sensor altitude (for airborne sensors), surface altitude, and atmospheric variables such as aerosol optical depth. MIP directly relates in-water absorption and scattering properties to the sensor radiances; thus, it considers a wide range of optical properties in natural waters, including e.g. extremely turbid water bodies.

For each sensor, the database is resampled to the sensor-specific spectral response functions. The MIP architecture then automatically adapts the retrieval modules to the optical conditions of the target area and specific sensor characteristics using sensor response functions. Hence, the retrieval modules deliver standardised, inter-comparable results for the sensors used. Precondition, however, is a physically correct and stable radiometric calibration of the used sensors. Resulting accuracies therefore strongly depend on the sensor characteristics.

Processing includes land-water-cloud-detection, ozone correction (Richter et al., 2014), adjacency correction (Kiselev et al., 2015), iterative retrieval of atmospheric properties, and an iterative retrieval of scattering and absorption properties of water column constituents for each water pixel. The iterative retrieval consists of a least-square minimisation between modelled and measured sensor radiances resulting in best-fit absorption- and backscattering spectra of the water body. Absorption and backscattering spectra can then be used to derive quantitative units of water constituent concentrations using the so-called specific inherent optical properties. The retrieval process enables the definition of different water types covering a range of varying specific inherent optical properties. In this study, we tested the capability of using a standard parameterisation to cover the variety of oligo- to hypertrophic lakes. Here, Heege et al. 2014 defined the wavelength dependency of scattering; the absorption of water constituents is a variable mixture between a Gaussian model by Gege 2000 and a phytoplankton specific absorption spectrum as defined in Heege and Fischer 2004. The processor provides various internal quality measures used for automated flagging and the adaptation to the specific inherent optical properties.

5.2.3.2 CHL concentration and eoHAB index

Using mass-specific conversion factors, MIP relates the inherent optical properties to water quality parameters. In this study, we focus on two water quality parameters, i.e. CHL and eoHAB (index on cyanobacteria presence). CHL retrieval relies on the retrieved absorption spectra. The total absorption consists of an inorganic and organic component. Organic absorption comprises of CHL related absorption and remaining absorbing components such as dissolved organic materials and tripton. Retrieving CHL concentration from CHL related absorption follows a relationship in which 1 $mg \cdot m^{-3}$ CHL equals 0.035 m^{-1} CHL absorption at 440 nm. This optimisation process additionally considers the specific scattering properties of phytoplankton.

The second parameter, the eoHAB index, refers to the presence of cyanobacteria. EoHAB is sensitive to the appearance of cyanobacteria-related pigments, i.e. phycocyanin and phycoerythrin. Both pigments show absorption features in green wavelengths from 500 nm to approx. 640 nm; phycoerythrin shows its absorption maximum at 540-570 nm, phycocyanin at 610-620 nm (Colyer et al., 2005). Most satellite sensors support the identification of this feature with only two bands, i.e. one in the green wavelength region (e.g. L7 and L8 at 530-590 nm) and in the red wavelength region at approx. 640-670 nm. The used standard parameterisation of phytoplankton absorption in MIP as described above, however, does not account phycocyanin and phycoerythrin absorption in the retrieval process. The modelled phytoplankton absorption therefore lacks the absorption features of these pigments. Nonetheless, if these pigments are present in the water a slight spectral mismatch between modelled water leaving reflectance ($R_{modelled}$) and satellite derived reflectance ($R_{satellite}$) occurs. The algorithm then compares the slope of $R_{modelled}$ and $R_{satellite}$ between the green and red band ($\delta R = R_{green} - R_{red}$).

Calculation of eoHAB (see also Fig. 5.5) follows Eq. 5.2.

$$eoHAB = 1 + 100 \cdot \Delta(\delta R_{satellite} - \delta R_{modelled}) \quad (5.2)$$

EoHAB values typically range between 95 and 110. A higher eoHAB value indicates a higher mismatch between Rsatellite and Rmodelled. Presence of phycocyanin and phycoerythrin result in lower $R_{satellite}$ values compared to $R_{modelled}$; we experienced that higher eoHAB values (> 100) point towards a higher probability of cyanobacteria presence.

5.2.4 Analyses of MIP products

Evaluation of MIP products includes three parts: (1) evaluating the temporal development of average CHL and eoHAB values from *in situ* samples and MIP products, (2) pixel-match-ups with *in situ* samples and (3) sensor inter-comparisons. Spatial and statistical analyses were conducted using ArcGIS version 10.3 (ESRI, 2016), R version 3.3.1 (R Core Team, 2016) and SNAP version 5.0 (SNAP, 2016).

To evaluate the temporal development of CHL we calculated the arithmetic mean and standard deviation of all valid pixels in a data set, i.e. pure deep-water pixels (no influence of bottom substrate or neighbouring land) with a good quality of parameter retrieval. To cover valid pixels from different sensors we had to define valid pixels differently: in case of MODTE and MODAQ, we considered data with a viewing angle < 45°. Since data processing and parameter retrieval become error prone with increasing viewing angles, data sets acquired with viewing angles > 45° provided inconsistent results and therefore have been left off. Moreover, a one-pixel buffer surrounding land-masked pixels prevented using mixed land-water pixels. To provide a sufficient number of pixels for statistical analysis, we only used MODTE and MODAQ data sets with at least ten connected deep-water pixels for further analysis.

For L 7/8 and S2A data, pixels with a water depth > 3 m (official bathymetric chart; LU-MV, 2002b) showed no signal from bottom substrate and were therefore included in processing. In case of cloud coverage, we calculated an additional two-pixel buffer (60 m) as an add-on to the cloud and cloud shadow mask to reduce the number of pixels influenced by cloud boundary effects. Referring to all sensors, we further excluded pixels with CHL below 1 mg·m^{-3} (or total absorption $\leq$ 0.1 m^{-1}) from the analysis since mesotrophic to eutrophic lakes normally show CHL > 3 mg·m^{-3} during summer months (Håkanson and Boulion, 2001; Wetzel, 2001). CHL below 1 mg·m^{-3} has never been measured at Lake Kummerow (Table 5.1). We applied a similar processing to the eoHAB product; afterwards we compared the eoHAB results with the cyanobacteria biomass fraction measured from *in situ* samples. In total, we analysed 33 remote sensing products, i.e. 13 MODTE, 11 MODAQ, four L7, four L8 and one S2A data sets.

To assess the accuracy of MIP retrieved CHL, we conducted pixel to sample match-ups for L7, L8 and S2A CHL products. We only considered match-ups where *in situ* sampling and satellite acquisition differed in maximum 48 hours. In each data comparison, we calculated arithmetic mean and standard deviation of CHL from a 5 x 5 pixel area surrounding the pixel which corresponded to the GPS location of the sampling site. To consider GPS and satellite positional inaccuracies, potential drift of boat and water masses we added the 5 x 5 pixel buffer. To address MODTE and MODAQ large pixel sizes of 500 x 500 m^2, we handled MODIS match-ups differently. With respect to MODIS pixel size, sampling sites were located too close to the shoreline. Strict masking of MODIS pixels resulted in a low number of positional matches between sampling sites and pixels. We therefore compared arithmetic mean and standard deviation of all sampling points to the arithmetic mean and standard deviation of all valid lake pixels at an acquisition date (including match-ups within 24 hours). Using R package hydroGOF (Zambrano-Bigiarini, 2014), we calculated Root-Mean-Squared-Error (RMSE), normalised RMSE, mean average error (MAE) and percentage bias (pbias) for each date and sensor.

To analyse sensor-inter-correlation, we compared CHL products derived from MODTE and MODAQ with those derived from L7, L8 and S2A, which have been acquired on the same day. To this end, we calculated arithmetic mean and standard deviation of all L7, L8 or S2A pixels, which fit into a valid MODTE or MODAQ pixel. Afterwards we determined Pearson's correlation coefficient.

We chose the first bloom event in summer 2015 to analyse the spatio-temporal patterns of algal blooms. To interpret the spatial patterns we further included hourly wind data and daily sunshine duration from nearby weather stations (Deutscher Wetterdienst, DWD, Fig. 5.1).

5.2.5 Trophic status assessment

In Germany, the WFD trophic status assessment follows the LAWA guidelines (Länder-Arbeitsgemeinschaft Wasser; Riedmüller, 2014). The trophic index (TI) combines season (March to September/October) averages of CHL (CHLSais), Secchi disk depth (STSais), total phosphorous concentration (TotPSais) and total phosphorous during spring (TotPSpr) with highest weighting of CHL (Riedmüller, 2014). Averaging and weighting of indices depends on the lake type. Eq. (5.3-5.7 are valid for polymictic lakes with an average depth > 3 m.

$$TI = \frac{(CHL\text{-}Ind \cdot 10 + STSais\text{-}Ind \cdot 7 + TotSpr\text{-}Ind \cdot 4)}{26}, \text{ with} \tag{5.3}$$

$$CHL\text{-}Ind = 0.856 \cdot ln(CHLSais[mg \cdot m^{-3}]) + 0.560 \tag{5.4}$$

$$ST\text{-}Ind = -1.304 \cdot ln(STSais[m]) + 3.5932 \tag{5.5}$$

$$TotPSais\text{-}Ind = 0.9987 \cdot ln(TotPSais[mg \cdot m^{-3}]) - 0.9384 \tag{5.6}$$

$$TotPSpr\text{-}Ind = 1.2232 \cdot ln(TotPSpr[mg \cdot m^{-3}]) - 1.7408 \tag{5.7}$$

For 2015, LU-MV provided measurement values for CHLSais, STSais, TotPSais and TotPSpr based on *in situ* measurements(LU-MV, 2015b). For calculating ChlaSais, we replaced the July, August and September *in situ* CHL by monthly average CHL values retrieved with MIP. To adress the temporal dynamic of CHL, we additionally assessed the trophic class using the minimum and maximum lake average CHL concentration per month based on satellite measurements. We then compared the retrieved TI and respective trophic classes based on either *in situ* data or integrating satellite CHL. To include the spatial variability of CHL, we conducted an attempt to retrieve a spatially explicit trophic class assessment. We created a 100 x 100 m^2 grid covering the lake to deal with the different resolutions of the used satellite sensors. We determined monthly average CHL concentrations and applied Eq. 5.3 for each grid cell, whereas ST-Ind, TotPaisSais-Ind and TotPSpr-Ind remained constant. TI values between 2.01 and 2.50 were classified as mesotrophic 2, between 2.51 and 3.00 as eutrophic 1 (Riedmüller, 2014).

5.3 Results

5.3.1 Uncertainty of *in situ* CHL concentrations

Fig. 5.2a shows a scatterplot of *in situ* CHL from CAU/TUM and UCL laboratory. The best-fit slope of the linear least square regression was 1.15 indicating that CAU/TUM values tended to be lower than the respective UCL results. Showing a Pearson's correlation coefficient of r = 0.85 (p-value < 0.001) the data sets were significantly correlated. Samples collected during the developing algal bloom deviated most. Fig. 2b depicts the histogram of RPD values, which revealed a measurement uncertainty of $\pm$ 48 % (95 % prediction interval).

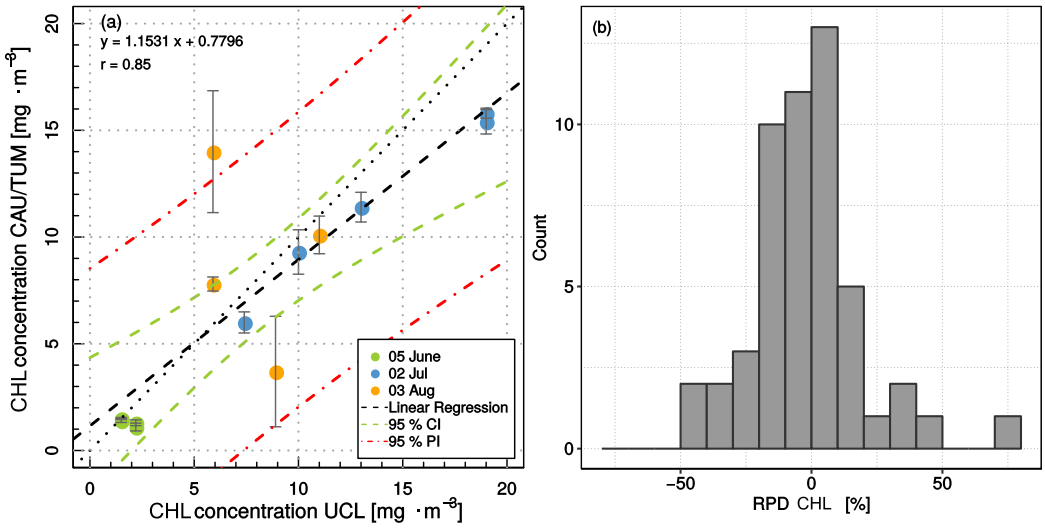

Figure 5.2: Scatterplot of CHL measured at UCL and CAU/TUM laboratory (a). Only one sample per sampling site was analysed by UCL, whereas CAU/TUM analysed three samples per sampling site (vertical error bars). Histogram of relative percentage difference (RPD, Eq. 5.1) for CHL (b).

5.3.2 Evaluation with satellite and *in situ* data match-ups

Fig. 5.3 shows the comparison of *in situ* CHL and CHL derived from S2A (Fig. 5.3a), L8 (Fig. 5.3b) and L7 (Fig. 5.3c). Two sampling dates (7 and 23 August) matched exactly with L8. For one L7 data set (7 July) a LU-MV sampling occurred two days after image acquisition. One S2A data set (6 August) is available, acquired one day before CAU sampling. Four sampling dates matched with MODTE and MODAQ image acquisitions (Fig. 5.3d, coloured points). Nine further samplings were within a ±1 day difference to MODTE or MODAQ acquisitions (Fig. 5.3d, grey points).

Table 5.4 summarises evaluation measures for each pair of satellite acquisition/sampling measurements. On 7 July, *in situ* CHL varied between 2 and 10 mg·m^{-3} whereas L7 retrieved CHL was distinctly higher (10-35 mg·m^{-3}). On 7 August, *in situ* and L8 derived CHL matched well within the uncertainty range of *in situ* measurements (± 48 %). Compared to L8, S2A data acquired the day before showed a higher variability in CHL indicated by the vertical error bars; despite the one-day difference S2A and *in situ* CHL corresponded well. On 23 August, L8 revealed a distinctly higher CHL than the corresponding *in situ* measurements. L7 matched only one sampling with a two-day difference. Table 5.4 and Fig. 5.3c show that *in situ* CHL varied between 2 and 10 mg·m^{-3} whereas L7 retrieved CHL was distinctly higher (10-35 mg·m^{-3}). The lake average CHL derived with MODTE and MODAQ only partially matched average *in situ* CHL. As presented in Fig. 5.3d both sensors provided outliers.

Table 5.4: Statistical evaluation measures between satellite retrieved CHL and *in situ* CHL acquired within 48 hours.

	***In situ* data time difference**	**RMSE [mg·m^{-3}]**	**MAE [mg·m^{-3}]**	**nRMSE [%]**	**pbias [%]**
L8 versus *in situ* 07 Aug	± 2 h	3.6	3.0	49.5	-7.5
L8 versus *in situ* 23 Aug	± 2 h	19.7	19.4	1120.6	363.2
L7 versus *in situ* 07 July	+ 48 h	6.2	6.2	110.3	124.3
S2A versus *in situ* 06 Aug	+ 1 d	5.1	4.5	69.2	-17.9
MODAQ versus *in situ* mean	± 24 h	14.9	11.5	68.3	64.6
MODTE versus *in situ* mean	± 24 h	7.1	5.9	32.6	20.5
MODAQ + MODTE versus *in situ* mean	± 24 h	12.8	9.7	58.6	55.1

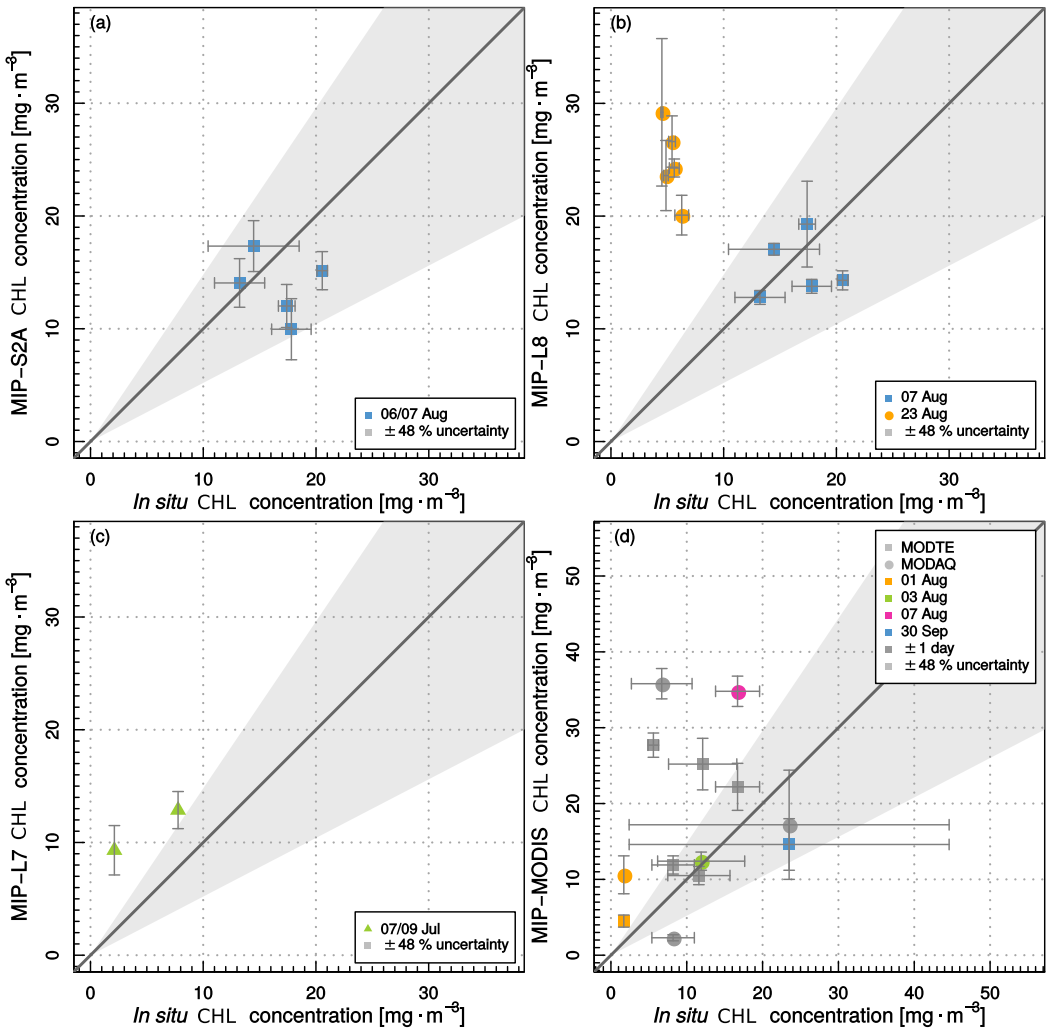

Figure 5.3: Comparison of CHL retrieved from *in situ* measurements and S2A (a), L8 (b), L7 (c), MODTE and MODAQ (d) acquisitions. Vertical error bars indicate the standard deviation of a 5 x 5 pixel environment (a-c) or of the lake (d). Horizontal error bars represent standard deviation of *in situ* measurements at the sampling sites, the grey shaded area indicates the 48 % uncertainty of *in situ* measurements.

5.3.3 Correlation in satellite CHL between different sensors

Fig. 5.4 shows a scatterplot between CHL values retrieved from MODTE/MODAQ and the other sensors acquired within ± 2 hours. Vertical error bars indicate variability of CHL of L7/8 or S2A within a MODTE/MODAQ pixel. For four satellite pairs, which have been acquired within 20 minutes, CHL values are close to the 1:1 line, i.e. L7 with MODTE/MODAQ and S2A with MODTE. S2A had a significant strong positive correlation with MODTE (Table 5.5) whereas S2A retrieved lower CHL (pbias = -22.5 %) than MODTE. On 31 August, the L7/MODTE pair matched well while on 7 July, both L7/MODIS pairs correlated insignificantly. The L7/MODTE pair, however, was closer to the 1:1 line (pbias = -9.3 %).

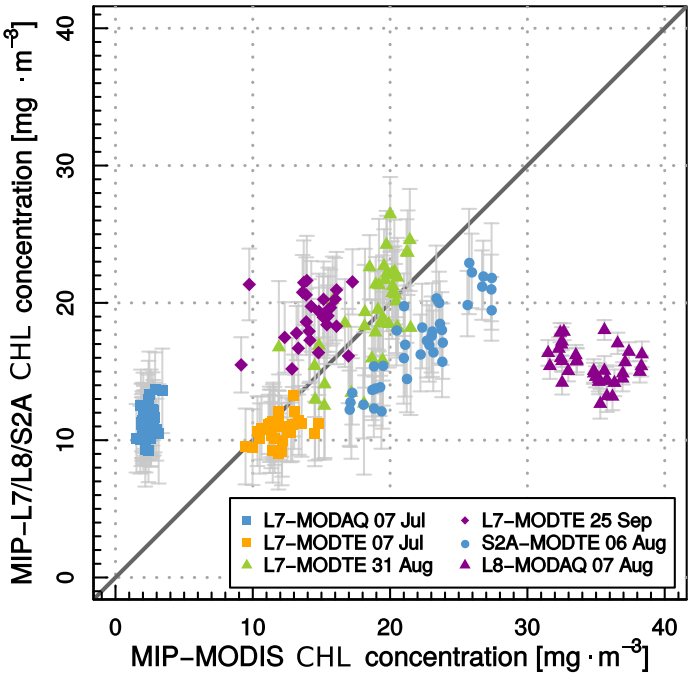

Figure 5.4: Comparison of L7, L8 or S2A and MODIS CHL acquired at the same day, error bars indicate standard deviations of L7, L8 and S2A within the corresponding MODIS pixel.

Table 5.5: Statistical relationship between the CHL values of L7, L8 or S2A and MODAQ or MODTE acquired on the same day.

Sensor pair	Time difference	n	Pearsons'r	p-value	RMSE [mg·m^{-3}]	MAE [mg·m^{-3}]	nRMSE [%]	pbias [%]
L7-MODAQ 07 Jul	2 h	42	0.35	0.012	9.0	9.0	478.6	385.1
L7-MODTE 07 Jul	20 min	42	0.38	0.017	1.6	1.2	30.1	-9.3
L7-MODTE 31 Aug	20 min	32	0.64	< 0.001	2.7	2.3	28.1	3.4
L7-MODTE 25 Sep	20 min	27	0.23	0.127	5.1	4.7	63.4	32.2
S2A-MODTE 06 Aug	10 min	37	0.89	< 0.001	5.2	5.0	50.2	-22.5
L8-MODAQ 07 Aug	1 h 15 min	35	-0.33	0.049	19.5	19.4	286.1	-55.6

5.3.4 Multi-sensor time series of CHL and eoHAB

Fig. 5.5a shows the time series of CHL at Lake Kummerow between 1 July and 3 October 2015. For the entire time span with 33 data acquisitions, satellite retrieved CHL varied between 2.3 and 35.8 mg·m^{-3}. At the beginning of July, satellite CHL started around 10 mg·m^{-3}. After a data gap due to bad weather conditions, satellite CHL rapidly increased from 5.0 to 35.8 mg·m^{-3} in the first half of August. Between mid-August and the beginning of October, satellite CHL fluctuated around 20 mmg·m^{-3}. CHL from *in situ* measurements is the arithmetic mean of all measurements at all sampling sites and the corresponding standard deviations (Fig. 5.5a). In total 14 *in situ* data sets are available (3 LU-MV and 11 CAU) with *in situ* CHL ranging between 1.7 and 23.5 mg·m^{-3}. At the beginning of July, *in situ* CHL was around 10.0 mg·m^{-3} similar to satellite average. In the first week of August, *in situ* CHL increased from 1.7 to 16.7 mg·m^{-3}; it decreased below 7.0 mg·m^{-3} in the second half of August, but increased again towards a maximum value on 30 September (23.5 mg·m^{-3}). In general, satellite CHL showed higher variation than *in situ* measurements. Overall, both approaches followed the trend with lower CHL in July an and higher CHL in late summer/ early autumn; satellite CHL reached its maximum in mid-August already (35.8 mg·m^{-3}). Significant deviations occurred in August, where *in situ* and satellite CHL indicated an algae bloom.

Fig. 5.5b shows the development of lake average eoHAB values for the same period. The Figure also illustrates

the cyanobacteria percentage of phytoplankton biomass at the LU-MV sampling days. In July, the cyanobacteria share was less than 4 %. Consistently, eoHAB values were low (< 100). At the beginning of August, eoHAB values increased to 100.5, slightly varied around this level until mid-September before it reached its maximum (101.8) at the end of September/beginning of October. The cyanobacteria fraction showed a similar behaviour with an increase up to 40 % in August and a subsequent high value in September.

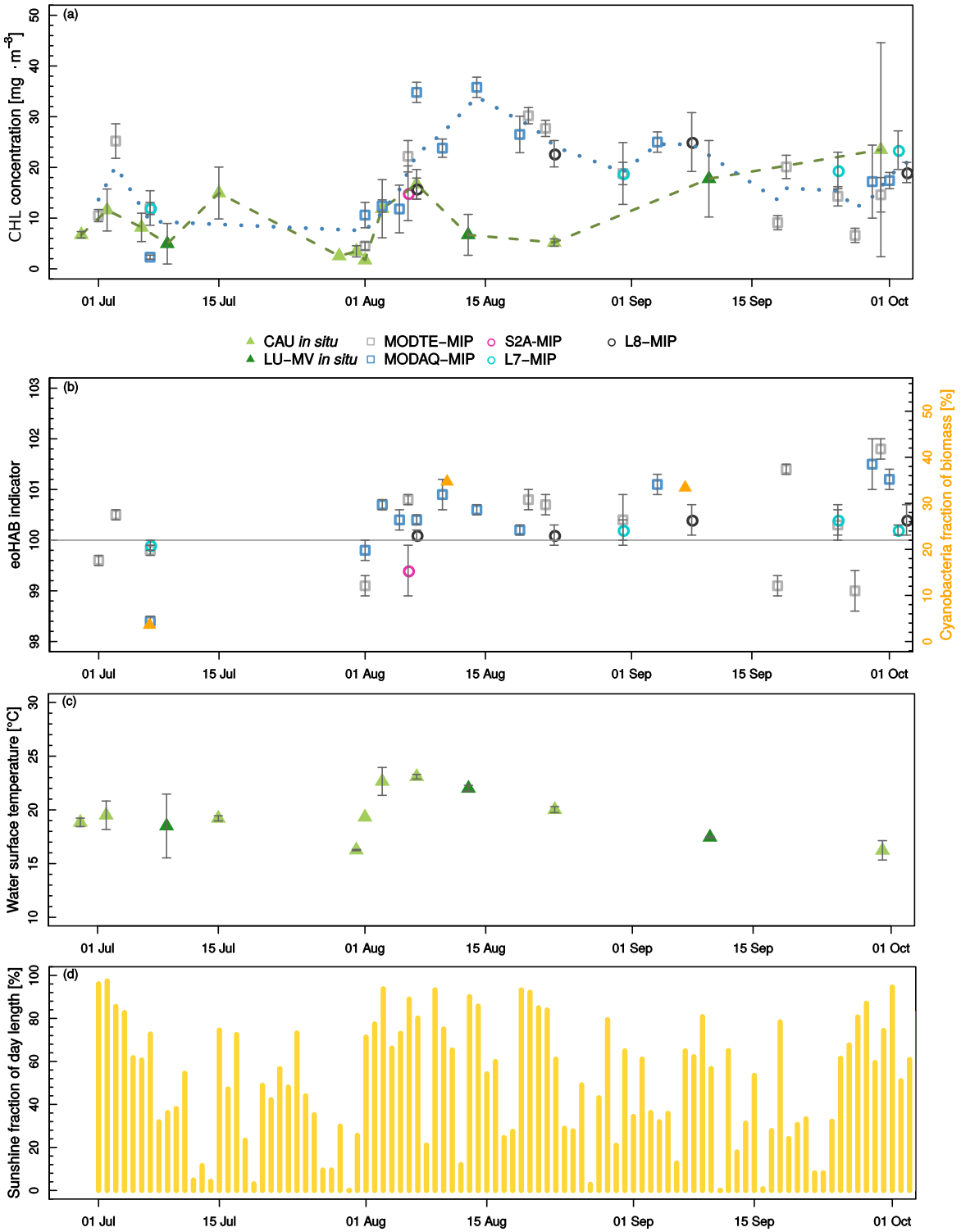

Figure 5.5: Lake average satellite CHL and *in situ* CHL between 1 July and 3 October 2015. Vertical bars indicate standard deviation (a). Lake average eoHAB and cyanobacteria fraction of biomass (LU-MV, 2015b) (b), measured water surface temperature (c) and daily sunshine fraction measured at DWD station Teterow (Deutscher Wetterdienst, 2016b) (d).

5.3.5 Spatio-temporal development of an algal bloom

Fig. 5.6 shows the spatio-temporal development of CHL between 1 and 7 August. Fig. 5.7 depicts wind speed and wind direction measured at a nearby weather station over the same period. On 1 August, MODAQ showed mean CHL of 10.6 mg·m^{-3} with an increase from the northern part (5 mg·m^{-3}) towards the southern part of the lake (12 mg·m^{-3}). Two days later, CHL was more homogenously distributed with an average CHL of 12.4 mg·m^{-3}. On 5 August, the distribution seems inverse to 1 August showing low CHL ($\sim$ 3-5 mg·m^{-3}) in the southern part and higher CHL (15 mg·m^{-3}) in the northern part. The high spatial resolution of S2A captured distinct spatial patterns of CHL on 6 August, i.e. low concentrations (3-5 mg·m^{-3}) in the north-eastern part and high concentrations up to 45 mg·m^{-3} in the western part. Ten minutes later, MODTE acquired similar patterns but a higher average CHL. Furthermore, MODTE was unable to monitor the veil-like structures with very high CHL apparent in the S2A data set. The coarse spatial resolution of the former also impeded a detection of low CHL areas close to the north-eastern shoreline. One day later, L8 depicted a rather homogenous CHL distribution with a relative maximum of 22 mg·m^{-3} in the south-eastern part.

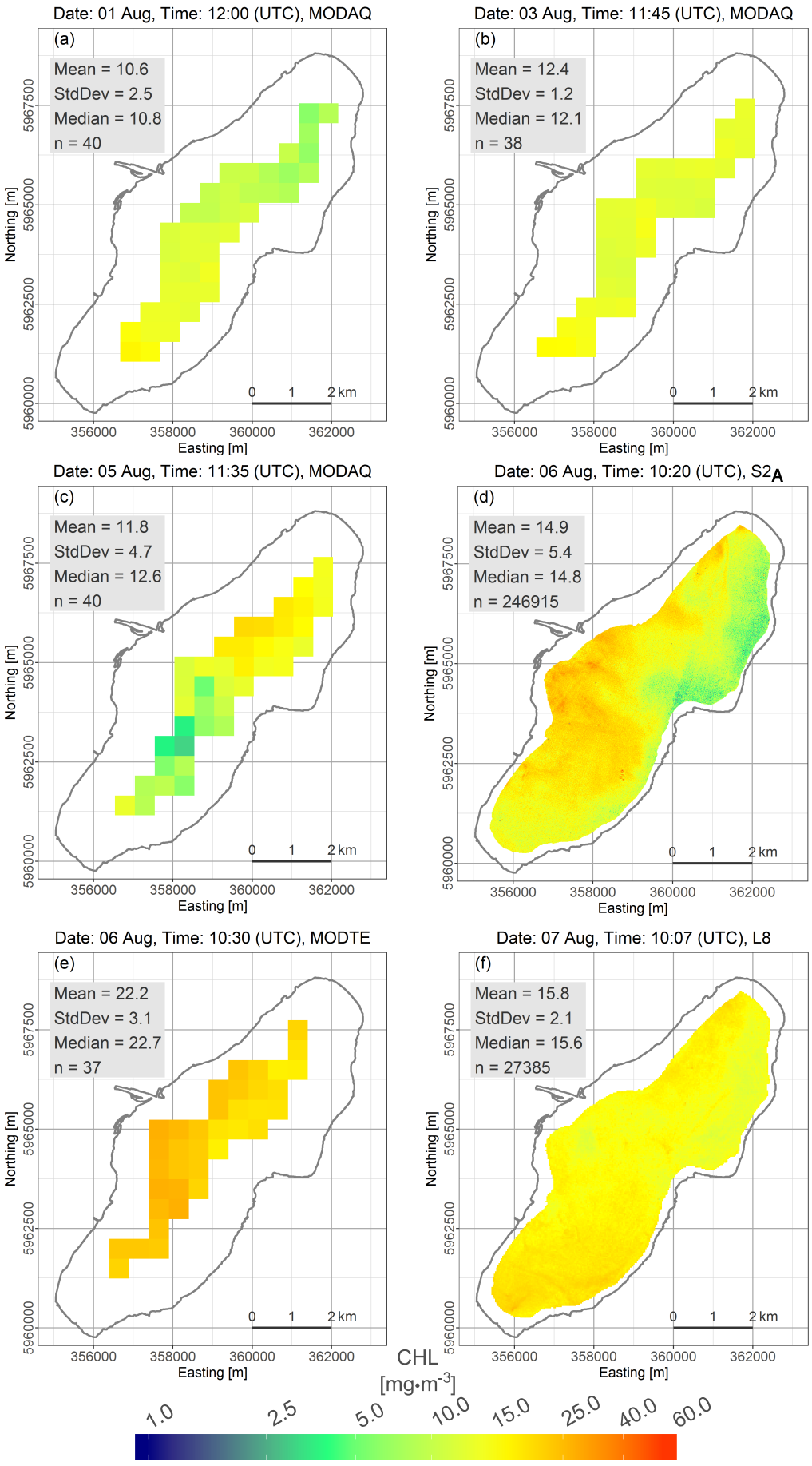

Figure 5.6: Multi-sensor CHL from 1 August to 7 August showing the spatio-temporal behaviour of an algal bloom. Coordinate system: UTM zone 33N, WGS 84.

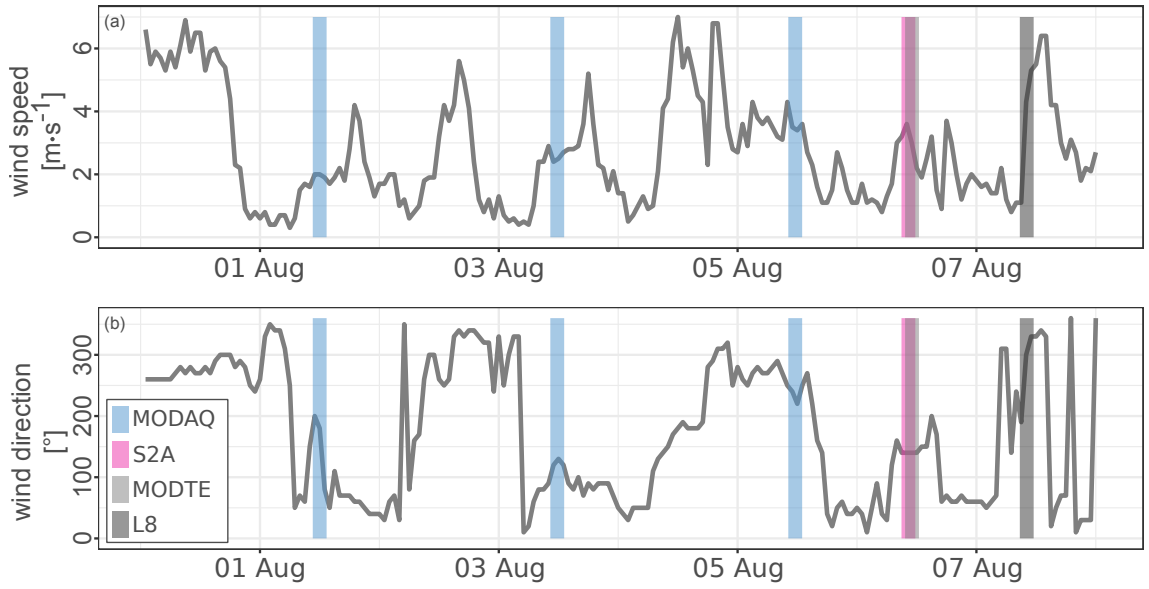

Figure 5.7: Hourly wind speed (a) and direction b) measured at DWD station Sukow-Levitzow from 31 July to 7 August. Vertical bars indicate satellite image acquisitions.

5.3.6 Integrating remote sensing data into WFD monitoring

Table 5.6 summarises season and spring average values of Secchi disk depth and total phosphorous concentration originating from *in situ* measurements (LU-MV, 2015b); it also lists the CHL values in more detail. Monthly averages from satellite products were distinctly higher in July and August, resulting in higher ChlaSais and ChlaSais-Index values. The final trophic index obtained with integrated satellite CHL showed a 0.13 higher value compared to the LU-MV index. Contrary to the classification according to *in situ* data (mesotrophic 2), Lake Kummerow was classified as eutrophic 1 using satellite based CHL data during the observation period. Using the maximum lake average satellite CHL, the trophic class was eutrophic 1; using the minimum lake average satellite CHL, the trophic class was mesotrophic 2 equal to the *in situ* based assessment.

Fig. 5.8a-c emphasise the monthly CHL arithmetic means based on a 100 x 100 m^2 grid showing the spatial variability of the trophic class assessment (Fig. 5.8d). The lake mainly achieved the class eutrophic 1 whereas parts along the eastern shoreline were classified as mesotrophic 2.

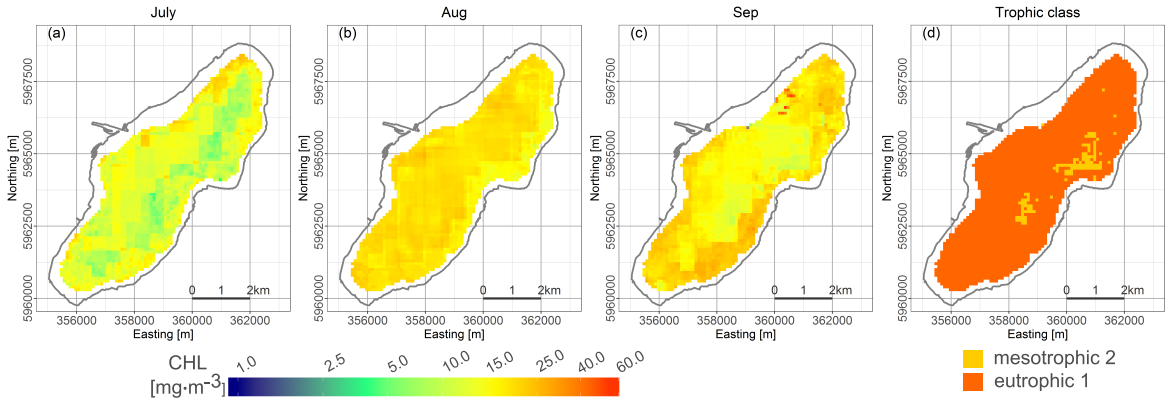

Figure 5.8: Monthly arithmetic mean for July (a), August (b) September (c) and trophic class (d) based on a 100 x 100 m^2 grid. Coordinate system: UTM zone 33N, WGS 84.

Table 5.6: Season and spring average values for trophic index calculation based on *in situ* measurements from LU-MV (2015c). Monthly average CHL based on satellite data are marked bold.

	StSais [m]	TotPSais [mg·m^{-3}]	TotPspr [mg·m^{-3}]		Monthly CHL [mg·m^{-3}]	CHLSais [mg·m^{-3}]	CHLSais-Index	Trophic index	Trophic class
Trophic class assessment based on *in situ* data	2.5	36	40	March May June July August September	5.1 5.0 2.3 5.0 6.7 17.8	7.0	2.2	2.44	mesotrophic 2
Trophic class assessment based on mean satellite measurement	2.5	36	40	March May June July August September	5.1 5.0 2.3 **12.4** **20.7** **16.8**	10.4	2.6	2.57	eutrophic 1
Trophic class assessment based on minimum satellite measurement	2.5	36	40	March May June July August September	5.1 5.0 2.3 **4.5** **6.6** **4.3**	4.3	1.8	2.28	mesotrophic 2
Trophic class assessment based on maximum satellite measurement	2.5	36	40	March May June July August September	5.1 5.0 2.3 **25.2** **35.8** **25.0**	16.4	3.0	2.72	eutrophic 1

5.4 Discussion

5.4.1 Inter-comparability based on match-ups

Comparisons between satellite CHL and *in situ* measurements collected within a specific time span are a common way to evaluate satellite derived results. Uncertainties associated with *in situ* measurements, however, often are ignored (Dörnhöfer and Oppelt, 2016). Major sources of uncertainty in CHL estimation are the filtration and the pigment extraction from filter using a solvent (McKee et al., 2014). To consider uncertainties associated with our *in situ* measurements we followed the approach by Claustre et al. 2004 to find an uncertainty range in which satellite CHL is allowed to vary. The calculated $\pm$ 48 % uncertainty of photometric measurements seemed to be comparable to uncertainties of HPLC (high pressure liquid chromatography) measurements published by McKee et al. 2014 ($\pm$ 28 %) or Claustre et al. 2004 ($\pm$ 20 %). One of the few published round robin tests conducted in German laboratories reported deviations up to 130 % in determining CHL photometrically using DIN 38412-L16 (AQS, 2008). A comparison between *in situ* and satellite CHL should therefore consider uncertainty ranges of *in situ* data and not merely focusing on exact matches.

L7 was slightly higher than *in situ* samples collected two days after image acquisition. Other than the time difference, this mismatch may be a result of its low radiometric resolution (8 bit). Further uncertainty of L7 products results from filling data gaps due to SLC-off; the data gaps are filled via interpolating neighbouring pixel, which may lead to artificial CHL variations independent from real conditions. Nonetheless, the match-up was included as being the closest and only match between *in situ* and a L7 data take.

Concerning L8 recent studies found that satellite and *in situ* CHL matched well at various concentrations ($\sim$1 mg·m^{-3}, (Giardino et al., 2014a), $\sim$11 mg·m^{-3} (Bresciani et al., 2016), up to 100 mg·m^{-3}, (Concha and Schott, 2016)). In case of S2A, Toming et al. 2016a retrieved promising results for CHL between 4 and 73 mg·m^{-3}, whereas Dörnhöfer et al. 2016b stated CHL of around 1 mg·m^{-3} too low for a solid retrieval. L8 and S2A CHL matched well with sampling results from 7 August (10-20 mg·m^{-3}) within the uncertainty range. Our

comparison with *in situ* measurements from 7 August emphasises S2A's and L8's suitability for CHL monitoring in mesotrophic-eutrophic lakes. The mismatch on 23 August with L8, however, contradicts this statement. On that day satellite measurements were in good agreement (20-25 mg·m^{-3}) whereas *in situ* CHL was on a much lower level ($\sim$5 mg·m^{-3}). Differences may result from surface scum captured by satellite and missed in the water samples (section 5.2.4). Otherwise, our sampling strategy just below the water surface may have excluded phytoplankton located deeper in the euphotic zone, which may have contributed to the satellite signal. A mixed water sample down to Secchi disk depth or profile measurements may improve the comparison between satellite and *in situ* data. Furthermore, vertical migration of cyanobacteria due to buoyancy effect can rapidly alter their concentration. Buoyancy performs most effective under stable water column conditions (Oliver et al., 2012). During the sampling on 23 August, wind speeds increased from 3.9 to 7.3 m·s^{-1} impeding a stable water column (Table 5.2). At this day, *in situ* CHL showed little variation between sampling sites and standard deviation was close to zero contrary to all other samplings. Therefore, the mismatch may also be attributed to errors in laboratory analyses such as improper pigment extraction. For MODAQ and MODTE, we compared lake average MODTE/MODAQ CHL with average *in situ* CHL. Only six out of 13 match-ups between MODTE/MODAQ and *in situ* sampling fell within the uncertainty range, suggesting a low performance of MODIS CHL retrieval. Comparing MODTE/MODAQ lake average CHL with *in situ* average may have introduced an offset, since sampling mostly focused on parts of lakes, i.e. south (LU-MV) and north (CAU/TUM). Overall, MODIS provided higher CHL values than *in situ* measurements. Furthermore, MODTE and MODAQ results also differed on days where both satellites provided valid data sets (e.g. 1 August, Fig. 5.3d or 7 July, Fig. 5.4). Politi et al. 2015 also reported such deviations and assumed MODTE sensor degradation and changes in atmospheric conditions between image acquisitions (MODAQ is 3 hours after MODTE) as possible reasons. In the match-ups (Fig. 5.3d), however, MODTE performed better than MODAQ. The cross-sensor comparison (Fig. 5.4) also shows that MODTE and L7/S2A pairs acquired within 20 minutes scattered closer to the 1:1 line, suggesting comparable results between satellites. Therefore, the observed differences between MODTE and MODAQ are probably due to changing water (e.g. buoyancy effect, sun glint) or atmospheric conditions (e.g. increasing aerosol optical thickness, water vapour content, wind speed or direction). These conditions may change rapidly; their effects on CHL retrieval are worth to be further investigated in upcoming multi-sensor constellations such as Sentinel-2 and Sentinel-3.

5.4.2 Inter-comparability based on temporal evolution

Combining different remote sensing systems and *in situ* measurements allowed generating time series of CHL and eoHAB values at Lake Kummerow. Comparing temporal development of *in situ* and satellite CHL may overcome the constraints associated with a limited number of match-ups. *In situ* and satellite CHL generally followed a similar trend with lower CHL levels at the beginning of July, and higher CHL levels in late summer/early autumn. We observed some obligations for satellite based monitoring due to bad weather conditions with high cloud coverages, which reduced the number of available satellite data – particularly in the second half of July.
A perfect match between satellite and *in situ* CHL development occurred in the first week of August when both methodological approaches described a forming algal bloom. During this week, sunshine fraction was $\geq$ 80 % leading to an increase in water surface temperatures from 17 °C to > 20 °C reaching a maximum of 24 °C on 7 August (Fig. 5.5c, d). For these temperatures, Paerl et al. 2016 reported growth rates of cyanobacteria around 80 % assuming non-nutrient limited conditions. Consequently, satellite and *in situ* CHL values increased and indicated the development of an algae bloom. EoHAB values increased accordingly (Fig. 5.5b). In mid-August, the increased eoHAB values matched well with predominating cyanobacteria indicated in the biomass analysis. Contrary, distinct discrepancies between *in situ* and satellite CHL occurred. Satellite CHL indicated an ongoing bloom event with lake average CHL > 30 mg·m^{-3}, whereas LU-MV and CAU/TUM sampling measured CHL between 5 and 7 mg·m^{-3}. We discussed presumable errors in laboratory analyses for CAU/TUM values (Section 5.4.1). Discrepancies between satellite and regular monitoring CHL (LU-MV), however, may be a result of methodological differences. Bertani et al. 2017 also observed such discrepancies during bloom events.

Cyanobacteria blooms often have patchy surface structures (Kutser et al., 2006). Depending on the sampling site and patch distribution, *in situ* CHL may be lower than satellite derived CHL data (Bertani et al., 2017). In cases, which involve a surface scum-forming bloom, satellites capture mainly the surface scum with high CHL concentrations. Water samples which were taken from below the surface may not contain surface scum (Bertani et al., 2017), which may again lead to lower CHL compared to average satellite CHL. Moreover, satellite derived CHL results from the sum of the absorption features of CHL and its degradation pigment phaeophytin-a (Trees et al., 2000). Separating CHL and phaeophytin-a is infeasible with the spectral resolution offered by sensors such as L8; the satellite based CHL therefore represents an indicator on living and degraded phytoplankton biomass. After the bloom peak in mid-August, phaeophytin-a from decaying algae may have contributed to the satellite signal; phaeophytin-a, however, was not measured *in situ* (CAU/TUM) and thus may represent a potential source of uncertainty.

5.4.3 Spatial development of an algal bloom

Spatial variation of phytoplankton depends on the variation of biological processes such as growth rate, grazing, regulated buoyancy and vertical migration (Reynolds, 2006; Winder and Sommer, 2012). The main abiotic factor driving spatial patterns of surface blooms is wind (Wu et al., 2015). Accordingly, wind conditions may explain the spatial patterns of the surface bloom at the beginning of August. Rainfalls and strong westerly winds at the end of July, which mixed the surface layer and increased nutrient availability (Winder and Sommer, 2012), probably initiated the first summer phytoplankton bloom in 2015. Phytoplankton started to grow in the southern part of the lake (inflows) on 1 August (Fig. 5.6a). Until the next MODAQ data acquisition on 3 August (Fig. 5.6b), high sunshine fraction strongly increased water surface temperature (Fig. 5.5c, from 17 °C to 24 °C) which resulted in a homogenous distribution of slightly higher CHL concentrations. Wind direction of around 250° before 5 August pushed phytoplankton towards the northern part of the lake, which was visible as high CHL area in the respective MODAQ data. The wind speed decreased below 2 $m \cdot s^{1}$ so cyanobacteria, which favour calm conditions (Harke et al., 2016), may have upwelled towards the surface. Similarly, the eoHAB indicator increased (Fig. 5.5b). Predominating easterly/ south-easterly winds with wind speeds up to 7 $m \cdot s^{1}$ resulted in an accumulation of higher CHL along the western lake region during S2A data acquisition (Fig. 5.6d). MODTE captured a similar pattern (Fig. 5.6e); average CHL, however, was higher since the large pixel sizes missed the low concentrations in the western lake region. 12 hours before L8 data acquisition, wind directions alternated between 90° and 320° with varying wind speeds, which may have resulted in the relatively homogenous distribution of CHL (Fig. 5.6f). The spatial resolution of L8 and S2A enabled a detailed view of spatial CHL patterns, which point-based sampling is unable to provide. These sensors may therefore help reducing uncertainties in ecological status classification (Søndergaard et al., 2016). Furthermore, public authorities or agencies may use these data to monitor the spatial development of blooms, to timely detect anomalies at bathing places (Potes et al., 2011) or to enhance site-specific management (Mercado et al., 2016).

5.4.4 Integration of satellite data into trophic state assessment

Søndergaard et al. (2016) proposed the integration of remote sensing into lake monitoring to reduce uncertainties in ecological status classification originating from spatial variability. We therefore tested the impact of integrating satellite CHL on the trophic class assessment at Lake Kummerow. According to German WFD assessment (Riedmüller, 2014) of 2015, Lake Kummerow achieved the status mesotrophic 2 (trophic index = 2.44) which meets its potential natural trophic class (mesotrophic LU-MV, 2015a). Substituting the LU-MV CHL values (July, August and September) by satellite average CHL resulted in the class eutrophic 1. This was mainly due to differences in satellite values in July and August, which were significantly higher (2.5-3 times) than *in situ* measurements. Particularly in August, LU-MV *in situ* monitoring (despite observing two sampling sites) seemed to miss the spatio-temporal variability of CHL as well as the bloom development. Using the monthly minimum and maximum satellite measurements intended to cover the temporal dynamics of CHL in the trophic

classification; two different trophic classes were the result. Temporal dynamics of CHL therefore may have an impact on the trophic classification, in particular when a lake is at the transition between two classes. Fig. 5.6 and the vertical bars in Fig. 5.5a emphasised a spatially variable CHL, which was supported by the gridded monthly averages of CHL (Fig. 5.8a-c). A spatially distributed trophic classification resulted in a predominantly eutrophic 1 lake. Using the satellite monthly average without addressing spatial variability yielded the same class. Nevertheless, neglecting the spatial variability misses eastern parts of the lake, which were classified as mesotrophic 2. Although the lake is well mixed and relatively uniform in shape, integrating spatial variability of CHL reveals spatially variable trophy. We assume such patterns to be more pronounced in lakes with higher shoreline development. In this study, Secchi disk depth and phosphorous concentrations remained spatially constant. Since nutrients lack optical influence in natural waters, optical remote sensing hardly can provide spatial information on phosphorous concentrations; approaches for estimating Secchi disk depth (Lee et al., 2015b) or indicators of transparency (references in Dörnhöfer and Oppelt, 2016) exist. Remote sensing may introduce temporal irregularities into a currently systematic *in situ* sampling scheme. Due to the dependence on cloud-free conditions, satellite data availability can lead to data gaps. Similar to different *in situ* or laboratory measurements, different sensors perform with different accuracies. Remote sensing can increase the number of observations and spatial variability of certain indicators used for trophic state assessment. Its integration into trophic state assessment would be associated with new challenges, which are worth to be investigated:

- combining temporally regular and irregular data
- fusing spatially variable and constant data
- integrating data from sensors with different accuracies

In our analysis, remote sensing data indicates that existing management strategies based on *in situ* data are incapable of reducing nutrient inputs to such an extent that the lake regain its natural trophic class. Bresciani et al. 2011c also reported misclassifications of lakes when based solely on *in situ* measurements. Their conclusions as well as a study of Kiefer et al. 2015 support the results of the present analysis that the spatio-temporal detail of satellite data is well placed to assist examining appropriate *in situ* monitoring sites.

5.4.5 Integrated multi-sensor monitoring of lakes

The overarching aim of this study was to evaluate the inter-comparability of CHL derived from different sensors and *in situ* measurements to promote a multi-sensor use for lake monitoring. A comparison of satellite and *in situ* based time series revealed a reasonable and generally similar development. Some discrepancies, especially during bloom events, may be due to methodological differences (Bertani et al., 2017). Referring to a limited *in situ* data set, S2A and L8 yielded promising results; match-ups with MODIS indicated a varying performance. Nevertheless, we have to bear in mind that satellite and *in situ* measurements rely on different methodological approaches, i.e. the former is based on a measurement of radiation from a large volume of water while the latter is a result of photometric measurement of a few millilitres of water in a laboratory. Such comparisons are inevitable; however, we should keep in mind their limited comparability. We therefore recommend using uncertainty ranges rather than aiming exact matches. Outliers of both satellite and *in situ* data further emphasised that neither approach should be credited without any doubts. Comparing CHL from S2A/L8/L7 with CHL from MODIS helped to overcome the general limitation of upscaling *in situ* measurements to satellite level.
Clouds and unfavourable meteorological conditions which complicate atmospheric correction and the subsequent CHL retrieval are the main shortcomings of optical remote sensing (Harvey et al., 2015). Cloud cover also reduced the number of suitable satellite scenes in our study. The high frequency of MODIS observation, however, significantly contributed to the large number of satellite observations. Using single MODIS pixel for analysing Lake Kummerow was ineffective leading to a further limitation, i.e. spatial resolution and subsequent problems with mixed pixels and adjacency effects. Using average values of 10-40 MODIS pixels, however, resulted in an unexpected reasonable match within the time series development. This finding also supports results of Matthews et al. 2010 who used average values of around 20 MERIS pixel when analysing algal blooms

at Lake Zeeklovei, South-Africa. The time series investigated emphasised a significant increase of temporal information when integrating multi-sensor data, i.e. sensors with high spatial/low temporal and low spatial/high temporal resolution. Future studies may therefore also integrate the OLCI instrument on board of Sentinel-3 with a spatial resolution of 300 x 300 m^2 (Berger et al., 2012).
There are other studies which discussed benefits of remote sensing due to the increased temporal information (e.g. Bresciani et al., 2011c; Matthews, 2014; Palmer et al., 2015c). Recently, Bresciani et al. 2016 detected a strong cyanobacterial bloom in Italian lakes in October and November, which standard monitoring programs (April to September) were unable to capture. We observed a similar situation at Lake Kummerow; rising eoHAB values indicated an algae bloom at the beginning of October which official WFD monitoring was missing. The World Health Organisation guidelines, however, recommend detailed analysis of potentially toxic cyanobacteria for CHL $\geq$ 10 mg·m^{-3} (Chorus et al., 2000), which would have applied to Lake Kummerow (> 20 mg·m^{-3}).
A synergetic use of suitable high spatial resolutions sensors, i.e. S2A and L8, in combination with the high temporal resolution of MODIS theoretically provides daily coverage, which increases the chance for cloud-free observations and a consistent monitoring of surface CHL. It may further improve observing, modelling and understanding ecological processes in lakes and their response to current stressors. Remote sensing cannot provide information on the toxicity of cyanobacteria (Stumpf et al., 2016) but a remote sensing based monitoring may support preventive health care at recreational sites. Additional integration of *in situ* sampling may cover cloudy periods as well as the vertical variability of CHL and additionally provides detailed information on phytoplankton species.

5.5 Conclusions

In the present study, we combined different sensors (MODTE, MODAQ, L7, L8, S2A) and *in situ* data to analyse a time series of CHL and eoHAB (indicator of cyanobacteria presence) at Lake Kummerow, Germany, during summer 2015. To ensure a comparable and consistent data processing for atmospheric correction and retrieval of hydro-biological parameters we applied the physically based model MIP using a standard parameterisation for oligo- to hypertrophic lakes. MIP-CHL products revealed a temporal development, which corresponded reasonably well with *in situ* data and weather conditions. Methodological differences between satellite and *in situ* measurements may have accounted for discrepancies observed in the CHL time series. Analysis and discussion of uncertainties for *in situ* and satellite data is crucial. Providing pixel based uncertainty measures, may increase confidence of end-users. They often doubt satellite products, while *in situ* data are considered as being the absolute truth. For *in situ* CHL, the present study revealed an uncertainty range of 48 %; for a valid discussion of results we therefore recommend the use of uncertainty measures for both, *in situ*and remote sensing data, to overcome the call for a perfect match.
Data derived from high spatial resolution (L7, L8, S2A) offered details on spatial patterns in surface CHL and phytoplankton blooms, which could be explained by prevailing wind conditions. By using temporally and spatially highly resolved information, end-users such as local authorities may optimise existing monitoring or management strategies. Comparisons based on limited *in situ* data showed promising results for L8 and S2A, but require further quantitative assessments. Satellite data enabled detecting phytoplankton blooms in early August and at the beginning of October which *in situ* monitoring was missing. The study also showed that combining remote sensing and *in situ* measurements offers great potential for trophic state assessment; integration of satellite data led to a more reliable trophic classification, which also highlights the importance of adequately considering the spatio-temporal variability of CHL in monitoring approaches.
Remote sensing may improve the existing monitoring of phytoplankton and cyanobacteria of lakes. Combining data from different satellite sensors with high spatial/low temporal and low spatial/high temporal resolution allows a theoretically daily coverage. The former provide spatial detail whereas the latter may fill time gaps by using lake average values. Satellite and *in situ* measurements, however, do have limitations and contain uncertainties in representing the actual conditions of a lake. A combined approach, which integrates traditional

in situ sampling and multi-sensor satellite products, enhances phytoplankton and cyanobacteria assessment and therefore may be a step towards a holistic monitoring of lakes.

Acknowledgements: We thank the anonymous reviewers for their effort and helpful comments. This work was conducted within the project LAKESAT (grant no: 50EE1340) funded by the Federal Ministry for Economic Affairs and Energy, Germany. We thank Christine Fritz (TUM) and Dr. Thomas Schneider (TUM) for laboratory analyses of CHL (LAKESAT grant no: 50EE1336). We acknowledge the Mecklenburg-Vorpommern Ministry for Agriculture, Environment and Consumer Protection for data supply from the lake monitoring programme. We further thank the USGS for providing Landsat 8, Landsat 7 and MODIS data. Many thanks are due to ESA for providing Sentinel-2A data.

Chapter 6

Water colour analysis of Lake Kummerow using time series of remote sensing and *in situ* data

Katja Dörnhöfer, Jorrit Scholze, Kerstin Stelzer and Natascha Oppelt
Journal of Photogrammetry, Remote Sensing and Geoinformation (2018), doi:10.1007/s41064-018-0046-3
Received: 19 September 2017, Accepted: 29 March 2018

Changes made to the published version:
To harmonise the style of the entire thesis, cross-references to figures are noted as Fig. instead of Figure. In case of value ranges units are only written after the second value.

Abstract

Monitoring water constituents of lakes using satellites is gaining increasing importance. Image archives of historic satellites represent valuable data sources to analyse the development of constituent concentrations over time and to derive trends. This study presents an analysis of the MERIS archive (2003-2011) using a neural network algorithm (FUB/WeW) to retrieve concentrations of Chlorophyll-a, total suspended matter and absorption by coloured dissolved organic matter (440 nm) at Lake Kummerow. All three constituents showed a clear seasonality: chlorophyll-a (0.3 - 45.8 $mg \cdot m^{-3}$) exhibited a spring bloom and multiple blooms during summer. Total suspended matter (0.1 - 10.0 $g \cdot m^{-3}$) and coloured dissolved organic matter (0.01 - 0.94 m^{-1}) revealed highest values during summer and lower values during autumn/winter. While total suspended matter (-1.3 $g \cdot m^{-3}$) and chlorophyll-a (-3.4 $mg \cdot m^{-3}$) showed a decreasing tendency from 2003-2011, coloured dissolved organic matter showed no clear trend. Chlorophyll-a retrieved from MERIS was around 20 % higher than *in situ* measurements. The other constituents (total suspended matter and coloured dissolved organic matter) were obtained by qualitative analysis due to the absence of *in situ* measurements. This analysis provides a first multi-year time series on these constituents over the whole lake and all seasons. Both, its size and its form, make Lake Kummerow a suitable lake for remote sensing validation activities. Recent and upcoming satellites, especially of the Sentinel missions, will provide further valuable information for integrating remote sensing into lake monitoring.

Keywords

inland waters, seasonality, spatial patterns, trend analysis

6.1 Introduction

Humans benefit from several ecosystem services offered by lakes including flood regulation, energy production, water and food supply, and recreational activities (Artell, 2013; Reynaud and Lanzanova, 2017). Moreover, lakes provide habitat for various species and are crucial components of nutrient, carbon and hydrological cycles (Moss 2012). Lake ecosystems, however, are seriously threatened by global change (Millennium Ecosystem Assessment, 2005); Climate change, intensified agricultural use and wastewater discharge have led to globally increasing nutrient concentrations and rising trophic levels (Rose et al., 2017; Smith and Schindler, 2009; Winder and Schindler, 2004). Thus, global change affects lakes directly or indirectly, i.e. via changes in their catchment (Adrian et al., 2009; Williamson et al., 2009). Changing lake condition and water quality also mirrors changes in the environmental status of the catchment (Randsalu-Wendrup et al. 2016). To understand and manage lake water quality, particularly in the context of global change, we need to understand how and why lakes respond to different drivers across space and time (Rose et al., 2017).

Passive remote sensing systems allow a spatial-temporal monitoring of water quality parameters that are optically active, i.e. that affect lake water colour through scattering and/or absorption (IOCCG, 2000). Prominent examples are chlorophyll-a (CHL), total suspended matter (TSM) and coloured dissolved organic matter (CDOM).

CHL is highly correlated with phytoplankton biomass and therefore a common indicator of lake trophic state (Solheim et al., 2013). In nutrient-rich, temperate lakes CHL typically exhibits a seasonal development with a spring bloom (high concentration) followed by a clear water phase (low concentration) and one or more blooms with very high concentrations during summer and autumn (Reynolds, 2006). Information on winter CHL is rarely available but it is expected to be considerably lower than in summer (Hampton et al., 2017). Remote sensing takes advantage of the specific absorption features located between 440 nm and 560 nm and at around 670 nm (Matthews 2011) but may also benefit from fluorescence maxima (e.g. fluorescence line height algorithm at 685 nm in Palmer et al., 2015a).

TSM consists of organic (detritus) and inorganic components (mineral particles) which enter the lake via tributaries (catchment erosion). TSM therefore represents an important carrier of nutrients and contaminants. In shallow lakes, wind-induced resuspension of bottom sediments and degrading phytoplankton may increase the TSM content in the water column (Madsen et al., 2001). Most remote sensing algorithms focus on the backscattering properties of TSM, which decline from 350 to 900 nm. In mineral-rich waters, however, TSM may also act as absorber that reduces the light penetration depth of the lake (Eder et al., 2016; Giardino et al., 2010b). High TSM concentration has a masking effect on the absorption features of CHL and CDOM.

CDOM is the optically active component of dissolved organic carbon (DOC). It is often considered as an indicator for DOC (Brezonik et al., 2015; Toming et al., 2016b) which in turn is an important response variable of lakes to climate change (Adrian et al., 2009). Statistical relationships between DOC and CDOM can vary within in a lake in space and time due to the variability of external inputs from the catchment or of lake internal production from phytoplankton or macrophytes (Hestir et al., 2015b). The spectral behaviour of CDOM exhibits an exponentially decreasing absorption from 350 to 900 nm. Its highest absorption in the blue wavelengths interferes strongly with the high absorption of CHL in this wavelength region.

The above-mentioned water constituents and their concentrations are related to processes in the catchment of a lake. CHL is a regularly monitored parameter within the European Water Framework Directive (Pasztaleniec, 2016). Less detailed information is available for CDOM and TSM. In this study, we therefore conducted an analysis of the MERIS archive to investigate the spatial-temporal development of water constituent concentrations in Lake Kummerow. To do so, we retrieved the first multi-year time series (2003-2011) on water constituents (CHL, TSM, CDOM) at Lake Kummerow using a well-established algorithm designed for MERIS data. Our specific aims were (1) to analyse the temporal development and trends, (2) to figure out seasonal cycles and (3) to map spatial patterns of water constituents.

6.2 Study area and *in situ* data

Lake Kummerow (53.808°N, 12.856° E, size: ∼32.5 km^2), Germany, formed as a proglacial lake during the last glacial period (Pomeranian stadium during Weichsel glacial). The wind-exposed location and the relatively shallow depth (average 8.1 m) cause a polymictic character. Thermal stratification rarely occurs during warm and windless summer days. The 'West Peene' in the south and 'Kleine Peene' in the west are the main inflows. The 'Peene' outflow is located at the northern end of lake (Fig. 1). The low gradient from the lake's outflow to the Baltic Sea (0.2-0.5 m) often leads to wind-induced backwater effects; these backwater effects mainly influence the northern part of the lake. The water residence time is less than 2 years (Wöbbecke et al., 2003). Sediment core analysis revealed a eutrophic development since several thousand years (Kalbe and Werner, 1974). Anthropogenic activities in the lake catchment such as deforestation, agricultural use and wastewater discharge have amplified eutrophication for the last 150 years. Today, agricultural cultivation (51.4 %) predominates the land use in the catchment (size: ∼1,150 km^2) followed by forests (19.1 %) and grasslands (17.1 %). Several bathing places and other water activities (e.g. sailing, windsurf, canoe, and fishing) make the lake a popular touristic area. Nevertheless, the shoreline remains an important breeding and resting area for waterfowl.

The lake's catchment is part of the terrestrial validation site 'Durable Environmental Multidisciplinary Monitoring Information Network' (DEMMIN; Borg et al., 2014). Located east of Lake Kummerow, DEMMIN represents an agricultural landscape of approximately 30,000 ha in the German North-Easthern Lowlands Observatory of TERENO (TERrestrial ENvironmental Observatory; Bogena et al., 2012). The lake's catchment partly covers and its outflow (river 'Peene') crosses DEMMIN as direct environmental connection. This special location, therefore, makes Lake Kummerow a connecting and integrative element of this intensively monitored landscape.

Since 1998, the lake monitoring programme of the federal state Mecklenburg-Western Pomerania (LU-MV) regularly samples (each year 4-6 times from March to October) two measurement sites (Fig. 6.1). Measurements include CHL, water temperature, pH, oxygen concentration/ saturation, Secchi disk depth, total and dissolved organic carbon, and nutrient concentrations from the surface to the lake bottom (see Dörnhöfer et al., 2018a). CHL photometric estimation of water samples follows DIN 38412-L16. Sampling also showed that diatoms (*Bacillariophyceae*) predominate the spring bloom whereas cyanobacteria, i.e. toxin producing *Microcystis spp*, prevail during summer blooms (LU-MV, 2016; Wöbbecke et al., 2003).

6.3 Earth observation data and methodology

6.3.1 MERIS data and image processing

MERIS (Medium Resolution Imaging Spectrometer) full swath geo-corrected full resolution datasets from 1 Jan 2003 to 31 Dec 2011 formed the basis for this study. The MERIS sensor operated in push-broom mode providing fifteen spectral channels between 412 and 900 nm with a spatial resolution of 300 x 300 m^2 on the ground (Bezy et al., 1999). MERIS was on board of the sun synchronous polar orbit earth-observation satellite ENVISAT at an altitude of 790 km, which terminated its operation on 9 May 2012. The last MERIS image was recorded on 8 April 2012.

MERIS acquired data of Lake Kummerow every one or two days. Cloud coverage, other atmospheric influences and influence by sun glint reduced the number of acquisitions suitable for data analysis. The processing of the MERIS data has been performed in four processing steps, which were all implemented in an automated processing chain. The processing steps comprised pre-processing, atmospheric correction, in-water retrieval and post-processing. All processing steps were conducted on the Calvalus cluster at Brockmann Consult, which holds the full MERIS archive and dedicated parallelised processing infrastructure. Pre-processing comprised improving the geometric correction with AMORGOS (Bicheron et al., 2011), the Coherent Noise Equalisation for reducing the striping (Bouvet and Ramino, 2010) and a smile correction which corrects small wavelength variations of each pixel along the image (Bourg et al., 2008; Delwart et al., 2010). Finally, the IdePix tool in

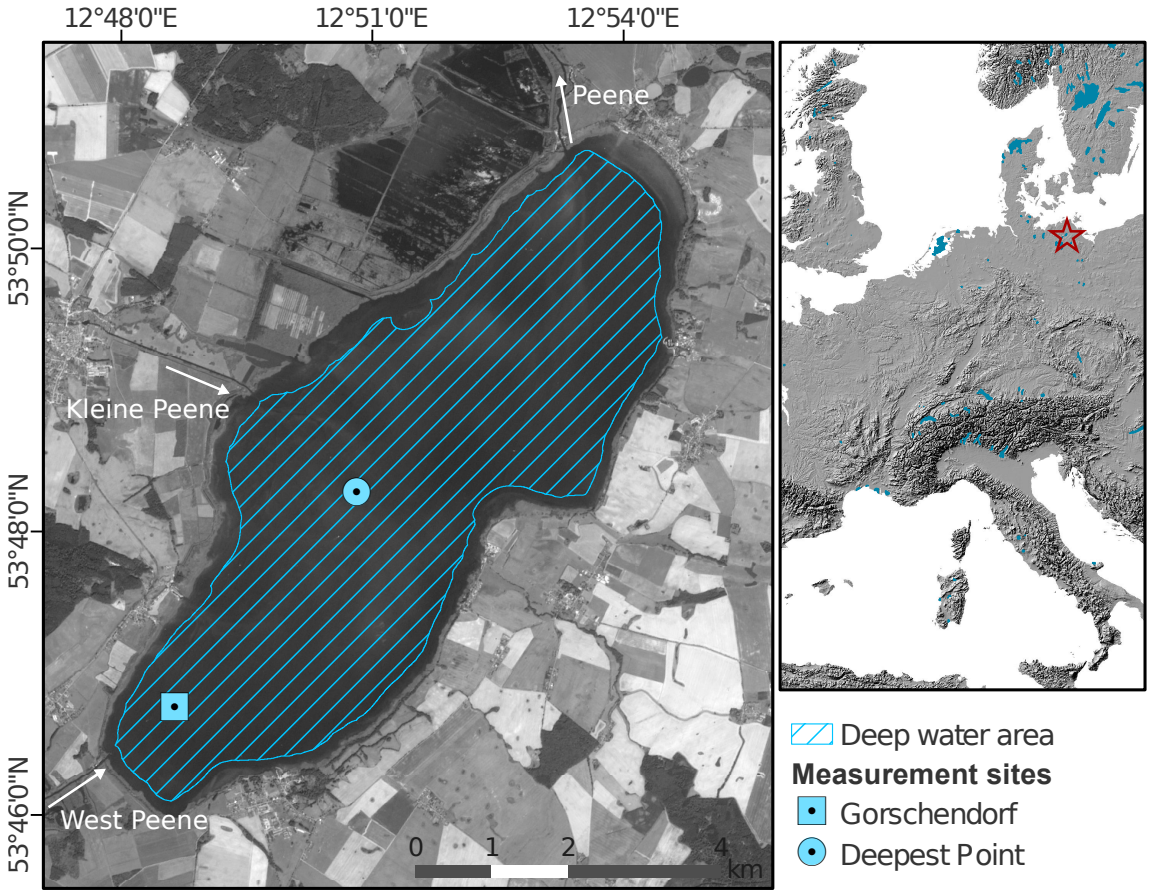

Figure 6.1: The study area Lake Kummerow and the location of measurement sites of the Ministry for Agriculture and Environment Mecklenburg-Western Pomerania. Water depth at measurement site Gorschendorf is 3 m and 22 m at site Deepest Point.

BEAM identified valid pixels including cloud and cloud shadow detection (Odermatt et al., 2015). The cloud detection with IdePix combines the output of a neural net with spectral tests. The neural net is trained with manually selected pixels of clouds, semi-transparent clouds and all kinds of clear surfaces. The cloud shadow is derived by the sun and viewing geometry and the cloud top height.

Adjacency effects caused by light scattering reflected from surrounding land surfaces towards the sensor strongly influence remote sensing data of inland waters. They result in higher radiances at the sensor at near-shore pixels compared to central lake pixels. To correct adjacency effects, we used the ICOL (Improved Contrast Between Ocean and Land) algorithm (Santer and Zagolski, 2000). MERIS studies which applied ICOL produced ambivalent results showing an improvement of subsequent analyses (e.g. Beltrán-Abaunza et al., 2014; Kallio et al., 2015; Philipson et al., 2016) but also generation of artefacts (e.g. Kiselev et al., 2015). In this case study, FUB/WeW results showed a higher consistency with applying ICOL.

ICOL corrects the measured signal for the adjacency effect and returns TOA (top of atmopshere) reflectances as they would have been measured without adjacency effect. Therefore, Rayleigh scattering and Fresnel reflectance at pixels close to land (distance < 30 km) are corrected and an aerosol model determines and corrects aerosol concentration for each pixel. The adjacency corrected TOA reflectances formed the so-called L1c product (Santer and Zagolski, 2000). This procedure was performed for the MERIS bands 1-10 and 12-14, which subsequently were the input for atmospheric correction and water constituent retrieval with the FUB algorithm.

To assess water constituents, i.e. CHL, TSM and absorption of CDOM at 440 nm, we used the FUB/WeW (hereafter FUB) processor developed by Freie Universität Berlin (FUB). The FUB algorithm (Schroeder et al.,

2007a,b) uses MERIS data as an input and comprises four separate artificial neural networks, which are trained with extensive radiative transfer simulations using the MOMO code (Fell and Fischer, 2001; Fischer and Grassl, 1984).

MOMO assumes a coupled atmosphere-ocean-system with plane parallel, horizontally homogeneous model layers subdividing the atmosphere and the water body (Schröder, 2005). The US-standard-atmosphere predefines the vertical distribution of the atmosphere into 11 layers. The simulation of the water body is implemented within three model layers (lowest at 500 m) assuming a rough surface and no reflectance from the bottom but neglecting foam on the surface. FUB further assumes a homogenous vertical concentration of each water constituent. Table 6.1 summarises concentration ranges for which the neural networks are trained.

Table 6.1: Concentration ranges of FUB (FUB/WeW MERIS processor developed by Freie Universität Berlin), where CHL = Chlorophyll-a , TSM = total suspended matter, CDOM = coloured dissolved organic matter.

Parameter	Minimum	Maximum	Unit
CHL	0.050	50	$mg \cdot m^{-3}$
TSM	0.050	50	$mg \cdot m^{-3}$
CDOM (440 nm)	0.005	1	m^{-1}

The four neural nets perform the atmospheric correction and the retrieval of each water constituent separately. The neural net for the atmospheric correction retrieves the aerosol optical thickness (AOT) and bottom of atmosphere (BOA) reflectance, while the other three retrieve water constituents directly from TOA reflectance.

Fig. 6.2 illustrates the FUB principle; the input vectors are L1c TOA remote sensing reflectance (RS_{TOA}), i.e. MERIS-Bands 1-7, 9, 10, 12-14 and geometric parameters x, y, z, sun zenith angle ($cos(\theta_O)$), surface air pressure (P) and wind speed (WS). The output vectors are logarithmic concentrations of CHL, TSM and CDOM, the aerosol optical depth for MERIS bands 2, 5, 7, 13 and water leaving reflectance for MERIS bands 1-8 (Schröder, 2005).

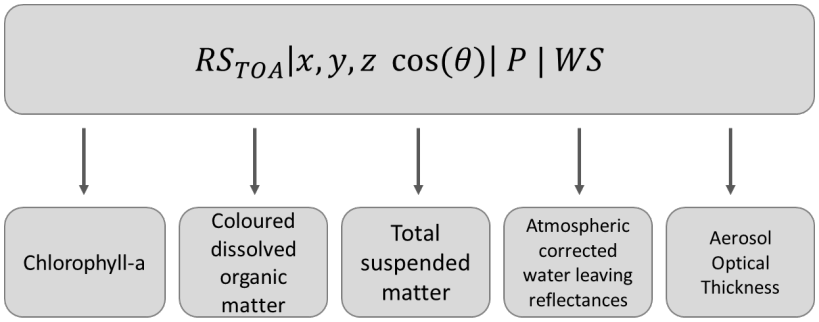

Figure 6.2: Flowchart of the direct algorithm, with the transformation of the geometry parameters $x = sin(\theta_O) \cdot cos(\Delta\phi)$, $y = sin(\theta_O) \cdot sin(\Delta\phi)$, $z = cos(\theta_O)$ where θ_O the MERIS zenith angle and $\Delta\phi$ is the azimuth difference (adopted from Schröder, 2005). RS_{TOA}=adjacency corrected TOA reflectance, P = surface air pressure, WS = wind speed.

Finally, the post-processing steps included spatial and temporal aggregation and time series generation (Sections 6.3.2 and 6.3.3) for the years 2003 to 2011. These steps were applied to all processed MERIS data and required a careful selection of valid pixels for all subsequent analysis steps. Table 6.2 lists all temporal and spatial aggregations used for the time series generation. To include only valid data for further analysis, we applied a valid-pixel-expression excluding pixels with the following flags:

- LAND Flag (=land pixels, also if covered by clouds)
- MIXPIXEL Flag (=mixed pixels of land and water)
- CLOUD Flag (=cloud covered pixels)

- CLOUDBUFF Flag (= pixel is located in a buffer zone around clouds; here: 2 pixels buffer)
- CLOUDSHADOW Flag (=pixel is influenced by cloud shadows)
- CHL_OUT Flag (= pixel CHL > 50 $mg \cdot m^{-3}$, i.e. is higher than FUB training range)
- AOT Flag (= pixel has an AOT > 1.0 at 440 nm))

To avoid analysis of pixels with signals of the lake bottom, we additionally excluded optically shallow water using the 2 m water depth line and a 100 m buffer from this depth line (Fig. 6.1; LU-MV, 2002b).

Table 6.2: Overview of temporal and spatial aggregation applied for the MERIS time series analyses. Long-term means a temporal aggregation over the entire period 2003-2011; short-term means a temporal aggregation separately for each year. CHL = Chlorophyll-a, TSM = total suspended matter, CDOM = coloured dissolved organic matter.

	Temporal aggregation	Spatial aggregation	Description	Results
CHL	$\pm$ 1 day	• mean of 3x3 pixel buffer • standard deviation of 3x3 pixel buffer • site Gorschendorf • site Deepest Point • $\geq$ 4 valid pixels in buffer	Section 6.3.2	Fig. 6.5
CHL, TSM, CDOM	daily	• lake-wide median • $\geq$ 50 valid pixels	Section 6.3.3	Fig. 6.4a, 6.9a
CHL, TSM, CDOM	monthly (short-term)	• lake-wide mean • lake-wide standard deviation	Section 6.3.3	Fig. 6.4a, 6.5, 6.7a, 6.7b, 6.9a
CHL, TSM, CDOM	monthly (long-term)	• lake-wide mean • lake-wide standard deviation	Section 6.3.3	Fig. 6.4c, 6.7a, 6.4c
CHL, TSM, CDOM	monthly (long-term)	• per pixel	Section 6.3.3	Fig. 6.6, 6.8

6.3.2 Evaluation

To evaluate the MERIS FUB products, we compared CHL from *in situ* measurements (LU-MV data) and CHL retrieved from MERIS products. We extracted the arithmetic mean and standard deviation from a 3 x 3 pixel buffer (i.e. macro-pixel) around the measurement site. To avoid inclusion of insufficiently masked pixels, we only considered pixel buffers covering at least four pixels. To reduce uncertainty due to spatially and temporally rapidly changing constituent concentrations, we only included *in situ* and MERIS data acquisition which differed a maximum of $\pm$1 days. We conducted linear regression analyses between *in situ* measurements and MERIS retrievals for each measurement site and for the combined data set. Outlier value pairs may strongly affect the results of regression analysis analyses. To omit such value pairs we first conducted a linear regression based on a 99 % confidence interval of the whole data set (n=28). Using R, we then calculated the studentized regression residuals (n=3) and determined three value pairs which were outside a 99 % confidence interval. For developing regression models such outlying value pairs are standardly excluded to improve fit quality (e.g. Matthews et al., 2012). We applied this procedure to account for potential uncertainties of *in situ* measurements and FUB algorithm in the matchup analysis, which may lead to few value pairs biasing a linear regression analyses. In order to remain transparent, we calculated the evaluation measures including and excluding value pairs strongly influencing the regression analyses.

We used the R package hydroGOF (Zambrano-Bigiarini, 2014) to calculate the root-mean-squared-error (RMSE), the normalised RMSE deviation (nRMSE), the mean average error (MAE) and the percentage bias (pBias). We further calculated the Pearson's correlation coefficient (r) and provided the regression equations.

6.3.3 Temporal development and trend analysis

To analyse the temporal development and trend of each water constituent for the entire lake we calculated the median of all valid water pixels of each MERIS acquisition, with at least 50 valid pixels (see Section 6.3.1, Ta-

ble 6.2). Furthermore, monthly arithmetic means and standard deviation (short-term) were calculated from all valid lake pixels for each year. Calculating anomalies based on daily medians aimed to detect single events, seasons or years with irregular concentrations in the time series. Anomalies were estimated similarly to the methodology provided by Matthews (2014). Long-term monthly means were retrieved from the entire time series. The anomaly based on the daily medians (CONSTITUENT') is defined as the difference between the daily median concentration ($CONSTITUENT_{Median\_day}$) and the long-term monthly average concentration ($CONSTITUENT_{Monthly\_Mean\_2003\text{-}2011}$).

$$CONSTITUENT' = (CONSTITUENT_{Median\_day}) - (CONSTITUENT_{Monthly\_Mean\_2003-2011}) \quad (6.1)$$

Thus, we could reduce the effect of seasonal variability by both, highlighting anomalies and performing a trend analysis (Matthews, 2014). By calculating a linear regression between anomalies and time, we retrieved the temporal trend of each constituent. We further calculated the linear trend of yearly arithmetic means. For CHL, *in situ* data was available. We therefore calculated anomalies and trends additionally based on the measurements at the site Deepest Point.

To analyse the seasonal cycles and development within one year, we calculated monthly arithmetic means of the entire lake for each water constituent and each year. Furthermore, seasonal cycles (2003 -2011) of each constituent were derived from daily arithmetic mean data of the entire lake. For CHL, we conducted the same calculations based on the *in situ* data of site Deepest Point. In case of CDOM, we also included measurements of dissolved organic carbon (DOC) as provided by LU-MV at the same site.

To figure out long-term monthly spatial differences, we calculated arithmetic means per pixel for each month based on the entire time series (2003-2011).

6.4 Results and discussion

6.4.1 Evaluation

Only 6 out of 50 sampling dates matched with the MERIS acquisition. Including value pairs with $\pm$ 1 day difference resulted in 25 observations at two sampling sites (Fig. 6.3). *In situ* measured CHL and MERIS CHL showed a significant linear correlation (Table 6.3). For concentrations > 10 mg·m^{-3} MERIS CHL tended to be higher than *in situ* measured CHL concentrations; for concentrations below 10 mg·m^{-3} MERIS CHL was lower than *in situ* values. Evaluation measures and regression coefficients, however, indicated a better match at site Gorschendorf (Table 6.3). Pearson's r (Table 6.3) indicated a higher correlation between *in situ* samples and MERIS CHL taken on the same day, but they have a higher pBias than the regression based on the entire data set. Compared to statistical requirements, the number of included value-pairs is, however, too low to make a definite statement.

Table 6.3: Linear regression coefficients and evaluation measures calculated between MERIS and *in situ* Chlorophyll-a. n = number of value pairs, pBias = percentage bias, MAE = mean average error, RMSE = root mean squared error, nRMSE = normalised RMSE. The first line contains evaluation measures including outlier value pairs, all other lines excluded outlier value pairs (n=3) in the calculations.

Match-up aggregation	n	regression	Pearson's r	p-value	pBias [%]	MAE [mg·m^{-3}]	RMSE [mg·m^{-3}]	nRMSE [mg·m^{-3}]
Total (incl. outlier value pairs)	28			0.0054	18.1	8.31	11.31	28.1
Total	25	y=-0.08+1.2·x	0.78	<0.0001	20.3	6.55	8.58	26.6
Gorschendorf	9	y=-0.40+1.25·x	0.92	0.0003	21.9	4.69	6.01	19.1
Deepest Point	16	y=0.55+1.16·x	0.69	0.0016	19.5	7.61	9.73	36.6
Same day	10	y=4.79+1.10·x	0.85	0.0009	51.3	6.23	7.19	32.8

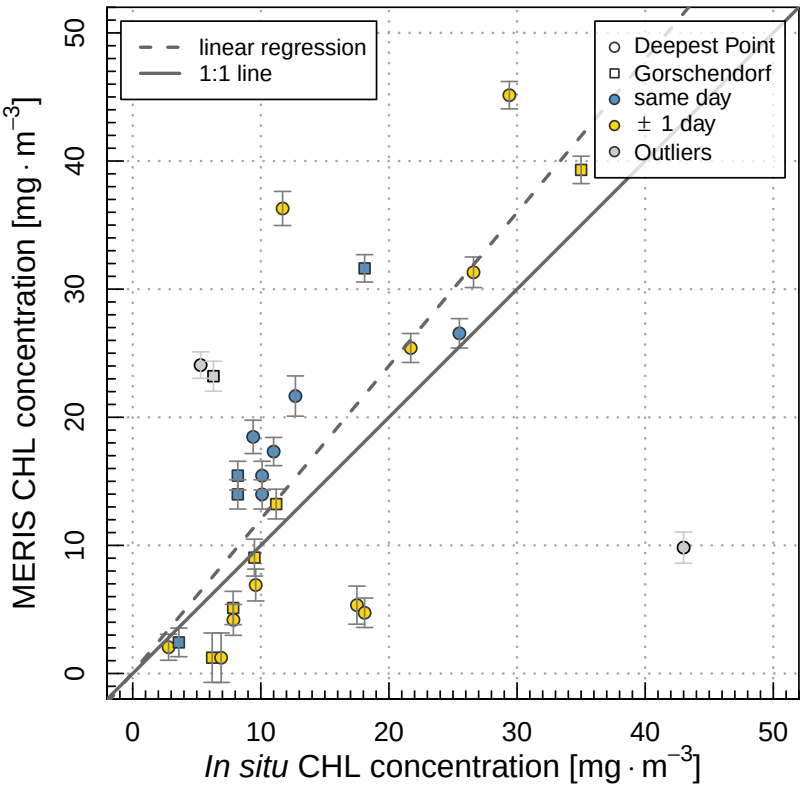

Figure 6.3: Scatterplot between MERIS Chlorophyll-a (CHL) and *in situ* measured CHL at sampling sites Gorschendorf and Deepest Point. Outliers (n = 3) excluded from the regression analysis are highlighted in light grey. Vertical bars indicate standard deviation within a MERIS macro-pixel (3 x 3 pixel buffer).

Comparisons between *in situ* collected water samples and satellite derived concentrations are a common way to assess the accuracy of remotely sensed water products (Dörnhöfer and Oppelt, 2016; Odermatt et al., 2012). The present evaluation of FUB CHL retrieval at Lake Kummerow achieved similar accuracies and tendencies as other studies using FUB: Philipson et al. (2016) obtained a Pearson's r of 0.85 for CHL at the CDOM-rich Lake Vänern, whereas MERIS CHL tended to be higher than *in situ* data. At the eutrophic-hypertrophic Lake Balaton, Palmer et al. (2015b) observed similar high correlations (Pearsons'r = 0.81), whereas MERIS CHL was on average 45.4 % (nRMSE) higher than *in situ* CHL (RMSE: 3.83 mg·m^{-3}). Recalibration equations obtained from matchups often serve as local adaptation to increase the correspondence of *in situ* and satellite data (e.g. Philipson et al., 2016). These approaches imply that *in situ* data are the absolute truth. Some studies, however, discovered uncertainties of *in situ* CHL ranging between 28 % (McKee et al., 2014) and 48 % (Dörnhöfer et al., 2018a); AQS reported even higher deviations of 130 % in a round robin test (AQS, 2008). We also have to consider that *in situ*-satellite comparisons suffer a distinct scale gap; comparing CHL from a water sample (few litres) and CHL retrieved from an area of 0.81 km^2 (3 x 3 pixel buffer) is problematic and may be misleading. Aside from the scale gap, existing differences may be due to erroneous *in situ* and/or satellite retrieval. Dörnhöfer and Oppelt (2016) therefore recommended using uncertainty ranges rather than expecting exact matches.

6.4.2 Seasonal cycles, trends and spatial patterns of CHL

During the period 2003-2011, MERIS CHL averaged for the entire lake varied between 0.3 (29 May 2005) and 45.8 mg·m^{-3} (3 September 2007). *In situ* CHL ranged between 2.0 (7 June 2010) and 69.6 mg·m^{-3} (5 August 2003). Site Gorschendorf (mean = 15.7 ±12.8 mg·m^{-3}) exhibited a slightly higher average and higher variability

of CHL than the site Deepest Point (mean = 14.1 $\pm$8.1 mg·m^{-3}). *In situ* measurements represent monthly CHL averages; we therefore calculated monthly MERIS CHL averages (green line in Fig. 6.4a) for a visual comparison. The standard deviation indicates the temporal variability within a month. In most cases, *in situ* CHL remained within the range of MERIS CHL monthly standard deviation.

The short- and long-term monthly means of MERIS CHL followed a seasonal pattern, which seems reasonable for a eutrophic, polymictic lake. The time series revealed a regularly occurring spring bloom in April with CHL around 10.7 $\pm$6.9 mg·m^{-3} (Fig. 6.4a, c, Fig. 6.5). Increasing light availability, water temperature and nutrient availability induce these diatom-dominated spring blooms (LU-MV, 2015a; Reynolds, 2006; Wöbbecke et al., 2003). After nutrient depletion, the clear water phase develops; decaying cells sink and the growing zooplankton population reduces phytoplankton through grazing (Winder and Schindler 2004). According to our MERIS time series, the clear water phase regularly occurred in May/June with CHL around 5-6 mg·m^{-3}. During the following summer months, CHL increased again to concentrations of up to 45 mg·m^{-3}. On average, September showed highest concentrations (Fig. 6.4c, Fig. 6.5). CHL strongly decreased again in November and remained around 5-6 mg·m^{-3} during the following winter months.

In situ CHL showed a similar seasonal development, i.e. a spring bloom in April, followed by a clear water phase in May/June, whereas *in situ* concentrations were generally higher than MERIS CHL. In late summer, however, *in situ* and MERIS CHL patterns differed. *In situ* CHL achieved its maximum in August, whereas MERIS CHL peaked in September (Fig. 6.4c, Fig. 6.5). Dörnhöfer et al. (2018a) found similar deviations when comparing CHL received from various satellite systems and *in situ* measurements. Methodological differences may account for the deviation: at Lake Kummerow, cyanobacteria predominate phytoplankton composition in late summer (LU-MV, 2016; Wöbbecke et al., 2003) which form patchy surface scums (Bertani et al., 2017). MERIS may have captured the signal from these patterns. In contrast, the *in situ* sampling may have missed the scum due to sampling below the water surface or spatial variability of surface scum (Bertani et al., 2017). Furthermore, degrading algal pigments of summer blooms (e.g. phaeophytin-a) may contribute to the signal acquired by MERIS and further lead to higher CHL concentration compared to *in situ* data.

Fig. 6.5 shows the monthly CHL averages (columns) for each year (rows) and highlights the information gain when integrating remote sensing in water quality monitoring. During 2003 and 2011, *in situ* measurements were available about 5 times per year, resulting in 48 monthly average values. The MERIS time series, however, provided twice as much values (112). Higher temporal coverage as provided by remote sensing data analyses may support lake monitoring and reduce uncertainties related to the temporally highly dynamic CHL. At Lake Kummerow, MERIS data indicated a variation of up to 35 mg·m^{-3} within a month (difference between monthly minimum and maximum arithmetic means of CHL). The monthly coefficient of variation (standard deviation/arithmetic mean) varied between 0.45 (September) and 1.1 (June, January). While *in situ* measurements were unavailable during winter months, MERIS provided CHL, which varied between 2.1 and 12 mg·m^{-3}. Therefore, this time series revealed unprecedented information on winter CHL in Lake Kummerow. For instance, Hampton et al. (2017) detected previously unexpected phytoplankton biomass in 101 lakes analysed during winter. They reported concentrations of mean CHL in winter being at average were 43.2 % that of CHL concentrations in summer (i.e. around 5.87 $\pm$0.88 mg·m^{-3}; Hampton et al., 2017). Accordingly, MERIS winter CHL concentrations at Lake Kummerow appear to be realistic.

The MERIS CHL time series showed several anomalies, which may have been the result of daily varying concentrations. The summers 2005 and 2007 exhibited a longer period of positive anomalies, i.e. higher CHL than average (Fig. 6.4b, Fig. 6.5). For both years, precipitation at a weather station in the catchment was above average in May (96 instead of 56 mm; Deutscher Wetterdienst, 2016b). Erosive precipitation at maize fields may have led to an increased nutrient availability in the lake (e.g. Vogel et al., 2016). In contrast, MERIS and *in situ* CHL showed irregularly low concentrations in summer 2009 (Fig. 6.4b, Fig. 6.5), whereas precipitation was average in spring. The same pattern applied to low summer CHL in 2010 and 2011, which also coincided with 'normal' precipitation patterns.

CHL monitoring and trend analyses may be a measure for a successful lake/catchment management, e.g. whether nutrient input has been reduced successfully. *In situ* measurements from the site Deepest Point re-

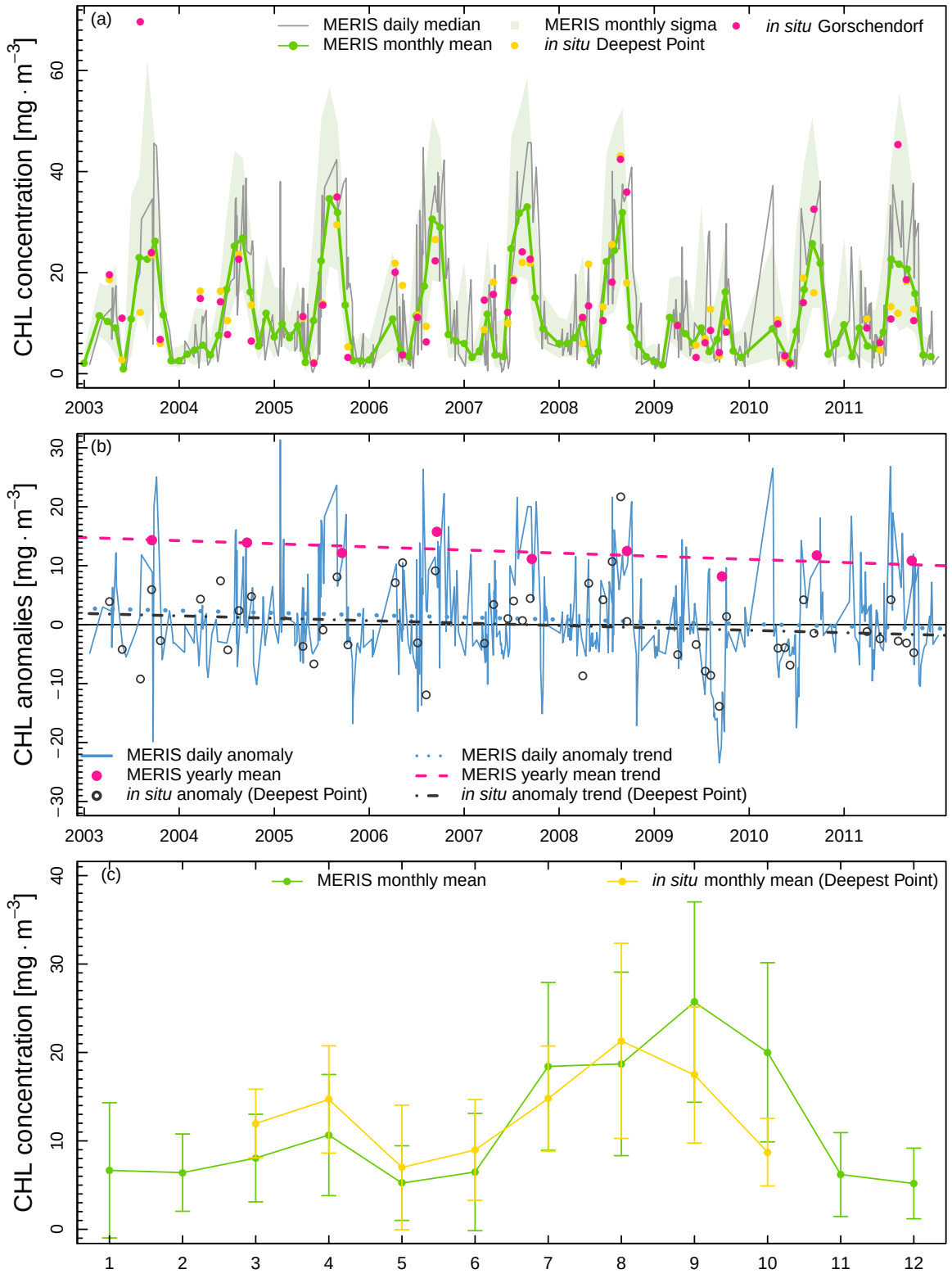

Figure 6.4: Daily median and monthly mean Chlorophyll-a (CHL) concentrations of the total lake (a). Daily CHL anomalies, yearly mean concentrations and linear trend lines based on MERIS, black circles indicate *in situ* CHL anomalies at site Deepest Point and *in situ* anomaly trend line (black line) (b). Seasonal cycle of CHL derived from the long-term monthly mean of the years 2003-2011 from MERIS and *in situ* data; vertical bars indicate monthly standard deviation (c).

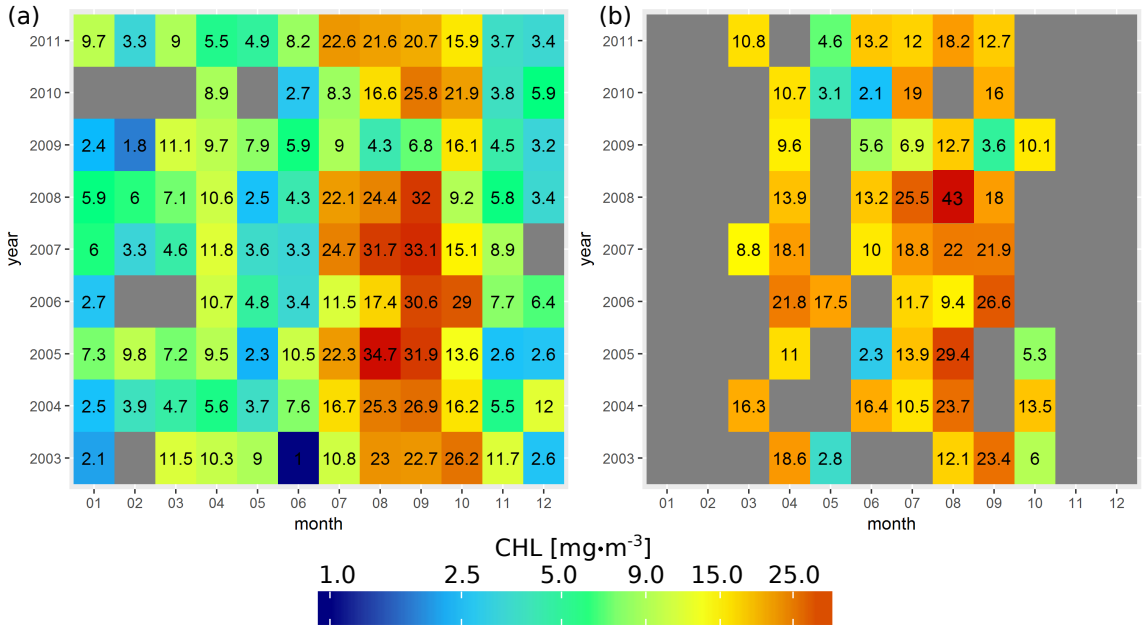

Figure 6.5: Monthly means of total lake Chlorophyll-a (CHL) concentrations based on MERIS (a) and *in situ* measurements at the site Deepest Point (b); data gaps are highlighted in grey.

vealed a weak negative trend of CHL during the period 2003-2011 (Table 6.4). MERIS data indicated a slightly lower CHL decrease than *in situ* values. Both, MERIS and *in situ* CHL, confirmed decreasing CHL concentrations and indicated a slight improvement of water quality.

Table 6.4: Linear trend and change of MERIS Chlorophyll-a (CHL; lake-wide) and *in situ* CHL (site Deepest Point) between 2003 and 2011.

	MERIS daily anomalie	MERIS yearly mean	*In situ* anomaly
Trend	CHL=-0.0010·date+15.3	CHL = -0.0015 ·date+32.2	CHL=-0.0011·date+15.4
Change	-3.4 mg·m^{-3}	-4.8 mg·m^{-3}	-3.7 mg·m^{-3}

In situ CHL indicated a spatial variability between the measurement sites. This spatial variability between sites became pronounced during summer, while spring values at both measurement sites resembled each other (Fig. 6.4a). MERIS monthly average maps (Fig. 6.6) showed similar patterns. In March/April (during spring blooms), CHL concentrations showed a homogenous distribution, which was most likely a result of a wind induced mixing of the water column and water surface. The clear water phase occurring in May/June also exhibited homogenously distributed CHL (around 5 mg·m^{-3}) at the lake surface. In July, CHL concentration increased. During August, higher CHL concentrations predominated in the western part of the lake; Dörnhöfer et al. (2018a) observed similar patterns for prevailing north-easterly winds in a detailed analysis of satellite data at Lake Kummerow in August 2015. In September, CHL was highest but distinct spatial patterns were not apparent; in October, the lake showed slightly lower, homogenously distributed concentrations. From November to February, CHL generally remained below 9 mg·m^{-3}.

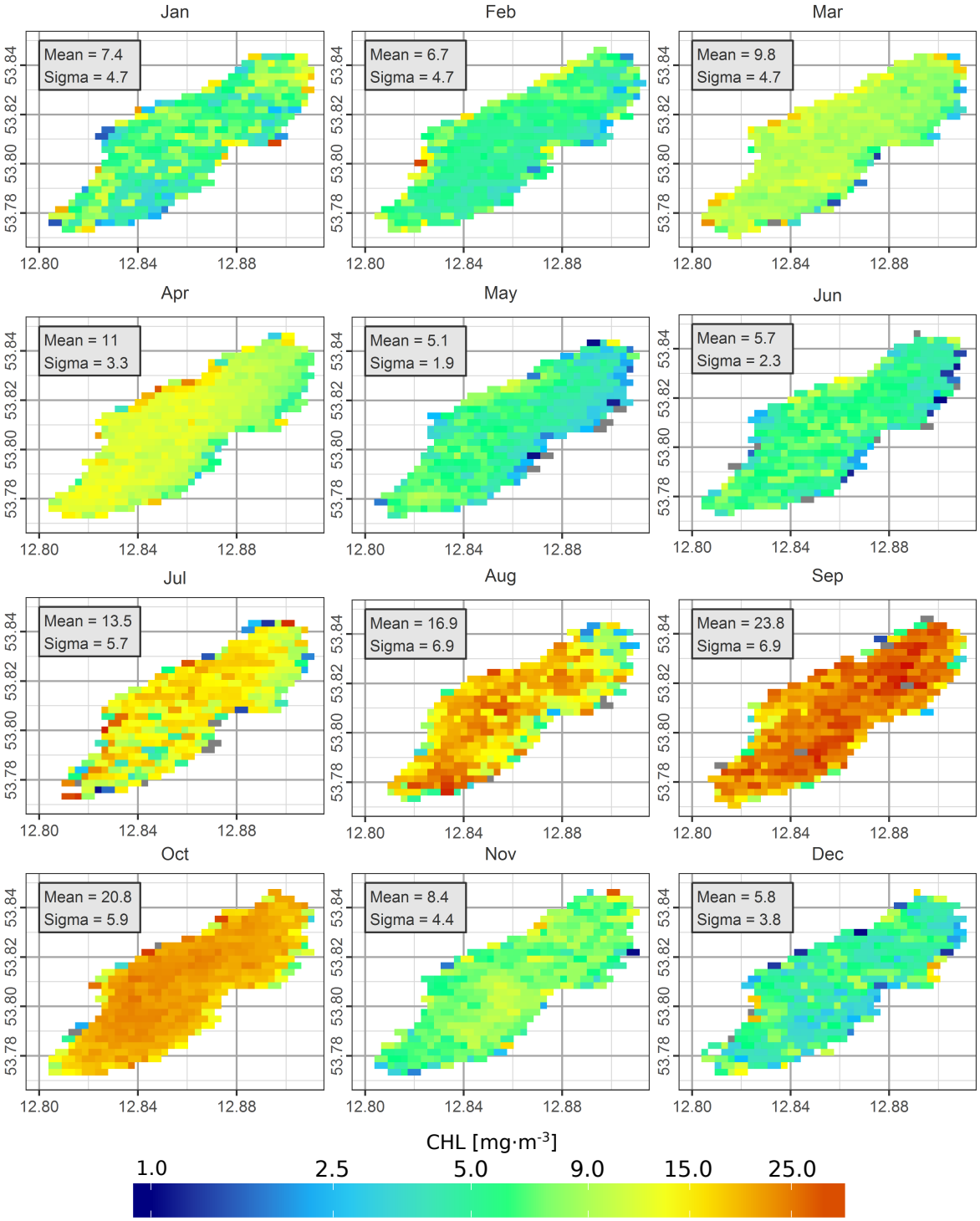

Figure 6.6: Spatial distribution of long-term monthly mean Chlorophyll-a (CHL) concentrations calculated from the entire MERIS time series (2003-2011). Mean is the lake wide arithmetic mean of the raster values in the map and sigma is the respective standard deviation, i.e. indicates the spatial variation.

6.4.3 Seasonal cycles, trends and spatial patterns of TSM

During the period 2003-2011, lake mean MERIS TSM varied between 0.1 $g \cdot m^{-3}$ on 25 May 2007 and 10.0 $g \cdot m^{-3}$ on 10 August 2003. LU-MV based *in situ* measurements of TSM or related parameters such as turbidity were not available. This time series therefore presents novel information on TSM concentrations and its temporal development. TSM concentrations showed a seasonal variability: during winter and spring, TSM remained below 1 $g \cdot m^{-3}$ on average. Between June and September, TSM increased up to 3 $g \cdot m^{-3}$ and decreased from October to November (Fig. 6.7a). In summer 2015, Fritz et al. (2017a) conducted *in situ* measurements which revealed TSM concentrations between 1 $g \cdot m^{-3}$ (June) and 4 $g \cdot m^{-3}$ (August). In reference to these measurements, the retrieved MERIS summer values were reasonable. Overall, the seasonal development was comparable in each year between 2003 and 2011. Only single years exhibited either very high values (August, September 2003 and 2005) or distinctly low values (throughout the year 2009; Fig. 6.7), which corresponded to the CHL anomalies mentioned earlier.

TSM consists of organic and inorganic particles. Unpublished measurements from summer 2016 revealed that organic particles predominated TSM in the northern part of Lake Kummerow. Organic components of TSM are phytoplankton and detritus (Matthews, 2011). Thus, the increasing TSM concentrations during summer and very high concentrations in summer 2005 may have resulted from accompanying high CHL concentrations. Similar to CHL, a trend analysis of TSM showed slightly decreasing concentrations between 2003 and 2011 (Table 6.5).

The monthly average maps showed spatially homogenous but low TSM concentrations from March to June (Fig. 6.8). In July, spatial variability increased. From August to October, TSM showed similar patterns as CHL indicating its predominating organic origin. Distinct patterns occurred in January and February when large parts of the lake exhibited low concentrations (< 0.9 $g \cdot m^{-3}$) whereas concentrations at the southern end exceeded 3 $g \cdot m^{-3}$. This pattern may be due to riverine inflow of the West Peene, which transports TSM (soil eroded in the catchment) into the southern part of the lake. When looking at precipitation patterns during the period 2003-2011, July showed highest precipitation rates (mean monthly sum: 81 mm, Deutscher Wetterdienst, 2016b). In January and February, however, average precipitation was around 50 mm (Deutscher Wetterdienst, 2016b), which may also have resulted in higher catchment erosion due to less protective vegetation cover during winter.

Table 6.5: Linear trend and change of MERIS total suspended matter (TSM; lake) between 2003 and 2011.

	MERIS daily anomalie	MERIS yearly mean
Trend	TSM = -0.0004·date+5.65	TSM = -0.0005·date+7.78
Change	-1.31 $g \cdot m^{-3}$	-1.5 $g \cdot m^{-3}$

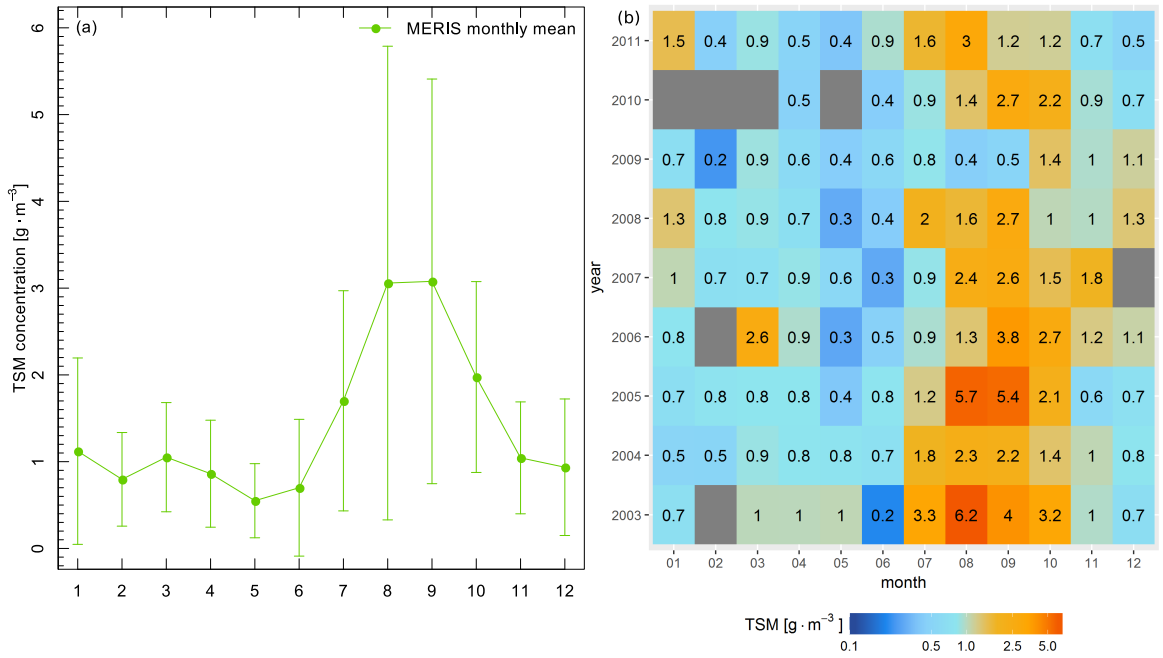

Figure 6.7: Seasonal cycle of total suspended matter (TSM) as long-term monthly average of the years 2003-2011; vertical bars indicate monthly standard deviation (a). Monthly means of TSM concentrations in the lake; data gaps are highlighted in grey (b).

6.4.4 Temporal development, seasonal cycles and spatial patterns of CDOM

During the period 2003-2011, lake mean MERIS CDOM varied between 0.01 (5 January 2009) and 0.94 m^{-1} (17 July 2006; Fig. 6.9a). Overall, CDOM showed a regularly appearing curve with minimum values during winter and maximum values during summer. Contrary to TSM and CHL, the time series showed no significant trend for CDOM (Fig. 6.9b) and lacked any spatial patterns (not shown here). The lake monitoring programme (LUMV, 2015a) lacks measurements of CDOM but included DOC as a parameter. Between 2005 and 2010, DOC formed 90-95 % of lake TOC (Fig. 6.9c). Several studies found a strong correlation between DOC and CDOM (e.g. Brezonik et al., 2015; Toming et al., 2016b), although seasonal and local variations have to be considered (Hestir et al., 2015b). At Lake Kummerow, *in situ* DOC and MERIS CDOM showed a similar seasonal behaviour during spring/early summer (Fig. 6.9c). DOC (9.7 - 10.3 g·m^{-3}) and CDOM (0.4 - 0.6 m^{-1}) increased from March to June. CDOM achieved its maximum in July (0.79 m^{-1}), DOC in August (10.7 g·m^{-3}). In late summer, CDOM started to decrease, whereas DOC varied from month to month. DOC, and therefore CDOM, originates from lake internal sources, i.e. macrophytes and phytoplankton (autochthonous production), or from soil organic matter and plants from the catchment (allochthonous production; Brezonik et al., 2015). Autochthonous DOC mainly consists of non-humic substances which have lower absorption properties, i.e. a lower influence on CDOM; allochthonous DOC mainly is composed of highly absorbing humic substances and has a high influence on CDOM (Thurman, 1985; Toming et al., 2016b). Peat bogs and swamps (allochthonous source) bordering the lake may therefore explain the relatively high CDOM values (e.g. Brezonik et al., 2015). Increased phytoplankton biomass in summer (as indicated by increased CHL, Section 6.4.2) may contribute to varying *in situ* DOC but may have a minor effect on MERIS CDOM (Fig. 6.9c).

Measurements conducted by Kiel University (CAU Kiel) in the summer of 2015 revealed CDOM around 1.3 m^{-1} (Fritz et al., 2017a). Assuming comparable CDOM conditions (no trend in Fig. 6.9b) FUB algorithm estimated lower CDOM (Fig. 6.9c) than recent *in situ* summer measurements. With *in situ* CDOM above 1.0 m^{-1}, Lake Kummerow exceeded the training range of FUB (Schroeder et al., 2007b, Section 6.3.1) which may have led to retrieval errors. Philipson et al. (2016) also documented CDOM values higher than the FUB

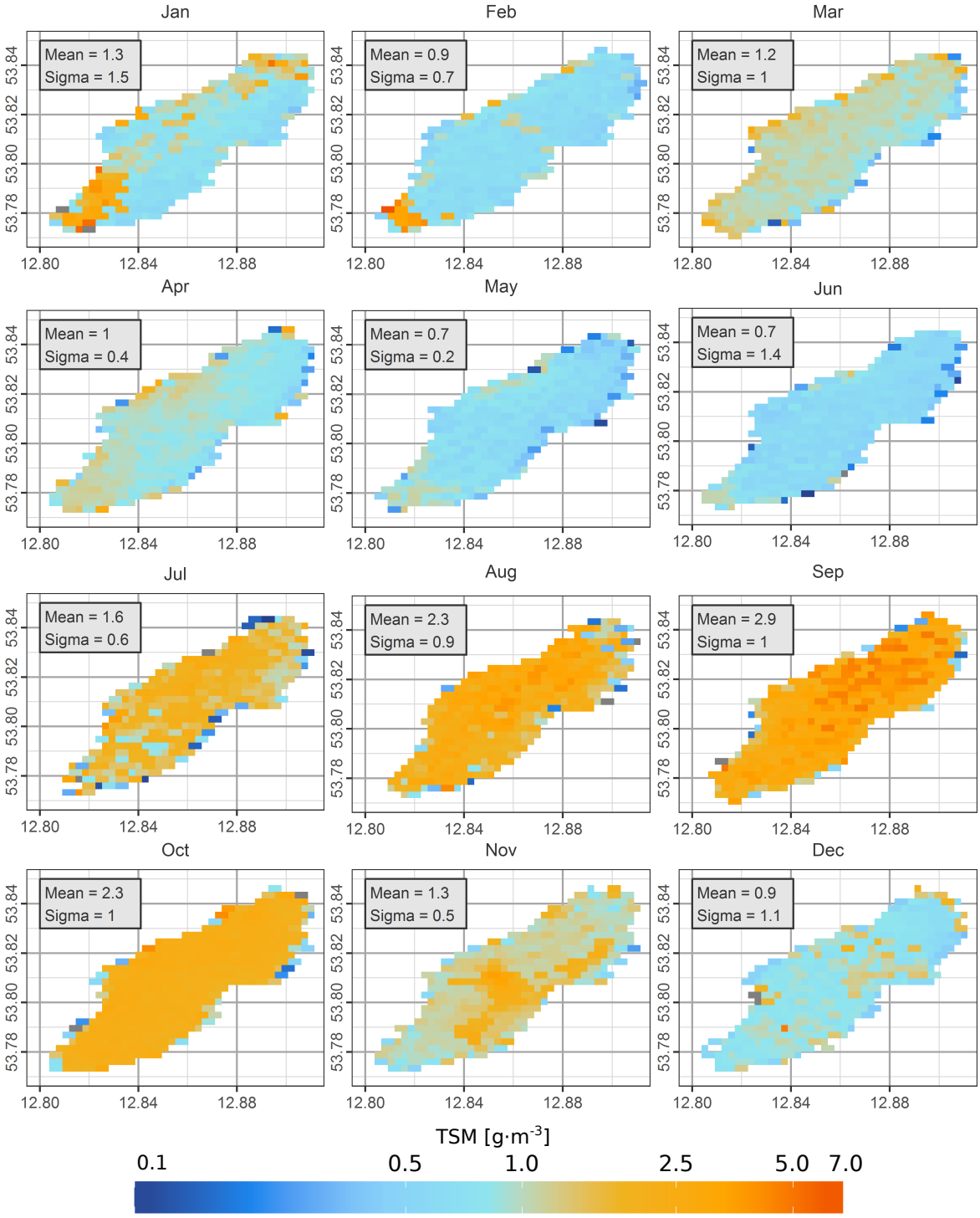

Figure 6.8: Spatial distribution of long-term monthly mean total suspended matter (TSM) concentrations calculated from the MERIS time series 2003-2011. Mean is the lake wide arithmetic mean of the raster values in the map and sigma is the respective standard deviation, i.e. indicates the spatial variation.

training range but observed a strong correlation with *in situ* data.

Apart from the accuracy of CDOM absolute values, a strong decline of CDOM appeared regularly during autumn/winter (Fig. 6.9a). Due to the lack of *in situ* measurements, however, we are unable to verify the decreasing autumn/winter CDOM observed by MERIS. Nevertheless, several other studies observed strong seasonal variations of CDOM, e.g. at US lakes (Brezonik et al., 2015, ; 30-50 % variation), Lake Võrtsjärv (Toming et al., 2016b, ; $\sim$6-12 m^{-1}) or Lake Balaton (Aulló-Maestro et al., 2017, ; $\sim$3.7-9.0 m^{-1}). Zhang et al. (2013b) reported that variations of CDOM sources, photobleaching and degradation might cause seasonal changes in CDOM. Aging and degrading DOC may also be a reasonable explanation for decreasing CDOM absorption at Lake Kummerow during winter months. Otherwise, the apparent seasonal behaviour may originate from potential retrieval artefacts. Due to its absorbing behaviour, very low reflectance signals aggravate CDOM-retrieval with remote sensing in CDOM-rich waters (Kutser et al., 2016). During the low light period (October to March) with low sun elevation angles, the water signal collected by the MERIS sensor was even lower. Thus, the retrieval may be even more complicated and subjected to algorithm artefacts. Sensitivity analyses of FUB/WeW indicated CDOM overestimation for concentrations < 0.1 and slight underestimation for concentrations > 0.1 m^{-1} under low sun elevation angles (Schröder, 2005). The behaviour of FUB under real conditions with low sun elevation conditions is still unknown due to a lack of *in situ* data from autumn and winter. In addition, published studies focused on the months April to October only. *In situ* measurements during winter are crucial in order to verify the seasonal behaviour or to detect algorithm artefacts.

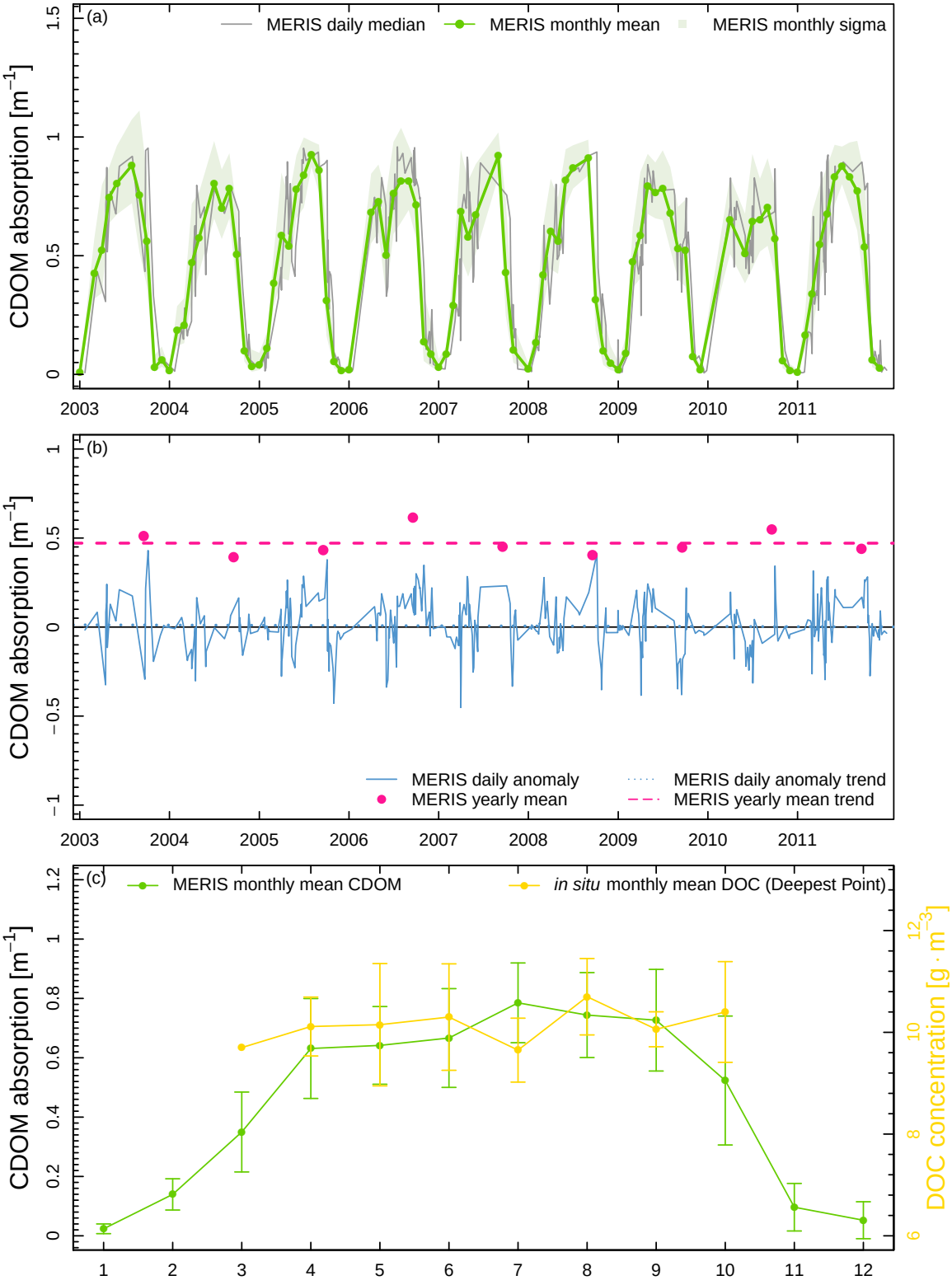

Figure 6.9: Daily median and monthly mean coloured dissolved organic matter (CDOM) absorption of the entire lake (a). Daily CDOM absorption, yearly mean and linear trend lines based on MERIS (b). Seasonal cycle of CDOM (2003-2011) and dissolved organic carbon (DOC; 2005-2010) as long-term monthly average values; vertical bars indicate monthly standard deviation (c).

6.4.5 Uncertainties and requirements for improved monitoring

Recent and future satellite systems suitable for inland water remote sensing (e.g. Sentinel-2, Sentinel-3, Landsat 8; HySpiri, EnMAP) boosted the development of sensor specific and generic algorithms for water constituent retrieval (Dörnhöfer and Oppelt, 2016). Testing algorithm performance, investigating weaknesses and improving existing applications such as shown in this study require validation data that cover both different spatial scales and lake characteristics (Nechad et al., 2015). However, permanent measurement sites such as in Lake Vänern, Sweden (e.g. Philipson et al., 2016) are rare. In Germany, *in situ* data of official lake monitoring programmes such as of LU-MV (LU-MV, 2015a) often serve as validation source for remote sensing studies. They provide valuable information, notably for historic satellite data analyses. These programmes, however, are designed to fulfil the reporting obligations of the European Water Framework Directive; they therefore cannot cover a sufficient basis for validating recent remote sensing missions and cannot achieve associated requirements.

Depending on the spatial-temporal variability of water constituents, validating satellite based algorithms for inland waters requires *in situ* measurements temporally proximate to image acquisition (best-case $\pm$2 hours, e.g. Dörnhöfer et al., 2016b; Giardino et al., 2014a; Philipson et al., 2016). Measured parameters should preferably include all optically active constituents and water leaving reflectance. In addition to water constituent validation, these measurements would enable the ability to optimise atmospheric correction procedures over optically complex inland waters (Palmer et al., 2015b). Individually organised measurement campaigns aim to bridge these gaps but have their limitations, which emphasise the need for a network of permanent measurement sites.

So far, individual data sets exist at different organisations without a central data management. Standardisation would facilitate international integration of measurements into shared databases, e.g. MERMAID database for ocean and coastal waters (Barker et al., 2008) or LIMNADES (Lake Bio-optical Measurements and Matchup Data for Remote Sensing: http://www.globolakes.ac.uk/limnades.html) for optical measurements of inland waters. First approaches of inter-comparison studies exist to support remote sensing validation studies with *in situ* measurement protocols (GLaSS, 2015; Zibordi et al., 2012). Many project-driven measurements still lack a standardisation of measurement setups, protocols and instrument (inter-) calibration and therefore are difficult to compare.

Moreover, these campaigns tend to focus on late spring to early autumn, while they rarely cover the winter months. To our knowledge, no published study exists which evaluates water constituent retrieval during the low-light period. Indeed, cloudy weather conditions, and influence of snow and ice at Lake Kummerow reduced the number of suitable MERIS acquisitions during winter. Nevertheless, the MERIS time series showed distinct seasonal cycles of CHL, TSM and CDOM. The absence of *in situ* measurements however impeded the assessment whether FUB is a valid predictor of CHL during the winter period or if increased TSM pattern at that time can be assessed to be a regular feature or a result from insufficient light condition. *In situ* observations in winter will also answer if the seasonality of CDOM concentration at Lake Kummerow or is a natural pattern or an algorithm artefact. The lack of regular TSM and CDOM measurements in this study only enabled for plausibility checks of their concentrations and spatial-temporal development.

This situation, together with the potentials of remote sensing for lake monitoring and the fact that lakes such as Lake Kummerow mirror environmental and climate changes in their catchments emphasise the necessity of integrated research at the landscape scale. It further underlines the call for permanent measurement sites for improved quantitative (validated) evaluations of lake water quality. Lake Kummerow, the seven largest lake of Germany, may be useful for such continuous *in situ* monitoring as its water cycle is closely linked with the terrestrial observation site DEMMIN in the TERENO network (Section 6.2).

6.5 Conclusions

In this study, we used the artificial neural network based and freely available algorithm FUB/WeW to analyse a MERIS time series (2003-2011) at Lake Kummerow, northern Germany. Water constituents of interest were CHL, TSM and CDOM. A comparison between MERIS and *in situ* CHL measured within the lake monitoring programme of the federal state Mecklenburg Western Pomerania (LU-MV 2015) revealed significant linear correlations. MERIS CHL was on average 20.3 % (pBias) higher than *in situ* measurements (MAE: 6.55 $m \cdot m^{-3}$). Due to the lack of *in situ* measurements, we evaluated TSM and CDOM on a qualitative basis. TSM was reasonable and within an expected value range. On the contrary, FUB likely underestimated CDOM since actual lake CDOM was out of the neural networks. Trend analyses of CHL and TSM showed a decreasing tendency during the analysed period, suggesting a slight improvement of water clarity and quality. CDOM displayed no clear trend.

Analysis of daily and monthly averages demonstrated that MERIS can monitor expected seasonal variabilities of CHL correctly, i.e. a spring bloom, followed by clear water phase in May/June and varying high CHL concentrations during summer/early autumn (summer blooms). Moreover, MERIS revealed unprecedented information on winter CHL ($\sim$ 5-6 $mg \cdot m^{-3}$). TSM showed highest concentrations (5 $g \cdot m^{-3}$) during summer; CDOM also exhibited maximum values during summer (around 0.7 m^{-1}) while winter values remained close to zero. For a quantitative validation of inland water approaches, however, permanent validation/calibration test sites in inland waters are imperative.

The results underline the information gain provided by remote sensing for inland water monitoring in terms of temporally frequent and spatially explicit data. Especially with a view on upcoming satellite systems, remote sensing-based algorithms offer an enormous potential for an operational monitoring of inland waters. Development, validation and improvement of algorithms, however, require permanently equipped measurement sites in lakes with different optical characteristics. One option that would also promote complex ecosystem-based research (e.g. at the catchment scale) may be the integration of lake measurement equipment into already established and well-equipped terrestrial sites for *in situ* observation and validation of satellite data and their derivatives.

Acknowledgements: This work was conducted within the project LAKESAT (grant no: 50EE1340) funded by the Federal Ministry for Economic Affairs and Energy, Germany. We acknowledge the Mecklenburg-Vorpommern Ministry for Agriculture, Environment and Consumer Protection for data supply from the lake monitoring programme. Many thanks are due to ESA for providing MERIS data.

Chapter 7

Synthesis

7.1 Summary of main achievements

Reviewing the research status of optical remote sensing for lake ecology and outlining future directions

To achieve the first objective, this thesis includes a comprehensive literature review (Chapter 3; Dörnhöfer and Oppelt, 2016). Previous published reviews (e.g. Chang et al., 2014; Matthews, 2011; Odermatt et al., 2012) focused on available algorithms for water constituent retrieval with remote sensing data. This updated literature review particularly emphasised studies which focused beyond algorithm development and contributed to the combination of passive remote sensing (subsequently referred to as remote sensing) and lake ecology. The considered lake ecology indicators were TSM, turbidity, CDOM, Secchi disk depth, K_d, phytoplankton (CHL, cyanobacteria), SAV, water depth, water temperature and ice phenology parameters. To build a link between remote sensing and lake ecology, the indicators retrieved in the remote sensing studies were summarised with respect to lake properties (according to Adrian et al., 2009), i.e. transparency, biota, hydrology and temperature. Special attention has been paid to feasible value ranges, achieved accuracies (Table 7.1) and a short description of which lake ecological processes or issues have been analysed with the remote sensing results.

Table 7.1: Summary of value ranges and accuracies depending on lake ecology indicators retrieved with remote sensing. k = Kappa coefficient, MAE = mean average error, RMSE = root mean squared error, R^2 = coefficient of determination (compiled based on Dörnhöfer and Oppelt, 2016).

Indicator	Min. value	Max. value	Min. accuracy	Max. accuracy
Transparancy				
TSM [g·m^{-3}]	0	2500	R^2 = 0.91	R^2 = 0.94
CDOM [m^{-1}]	0	20	R^2 = 0.62	R^2 = 0.78
$K_d(\lambda)$ [m^{-1}]	0	24	R^2 = 0.56	R^2 = 0.76
Secchi disk depth [m]	0.13	7.53	R^2 = 0.67	RMSE = 0.48 m
Biota				
CHL [mg·m^{-3}]	0	500	R^2 = 0.83	R^2 = 0.98
SAV	habitat classes	% coverage	k = 0.66	k = 0.87
Hydrology				
Water depth [m]	0	10.45	R^2 = 0.84	R^2 = 0.92
Water temperature				
Surface Temperature [°C]	-2	35	RMSE = 4.18	$R^2 \sim 0.9$
Lake ice phenology				
ice-on/out [days]	-	-	MAE = 11.9	MAE = 4.2

The majority of reviewed studies retrieved water constituents, i.e. CDOM, TSM (transparency; Table 3.4) and CHL (biota and transparency; Table 3.4, 3.5), with CHL being the most frequently assessed indicator.

Retrieval of CHL was mainly related to trophic state monitoring (e.g. Bresciani et al., 2011c; Keith et al., 2012; Matthews, 2014) and the identification of phytoplankton blooms (Palmer et al., 2015c), in particular potentially harmful blooms of cyanobacteria (e.g. Gómez et al., 2011; Wu et al., 2015). CDOM was associated with lake carbon content (e.g. Kutser, 2012; Kutser et al., 2009). Time series of TSM concentrations revealed influences of anthropogenic activities or event-driven discharge on water transparency (e.g. Binding et al., 2010; Lobo et al., 2015; Long and Pavelsky, 2013). Published analyses with direct indicators of water transparency (i.e. Secchi disk depth, the depth at which 90 % of the incoming solar irradiance are still available and $K_d(\lambda)$) existed less often than water constituent analyses (e.g. Majozi et al., 2014; Shi et al., 2014). Most studies which combined remotely sensed water constituents with lake ecology issues considered time series (Table 3.4, 3.5). Analyses thus benefited from regularly available data covering one or multiple lakes. These studies, however, mainly relied on large scale sensors (MODIS, MERIS) and occasionally Landsat. Indicators were often retrieved along with other indicators to study interactions among water constituents but also catchment processes (e.g. land use) or meteorological data. Still, most of these studies applied empirical algorithms or ready-to-use algorithms (mainly for the ocean colour sensor MERIS) which are implemented in software packages such as BEAM (Fomferra and Brockmann, 2015), a phenomenon also observed by Odermatt et al. (2012). Physically-based bio-optical algorithms which are easier to transfer to other lakes and sensors already exist and are freely available. Nevertheless, the developing research groups mainly apply these more sophisticated approaches. In-depth knowledge to apply these algorithms properly presumably hinders a widespread application.

Owing to the need for a high spatial and spectral resolution, SAV and lake bottom substrate analyses were mainly based on airborne, hyperspectral images which were acquired during the growing season. Retrieval algorithms included supervised/unsupervised classification techniques and spectral unmixing whereas bio-optical modelling or depth-invariant indices accounted for the effect of the overlying water column (Table 3.5). Analyses between data acquisitions in different years aimed to detect changes in SAV colonisations and relations to water quality (e.g. Brooks et al., 2015; Giardino et al., 2007; Heblinski et al., 2011). Differentiations between bare substrate and SAV covered areas were feasible in extended shallow water areas using satellite data (e.g. Brooks et al., 2015; Shuchman et al., 2013b). Still, the differentiation between species is challenging even using hyperspectral imagery (e.g. Giardino et al., 2015; Rößler et al., 2013). Lake bottom analyses often go along with the retrieval of water depth. Studies retrieving water depth from remote sensing data mainly focused on model and methodological development (e.g. Gege, 2014a; Giardino et al., 2014a). Hitherto, remotely sensed water depth is rarely related to lake ecological issues.

Remote sensing data were also implemented to retrieve lake water surface temperature. These analyses mainly considered time series to derive trends in lake water temperature studies (e.g. Alcântara et al., 2010; Politi et al., 2012; Schneider and Hook, 2010). Although radar techniques are the main source for retrieving ice phenology parameters with remote sensing, some studies used large-scale optical sensors to delineate trends in ice phenology and improve the understanding of drivers influencing ice-on and ice-off (e.g. Kropáček et al., 2013; Latifovic and Pouliot, 2007).

In summary, the reviewed studies showed that remote sensing may support analyses and monitoring in lake ecology; several studies already connected remote sensing with lake ecological issues. Globally, remote sensing still has a small share in published studies on lake water quality (Fig. 3.4; Dörnhöfer and Oppelt, 2016). A lack of training and knowledge about the possibilities of remote sensing may be a key reason (Schaeffer et al., 2013). Studies which highlight new insights gathered from remote sensing and address uncertainties at lakes which are familiar to decision makers and authorities may help to increase the understanding for the potential of remote sensing (Schaeffer et al., 2013). Such analyses, however, require *in situ* measurements which often are associated with logistic challenges and costs. The scarcity of *in situ* data might be one reason why remote sensing research is concentrated on lakes within the close vicinity of research groups. *In situ* measurements form the basis for algorithm development, evaluation and validation to state accuracy measures for the retrieved lake ecology indicators. These comparisons normally consider *in situ* measurements as the reference whereas

uncertainties of *in situ* measurements are rarely included. It further remains challenging to upscale the *in situ* point measurement to the spatial measurement of a remote sensor. Nevertheless, Tables 7.1 and 3.4-3.8 demonstrate that retrieval was possible with accuracies which, however, varied among indicators, concentration ranges, sensors and algorithms used.

Apart from a certain scepticism about remote sensing compared to *in situ* measurements, reviewing the literature pointed out several unresolved challenges and issues still restraining a widespread combination of lake ecology and remote sensing (see Chapter 1.1). These issues include the unresolved problem of sensor-independent atmospheric correction algorithms designed for the specific conditions of lakes, e.g. adjacency effects, sun and sky glint at the water surface, and aerosol composition. Furthermore, knowledge about the more advanced bio-optical, inversion approaches should be increased. Nevertheless, ecologists may also benefit from a distribution of easy-to-apply algorithms and ready-to-use products. In addition, collaboration among disciplines may overcome knowledge gaps in technical or ecological issues. Validation exercises gain increasing importance with the availability of image data from the promising S2, L8 and S3 sensors with improved radiometric, spectral and, in case of the former, spatial resolution. While investigating the true performance of new sensors, the value of archived image data should also be explored. Integrating uncertainties of *in situ* measurements in validation exercises may raise the awareness of disadvantages associated with using only established methods. In this vein, clarifying the constraints of remote sensing is inevitable to promote a reasonable synergetic use of *in situ* and remote sensing methods. This thesis addressed these issues in Chapters 4 (Dörnhöfer et al., 2016b), 5 (Dörnhöfer et al., 2018a) and 6 (Dörnhöfer et al., 2018b).

Since the online publication of the review paper at the beginning of 2016 (Chapter 3; Dörnhöfer and Oppelt (2016)), various studies contributed to the progress in the field of inland water remote sensing and its combination with lake ecology (Table 7.2). More than 70 research papers have been published in peer-reviewed journals. Again, most publications focused on water constituent retrieval addressing lake ecology indicators of transparency and biota. Table 7.2 provides an overview about the new literature which was categorised in accordance to the tables in Chapter 3. A summary of the content showed that studies based on large-scale MODIS and archived MERIS data continued. They focused on time series $\geq$ 10 years to figure out drivers of trends and changes in water constituent concentrations (e.g. Breunig et al., 2017; Cao et al., 2017; Hou et al., 2017; Sayers et al., 2016; Yousef et al., 2017; Zhang et al., 2016c). With the availability of short time series of L8, studies have been published using L8 to retrieve TSM time series with high spatial detail in lakes (e.g. Robert et al., 2017; Zhang et al., 2016d; Zheng et al., 2016) and to evaluate L8 specific algorithms for water constituent retrieval (e.g. Concha and Schott, 2016; Ogashawara et al., 2017a; Rodrigues et al., 2017; Zheng et al., 2016). Reviewing studies of coastal areas showed L8 time series analyses which supported the identification of detailed spatial patterns and environmental drivers of river plumes (Braga et al., 2017; Manzo et al., 2018). Initial studies which retrieved water constituents in lakes from S2 were published (e.g. Chen et al., 2017; Dörnhöfer et al., 2016b; Ha et al., 2017; Liu et al., 2017; Toming et al., 2016a). Water constituents in the analysed lakes varied from low to high TSM (0-4200 $g \cdot m^{-3}$), CDOM (0-16 m^{-1}) and CHL (0-250 $mg \cdot m^{-3}$) concentrations (cf. Table 7.1).

Studies mapping SAV in lakes with L8 or S2 were rarely published (e.g. Dörnhöfer et al., 2016b; Yadav et al., 2017). Nevertheless, S2A and L8 were already applied to map seagrass and SAV in coastal zones (Giardino et al., 2016; Traganos and Reinartz, 2017). Various new studies investigated thermal trends in lakes with L7 and L8 data (e.g. Allan et al., 2016; Huang et al., 2017b; Ling et al., 2017). Two further studies analysed large-scale optical data to figure out trends in ice phenology (Murfitt and Brown, 2017; Weber et al., 2016). Studies about ice phenology and lake surface temperature already have benefited from combining multi-sensor data (Chapter 3).

New studies published since 2016 have increasingly combined multi-sensor data to monitor water constituents: Coelho et al. (2017) combined L8 and RapidEye data to derive CDOM and CHL in order to assess trophic states. Olmanson et al. (2016) obtained CDOM and Secchi disk depth from L7 and L8, while Robert

et al. (2017) figured out environmental drivers of varying TSM concentrations combining L7 and L8 with MODIS. Dörnhöfer et al. (2018a) (Chapter 5) combined L7, L8, MODIS and S2A to capture phytoplankton development in a eutrophic lake. Such multi-sensor studies rely on sensor-independent algorithms and require sensor comparison analyses. In a multi-sensor time series, Lymburner et al. (2016) figured out that TSM retrievals are consistent between L5 and L7 as well as between L7 and L8. Dörnhöfer et al. (2018a) (Chapter 5) found significant correlations of CHL between MODIS and L7 or S2A within a 1 hour image acquisition difference. Olmanson et al. (2016) retrieved comparable Secchi disk depth values between L7 and L8; CDOM retrievals were, however, only comparable in waters with low to moderate CDOM levels. Liu et al. (2017) obtained highly correlated TSM concentrations between MODIS and S2. The results of these first studies testing sensor intercomparability are promising for future limnologically orientated investigations that synergetically use different sensors.

Table 7.2: Studies published since the beginning of 2016 deducing indicators of lake ecology. When several algorithms have been tested, the table indicates the approach with the highest accuracy. NN = neural network, LUT = look-up table, k = Kappa coefficient, OA = overall accuracy, MAPE = mean average percentage error, r = correlation coefficient, RMSE = root mean square error, R^2 = determination coefficient. *Airborne, hyperspectral sensor.

Authors	Techniques	Sensor	Parameter	Range	Accuracy	Study area	Time	Process
Transparency								
Alcântara et al. (2016)	empirical	L8	CDOM	0.616-1.69 m^{-1}	R^2 = 0.7 RMSE = 10.65 %	Barra Bonita hydro-electric reservoir (Brazil)	autumn/winter 2014	spatial differences
Alikas and Kratzer (2017)	empirical semi-analytical	MERIS	Z_{SD}	0.2-15.0 m	R^2 = 0.75 RMSE = 1.33 m	Scandinavian lakes and coastal areas	2010	potential for WFD monitoring
Bernardo et al. (2017)	empirical	L8	TSM	3.2 - 53 $g{\cdot}m^{-3}$	MAPE = 10 %	Barra Bonita hydro-electric reservoir (Brazil)	13 Oct 2014	influence of different atmospheric corrections
Breunig et al. (2017)	empirical	MODIS	TSM CHL	0-18 $g{\cdot}m^{-3}{\cdot}m^{-3}$, 0-21 $mg{\cdot}m^{-3}$,	RMSE = 2.98 $g{\cdot}m^{-3}$ RMSE = 2.33 $mg{\cdot}m^{-3}$	Passo Real reservoir (Brazil)	2002-2014	spatial patterns, driver analyses
Cao et al. (2017)	empirical	MODIS	TSM	10 - 80 $g{\cdot}m^{-3}$	RMSE $\sim$ 7.7 $g{\cdot}m^{-3}$	Lake Hongze (China)	2002-2015	spatial patterns, driver analyses
Chen et al. (2017)	NN	S2	CDOM CHL	0-5.02 m^{-1} 0-55.14 $mg{\cdot}m^{-3}$	R^2 = 0.913 R^2 = 0.95	Lake Huron (Canada/USA)	7 Oct 2016	sensor and algorithm evaluation
Coelho et al. (2017)	empirical	L8 RapidEye	CDOM CHL	2-12 m^{-1} 0-250 $mg{\cdot}m^{-3}$	r = -0.47 r = 0.84	3 small reservoirs (Brazil)	2014-2016	trophic state assessment
Concha and Schott (2016)	LUT optimisation	L8	CDOM CHL TSM	0.11-1.2 m^{-1} 0.1-100 $mg{\cdot}m^{-3}$ 1-50 $g{\cdot}m^{-3}$	R^2 = 0.98 R^2 = 0.84 R^2 = 0.88	Rochester Embayment (USA)	Sep 2013, 2014, 2015	sensor and algorithm evaluation
Dörnhöfer et al. (2018b)	NN FUB-WeW	MERIS	CDOM CHL TSM	0.01-0.94 m^{-1} 0.3-45.8 $mg{\cdot}m^{-3}$ 0.1-10.0 $g{\cdot}m^{-3}$	qualitative R^2 = 0.78 qualitative	Lake Kummerow (Germany)	2003-2011	trend analyses
Dörnhöfer et al. (2016b)	bio-optical inversion	S2A	CDOM TSM z_B SAV	0.1-0.74 m^{-1} 1.1-5.1 $g{\cdot}m^{-3}$ 0-4 m coverage	relative comparisons r = 0.83 relative comparisons	Lake Starnberg (Germany)	13 Aug 2015	sensor and algorithm evaluation
Hou et al. (2017)	empirical	MODIS	TSM	1-300 $g{\cdot}m^{-3}$	30-40 % uncertainty	lakes in Yangtze river basin (China)	2000-2014	monitoring trends in water quality

Continued on next page

Table 7.2 – *Continued from previous page*

Authors	Techniques	Sensor	Parameter	Range	Accuracy	Study area	Time	Process
Huang et al. (2017a)	empirical	GOCI	DOC	1-13 $g \cdot m^{-3}$	RMSE = 0.69 $g \cdot m^{-3}$	Lake Taihu (China)	2014-2015	monitoring hourly DOC concentrations
Lee et al. (2016)	quasi-analytical algorithm	L8	Z_{SD}	0.1-30 m	R^2 = 0.96	Jiulongjiang river estuary	4 Aug 2013	sensor and algorithm evaluation
Liu et al. (2017)	empirical	S2 MODIS	TSM	0-300 $g \cdot m^{-3}$	R^2 = 0.77-0.93	Poyang Lake (China)	15 Aug 2016, 2 Apr 2017	sensor and algorithm evaluation
Lymburner et al. (2016)	semi-analytical	L5/7/8	TSM	0-178 $g \cdot m^{-3}$	R^2 = 0.97	lakes in New South Wales/Queensland (Australia)	1987-2014	sensor inter-comparability, TSM trend
Lyu et al. (2017)	semi-empirical	MERIS	POC	2-15 $mg \cdot m^{-3}$	MAPE = 0.1 - 85 %	Lake Taihu (China)	Aug, Dec 2010	algorihm development
Olmanson et al. (2016)	empirical	L7/8	CDOM	0.5-22.6 m^{-1}	$R^2 \sim 0.7$	lakes in Minnesota (USA)	summer 2008, 2013, 2014	sensor-comparison, algorithm evaluation
			Z_{SD}	0.15-8.8 m	$R^2 \sim 0.82$			
Philipson et al. (2016)	NN, FUB-WeW	MERIS	CHL	0-49 $mg \cdot m^{-3}$	r = 0.85	Lake Vänern (Sweden)	2002-2012	algorithm evaluation, spatial patterns
			TSM	0.21-24 FNU	r = 0.9			
			CDOM	0.005-0.201 m^{-1}	r = 0.87			
Robert et al. (2017)	empirical	L7/8, MODIS	TSM	106-4178 $g \cdot m^{-3}$	R^2 = 0.79	Agoufou Lake (Mali)	2013-2016	time series, driver analysis
Rodrigues et al. (2017)	semi-analytical	L8	Z_{SD}	2-4 m	MAPE = 8.7-19.8 %	reservoirs alsong Tietê River (Brasil)	2014, 2016	algorithm evaluation
			K_d	0.3-0.5 m^{-1}	MAPE = 8.9-18.8 %			
Shen et al. (2017)	empirical	S3A	K_d	0-12 m^{-1}	R^2=0.81	Lake Taihu (China)	2017	sensor and algorithm evaluation
Toming et al. (2016a)	empirical	S2A	CHL	0-70 $mg \cdot m^{-3}$	R^2 = 0.83	11 lakes in Estonia	Aug 2015	sensor and algorithm evaluation
			CDOM	2-16 $g \cdot m^{-3}$	R^2 = 0.72			
			DOC	6-21 $g \cdot m^{-3}$	R^2 = 0.92			
Yousef et al. (2017)	empirical (NASA)	SeaWiFS MODIS	K_d	0.091-0.121	R^2 = 0.72 R^2 = 0.88	Great Lakes (Canada/USA)	1998-2012	trend analysis of water clarity, influence of invasive mussel
Zhang et al. (2016d)	semi-analytical	L8	TSM	0-20 $g \cdot m^{-3}$	R^2 = 0.85	Xin'anjiang reservoir (China)	Dec 2013 - Apr 2015	spatial and seasonal patterns
Zhang et al. (2016c)	empirical; Shi et al. (2015)	MODIS	TSM	0-450 $g \cdot m^{-3}$	Shi et al. (2015)	Lake Taihu (China)	2004-2013	driver analysis of river plume
Zheng et al. (2016)	empirical	L8	K_d	2-16 m^{-1}	MAPE = 23.18 %	Dongting Lake (China)	2013-2016	algorithm evaluation, pattern and driver analysis

Continued on next page

Table 7.2 – *Continued from previous page*

Authors	Techniques	Sensor	Parameter	Range	Accuracy	Study area	Time	Process
Biota - Phytoplankton and Cyanobacteria								
Beck et al. (2016)	empirical, semi-analytical	CASI*	CHL	30-80 mg·m^{-3}	R^2 = 0.729	Lake Harsha (USA)	27 June 2014	algorithm comparison and sensor transfer
Bertani et al. (2017)	product by NOAA-NCCOS	MERIS, MODIS	cyano bloom size	-	-	Lake Erie (Canada/USA)	2002-2013	comparision of different monitoring methods
Bresciani et al. (2018)	bio-optical inversion	S2A, L8	CHL	0-20 mg·m^{-3}	R^2=0.82	subalpine lakes (Italy)	2015-2017	sensor evaluation, WFD monitoring
Bresciani et al. (2016)	empirical, bio-optical inversion, MERIS MPH	L8, MERIS, MIVIS*, APEX*	cyano, CHL	20-100 mg·m^{-3}	relative comparisons	subalpine lakes; Mantua lakes (Italy)	2003-2015	cyanobacteria bloom monitoring
Clark et al. (2017)	empirical	MERIS in prep. for S3-OLCI	cyanoHAB frequency	10^4-10^7 cells·mL^{-1}	R^2 = 0.95	lakes in the USA	2003-2015	detection of cyano HABs in recreational and drinking water bodies
Dlamini et al. (2016)	empirical	MODIS	CHL	0.1-0.84 mg·m^{-3}	R^2 = 0.89	Lake Chivero (Zimbabwe)	Feb to May 2012	relation to land use
Dörnhöfer et al. (2018a)	bio-optical inversion	MODIS, L7/8, S2A	CHL	2.3-35.8 mg·m^{-3}	RMSE = 3.6 - 19.7 mg·m^{-3}	Lake Kummerow (Germany)	July-Oct 2015	combination of different sensors and *in situ* data
Duan et al. (2017)	empirical	MODIS	CHL PC	5-250 mg·m^{-3}	R^2 = 0.64 R^2 = 0.4	Lake Chaohu (China)	2000-2014	relationship PC:CHL analysis, developing management guidelines
Fahnenstiel et al. (2016)	semi-analytical (Shuchman et al., 2013a)	MODIS	CHL	0.2-8 mg·m^{-3}	R^2=0.83	Upper Great Lakes (Canada/USA)	2010-2013	modelling primary production
Ha et al. (2017)	empirical	S2A	CHL	1-9 mg·m^{-3}	R^2=0.68	Lake Be Be (Vietnam)	2015-2017	sensor and algorithm evaluation, seasonal development
Ho et al. (2017)	empirical	L5	bloom area	-	relative assessement to MERIS	Lake Erie (Canada/USA)	1984-2011	generation of a long-term phytoplankton bloom recors
Jin et al. (2017)	empirical	MERIS	cyano	0-100 %	MAPE = 13.44 %	Lake Taihu (China)	12 Aug 2010	mapping cyanobacteria abundance

Continued on next page

Table 7.2 – *Continued from previous page*

Authors	Techniques	Sensor	Parameter	Range	Accuracy	Study area	Time	Process
Li et al. (2018)	empirical	L8	CHL	0-30 $mg \cdot m^{-3}$	MAPE = 14.05 %	Xin'anjiang reservoir (China)	2013-2015	sensor and algorithm evaluation, driver analysis
Ogashawara et al. (2017a)	empirical	L8	bloom	3 classes: water, severe/ moderate bloom	OA = 88.46 %	Eagle Creek Reservoir (USA), Lake Erie (Canada/USA), Lake Tai (China)	summer 2014	development of an easy to use algorithm
Pitarch et al. (2017)	Maximum Peak Height	MERIS	cyano, CHL	0-734 $mg \cdot m^{-3}$	R^2 = 0.62	Albufera de valencia (Spain)	2002-2014	time series, seasonal cycles
Salem et al. (2017)	7 MERIS algorithms	MERIS	CHL	8.1 - 187.4 $mg \cdot m^{-3}$	R^2 = 0.42-0.65	Lake Kasumigaura (Japan)	2002-2012	time series, algorithm comparison
Sayers et al. (2016)	empirical; classification tree	MODIS	cyano blooms	classes	OA = 83 %	Greta Lakes (Canadan/USA)	2002-2013	time series, driver analysis, monitoring
Shuchman et al. (2017)	products from Color Producing Agents Algorithm	several sensors	water clarity, SAV, primary productivity, harmful algal bloom			Great Lakes (Canadan/USA)	1970-2016	effect of invasive mussels on water clarity
Zhang et al. (2016b)	empirical, sub-pixel analysis	MODIS	cyanoHAB area	50 - >200 km^2	-	Lake Taihu (China)	2001-2013	time series, driver analysis of cyanoHAB
Zolfaghari and Duguay (2016)	empirical	MERIS	CHL	10-1000 $mg \cdot m^{-3}$	RMSE= 0.31	Lake Erie (Canada/USA)	2004-2012	time series and driver analysis
			Z_{SD}	0.01 - 7.9 m	RMSE=0.19			
Biota - Submerged aquatic vegetation								
Fritz et al. (2017a)	depth-invariant index	RapidEye	SAV	coverage	k=0.61	Lake Kummerow (Germany)	June-Aug 2015	seasonal SAV development
Grimm et al. (2016)	depth-invariant index	Pléiades	SAV	-	-	Lake Huron (Canada/USA)	2013	maps of lake trout spwaning sites
Liang et al. (2017)	classification tree	MODIS	SAV, emergent, cyano scums	classes	OA = 86 %	Lake Taihu (China)	2010-2016	algorithm development
Luo et al. (2017)	classification tree	HJ-CCD	SAV	classes, species differentation	k = 0.63	Lake Taihu (China)	Feb - Oct 2013	algorithm development based on SAV phenology

Continued on next page

Table 7.2 – *Continued from previous page*

Authors	Techniques	Sensor	Parameter	Range	Accuracy	Study area	Time	Process
Luo et al. (2016)	classification tree	L5, HJ-CCD	SAV	habitat classes, SAV area	-	Lake Taihu (China)	1984-2013	long-term SAV trend analysis, driver analysis
Yadav et al. (2017)	classification	L8	SAV	20-40% coverage	OA = 86.5%	Lake Biwa (Japan)	Sep/Oct 2013-2016	change detection
			biomass	3390 - 4550 t	R^2 = 0.79			
Zhang et al. (2016a)	classification tree	MODIS	aquatic vegetation	classes	-	Lake Taihu (China)	2003-2014	implications for lake restoration
Lake Surface Temperature								
Allan et al. (2016)	analytical	L7	T	6.1-23.1 °C	RMSE = 0.48 K	Rotura lakes (New Zealand)	2005-2008	combination of *in situ*, remote sensning and 3-D modelling
Huang et al. (2017b)	mono-window	L8	T	2.33-15.75 °C	R^2 = 0.9578	Arctic thermokarst lakes ()	July-Aug 2013	inter- and intra-lake patterns and gradients
Li et al. (2017)	mono-window	L7	T	3-35 °C	R^2 = 0.92	Poyang Lake (China)	2015	combination iwth limnologic model
Ling et al. (2017)	mono-window	L7	T	5-30 °C	R^2 = 0.9268	dams in Qingjiang River (China)	2000-2014	monitoring thermal pollution by dams
Pareeth et al. (2017)	homogenisation approach, split-window	13 sensors	T	-'10 -30 °C	$R^2 \sim 0.98$	peri-alpine lakes (Italy)	1986-2015	trend analysis
Pareeth et al. (2016)	homogenisation approach, split-window	13 sensors	T	7-26 °C	RMSE = 0.38-1.19 °C	Lake Garda (Italy)	1986-2015	trend analysis, diurnal cycles
Zhong et al. (2016)	homogenised product	OISST2, GLSEA2 LST products	T	0.5-24 °C	-	Great Lakes (Canada/USA)	1982-2012	understanding aprubt warming from 1997-1998, combination with modelling
Ice phenology								
Murfitt and Brown (2017)	MODIS product	MODIS	ice phenology, T			lakes in Ontario/Manitoba (Canada)	2001-2014	trend analysis

Continued on next page

Table 7.2 – *Continued from previous page*

Authors	Techniques	Sensor	Parameter	Range	Accuracy	Study area	Time	Process
Weber et al. (2016)	classification tree	AVHRR	ice phenology	Day of year	r = 0.2 - 0.73	Lake Neusiedel (Austria), Lake Pepsi, Lake Võrtsjärv (Estonia)	1990-2012	tlong-term time series of freeze-thaw cycles

Evaluating the suitability of the new Sentinel-2A satellite for mapping lake ecology indicators

Chapter 4 and Chapter 5 addressed the second objective of this thesis. Evaluations were conducted at both considered lakes. At Lake Starnberg, evaluations comprised TSM, CHL and CDOM as well as water depth and substrate coverage. At Lake Kummerow, the main main focus was on CHL.

Relatively clear, optically deep water - Lake Starnberg

At Lake Starnberg, colleagues from DLR Oberpfaffenhofen and TU Munich provided *in situ* data measured timely to a S2A image acquisition on 13. August 2015. The analysis (Chapter 4; Dörnhöfer et al., 2016b) included comparisons among three different atmospheric correction algorithms (MIP, ACOLITE, Sen2Cor), from which the former two were specifically developed for water bodies. The comparison revealed R_{rs} spectra which varied in shape and intensity among the three approaches. Such differences were, however, expected and are anticipated for sensors other than S2A as well. Doxani et al. (2018) and GLaSS (2014) reported similar variations among different correction algorithms. Examining the atmospherically corrected R_{rs} spectra at the measurement sites also highlighted differences to the *in situ* measured R_{rs} spectra. These differences probably resulted from imperfect removal of atmospheric and water surface effects but also from the scale difference between the point *in situ* measurements and the spatially extended satellite measurements. These differences result in large relative errors due to the low signal gathered from the water and are therefore essential in lake remote sensing. The entirely physically based model MIP turned out to produce spectra closest to *in situ* measurements. It therefore formed the input for the subsequent analyses with the bio-optical model WASI-2D to retrieve water constituents (TSM, CDOM), water depths and lake bottom substrate.

The bio-optical analyses with WASI-2D showed that S2A was capable of capturing and resolving small variations of TSM concentrations (1.1-5.1 $g \cdot m^{-3}$, mean: 1.8 ± 0.2 $g \cdot m^{-3}$) and CDOM absorption (0.1-0.74 m^{-1}, mean: 0.14 ± 0.02 m^{-1}) at high spatial detail. CDOM obtained from S2A was lower than the CDOM modelled from *in situ* measurements (0.42-0.44 m^{-1}). TSM concentration analysed from water samples matched with the lower boundary of the TSM concentrations retrieved from S2A. CDOM is normally stated as an absorption value (Brezonik et al., 2015), i.e. in the same physical unit as is retrieved during inverse modelling. Otherwise, TSM is indirectly derived from the inherent optical properties (IOP) 'backscattering by TSM' ($b_{b,TSM}(\lambda)$) using a mass-specific conversion factor (cf. section 4.2.3). To assess the suitability of S2A for lake water remote sensing, the analysis included a comparison of $b_{b,TSM}$(550 nm) values retrieved from S2A and *in situ* measurements. A comparison based on IOPs is independent of the accuracy of the mass-specific conversion and resulted in an even closer match between *in situ* and S2A values.

The evaluation of 13 August 2015 indicated that CHL concentrations of $\sim$ 1 $mg \cdot m^{-3}$ were too low for a retrieval with S2A and WASI-2D. Analyses of other images acquired in August 2015 using WASI-2D allowed retrieval of CHL concentrations on average between 1 and 3.5 $mg \cdot m^{-3}$ (Fritz et al., prep). Varying conditions in the atmosphere may have facilitated the removal of atmospheric effects and subsequently the retrieval of water constituents which again may be influenced by varying conditions within the lake. These results underpin the conclusion in Chapter 4: using a single image acquisition with a limited set of *in situ* data represented an initial evaluation and was valuable in obtaining a first assessment and encouraging the use of S2A for lake analyses. Further robust validations require assessments over several acquisition dates and lakes with different optical characteristics. Such assessments in turn necessitate extensive *in situ* campaigns which are only feasible through collaborations of multiple groups, ideally through financially sound projects.

Phytoplankton- and CDOM-rich, optically deep water - Lake Kummerow

S2A evaluation for CHL retrieval in eutrophic, phytoplankton-rich waters was considered in Chapter 5 (Dörnhöfer et al., 2018a). The investigated CHL product originated from a different physically based, bio-optical inversion model, i.e. MIP, and was analysed during a phytoplankton bloom with cyanobacterial predominance. The fine spatial resolution of S2A revealed detailed structures of spatial gradients in CHL concentrations (3 - 45 $mg \cdot m^{-3}$), such as distinct streaks with very high concentrations traversing patches with lower concentrations. Comparisons with *in situ* CHL samples (1 day later) showed that S2A retrieved CHL matched within the uncer-

tainty range of *in situ* data. Another option to assess the suitability of S2A for lake water remote sensing could be a comparison with another sensor which is already established for water analyses and still in orbit, such as MODTE/ MODAQ (see references in Table 3.4, 3.5 and 7.2). Correlation analysis between CHL retrieved from S2A and from timely acquired MODTE data demonstrated a strong linear relationship between both sensors (r=0.89).

Relatively clear, optically shallow water - Lake Starnberg

S2A's suitability for mapping lake ecology indicators in optically shallow water was tested in the relatively clear waters of Lake Starnberg (Chapter 4 Dörnhöfer et al., 2016b). Water depth and substrate coverage represented the indicators of interest. The spectral resolution of S2A allowed for the differentiation between two bottom types, i.e. SAV and bare sediment. The high spatial resolution of 10 m enabled the delineation of the partially narrow shallow water areas at Lake Starnberg which, for instance, would hardly be detectable with Landsat's 30 m or even Sentinel-3's/MERIS 300 m. Thus, small-scale variations and transitions between areas covered by dense SAV or bare substrate became apparent. A problem in mapping SAV with remote sensing is the scarce availability of *in situ* data about substrate coverage as a basis for sensor and algorithm evaluations (see also Fritz et al., 2017a, prep). If such data are available, different scales of *in situ* mapping (e.g. species abundance estimations by divers at points along transects) and absence of large homogenous patches hamper an adequate comparison to the spatial coverage of a remote sensor. Due to the lack of SAV and substrate mappings, the S2A results were qualitatively compared with retrievals in previous studies as conducted by Rößler et al. (2012, 2013). Indeed, S2A found similar structures of dense SAV as Rößler et al. (2012, 2013) using hyperspectral and RapidEye data from 2011 which indicates a certain coherence with other sensors; however, different SAV mapping approaches were considered in the studies. A distinct detection of bare sediment at well known sandy shoreline sections (e.g. Roseninsel and south-eastern shoreline at Seeshaupt) underpinned meaningful S2A substrate mappings.

To consider the effect of the water depth on R_{rs} spectra in shallow waters, substrate unmixing using WASI-2D includes concurrent water depth retrieval. Assessing the accuracy of fitted water depths in comparison to, for instance, echo sounding data provides a further indication on the quality of analysing shallow water lake ecology indicators with S2A. Archived echo sounding data from 2012 highly correlated with S2A derived water depths (r=0.95) but were slightly underestimated ($\sim$ 0.5 m) between 0.5 and 2.5 m. Water depths shallower than 0.5 m lacked echo sounding data. In water depths deeper than 2.5 m, WASI-2D retrieved erroneous water depths (underestimation) using S2A. Further analyses which considered a fixed substrate type indicated that S2A did not provide enough spectral information for WASI-2D to correctly differentiate between mixed SAV and bare sediment patches in water depths deeper than 2.5 m.

Combination of multi-sensor data for phytoplankton monitoring

Chapter 5 addressed the third objective of this thesis. The idea of combining multiple sensors aims to increase the chance of obtaining cloud-free images of a lake, enabling more continuous time series. Sensors or sensor constellations with high spatial resolution (tens of metres) such as S2 or L8 have a revisit time between 5 and 16 days (Drusch et al., 2012; Irons et al., 2012). In cloud-prone regions, such as the study area Lake Kummerow, clouds often reduce the number of suitable images. Low spatial resolution sensors (hundreds of metres), such as MODIS or S3, acquire data at a daily or even higher temporal rate (Donlon et al., 2012), increasing the chance for cloud-free images. If a lake's size provides at least a few pure water pixels (e.g. 10-15 MERIS pixels in a $\sim$ 250 ha lake; Matthews et al., 2010) that a sensor records, the retrieved lake indicator information from low spatial resolution sensors may fill temporal gaps between the high spatial resolution data acquisitions. A multi-sensor approach requires a sensor-independent physical model to guarantee a comparison based on the same methodology including the atmospheric correction and lake ecology indicator retrieval.

This thesis examined such a multi-sensor approach in Chapter 5 (Dörnhöfer et al., 2018a) with the case study of Lake Kummerow and its phytoplankton development during summer 2015. To this end, CHL products

and an indicator of harmful algal blooms (eoHAB) were obtained from MIP, which conducts both atmospheric correction and water constituent retrieval ensuring methodologically comparable results among sensors. A series of sensors served as the basis for parameter retrieval, i.e. MODIS-Aqua and MODIS-Terra as low spatial with high temporal resolution sensors and L7, L8, S2A as high spatial with low temporal resolution sensors. Combining suitable and cloud-free data sets resulted in a total of 33 images between 1st July and 3rd October 2015. The time series captured low CHL concentrations below 10 mg·m^{-3} during early summer and the development of a phytoplankton bloom at the beginning of August with a lake average CHL maximum of 35.8 mg·m^{-3}. Subsequently, CHL concentrations slightly varied around a relatively high level ($\sim$ 20 mg·m^{-3}) until the beginning of October. Combining, for instance, lake-wide average results of a sensor-independent model within a time series was feasible. Nevertheless, it is a question of whether different sensors provide coherent results. Examining the time series, lake average CHL concentrations from different sensors followed a reasonable and consistent temporal development. At the beginning of August, in particular, CHL concentrations derived from different sensors exhibited a coherent increase.

Few (6 times) match-ups between the high and low spatial resolution sensors on the same day enabled a quantitative analysis of coherence. Between 250 and 2500 L7/L8 or S2A pixels occurred within a MODTE or MODAQ pixel. High standard deviations indicated a certain spatial variability within the 500x500 m^2 MODTE/ MODAQ pixels. Nevertheless, CHL concentrations from match-ups within a small time slot ($\sim$ 20 min) scattered around the 1:1 line and showed acceptable measures of value differences: MAE varied between 1.2 and 5.0 mg·m^{-3} with relative errors (nRMSE) between 28 and 63 %. A strong correlation, however, existed only between S2A and MODTE (r=0.89) and one match-up between L7 and MODTE (r = 0.64). Strong discrepancies between CHL from different sensors occurred in match-ups with a time slot larger than 1 hour, e.g. L8 and MODAQ. Here, nRMSE values > 286 % were observed, indicating that lake conditions or atmospheric conditions may have changed within hours and complicated CHL retrieval. A comparison with *in situ* data from 7 August (uncorrelated match-up between L8 and MODAQ) showed that L8 retrieved CHL was closer to *in situ* CHL than MODAQ.

This comparison with *in situ* data emphasised the challenge of considering different accuracies when combining multiple sensors. Since MODIS acquires data daily, the number of match-ups with *in situ* measurements acquired within $\pm$ 1 day was higher (13 times) compared to L7/L8/S2A (1-2 times). Moreover, the suitability of several litres water sample for evaluating CHL retrievals with 500 x 500 m^2 MODIS pixels can be questioned. Considering the uncertainty of *in situ* data, calculated accuracy measures ranged between 3.0 and 19.4 mg·m^{-3} (MAE) whereas L8 and S2A agreed best at the beginning of August. In contrast, L8 also offered the highest discrepancy at a different match-up date. Around this date (23 August), CHL from different satellites followed a similar trend whereas *in situ* data from two measurement days were distinctly lower. Methodological differences such as sampling below the surface vs. at the surface covered with scums and the influence of degrading pigments in satellite signal which were not considered in *in situ* samples or erroneous analysis of both *in situ* and satellite data may explain the discrepancies.

Such comparisons demonstrate the challenges associated with combining multiple sensors and also integrating *in situ* data. The gathered, detailed time series on the phytoplankton development at the study area Lake Kummerow, however, shows that the effort in combining multiple sensors and *in situ* data is worthwile. *In situ* data alone were not able to delineate the variable spatio-temporal CHL development. Nevertheless, *in situ* data are indispensable since they supply information which remote sensing is unable to provide, such as water column profiles, information beyond euphotic depth, detailed analyses on e.g. species composition and information during cloudy periods (e.g. second half of July). Meanwhile, combined satellite data represents a valuable information source on spatial surface patterns at a theoretically higher temporal resolution. Even the low spatial resolution of MODIS sensors captured spatial tendencies. The higher spatially resolved data acquired by Landsat and S2A sensors provided detailed insights into surface structures before and after the MODIS acquisitions. Thus, combining multiple sensors allowed spatially tracking surface CHL evolution and

pattern shifts during the development phase of a phytoplankton bloom.

Assessing the value of archived MERIS satellite imagery for monitoring lake ecology indicators

Although new sensors are available with improved spatial, radiometric and spectral resolutions suitable for lake remote sensing, archived imagery may also represent a valuable data source for retrieving earlier information and time series on lake ecology indicators. The archive of the ocean colour sensor MERIS (300 x 300 m^2 spatial resolution) provides consistent data from March 2002 until April 2012 which are well suited for lakes with a sufficient spatial extent. Chapter 6 (Dörnhöfer et al., 2018b) of this thesis therefore includes an analysis of water constituents, i.e. CHL, TSM and CDOM, retrieved from the MERIS archive. The study was conducted at Lake Kummerow using the well established (e.g. Palmer et al., 2015c; Philipson et al., 2016) neural network algorithm FUB-WeW. Thus, a 9-year time series (2003-2011) of CHL, TSM and CDOM covering all seasons could be generated.

Regular monitoring data acquired by LU-MV during the growing season enabled a comparison of MERIS with *in situ* CHL. The quantitative assessment indicated correlating MERIS and *in situ* CHL concentrations (r = 0.78), whereas MERIS CHL concentrations > 10 $mg \cdot m^{-3}$ were higher than *in situ* measurements. Calculating long-term (9 years) monthly lake average concentrations delineated the seasonal behaviour of CHL throughout the year. According to the MERIS data, a phytoplankton spring bloom regularly occured in April ($\sim$ 11 $mg \cdot m^{-3}$) followed by the clear water phase ($\lesssim$ 6 $mg \cdot m^{-3}$) in May/June. Subsequent increasing CHL concentrations peaked in September ($\sim$ 30 $mg \cdot m^{-3}$) and decreased until November. During winter months, CHL concentrations remained $\sim$ 5 $mg \cdot m^{-3}$. Knowledge about the spring bloom, clear water phase and high summer concentrations were already well-known from *in situ* data with the difference that *in situ* measurements indicated highest CHL concentrations in August. However, no information on winter CHL concentrations at Lake Kummerow has been available so far. Otherwise, the lack of *in situ* measurements impeded quantitatively verifying the reliability of the retrieved concentrations during winter months.

The same issue applied for TSM and CDOM. Both parameters have not been measured at the lake; the MERIS time series therefore revealed the first spatio-temporal information on their concentrations. TSM demonstrated a similar seasonal behaviour as CHL with highest concentrations occurring during summer months ($\sim 3\, g \cdot m^{-3}$) and hardly varying concentrations $\sim$ 1 $g \cdot m^{-3}$ during the rest of the year. This behaviour was reasonable since TSM at Lake Kummerow mainly consists of organic particles, i.e. phytoplankton and detritus. According to the analysed MERIS data, CDOM exhibited a distinct seasonal behaviour with increasing values from January to April ($\sim$ 0.05 - 0.6 m^{-1}); during the summer they slightly varied between 0.6 and 0.7 m^{-1} before they decreased again during autumn. *In situ* DOC measurements (CDOM may correlate with DOC; e.g. Hestir et al., 2015b; Toming et al., 2016b) indicated only slightly varying concentrations between March and October which also lacked any measurements during autumn and winter. An algorithm failure during the low light period, which aggravates a proper retrieval of light absorbing water constituents such as CDOM, might be plausible but cannot be finally resolved without any winter/autumn *in situ* measurements.

Nonetheless, the time series of Lake Kummerow provided a valuable source for calculating trends of water constituent development. Analysing the MERIS CHL data set revealed a decreasing tendency of -3.4 $mg \cdot m^{-3}$ between 2003 and 2011. A similar trend was found based on the *in situ* data (-3.7 $mg \cdot m^{-3}$) which reinforces that remote sensing and *in situ* data may complement each other in reaching a similar conclusion. TSM also decreased during the period (-1.3 $g \cdot m^{-3}$) whereas CDOM showed no trend. This information was only available through analysing the MERIS data archive. Such analyses with well-established algorithms provide valuable time series information of non-investigated lakes and irregularly or not measured water constituents. Indeed, comparisons with *in situ* measurements entail various issues such as temporal mismatch, up-scaling or methodological differences (e.g. Dörnhöfer et al., 2018a; Pahlevan et al., 2016; Salama and Su, 2011; Toming et al., 2016a). Without any *in situ* data serving for quantitative assessments or at least plausibility checks, such time series have to be interpreted carefully and cross-checked with literature to check their reliability.

7.2 Answers to research questions

The key achievements of this thesis summarised in section 7.1 aimed to contribute to answer the two main research questions underpinning the entire text.

Do new sensors fulfill the promise on their predicted suitability for lake remote sensing?

The conducted evaluations indicated a well performance of S2A and L8 for retrieving lake ecology indicators. In detail, the noise equivalent R_{rs} difference of S2A data was high enough to be suited for remote sensing of deep water in relatively clear lakes. TSM retrievals achieved reliably concentrations $\sim$ 1.5 g·m^{-3} whereas CDOM was slightly lower compared to *in situ* values. CHL retrievals with concentrations $\sim$ 1 mg·m^{-3} performed unevenly. In the phytoplankton and CDOM-rich waters of Lake Kummerow, S2A turned out to be well-suited for retrieving CHL concentrations within the uncertainty range of *in situ* measurements. Compared to L8, the additional bands of S2 sensors > 700 nm are advantageous for lake remote sensing. Indeed, the CHL results of L8 were ambivalent with one match-up-date falling within the uncertainty range and one completely out of the range (a laboratory error cannot be excluded). Nevertheless, other analysed scenes without *in situ* data reasonably followed the temporal development of CHL so that it is worth to continue analyses with L8 for lake remote sensing. In optically shallow waters, S2's high spatial resolution of up to 10 m was anticipated to support SAV and water depth mapping. Indeed, S2 allows unprecedented discrimination of lake bottom coverage with freely available data. With Secchi disk depth of around 4 m, S2A data enabled a reasonable differentiation between dense SAV, mixed and bare sediment areas up to 2.5 m water depths using a bio-optical modelling approach at Lake Starnberg. In deeper waters, erroneous water depth retrieval indicated an insufficient spectral information provided by S2A to reliably differentiate between SAV covered, bare sediment and mixed areas using the applied approach.

These evaluations, however, open a discussion about the reference to which the suitability of these new sensors is examined. The literature review in Chapter 3 and section 7.1 pointed out *in situ* measurements timely to image acquisitions ($\pm$ 2 hours up to 1 day) as a major means for evaluating lake ecology indicator values retrieved in a pixel or pixel environment (macro-pixel) surrounding the coordinate of the measurement site. These comparisons, however, often focused on exact match-ups or strong correlations but neglect uncertainties associated with *in situ* sampling, e.g. GPS positional inaccuracies, sample variability, device accuracies, methodological differences. Evaluation plots often depict error bars as standard deviation of the mean value of several pixels surrounding the measurement site; *in situ* data rarely contain an error bar in remote sensing studies. To overcome forcing exact match-ups, Chapter 3 and 5 suggested the integration of *in situ* uncertainty ranges in comparisons between *in situ* and satellite data. Chapter 4, for instance, therefore included the standard deviation of repeated radiometric measurements conducted at one measurement site in comparison to S2A R_{rs} spectra from different atmospheric correction algorithms. At the case study of water constituents at Lake Kummerow, *in situ* measurements conducted in this thesis included three samples taken at each measurement site for each analysed water constituent (cf. Chapter 2). Three samples represented a trade-off between a minimum of multiple samples at a measurement site to indicate sample variability and a feasible sample transport and analyses while covering a certain spatial area. Additional samples which were analysed by an external laboratory and subsequent uncertainty calculations defined an uncertainty range of CHL samples ($\pm$ 48 %) taken at Lake Kummerow, into which the satellite derived values should preferably fall (cf. Chapter 5).

In summary, the short operating time of S2A and cloud coverage during the main measurement phase of this thesis limited the evaluation of S2A's and L8 suitability for lake remote sensing to a few scenes. Analyses focused on two lakes with highly differing optical characteristics but statements are limited to conditions similar to these lakes at acquisition dates and based on a small sample size. Stating a real suitability of S2 and L8 for lake remote sensing certainly is a preliminary evaluation but promising to encourage further research with these sensors in lakes. Results from other case studies conducted at various lakes on the globe and mainly focusing

on water constituents support the positive statement of this evaluation. Nevertheless, Pahlevan et al. (2017) figured out S2A and L8 on-orbit signal to noise ratio in short wavelengths is distinctly lower than recommended for ocean colour sensors. Resampling S2A data to 20-30 m may reduce image noise and provide L8 comparable data valuable for lake remote sensing (Pahlevan et al., 2017). Furthermore, S2's acquisition characteristics lead to slight mis-registrations between bands which is problematic for proper sun glint detections and corrections (Harmel et al., 2017; Pahlevan et al., 2017). In this context, one has to bear in mind that L8 and S2 were not specifically designed for water analyses. Nevertheless, combining this thesis's results with the results of other studies reviewed in Chapter 3 and its update (Table 7.2), S2 and L8 seem to hold promise for use in lake remote sensing.

Can different satellite sensors synergetically be used to contribute to lake monitoring?.

The example of Lake Kummerow which combined retrieved CHL products from different sensors (MODAQ, MODTE, L7, L8 ad S2A) demonstrated that synergetic use of different sensors is feasible. This synergetic combination provided a time series which indicated spatial variability within the lake through lake-wide standard deviations; the temporal dynamics of phytoplankton development became apparent through lake average CHL concentrations at a higher temporal resolution than obtained by *in situ* sampling. This example further examined how such information may be integrated into lake monitoring, e.g. into the programmes within the WFD. To this end, the lake's trophic state was first determined based solely on *in situ* data and secondly with CHL monthly averages obtained from satellite derived values. Indeed, using synergetic satellite CHL values revealed a higher trophic state (eutrophic 1) compared to the pure *in situ* calculation (mesotrophic 2). This difference mainly originated from higher satellite than *in situ* average concentrations in late summer months. Integrating satellite data into trophic state calculations further enabled generating a spatial depiction of the trophic state. This map showed the majority of the lake as eutrophic 1 and a part close to the eastern shoreline as mesotrophic.

Discussing these results emphasised that satellite data may assist traditional monitoring approaches; a robust support, however, may not simply combine satellite and *in situ* measurements in an established index calculation. Index calculations such as the trophic state classification were specifically developed and tested for *in situ* data (e.g. Riedmüller, 2014). Satellite data involve different issues than *in situ* data which have to be considered for index calculations based on lake monitoring data. Although synergetically combined satellite data have a theoretically high temporal resolution, longer periods of cloudy weather lead to temporally irregular data supply (see Chapter 5). The derived concentration originates from a mixed signal between the surface and light penetration depth (Gege, 2017) compared to fixed depths of water samples. Nevertheless, satellite data may reduce uncertainties in trophic state assessments and lake monitoring arising from spatial variabilities undetected by point based *in situ* measurements (Kiefer et al., 2015; Søndergaard et al., 2016). Furthermore, physically sound and transferable remote sensing algorithms which may work similarly and comparably among different regions are advantageous compared to the recently 'Three hundred ways to assess Europe's surface waters' (Birk et al., 2012). This advantage requires sensor-independent algorithms for both atmospheric correction and lake ecology indicator retrieval. Cross-sensor comparisons such as those conducted in Chapter 5 and other studies (e.g. Liu et al., 2017; Lymburner et al., 2016; Pahlevan et al., 2017) form the basis to analyse the comparability of lake ecology indicators from different sensors. Assessing and providing sensor-specific uncertainty measures which can then be considered in lake monitoring may support a multi-sensor use.

Satellites acquire data beyond the main monitoring phase during the growing season. Thus, multi-sensor satellite CHL showed increased concentrations at Lake Kummerow likeley explained by a surface bloom occurring after the official measurement period which terminated in the first half of September. Bresciani et al. (2016) reported similar observations where satellite data revealed cyanobacteria blooms which may also be relevant for human health issues. Indicators on cyanobacteria presence such as eoHAB (Chapter 5) or the Cyano Index published by Clark et al. (2017) combined with near real-time satellite data may help to identify hot spot areas. Thus, authorities may react in a timely manner and check potential toxins with *in situ* water samples. Outside the official measurement periods, operational but also archived imagery provide information about water con-

stituents during autumn and winter. Often lacking measurement data and low sun angles for remote sensing data hamper autumn and winter analyses for lake monitoring.

Analysing archived imagery such as that of MERIS may also create synergies of operating sensors and lake monitoring. At Lake Kummerow, MERIS data enabled the calculation of trends in water constituent development and seasonal behaviour. Comparisons between CHL development based on the MERIS analyses (Chapter 6) and observations from the multi-sensor time series Chapter 5) indicated similar behaviours during summer months. OLCI as the heritage sensor of MERIS on-board S3 (Berger et al., 2012) ensures continuity of these data and may help to optimise, for instance, the location of monitoring sites (e.g. MERIS-study by Kiefer et al., 2015).

In summary, various issues associated with climate change, eutrophication and alien species invasion threaten lake environments and demand a rethinking of established, traditional monitoring approaches. New sensor techniques, progress in algorithm development and computational capacities facilitate a multi-sensor combination to support lake monitoring. As Bertani et al. (2017) suggested for cyanobacterial monitoring, a combination of different approaches including remote sensing, *in situ* measurements and modelling may tackle current challenges associated with lake monitoring.

7.3 Conclusions and future challenges

Using satellite data from sensors with varying spatial, spectral and temporal resolutions, this thesis demonstrated how water colour analyses can contribute to lake monitoring. The created *in situ* data bases and conducted analyses aimed to contribute to investigations of the open issues stated in the introduction to progress lake remote sensing. Uncertainty analyses of *in situ* water samples for CHL retrieval revealed a $\pm$ 48 % measurement uncertainty of samples in this thesis. Coefficients of variation up to 37 % occurred in CHL concentrations from multiple samples taken at one measurement site; this observation indicated coincidently varying water at a measurement site and variabilities through sample analysis. Thus, one conclusion of this thesis is a strong recommendation to include *in situ* data uncertainty analyses in remote sensing validations and aim at a match-up within uncertainty ranges rather than an exact match-up.

In doing so, suitability analyses of S2A and L8 as new sensors produced promising results under relatively clear and phytoplankton-/CDOM-rich conditions in optically deep waters. S2A further turned out to be a valuable data source for shallow water analyses if the water column is relatively clear and substrate types are spectrally, clearly distinguishable. Nevertheless, the limited number of *in situ* data and match-ups between satellite and *in situ* measurements resulted in a preliminary evaluation of these sensors. Further robust validations are required which cover even more water types. For such analyses, a variety of retrieval algorithms exists ranging from empirical, semi-analytical, neural networks and bio-optical inversion approaches.

This thesis focused on two physically-based, bio-optical inversion approaches (WASI-2D, MIP) and a neural network algorithm (FUB-WeW) which all offered different advantages and disadvantages. FUB-WeW is freely available and combines atmospheric correction and water constituent retrieval; it is, however, restricted to the water constituent concentrations for which the neural network was trained and sensor-specific, i.e. MERIS and further developed for S3. MIP combines a coupled atmospheric correction and water constituent, water depth or substrate retrieval and is applicable to any suited sensor. Since only the products are distributed by EOMAP GmbH & Co.KG, the model itself remains a black box. WASI-2D is freely available and enables the derivation of water constituents, water depths and substrates. Its structure allows adaptations to any suited sensor and lake conditions if the required data is available. The remote sensing input data, however, must be atmospherically corrected. The performance of physically-based, bio-optical inversion models strongly relies on the performance of the applied atmospheric correction algorithm. WASI-2D, however, includes an analytical algorithm for considering water surface effects such as sun and sky glint during parameter retrieval.

The atmospheric correction algorithms evaluated in this thesis were partially designed for water bodies. Only MIP was sensor-independent and performed best in relation to radiometric *in situ* measurements under relatively clear water conditions. Meanwhile developments of atmospheric correction algorithm progressed and a comparison among recently available approaches for L8 and S2 was published (Doxani et al., 2018). A sensor-independent and water body specific algorithm, however, is still lacking for lake remote sensing.

Combining this thesis's results with the reviewed literature could answer the two research questions positively: S2 and L8 provided promising results for lake remote sensing. In combination with archived imagery, a synergetic use of multiple recently operating and suitable sensors is expected to strongly support lake monitoring. Lake remote sensing and its combination with *in situ* measurements has made a lot progress over the last few years. Reviewing the published literature and the results of this thesis also emphasised still unresolved challenges and a variety of topics arose which are worth being investigated in the near future to continue the (rapid) progress in lake remote sensing:

- The essential basis for lake remote sensing is an accurate correction of atmospheric and water surface effects. Meanwhile, a variety of approaches also specifically designed for water bodies is available. None of them are both sensor-independent and open-source. Still, the available algorithms face challenges in correcting adjacency effects, sun and sky glint in addition to the 'normal' atmosphere at once while having only a limited number of multispectral bands in case of e.g. S2 and L8. The specific acquisition

modes of these sensors, however, hamper sun glint corrections (e.g. Harmel et al., 2017; Pahlevan et al., 2017). The development of a sensor-independent and open-source approach which considers the specific requirements of water surfaces may significantly contribute to the progress in lake remote sensing research and its combination with lake ecology. In this vein, assessing the influence of different atmospheric correction algorithms on the retrieval of lake ecology indicators should be a next step.

- The newly available sensors provided promising results regarding their use for lake remote sensing. Nonetheless, none of them are specifically designed to map lakes. Lake remote sensing may benefit from these sensors by means of a synergetic combination. With the launch of S3, the integration of S3 into this synergetic multi-sensor use for lakes should be evaluated. As already started, cross-sensor evaluations should be continued in order to increase knowledge about the comparability of retrieval algorithm products from different sensors. Such combinations require sensor-independent models for atmospheric correction and lake ecology indicator retrieval to ensure comparable data processing. Developing algorithm specific, pixel-based uncertainty measures, such as quality flags, may help to exclude uncertain pixels.
- *In situ* data are and remain the major source for evaluating sensors and algorithms in lake remote sensing. Robust evaluations or validations require large data bases with match-ups of lakes having varying optical characteristics. Collaborations among different groups from remote sensing and lake ecology disciplines may strengthen such evaluations by using capacities effectively and increasing knowledge and data from various lake types. Developing national or international data repositories may facilitate data access and usage. Advancing a common comprehension on (standardised) measurement protocols and metadata management therefore is crucial. Lack of financing often hampers *in situ* or laboratory inter-calibration of measurement devices and round robin tests of laboratories to increase knowledge about uncertainties originating from different measurement devices/ analysis procedures. A first attempt would be to increase sample sizes and measurements at each measurement site to obtain a degree of certainty and variability of *in situ* measurements. Further uncertainty analyses may improve remote sensing evaluations.
- Remote sensing depicts the spatial variability and patterns of lake ecology indicators at or near the water surface. A next step would be to use this spatially explicit and temporally highly available data in a combination with lake modelling and *in situ* data. Such a combination may extrapolate the spatial information vertically into the depth and temporally during cloudy or low light periods. Within this modelling context, remote sensing products may serve as input, comparison and/ or evaluation data for modelling such as for primary production modelling conducted by Kauer et al. (2015). The complexity of the different approaches requires the collaboration of different disciplines, e.g. remote sensing, lake ecology and modelling researchers.

The future about monitoring, understanding and managing lakes is about a synergetic combination of different approaches: *in situ* measurements with remotely sensed indicators from various suitable sensors together with lake modelling. Each of the approaches has its specific advantages and constraints. Some open research issues were elaborated which may be addressed in the near future to progress lake remote sensing. The data base created at Lake Kummerow and expanded at Lake Starnberg during this thesis is not yet fully exploited and offers potential for future analyses considering these issues. The contrasting characters and sizes of the two lakes make them suitable for advancing lake remote sensing and modelling making it worthwhile to continue measurements there.

References

Adrian, R., O'Reilly, C. M., Zagarese, H., Baines, S. B., Hessen, D. O., Keller, W., Livingstone, D. M., Sommaruga, R., Straile, D., van Donk, E., Weyhenmeyer, G. A., and Winder, M. (2009). Lakes as sentinels of climate change. *Limnology and Oceanography*, 54(6):2283–2297.

Albert, A. and Mobley, C. D. (2003). An analytical model for subsurface irradiance and remote sensing reflectance in deep and shallow case-2 waters. *Optics Express*, 11(22):2873–2890.

Alcântara, E., Bernardo, N., Watanabe, F., Rodrigues, T., Rotta, L., Carmo, A., Shimabukuro, M., Gonçalves, S., and Imai, N. (2016). Estimating the CDOM absorption coefficient in tropical inland waters using OLI/Landsat-8 images. *Remote Sensing Letters*, 7(7):661–670.

Alcântara, E. H., Stech, J. L., Lorenzzetti, J. A., Bonnet, M. P., Casamitjana, X., Assireu, A. T., and de Moraes Novo, E. M. L. (2010). Remote sensing of water surface temperature and heat flux over a tropical hydroelectric reservoir. *Remote Sensing of Environment*, 114(11):2651–2665.

Alikas, K. and Kratzer, S. (2017). Improved retrieval of Secchi depth for optically-complex waters using remote sensing data. *Ecological Indicators*, 77:218–227.

Allan, M. G., Hamilton, D. P., Trolle, D., Muraoka, K., and McBride, C. (2016). Spatial heterogeneity in geothermally-influenced lakes derived from atmospherically corrected Landsat thermal imagery and three-dimensional hydrodynamic modelling. *International Journal of Applied Earth Observation and Geoinformation*, 50:106–116.

Andrew, M. E., Wulder, M. A., and Nelson, T. A. (2014). Potential contributions of remote sensing to ecosystem service assessments. *Progress in Physical Geography*, 38(3):328–353.

Anzaldua, G., Gerner, N. V., Lago, M., Abhold, K., Hinzmann, M., Beyer, S., Winking, C., Riegels, N., Krogsgaard Jensen, J., Termes, M., Amorós, J., Wencki, K., Strehl, C., Ugarelli, R., Hasenheit, M., Nafo, I., Hernandez, M., Vilanova, E., Damman, S., Brouwer, S., Rouillard, J., Schwesig, D., and Birk, S. (2018). Getting into the water with the Ecosystem Services Approach: The DESSIN ESS evaluation framework. *Ecosystem Services*.

AQS (2008). Länderübergreifender Ringversuch - Chlorophyll in Oberflächenwasser - Chlorophyll-a, Phaeopigment: AQS (Analytische Qualitätssicherung Baden-Württemberg).

Arle, J., Blondzik, K., Claussen, U., Duffek, A., Grimm, S., Hiliges, F., Hoffmann, A., Leujak, W., Mohaupt, V., Naumann, S., Pirntke, U., Richter, S., Schilling, P., Schroeter-Kermani, C., Ullrich, A., Wellmitz, J., Werner, S., and Wolter, R. (2013). Wasserwirtschaft in Deutschland. Teil 2. Gewässergüte. Umweltbundesamt (UBA). Bonn, Germany.

Arp, C. D., Jones, B. M., and Grosse, G. (2013). Recent lake ice-out phenology within and among lake districts of Alaska, U.S.A. *Limnology and Oceanography*, 58(6):2013–2028.

Artell, J. (2013). Lots of value? A spatial hedonic approach to water quality valuation. *Journal of Environmental Planning and Management*, 57(6):862–882.

Aulló-Maestro, M. E., Hunter, P., Spyrakos, E., Mercatoris, P., Kovács, A., Horváth, H., Preston, T., Présing, M., Torres Palenzuela, J., and Tyler, A. (2017). Spatio-seasonal variability of chromophoric dissolved organic matter absorption and responses to photobleaching in a large shallow temperate lake. *Biogeosciences*, 14(5):1215–1233.

Australian Government (2000). National Water Management Strategy of Australia and New Zealand.

Barker, K., Mazeran, C., Lerebourg, C., Bouvet, M., Antoniades, D., Ondrusek, M. E., Zibordi, G., and Lavender, S. (2008). Mermaid: The MERIS matchup in-situ database. In ESA, editor, *Proceedings of the 2nd MERIS*, ESA SP, 1609-042X. European Space Agency, Noordwijk, The Netherlands.

Bavarian Environmental Agency (2000). Digital Elevation Model of Lake Starnberg. Augsburg, Germany.

Bavarian Environmental Agency (2016). Download Gauge Starnberg. Starnberger See. Bavarian Environmental Agency (BEA).

Bayern, G. (2013). Data of measure point Lake Starnberg.

Beck, R., Zhan, S., Liu, H., Tong, S., Yang, B., Xu, M., Ye, Z., Huang, Y., Shu, S., Wu, Q., Wang, S., Berling, K., Murray, A., Emery, E., Reif, M., Harwood, J., Young, J., Nietch, C., Macke, D., Martin, M., Stillings, G., Stump, R., and Su, H. (2016). Comparison of satellite reflectance algorithms for estimating chlorophyll-a in a temperate reservoir using coincident hyperspectral aircraft imagery and dense coincident surface observations. *Remote Sensing of Environment*, 178:15–30.

Beltrán-Abaunza, J. M., Kratzer, S., and Brockmann, C. (2014). Evaluation of MERIS products from Baltic Sea coastal waters rich in CDOM. *Ocean Science*, 10(3):377–396.

Benson, B. J., Magnuson, J. J., Jensen, O. P., Card, V. M., Hodgkins, G., Korhonen, J., Livingstone, D. M., Stewart, K. M., Weyhenmeyer, G. A., and Granin, N. G. (2012). Extreme events, trends, and variability in Northern Hemisphere lake-ice phenology (1855–2005). *Climatic Change*, 112(2):299–323.

Berger, M., Moreno, J., Johannessen, J. A., Levelt, P. F., and Hanssen, R. F. (2012). ESA's sentinel missions in support of Earth system science. *Remote Sensing of Environment*, 120:84–90.

Bernardo, N., Watanabe, F., Rodrigues, T., and Alcântara, E. (2017). Atmospheric correction issues for retrieving total suspended matter concentrations in inland waters using OLI/Landsat-8 image. *Advances in Space Research*, 59(9):2335–2348.

Bertani, I., Steger, C. E., Obenour, D. R., Fahnenstiel, G. L., Bridgeman, T. B., Johengen, T. H., Sayers, M. J., Shuchman, R. A., and Scavia, D. (2017). Tracking cyanobacteria blooms: Do different monitoring approaches tell the same story? *Science of the Total Environment*, 575:294–308.

Bezy, J.-L., Gourmelon, G., Bessudo, R., Baudin, G., Sontag, H., and Weiss, S. (1999). The ENVISAT Medium Resolution Imaging Spectrometer (MERIS). In Stein, T. I., editor, *IGARSS'99*, pages 1432–1434. IEEE.

Bicheron, P., Amberg, V., Bourg, L., Petit, D., Huc, M., Miras, B., Brockmann, C., Hagolle, O., Delwart, S., Ranera, F., Leroy, M., and Arino, O. (2011). Geolocation Assessment of MERIS GlobCover Orthorectified Products. *IEEE Transactions on Geoscience and Remote Sensing*, 49(8):2972–2982.

Binding, C. E., Greenberg, T. A., Watson, S. B., Rastin, S., and Gould, J. (2015). Long term water clarity changes in North America's Great Lakes from multi-sensor satellite observations. *Limnology and Oceanography*, 60(6):1976–1995.

Binding, C. E., Jerome, J. H., and Booty, W. G. (2010). Suspended particulate matter in Lake Erie derived from MODIS aquatic colour imagery. *International Journal of Remote Sensing*, 31:5239–5255.

Birk, S., Bonne, W., Borja, A., Brucet, S., Courrat, A., Poikane, S., Solimini, A., van de Bund, W., Zampoukas, N., and Hering, D. (2012). Three hundred ways to assess Europe's surface waters: An almost complete overview of biological methods to implement the Water Framework Directive. *Ecological Indicators*, 18:31–41.

Birk, S. and Ecke, F. (2014). The potential of remote sensing in ecological status assessment of coloured lakes using aquatic plants. *Ecological Indicators*, 46:398–406.

Bogena, H. R., Kunkel, E., Krüger, E., Zacharias, S., Pütz, T., Schwank, M., Bens, O., Borg, E., Brauer, A., Dietrich, P., Hajnsek, I., Kunstmann, H., Munch, J.-C., Papen, H., Priesack, E., Schmid, H. P., Wollschläger, U., and Vereecken, H. (2012). TERENO - Ein langfristiges Beobachtungsnetzwerk für die terrestrische Umweltforschung. *HyWa*, 3:138–143.

Bojanowski, A. (2014). Sauerstoffmangel: Todeszonen in der Ostsee haben sich verzehnfacht: Spiegel Online.

Bolpagni, R., Bresciani, M., Laini, A., Pinardi, M., Matta, E., Ampe, E. M., Giardino, C., Viaroli, P., and Bartoli, M. (2014). Remote sensing of phytoplankton-macrophyte coexistence in shallow hypereutrophic fluvial lakes. *Hydrobiologia*, 737(1):67–76.

Bonansea, M., Rodriguez, M. C., Pinotti, L., and Ferrero, S. (2015). Using multi-temporal Landsat imagery and linear mixed models for assessing water quality parameters in Río Tercero reservoir (Argentina). *Remote Sensing of Environment*, 158:28–41.

Borg, E., Fichtelmann, B., Schiller, C., Kuenlenz, S., Renke, F., Jahnke, D., and Wloczyk, C. (2014). DEMMIN - Test Site for Remote Sensing in Agricultural Application: JECAM Science Meeting, 21 - 23 July 2014, Ottawa, Ontario, Canada.

Bourg, L., D'Alba, L., and Colagrande, P. (2008). MERIS SMILE effect characterisation and correction: Technical Note.

Bouvet, M. and Ramino, F. (2010). Equalization of MERIS L1b products from the 2nd reprocessing: Technical Report ESA TN TECEEP/2009.521/MB, ESA.

Braga, F., Zaggia, L., Bellafiore, D., Bresciani, M., Giardino, C., Lorenzetti, G., Maicu, F., Manzo, C., Riminucci, F., Ravaioli, M., and Brando, V. E. (2017). Mapping turbidity patterns in the Po river prodelta using multi-temporal Landsat 8 imagery. *Estuarine, Coastal and Shelf Science*, 198:555–567.

Brando, V. E. and Dekker, A. G. (2003). Satellite hyperspectral remote sensing for estimating estuarine and coastal water quality. *IEEE Transactions on Geoscience and Remote Sensing*, 41(6):1378–1387.

Bresciani, M., Cazzaniga, I., Austoni, M., Sforzi, T., Buzzi, F., Morabito, G., and Giardino, C. (2018). Mapping phytoplankton blooms in deep subalpine lakes from Sentinel-2A and Landsat-8. *Hydrobiologia*, 3(1):31.

Bresciani, M., Giardino, C., and Boschetti, L. (2011a). Multi-temporal assessment of bio-physical parameters in lakes Garda and Trasimeno from MODIS and MERIS. *Italian Journal of Remote Sensing*, pages 49–62.

Bresciani, M., Giardino, C., Lauceri, R., Matta, E., Cazzaniga, I., Pinardi, M., Lami, A., Austoni, M., Viaggiu, E., Congestri, R., and Morabito, G. (2016). Earth observation for monitoring and mapping of cyanobacteria blooms. Case studies on five Italian lakes. *Journal of Limnology*.

Bresciani, M., Sotgia, C., Fila, G. L., Musanti, M., and Bolpagni, R. (2011b). Assessing common reed bed health and management strategies in Lake Garda (Italy) by means of Leaf Area Index measurements. *Italian Journal of Remote Sensing*, pages 9–22.

Bresciani, M., Stroppiana, D., Odermatt, D., Morabito, G., and Giardino, C. (2011c). Assessing remotely sensed chlorophyll-a for the implementation of the Water Framework Directive in European perialpine lakes. *Science of the Total Environment*, 409(17):3083–3091.

Breunig, F. M., Pereira Filho, W., Galvao, L. S., Wachholz, F., and Cardoso, M. A. G. (2017). Dynamics of limnological parameters in reservoirs: A case study in South Brazil using remote sensing and meteorological data. *Science of the Total Environment*, 574:253–263.

Brezonik, P. L., Olmanson, L. G., Finlay, J. C., and Bauer, M. E. (2015). Factors affecting the measurement of CDOM by remote sensing of optically complex inland waters. *Remote Sensing of Environment*, 157:199–215.

Bricaud, A., Morel, A., and PRIEUR, L. (1981). Absorption by dissolved organic matter of the sea (yellow substance) in the UV and visible domains. *Limnology and Oceanography*, 26(1):43–53.

Brönmark, C. and Hansson, L.-A. (2002). Environmental issues in lakes and ponds: current state and perspectives. *Environmental Conservation*, 29(03).

Brooks, B. W., Lazorchak, J. M., Howard, M. D. A., Johnson, M.-V. V., Morton, S. L., Perkins, D. A. K., Reavie, E. D., Scott, G. I., Smith, S. A., and Steevens, J. A. (2016). Are harmful algal blooms becoming the greatest inland water quality threat to public health and aquatic ecosystems? *Environmental toxicology and chemistry*, 35(1):6–13.

Brooks, C. N., Grimm, A. G., Shuchman, R., Sayers, M., and Jessee, N. (2015). A satellite-based multi-temporal assessment of the extent of nuisance Cladophora and related submerged aquatic vegetation for the Laurentian Great Lakes. *Remote Sensing of Environment*, 157:58–71.

Brown, L. C. and Duguay, C. R. (2010). The response and role of ice cover in lake-climate interactions. *Progress in Physical Geography*, 34(5):671–704.

Brown, L. C. and Duguay, C. R. (2012). Modelling Lake Ice Phenology with an Examination of Satellite-Detected Subgrid Cell Variability. *Advances in Meteorology*, 2012:529064.

Brucet, S., Poikane, S., Solheim, A. L., and Birk, S. (2013). Biological assessment of European lakes: ecological rationale and human impacts. *Freshwater Biology*, 58(6):1106–1115.

Bulgarelli, B., Kiselev, V., and Roberti, L. (1999). Radiative transfer in the atmosphere-ocean system: the finite-element method. *Applied Optics*, 38(9):1530–1542.

Cao, Y. and Hawkins, C. P. (2011). The comparability of bioassessments: A review of conceptual and methodological issues. *Journal of the North American Benthological Society*, 30(3):680–701.

Cao, Z., Duan, H., Feng, L., Ma, R., and Xue, K. (2017). Climate- and human-induced changes in suspended particulate matter over Lake Hongze on short and long timescales. *Remote Sensing of Environment*, 192:98–113.

Carpenter, S. R., Stanley, E. H., and Vander Zanden, M. J. (2011). State of the World's Freshwater Ecosystems: Physical, Chemical, and Biological Changes. *Annual Review of Environment and Resources*, 36(1):75–99.

Carvalho, G. A., Minnett, P. J., Banzon, V. F., Baringer, W., and Heil, C. A. (2011). Long-term evaluation of three satellite ocean color algorithms for identifying harmful algal blooms (Karenia brevis) along the west coast of Florida: A matchup assessment. *Remote Sensing of Environment*, 115(1):1–18.

Carvalho, L., McDonald, C., de Hoyos, C., Mischke, U., Phillips, G., Borics, G., Poikane, S., Skjelbred, B., Solheim, A. L., van Wichelen, J., Cardoso, A. C., and Cadotte, M. (2013a). Sustaining recreational quality of European lakes: minimizing the health risks from algal blooms through phosphorus control. *Journal of Applied Ecology*, 50(2):315–323.

Carvalho, L., Poikane, S., Solheim, A. L., Phillips, G., Borics, G., Catalan, J., de Hoyos, C., Drakare, S., Dudley, B. J., Järvinen, M., Laplace-Treyture, C., Maileht, K., McDonald, C., Mischke, U., Moe, J., Morabito, G., Nõges, P., Nõges, T., Ott, I., Pasztaleniec, A., Skjelbred, B., and Thackeray, S. J. (2013b). Strength and uncertainty of phytoplankton metrics for assessing eutrophication impacts in lakes. *Hydrobiologia*, 704(1):127–140.

Ceyhun, Ö. and Yalçın, A. (2010). Remote sensing of water depths in shallow waters via artificial neural networks. *Estuarine, Coastal and Shelf Science*, 89(1):89–96.

Chang, N.-B., Imen, S., and Vannah, B. W. (2014). Remote Sensing for Monitoring Surface Water Quality Status and Ecosystem State in Relation to the Nutrient Cycle: A 40-Year Perspective. *Critical Reviews in Environmental Science and Technology*, 45(2):101–166.

Chao Rodríguez, Y., el Anjoumi, A., Domínguez-Gómez, J. A., Rodríguez Pérez, D., and Rico, E. (2014). Using Landsat image time series to study a small water body in Northern Spain. *Environmental monitoring and assessment*, 186(6):3511–3522.

Chen, J., Zhu, W., Tian, Y. Q., Yu, Q., Zheng, Y., and Huang, L. (2017). Remote estimation of colored dissolved organic matter and chlorophyll-a in Lake Huron using Sentinel-2 measurements. *Journal of Applied Remote Sensing*, 11(03):1.

Chen, Q., Zhang, Y., Ekroos, A., and Hallikainen, M. (2004). The role of remote sensing technology in the EU water framework directive (WFD). *Environmental Science & Policy*, 7(4):267–276.

Chorus, I., Falconer, I. R., Salas, H. J., and Bartram, J. (2000). Health risks caused by freshwater cyanobacteria in recreational waters. *Journal of toxicology and environmental health. Part B, Critical reviews*, 3(4):323–347.

Clark, J. M., Schaeffer, B. A., Darling, J. A., Urquhart, E. A., Johnston, J. M., Ignatius, A. R., Myer, M. H., Loftin, K. A., Werdell, P. J., and Stumpf, R. P. (2017). Satellite monitoring of cyanobacterial harmful algal bloom frequency in recreational waters and drinking water sources. *Ecological Indicators*, 80:84–95.

Claustre, H., Hooker, S. B., van Heukelem, L., Berthon, J.-F., Barlow, R., Ras, J., Sessions, H., Targa, C., Thomas, C. S., van der Linde, D., and Marty, J.-C. (2004). An intercomparison of HPLC phytoplankton pigment methods using in situ samples: Application to remote sensing and database activities. *Marine Chemistry*, 85(1-2):41–61.

Coelho, C., Heim, B., Foerster, S., Brosinsky, A., and de Araújo, J. (2017). In Situ and Satellite Observation of CDOM and Chlorophyll-a Dynamics in Small Water Surface Reservoirs in the Brazilian Semiarid Region. *Water*, 9(12):913.

Colyer, C. L., Kinkade, C. S., Viskari, P. J., and Landers, J. P. (2005). Analysis of cyanobacterial pigments and proteins by electrophoretic and chromatographic methods. *Analytical and bioanalytical chemistry*, 382(3):559–569.

Concha, J. A. and Schott, J. R. (2016). Retrieval of color producing agents in Case 2 waters using Landsat 8. *Remote Sensing of Environment*, 185:95–107.

Cox, C. and Munk, W. (1954). Measurement of the Roughness of the Sea Surface from Photographs of the Sun's Glitter. *Journal of the Optical Society of America*, 44(11):838.

Crosman, E. T. and Horel, J. D. (2009). MODIS-derived surface temperature of the Great Salt Lake. *Remote Sensing of Environment*, 113(1):73–81.

de Araujo Barbosa, C.C., Atkinson, P. M., and Dearing, J. A. (2015). Remote sensing of ecosystem services: A systematic review. *Ecological Indicators*, 52:430–443.

Dekker, A. G., Brando, V. E., Anstee, J. M., Pinnel, N., Kutser, T., Hoogenboom, E., Peters, S., Pasterkamp, R., Vos, R., Olbert, C., and Malthus, T. (2002). Imaging Spectrometry of Water. In van der Meer, F. D. and Jong, S., editors, *Imaging Spectrometry*, volume 4 of *Remote Sensing and Digital Image Processing*, pages 307–359. Springer Netherlands.

Dekker, A. G. and Hestir, E. L. (2012). Evaluating the feasibility of systematic inland water quality monitoring with satellite remote sensing. Canberra, Australia.

Dekker, A. G., Phinn, S. R., Anstee, J. M., Bissett, W. P., Brando, V. E., Casey, B., Fearns, P. R., Hedley, J. D., Klonowski, W., Lee, Z. P., Lynch, M., Lyons, M., Mobley, C. D., and Roelfsema, C. M. (2011). Intercomparison of shallow water bathymetry, hydro-optics, and benthos mapping techniques in Australian and Caribbean coastal environments. *Limnology and Oceanography: Methods*, 9:396–425.

Delwart, S., Preusker, R., Bourg, L., Santer, R., Ramon, D., and Fischer, J. (2010). MERIS in–flight spectral calibration. *International Journal of Remote Sensing*, 28(3-4):479–496.

Deutscher Wetterdienst (2016b). Climatological time series of station Teterow. WebWerdis. Deutscher Wetterdienst (DWD).

Deutscher Wetterdienst (5.7.2016a). Climatological time series of station Starnberg and Attenkam. WebWerdis. Deutscher Wetterdienst.

Diamond, J., Stribling, J. B., Stribling, J. R., Huff, L., and Gilliam, J. (2012). An approach for determining bioassessment performance and comparability. *Environmental monitoring and assessment*, 184(4):2247–2260.

Dlamini, S., Nhapi, I., Gumindoga, W., Nhiwatiwa, T., and Dube, T. (2016). Assessing the feasibility of integrating remote sensing and in-situ measurements in monitoring water quality status of Lake Chivero, Zimbabwe. *Physics and Chemistry of the Earth, Parts A/B/C*, 93:2–11.

Doerffer, R. and Schiller, H. (2007). The MERIS Case 2 water algorithm. *International Journal of Remote Sensing*, 28(3-4):517–535.

Doerffer, R. and Schiller, H. (2008). MERIS Regional Coastal and Lake Case 2 Water Project - Atmospheric Correction ATBD: GKSS Research Center 21502 Geesthacht.

Dogan, O. K., Akyurek, Z., and Beklioglu, M. (2009). Identification and mapping of submerged plants in a shallow lake using Quickbird satellite data. *Journal of environmental management*, 90(7):2138–2143.

Donlon, C., Berruti, B., Buongiorno, A., Ferreira, M.-H., Féménias, P., Frerick, J., Goryl, P., Klein, U., Laur, H., Mavrocordatos, C., Nieke, J., Rebhan, H., Seitz, B., Stroede, J., and Sciarra, R. (2012). The Global Monitoring for Environment and Security (GMES) Sentinel-3 mission. *Remote Sensing of Environment*, 120:37–57.

Dörnhöfer, K., Gege, P., Pflug, B., and Oppelt, N. (2016a). Mapping indicators of lake ecology at Lake Starnberg, Germany – First results of Sentinel-2A. In Ouwehand, L., editor, *Living planet symposium 2016*, SP / ESA. ESA Communications, Noordwijk.

Dörnhöfer, K., Göritz, A., Gege, P., Pflug, B., and Oppelt, N. (2016b). Water Constituents and Water Depth Retrieval from Sentinel-2A—A First Evaluation in an Oligotrophic Lake. *Remote Sensing*, 8(11):941.

Dörnhöfer, K., Klinger, P., Heege, T., and Oppelt, N. (2018a). Multi-sensor satellite and in situ monitoring of phytoplankton development in a eutrophic-mesotrophic lake. *Science of The Total Environment*, 612:1200–1214.

Dörnhöfer, K. and Oppelt, N. (2014). Mapping benthic substrate coverage and bathymetry using bio-optical modelling — An enmap case study in the coastal waters of helgoland. In *2014 6th Workshop on Hyperspectral Image and Signal Processing: Evolution in Remote Sensing (WHISPERS)*, pages 1–6. IEEE.

Dörnhöfer, K. and Oppelt, N. (2016). Remote sensing for lake research and monitoring – Recent advances. *Ecological Indicators*, 64:105–122.

Dörnhöfer, K. and Oppelt, N. (2018). LAKESAT. Synergetische Nutzung von hoch- und mittelaufgelösten Satellitendaten zur Operationalisierung der Analyse von Binnengewässern . Grant no.: 50EE1340: Unpublished final report.

Dörnhöfer, K., Scholze, J., Stelzer, K., and Oppelt, N. (2018b). Water colour analysis of Lake Kummerow using time series of remote sensing and in situ data. *Journal of Photogrammetry, Remote sensing and Geoinformation*.

Doxani, G., Vermote, E., Roger, J.-C., Gascon, F., Adriaensen, S., Frantz, D., Hagolle, O., Hollstein, A., Kirches, G., Li, F., Louis, J., Mangin, A., Pahlevan, N., Pflug, B., and Vanhellemont, Q. (2018). Atmospheric Correction Inter-Comparison Exercise. *Remote Sensing*, 10(3):352.

Drusch, M., Del Bello, U., Carlier, S., Colin, O., Fernandez, V., Gascon, F., Hoersch, B., Isola, C., Laberinti, P., Martimort, P., Meygret, A., Spoto, F., Sy, O., Marchese, F., and Bargellini, P. (2012). Sentinel-2: ESA's Optical High-Resolution Mission for GMES Operational Services. *Remote Sensing of Environment*, 120:25–36.

Duan, H., Tao, M., Loiselle, S. A., Zhao, W., Cao, Z., Ma, R., and Tang, X. (2017). MODIS observations of cyanobacterial risks in a eutrophic lake: Implications for long-term safety evaluation in drinking-water source. *Water research*, 122:455–470.

Dudgeon, D., Arthington, A. H., Gessner, M. O., Kawabata, Z.-I., Knowler, D. J., Lévêque, C., Naiman, R. J., Prieur-Richard, A.-H., Soto, D., Stiassny, M. L. J., and Sullivan, C. A. (2006). Freshwater biodiversity: importance, threats, status and conservation challenges. *Biological reviews of the Cambridge Philosophical Society*, 81(2):163–182.

Eder, E., Dörnhöfer, K., Gege, P., Schenk, K., Klinger, P., Wenzel, J., Oppelt, N., and Gruber, N. (2016). Analysis of mineral-rich suspended matter in glacial lakes using simulations and satellite data. In Ouwehand, L., editor, *Living planet symposium 2016*, SP / ESA. ESA Communications, Noordwijk.

Effler, S. W., Peng, F., O'Donnell, D. M., and Strait, C. (2013). The backscattering coefficient and its components in the Great Lakes: A review and synthesis. *Journal of Great Lakes Research*, 39:108–122.

ESA (2014a). The Sentinel-2 Toolbox.

ESA (2014b). The Sentinel-3 Toolbox.

ESA (2015). Sentinel-2A Spectral Response Functions (S2A-SRF).

ESRI (2016). ArcGIS Version 10.3.1.

European Commission (2000). Directive 2000/60/EC of the European Parliament and of the Council of 23 October 2000 establishing a framework for Community action in the field of water policy.

European Space Agency (2016). S2 MPC. Data Quality Report. Reference S2-PDGS-MPC-DQR. Issue 02. Date: 2016-04-11.

Fahnenstiel, G. L., Sayers, M. J., Shuchman, R. A., Yousef, F., and Pothoven, S. A. (2016). Lake-wide phytoplankton production and abundance in the Upper Great Lakes: 2010–2013. *Journal of Great Lakes Research*, 42(3):619–629.

Fell, F. and Fischer, J. (2001). Numerical simulation of the light field in the atmosphere–ocean system using the matrix-operator method. *Journal of Quantitative Spectroscopy and Radiative Transfer*, 69(3):351–388.

Fischer, J. and Grassl, H. (1984). Radiative transfer in an atmosphere–ocean system: An azimuthally dependent matrix-operator approach. *Applied Optics*, 23(7):1032.

Flener, C., Lotsari, E., Alho, P., and Käyhkö, J. (2012). Comparison of empirical and theoretical remote sensing based bathymetry models in river environments. *River Research and Applications*, 28(1):118–133.

Fomferra, N. and Brockmann, C. (2015). BEAM-VISAT. The BEAM Project Website.

Fritz, C., Dörnhöfer, K., Schneider, T., Geist, J., and Oppelt, N. (2017a). Mapping Submerged Aquatic Vegetation Using RapidEye Satellite Data: The Example of Lake Kummerow (Germany). *Water*, 9(7):510.

Fritz, C., Dörnhöfer, K., Schneider, T., Geist, J., and Oppelt, N. (in prep.). Mapping submerged aquatic vegetation development by using a Sentinel-2A time series at Lake Starnberg (Germany). *Journal of Limnology*.

Fritz, C. and Schneider, T. (2018). LAKESAT. Synergetische Nutzung von hoch- und mittelaufgelösten Satellitendaten zur Operationalisierung der Analyse von Binnengewässern . Grant no.: 50EE1336: Unpublished final report.

Fritz, C., Schneider, T., and Geist, J. (2017b). Seasonal Variation in Spectral Response of Submerged Aquatic Macrophytes: A Case Study at Lake Starnberg (Germany). *Water*, 9(12):527.

Gao, J. (2009). Bathymetric mapping by means of remote sensing: methods, accuracy and limitations. *Progress in Physical Geography*, 33(1):103–116.

Garcia, R. A., Fearns, P. R., and McKinna, L. I. (2014). Detecting trend and seasonal changes in bathymetry derived from HICO imagery: A case study of Shark Bay, Western Australia. *Remote Sensing of Environment*, 147:186–205.

Gege, P. (2000). Gaussian model for yellow substance absorption spectra. In: Ocean Optics XV, 16-20 October, 2000, Monaco.

Gege, P. (2012). Estimation of phytoplankton concentration from downwelling irradiance measurements in water. *Israel Journal of Plant Sciences*, 60(1):193–207.

Gege, P. (2014a). A case study at Starnberger See for hyperspectral bathymetry mapping using inverse modelling. In IEEE, editor, *Proceedings of the WHISPERS conference*.

Gege, P. (2014b). WASI-2D: A software tool for regionally optimized analysis of imaging spectrometer data from deep and shallow waters. *Computers & Geosciences*, 62:208–215.

Gege, P. (2017). Radiative Transfer Theory for Inland Waters. In Mishra, D. R., Ogashawara, I., and Gitelson, A. A., editors, *Bio-optical modeling and remote sensing of inland waters*. Elsevier, Amsterdam.

Gege, P. and Groetsch, P. (2016). A spectral model for correcting sun glint and sky glint. Ocean Optics XXIII, CD-ROM. 23-28 October, 2016, Victoria, Canada. *Proceedings of Ocean Optics XXIII 2016*.

Giardino, C., Bartoli, M., Candiani, G., Bresciani, M., and Pellegrini, L. (2007). Recent changes in macrophyte colonisation patterns: an imaging spectrometry-based evaluation of southern Lake Garda (northern Italy). *Journal of Applied Remote Sensing*, 1(1):011509.

Giardino, C., Bresciani, M., Cazzaniga, I., Schenk, K., Rieger, P., Braga, F., Matta, E., and Brando, V. E. (2014a). Evaluation of multi-resolution satellite sensors for assessing water quality and bottom depth of Lake Garda. *Sensors (Basel, Switzerland)*, 14(12):24116–24131.

Giardino, C., Bresciani, M., Fava, F., Matta, E., Brando, V. E., and Colombo, R. (2016). Mapping Submerged Habitats and Mangroves of Lampi Island Marine National Park (Myanmar) from in Situ and Satellite Observations. *Remote Sensing*, 8(1):2.

Giardino, C., Bresciani, M., Stroppiana, D., Oggioni, A., and Morabito, G. (2014b). Optical remote sensing of lakes: An overview on Lake Maggiore. *Journal of Limnology*, 73(s1).

Giardino, C., Bresciani, M., Valentini, E., Gasperini, L., Bolpagni, R., and Brando, V. E. (2015). Airborne hyperspectral data to assess suspended particulate matter and aquatic vegetation in a shallow and turbid lake. *Remote Sensing of Environment*, 157:48–57.

Giardino, C., Bresciani, M., Villa, P., and Martinelli, A. (2010a). Application of Remote Sensing in Water Resource Management: The Case Study of Lake Trasimeno, Italy. *Water Resources Management*, 24(14):3885–3899.

Giardino, C., Candiani, G., Bresciani, M., Lee, Z. P., Gagliano, S., and Pepe, M. (2012). BOMBER: A tool for estimating water quality and bottom properties from remote sensing images. *Computers & Geosciences*, 45:313–318.

Giardino, C., Oggioni, A., Bresciani, M., and Yan, H. (2010b). Remote Sensing of Suspended Particulate Matter in Himalayan Lakes. *Mountain Research and Development*, 30(2):157–168.

Ginn, B. K. (2011). Distribution and limnological drivers of submerged aquatic plant communities in Lake Simcoe (Ontario, Canada): Utility of macrophytes as bioindicators of lake trophic status. *Journal of Great Lakes Research*, 37:83–89.

Gitelson, A., Dall'Olmo, G., Moses, W., Rundquist, D. C., Barrow, T., Fisher, T. R., Gurlin, D., and Holz, J. (2008). A simple semi-analytical model for remote estimation of chlorophyll-a in turbid waters: Validation. *Remote Sensing of Environment*, 112(9):3582–3593.

Gitelson, A. and Kondratyev, K. Y. (1991). Optical models of mesotrophic and eutrophic water bodies. *International Journal of Remote Sensing*, 12(3):373–385.

GKD Bayern (2013a). Befunde Tiefste Stelle/ Starnberger See. Biokomponente Phytoplankton.

GKD Bayern (2013b). Stammdaten Messstelle Starnberger See.

GLaSS (2014). Global Lakes Sentinel Services, D3.2: Harmonized Atmospheric Correction Method: GLaSS Deliverable 3.2.

GLaSS (2015). Global Lakes Sentinel Services. Technical report about measurement protocols: Grant number 313256.

Gómez, J. A. D., Alonso, C. A., and García, A. A. (2011). Remote sensing as a tool for monitoring water quality parameters for Mediterranean Lakes of European Union water framework directive (WFD) and as a system of surveillance of cyanobacterial harmful algae blooms (SCyanoHABs). *Environmental monitoring and assessment*, 181(1-4):317–334.

Government of Canada (1985). Canada Water Act.

Government of South Africa (1998). National Water Act.

Gower, J. F., Brown, L. C., and Borstad, G. A. (2004). Observation of chlorophyll fluorescence in west coast waters of Canada using the MODIS satellite sensor. *Canadian Journal of Remote Sensing*, 30(1):17–25.

Gray, W. B. and Shimshack, J. P. (2011). The Effectiveness of Environmental Monitoring and Enforcement: A Review of the Empirical Evidence. *Review of Environmental Economics and Policy*, 5(1):3–24.

Gregg, W. W. and Carder, K. L. (1990). A simple spectral solar irradiance model for cloudless maritime atmospheres. *Limnology and Oceanography*, 35(8):1657–1675.

Grimm, A. G., Brooks, C. N., Binder, T. R., Riley, S. C., Farha, S. A., Shuchman, R. A., and Krueger, C. C. (2016). Identification of lake trout Salvelinus namaycush spawning habitat in northern Lake Huron using high-resolution satellite imagery. *Journal of Great Lakes Research*, 42(1):127–135.

Ha, N. T. T., Thao, N. T. P., Koike, K., and Nhuan, M. T. (2017). Selecting the Best Band Ratio to Estimate Chlorophyll-a Concentration in a Tropical Freshwater Lake Using Sentinel 2A Images from a Case Study of Lake Ba Be (Northern Vietnam). *ISPRS International Journal of Geo-Information*, 6(12):290.

Håkanson, L. and Boulion, V. V. (2001). Regularities in Primary Production, Secchi Depth and Fish Yield and a New System to Define Trophic and Humic State Indices for Lake Ecosystems. *International Review of Hydrobiology*, 86(1):23–62.

Hampton, S. E., Galloway, A. W. E., Powers, S. M., Ozersky, T., Woo, K. H., Batt, R. D., Labou, S. G., O'Reilly, C. M., Sharma, S., Lottig, N. R., Stanley, E. H., North, R. L., Stockwell, J. D., Adrian, R., Weyhenmeyer, G. A., Arvola, L., Baulch, H. M., Bertani, I., Bowman, JR, L. L., Carey, C. C., Catalan, J., Colom-Montero, W., Domine, L. M., Felip, M., Granados, I., Gries, C., Grossart, H.-P., Haberman, J., Haldna, M., Hayden, B., Higgins, S. N., Jolley, J. C., Kahilainen, K. K., Kaup, E., Kehoe, M. J., MacIntyre, S., Mackay, A. W., Mariash, H. L., McKay, R. M., Nixdorf, B., Noges, P., Noges, T., Palmer, M., Pierson, D. C., Post, D. M., Pruett, M. J., Rautio, M., Read, J. S., Roberts, S. L., Rucker, J., Sadro, S., Silow, E. A., Smith, D. E., Sterner, R. W., Swann, G. E. A., Timofeyev, M. A., Toro, M., Twiss, M. R., Vogt, R. J., Watson, S. B., Whiteford, E. J., and Xenopoulos, M. A. (2017). Ecology under lake ice. *Ecology letters*, 20(1):98–111.

Harke, M. J., Steffen, M. M., Gobler, C. J., Otten, T. G., Wilhelm, S. W., Wood, S. A., and Paerl, H. W. (2016). A review of the global ecology, genomics, and biogeography of the toxic cyanobacterium, Microcystis spp. *Harmful Algae*, 54:4–20.

Harmel, T., Chami, M., Tormos, T., Reynaud, N., and Danis, P.-A. (2017). Sunglint correction of the Multi-Spectral Instrument (MSI)-SENTINEL-2 imagery over inland and sea waters from SWIR bands. *Remote Sensing of Environment*.

Harvey, E. T., Kratzer, S., and Philipson, P. (2015). Satellite-based water quality monitoring for improved spatial and temporal retrieval of chlorophyll-a in coastal waters. *Remote Sensing of Environment*, 158:417–430.

Heblinski, J., Schmieder, K., Heege, T., Agyemang, T. K., Sayadyan, H., and Vardanyan, L. (2011). High-resolution satellite remote sensing of littoral vegetation of Lake Sevan (Armenia) as a basis for monitoring and assessment. *Hydrobiologia*, 661(1):97–111.

Hedley, J. D., Roelfsema, C., Koetz, B., and Phinn, S. (2012). Capability of the Sentinel 2 mission for tropical coral reef mapping and coral bleaching detection. *Remote Sensing of Environment*, 120:145–155.

Heege, T. (2000). *Flugzeuggestützte Fernerkundung von Wasserinhaltsstoffen am Bodensee: published as Research Report Vol. 2000-40 by Deutsches Zentrum für Luft- und Raumfahrt, Köln*. PhD thesis, Freie Universität Berlin, Berlin.

Heege, T. and Fischer, J. (2004). Mapping of water constituents in Lake Constance using multispectral airborne scanner data and a physically based processing scheme. *Canadian Journal of Remote Sensing*, 30(1):77–86.

Heege, T., Häse, C., Bogner, A., and Pinnel, N. (2003). Airborne Multi-spectral Sensing in Shallow and Deep Waters. *Backscatter*, 1/2003:17–19.

Heege, T., Kiselev, V., Wettle, M., and Hung, N. N. (2014). Operational multi-sensor monitoring of turbidity for the entire Mekong Delta. *International Journal of Remote Sensing*, 35(8):2910–2926.

Heege, T., Schenk, K., Klinger, P., Broszeit, A., Wenzel, J., and Kiselev, V. (2015). Monitoring status and trends of water quality in inland waters using earth observation technologiesProceedings "Water Quality in Europe: Challenges and Best Practice" UNESCO-IHP European Regional Consultation Workshop, Koblenz, Germany, Dec 2015, p. 1-4.

Hering, D., Borja, A., Carstensen, J., Carvalho, L., Elliott, M., Feld, C. K., Heiskanen, A.-S., Johnson, R. K., Moe, J., Pont, D., Solheim, A. L., and de van Bund, W. (2010). The European Water Framework Directive at the age of 10: a critical review of the achievements with recommendations for the future. *Science of the Total Environment*, 408(19):4007–4019.

Hestir, E. L., Brando, V. E., Bresciani, M., Giardino, C., Matta, E., Villa, P., and Dekker, A. G. (2015a). Measuring freshwater aquatic ecosystems: The need for a hyperspectral global mapping satellite mission. *Remote Sensing of Environment*, 167:181–195.

Hestir, E. L., Brando, V. E., Campbell, G., Dekker, A. G., and Malthus, T. (2015b). The relationship between dissolved organic matter absorption and dissolved organic carbon in reservoirs along a temperate to tropical gradient. *Remote Sensing of Environment*, 156:395–402.

Hicks, B. J., Stichbury, G. A., Brabyn, L. K., Allan, M. G., and Ashraf, S. (2013). Hindcasting water clarity from Landsat satellite images of unmonitored shallow lakes in the Waikato region, New Zealand. *Environmental monitoring and assessment*, 185(9):7245–7261.

Ho, J. C., Stumpf, R. P., Bridgeman, T. B., and Michalak, A. M. (2017). Using Landsat to extend the historical record of lacustrine phytoplankton blooms: A Lake Erie case study. *Remote Sensing of Environment*, 191:273–285.

Horion, S., Bergamino, N., Stenuite, S., Descy, J.-P., Plisnier, P.-D., Loiselle, S. A., and Cornet, Y. (2010). Optimized extraction of daily bio-optical time series derived from MODIS/Aqua imagery for Lake Tanganyika, Africa. *Remote Sensing of Environment*, 114(4):781–791.

Hou, X., Feng, L., Duan, H., Chen, X., Sun, D., and Shi, K. (2017). Fifteen-year monitoring of the turbidity dynamics in large lakes and reservoirs in the middle and lower basin of the Yangtze River, China. *Remote Sensing of Environment*, 190:107–121.

Huang, C., Yunmei, L., Liu, G., Guo, Y., Yang, H., Zhu, A.-x., Song, T., Huang, T., Zhang, M., and Shi, K. (2017a). Tracing high time-resolution fluctuations in dissolved organic carbon using satellite and buoy observations: Case study in Lake Taihu, China. *International Journal of Applied Earth Observation and Geoinformation*, 62:174–182.

Huang, Y., Liu, H., Hinkel, K., Yu, B., Beck, R., and Wu, J. (2017b). Analysis of Thermal Structure of Arctic Lakes at Local and Regional Scales Using in Situ and Multidate Landsat-8 Data. *Water Resources Research*, 53(11):9642–9658.

Hulley, G. C., Hook, S. J., and Schneider, P. (2011). Optimized split-window coefficients for deriving surface temperatures from inland water bodies. *Remote Sensing of Environment*, 115(12):3758–3769.

Hunter, P. D., Gilvear, D. J., Tyler, A. N., Willby, N. J., and Kelly, A. (2010a). Mapping macrophytic vegetation in shallow lakes using the Compact Airborne Spectrographic Imager (CASI). *Aquatic Conservation: Marine and Freshwater Ecosystems*, 20(7):717–727.

Hunter, P. D., Tyler, A. N., Carvalho, L., Codd, G. A., and Maberly, S. C. (2010b). Hyperspectral remote sensing of cyanobacterial pigments as indicators for cell populations and toxins in eutrophic lakes. *Remote Sensing of Environment*, 114(11):2705–2718.

International Ocean-Colour Coordinating Group (2012). Mission Requirements for Future Ocean-Colour Sensors. Reports of the International Ocean-Colour Coordinating Group. Dartmouth, NS, Canada.

IOCCG (2000). Remote Sensing of Ocean Colour in Coastal, and other Optically-Complex, Waters: , Reports of the International Ocean-Colour Coordinating Group, No. 3. Dartmouth, Canada.

Irons, J. R., Dwyer, J. L., and Barsi, J. A. (2012). The next Landsat satellite: The Landsat Data Continuity Mission. *Remote Sensing of Environment*, 122:11–21.

Jeppesen, E., SONDERGAARD, M., JENSEN, J. P., Havens, K. E., Anneville, O., Carvalho, L., COVENEY, M. F., DENEKE, R., Dokulil, M. T., FOY, B. O., GERDEAUX, D., Hampton, S. E., HILT, S., Kangur, K., KOHLER, J. A., LAMMENS, E. H., Lauridsen, T. L., MANCA, M., MIRACLE, M. R., Moss, B., Noges, P., PERSSON, G., Phillips, G., PORTIELJE, R. O., Romo, S., SCHELSKE, C. L., Straile, D., TATRAI, I., WILLEN, E. V., and Winder, M. (2005). Lake responses to reduced nutrient loading - an analysis of contemporary long-term data from 35 case studies. *Freshwater Biology*, 50(10):1747–1771.

Jiang, G., Ma, R., Loiselle, S. A., Duan, H., Su, W., Cai, W., Huang, C., Yang, J., and Yu, W. (2015). Remote sensing of particulate organic carbon dynamics in a eutrophic lake (Taihu Lake, China). *Science of the Total Environment*, 532:245–254.

Jimenez-Munoz, J. C., Cristobal, J., Sobrino, J. A., Soria, G., Ninyerola, M., and Pons, X. (2009). Revision of the Single-Channel Algorithm for Land Surface Temperature Retrieval From Landsat Thermal-Infrared Data. *IEEE Transactions on Geoscience and Remote Sensing*, 47(1):339–349.

Jin, Q., Lyu, H., Shi, L., Miao, S., Wu, Z., Li, Y., and Wang, Q. (2017). Developing a two-step method for retrieving cyanobacteria abundance from inland eutrophic lakes using MERIS data. *Ecological Indicators*, 81:543–554.

Jørgensen, S. E. (2010). A review of recent developments in lake modelling. *Ecological Modelling*, 221(4):689–692.

Kachelriess, D., Wegmann, M., Gollock, M., and Pettorelli, N. (2014). The application of remote sensing for marine protected area management. *Ecological Indicators*, 36:169–177.

Kalbe, L. and Werner, H. (1974). Das Sediment des Kummerower Sees. Untersuchungen des Chemismus und der Diatomeenflora. *Internationale Revue der gesamten Hydrobiologie und Hydrographie*, 59(6):755–782.

Kallio, K., Koponen, S., Ylöstalo, P., Kervinen, M., Pyhälahti, T., and Attila, J. (2015). Validation of MERIS spectral inversion processors using reflectance, IOP and water quality measurements in boreal lakes. *Remote Sensing of Environment*, 157:147–157.

Kandziora, M., Dörnhöfer, K., Oppelt, N., and Müller, F. (2014). Detecting Land Use And Land Cover Changes In Northern German Agricultural Landscapes To Assess Ecosystem Service Dynamics. *Landscape Online*, pages 1–24.

Kauer, T., Kutser, T., Arst, H., Danckaert, T., and Nõges, T. (2015). Modelling primary production in shallow well mixed lakes based on MERIS satellite data. *Remote Sensing of Environment*, 163:253–261.

Kay, S., Hedley, J. D., and Lavender, S. (2009). Sun Glint Correction of High and Low Spatial Resolution Images of Aquatic Scenes: A Review of Methods for Visible and Near-Infrared Wavelengths. *Remote Sensing*, 1(4):697–730.

Keith, D. J., Milstead, B., Walker, H., Snook, H., Szykman, J., Wusk, M., Kagey, L., Howell, C., Mellanson, C., and Drueke, C. (2012). Trophic status, ecological condition, and cyanobacteria risk of New England lakes and ponds based on aircraft remote sensing. *Journal of Applied Remote Sensing*, 6(1):063577–1.

Kelly, M. G., Birk, S., Willby, N. J., Denys, L., Drakare, S., Kahlert, M., Karjalainen, S. M., Marchetto, A., Pitt, J.-A., Urbanic, G., and Poikane, S. (2016). Redundancy in the ecological assessment of lakes: Are phytoplankton, macrophytes and phytobenthos all necessary? *Science of the Total Environment*, 568:594–602.

Kiefer, I., Odermatt, D., Anneville, O., Wüest, A., and Bouffard, D. (2015). Application of remote sensing for the optimization of in-situ sampling for monitoring of phytoplankton abundance in a large lake. *Science of the Total Environment*, 527-528:493–506.

Kirillin, G., Leppäranta, M., Terzhevik, A., Granin, N., Bernhardt, J., Engelhardt, C., Efremova, T., Golosov, S., Palshin, N., Sherstyankin, P., Zdorovennova, G., and Zdorovennov, R. (2012). Physics of seasonally ice-covered lakes: A review. *Aquatic Sciences*, 74(4):659–682.

Kirk, J. T. O. (2011). *Light and photosynthesis in aquatic ecosystems*. Cambridge University Press, Cambridge, UK and New York, 3rd ed. edition.

Kiselev, V., Bulgarelli, B., and Heege, T. (2015). Sensor independent adjacency correction algorithm for coastal and inland water systems. *Remote Sensing of Environment*, 157:85–95.

Kiselev, V., Roberti, L., and Perona, G. (1995). Finite-element algorithm for radiative transfer in vertically inhomogeneous media: numerical scheme and applications. *Applied Optics*, 34(36):8460–8471.

Kosten, S., Huszar, V. L. M., Bécares, E., Costa, L. S., Donk, E., Hansson, L.-A., Jeppesen, E., Kruk, C., Lacerot, G., Mazzeo, N., Meester, L., Moss, B., Lürling, M., Nõges, T., Romo, S., and Scheffer, M. (2012). Warmer climates boost cyanobacterial dominance in shallow lakes. *Global Change Biology*, 18(1):118–126.

Kropáček, J., Maussion, F., Chen, F., Hoerz, S., and Hochschild, V. (2013). Analysis of ice phenology of lakes on the Tibetan Plateau from MODIS data. *The Cryosphere*, 7(1):287–301.

Kuenzer, C. and Dech, S. (2013). *Thermal Infrared Remote Sensing. Sensors, Methods, Applications.*, volume 17. Springer Netherlands, Dordrecht.

Kutser, T. (2009). Passive optical remote sensing of cyanobacteria and other intense phytoplankton blooms in coastal and inland waters. *International Journal of Remote Sensing*, 30(17):4401–4425.

Kutser, T. (2012). The possibility of using the Landsat image archive for monitoring long time trends in coloured dissolved organic matter concentration in lake waters. *Remote Sensing of Environment*, 123:334–338.

Kutser, T., Metsamaa, L., Strömbeck, N., and Vahtmäe, E. (2006). Monitoring cyanobacterial blooms by satellite remote sensing. *Estuarine, Coastal and Shelf Science*, 67(1-2):303–312.

Kutser, T., Paavel, B., Verpoorter, C., Ligi, M., Soomets, T., Toming, K., and Casal, G. (2016). Remote Sensing of Black Lakes and Using 810 nm Reflectance Peak for Retrieving Water Quality Parameters of Optically Complex Waters. *Remote Sensing*, 8(6):497.

Kutser, T., Tranvik, L., and Pierson, D. C. (2009). Variations in colored dissolved organic matter between boreal lakes studied by satellite remote sensing. *Journal of Applied Remote Sensing*, 3(1):33538.

Kutser, T., Verpoorter, C., Paavel, B., and Tranvik, L. J. (2015). Estimating lake carbon fractions from remote sensing data. *Remote Sensing of Environment*, 157:138–146.

Labsphere (undated). Spectralon. Diffuse Reflectance Targets. 10 % nominal reflectance value. SRT 10-050 Nr. 50 039084 000.

Latifovic, R. and Pouliot, D. (2007). Analysis of climate change impacts on lake ice phenology in Canada using the historical satellite data record. *Remote Sensing of Environment*, 106(4):492–507.

Lee, C. M., Cable, M. L., Hook, S. J., Green, R. O., Ustin, S. L., Mandl, D. J., and Middleton, E. M. (2015a). An introduction to the NASA Hyperspectral InfraRed Imager (HyspIRI) mission and preparatory activities. *Remote Sensing of Environment*, 167:6–19.

Lee, Z. P., Shang, S., Hu, C., Du, K., Weidemann, A., Hou, W., Lin, J., and Lin, G. (2015b). Secchi disk depth: A new theory and mechanistic model for underwater visibility. *Remote Sensing of Environment*, 169:139–149.

Lee, Z. P., Shang, S., Qi, L., Yan, J., and Lin, G. (2016). A semi-analytical scheme to estimate Secchi-disk depth from Landsat-8 measurements. *Remote Sensing of Environment*, 177:101–106.

Legleiter, C. J., Roberts, D. A., and Lawrence, R. L. (2009). Spectrally based remote sensing of river bathymetry. *Earth Surface Processes and Landforms*, 34(8):1039–1059.

Legleiter, C. J., Tedesco, M., Smith, L. C., Behar, A. E., and Overstreet, B. T. (2014). Mapping the bathymetry of supraglacial lakes and streams on the Greenland ice sheet using field measurements and high-resolution satellite images. *The Cryosphere*, 8(1):215–228.

Lehner, B. and Döll, P. (2004). Development and validation of a global database of lakes, reservoirs and wetlands. *Journal of Hydrology*, 296(1-4):1–22.

LfU (2012). Gewässerkundlicher Jahresbericht 2011. Bayerisches Landesamt für Umwelt (LfU).

Li, Y., Zhang, Q., Zhang, L., Tan, Z., and Yao, J. (2017). Investigation of Water Temperature Variations and Sensitivities in a Large Floodplain Lake System (Poyang Lake, China) Using a Hydrodynamic Model. *Remote Sensing*, 9(12):1231.

Li, Y., Zhang, Y., Shi, K., Zhou, Y., Zhang, Y., Liu, X., and Guo, Y. (2018). Spatiotemporal dynamics of chlorophyll-a in a large reservoir as derived from Landsat 8 OLI data: Understanding its driving and restrictive factors. *Environmental science and pollution research international*, 25(2):1359–1374.

Liang, Q., Zhang, Y., Ma, R., Loiselle, S., Li, J., and Hu, M. (2017). A MODIS-Based Novel Method to Distinguish Surface Cyanobacterial Scums and Aquatic Macrophytes in Lake Taihu. *Remote Sensing*, 9(2):133.

Lichtenthaler, H. K. and Buschmann, C. (2000). Chlorophylls and Carotenoids: Measurement and Characterization by UV-VIS Spectroscopy. In Wrolstad, R. E., editor, *Current protocols in food analytical chemistry. F:F4:F4.3*. John Wiley, New York.

Lindström, M., Håkanson, L., Abrahamsson, O., and Johansson, H. (1999). An empirical model for prediction of lake water suspended particulate matter. *Ecological Modelling*, 121(2–3):185–198.

Ling, F., Foody, G., Du, H., Ban, X., Li, X., Zhang, Y., and Du, Y. (2017). Monitoring Thermal Pollution in Rivers Downstream of Dams with Landsat ETM+ Thermal Infrared Images. *Remote Sensing*, 9(11):1175.

Linnemann, K., Gege, P., Rößler, S., Schneider, T., and Melzer, A. (2013). CDOM retrieval using measurements of downwelling irradiance. In Bostater, C. R., Mertikas, S. P., and Neyt, X., editors, *SPIE Remote Sensing*, SPIE Proceedings, page 88880I. SPIE.

Liu, H., Li, Q., Shi, T., Hu, S., Wu, G., and Zhou, Q. (2017). Application of Sentinel 2 MSI Images to Retrieve Suspended Particulate Matter Concentrations in Poyang Lake. *Remote Sensing*, 9(12):761.

Lobo, F. L., Costa, M. P., and Novo, E. M. (2015). Time-series analysis of Landsat-MSS/TM/OLI images over Amazonian waters impacted by gold mining activities. *Remote Sensing of Environment*, 157:170–184.

Long, C. M. and Pavelsky, T. M. (2013). Remote sensing of suspended sediment concentration and hydrologic connectivity in a complex wetland environment. *Remote Sensing of Environment*, 129:197–209.

LU-MV (2002a). Above ground catchment area of Lake Kummerow - Land use. BNTK. ID 200010. Ministry for Agriculture, Environment and Consumer Protection. Department for inland waters.

LU-MV (2002b). Bathymetric contours Lake Kummerow. ID 200010. Ministry for Agriculture, Environment and Consumer Protection. Department for inland waters.

LU-MV (2015a). Chemical monitoring data from 2003 to 2011. Lake Kummerow (200010).

LU-MV (2015b). Chemical monitoring data from 2004 to 2015. Lake Kummerow (200010).

LU-MV (2015c). Trophic levels assessements of Lake Kummerow 2004-2015. ID 200010. Ministry for Agriculture, Environment and Consumer Protection. Department for inland waters. Seenprogramm Mecklenburg-Vorpommern.

LU-MV (2016). Phytoplankton monitoring data from 2003 to 2011. Lake Kummerow (200010).

Luo, J., Duan, H., Ma, R., Jin, X., Li, F., Hu, W., Shi, K., and Huang, W. (2017). Mapping species of submerged aquatic vegetation with multi-seasonal satellite images and considering life history information. *International Journal of Applied Earth Observation and Geoinformation*, 57:154–165.

Luo, J., Li, X., Ma, R., Li, F., Duan, H., Hu, W., Qin, B., and Huang, W. (2016). Applying remote sensing techniques to monitoring seasonal and interannual changes of aquatic vegetation in Taihu Lake, China. *Ecological Indicators*, 60:503–513.

Lymburner, L., Botha, E., Hestir, E., Anstee, J., Sagar, S., Dekker, A., and Malthus, T. (2016). Landsat 8: Providing continuity and increased precision for measuring multi-decadal time series of total suspended matter. *Remote Sensing of Environment*, 185:108–118.

Lyu, H., Wang, Y., Jin, Q., Shi, L., Li, Y., and Wang, Q. (2017). Developing a semi-analytical algorithm to estimate particulate organic carbon (POC) levels in inland eutrophic turbid water based on MERIS images: A case study of Lake Taihu. *International Journal of Applied Earth Observation and Geoinformation*, 62:69–77.

Madsen, J. D., Chambers, P. A., James, W. F., Koch, E. W., and Westlake, D. F. (2001). The interaction between water movement, sediment dynamics and submersed macrophytes. *Hydrobiologia*, 444(1-3):71–84.

Majozi, N. P., Salama, M. S., Bernard, S., Harper, D. M., and Habte, M. G. (2014). Remote sensing of euphotic depth in shallow tropical inland waters of Lake Naivasha using MERIS data. *Remote Sensing of Environment*, 148:178–189.

Manzo, C., Bresciani, M., Giardino, C., Braga, F., and Bassani, C. (2015). Sensitivity analysis of a bio-optical model for Italian lakes focused on Landsat-8, Sentinel-2 and Sentinel-3. *European Journal of Remote Sensing*, 48:17–32.

Manzo, C., Federica, B., Luca, Z., Ernesto, B. V., Claudia, G., Mariano, B., and Cristiana, B. (2018). Spatio-temporal analysis of prodelta dynamics by means of new satellite generation: The case of Po river by Landsat-8 data. *International Journal of Applied Earth Observation and Geoinformation*, 66:210–225.

Matthews, M. W. (2011). A current review of empirical procedures of remote sensing in inland and near-coastal transitional waters. *International Journal of Remote Sensing*, 32(21):6855–6899.

Matthews, M. W. (2014). Eutrophication and cyanobacterial blooms in South African inland waters: 10 years of MERIS observations. *Remote Sensing of Environment*, 155:161–177.

Matthews, M. W., Bernard, S., and Robertson, L. (2012). An algorithm for detecting trophic status (chlorophyll-a), cyanobacterial-dominance, surface scums and floating vegetation in inland and coastal waters. *Remote Sensing of Environment*, 124:637–652.

Matthews, M. W., Bernard, S., and Winter, K. (2010). Remote sensing of cyanobacteria-dominant algal blooms and water quality parameters in Zeekoevlei, a small hypertrophic lake, using MERIS. *Remote Sensing of Environment*, 114(9):2070–2087.

Matthews, M. W. and Odermatt, D. (2015). Improved algorithm for routine monitoring of cyanobacteria and eutrophication in inland and near-coastal waters. *Remote Sensing of Environment*, 156:374–382.

McKee, D., Röttgers, R., Neukermans, G., Calzado, V. S., Trees, C., Ampolo-Rella, M., Neil, C., and Cunningham, A. (2014). Impact of measurement uncertainties on determination of chlorophyll-specific absorption coefficient for marine phytoplankton. *Journal of Geophysical Research: Oceans*, 119(12):9013–9025.

Melzer, A., Zimmermann, S., and Schorer, A. (2003). Seelitorale in Bayern. Starnberger See. Makrophyten-Kartierungen 1979, 1989 und 2000: Materialien Nr. 110.

Mercado, J. M., Gómez-Jakobsen, F., Cortés, D., Yebra, L., Salles, S., León, P., and Putzeys, S. (2016). A method based on satellite imagery to identify spatial units for eutrophication management. *Remote Sensing of Environment*, 186:123–134.

Millennium Ecosystem Assessment (2005). Ecosystems and Human Well-Being: Wetlands and Water Synthesis. World Resources Institute, Washington, DC.

Mobley, C. D. (1989). A numerical model for the computation of radiance distributions in natural waters with wind-roughened surfaces. *Limnology and Oceanography*, 34(8):1473–1483.

Mobley, C. D. (1999). Estimation of the remote-sensing reflectance from above-surface measurements. *Applied Optics*, 38(36):7442.

Mobley, C. D., Boss, E., and Roesler, C. (2015). Ocean Optics Web Book.

Morel, A. and Prieur, L. (1977). Analysis of variations in ocean color1. *Limnology and Oceanography*, 22(4):709–722.

Morel, A. Y. and Gordon, H. R. (1980). Report of the working group on water color. *Boundary-Layer Meteorology*, 18(3):343–355.

Moses, W. J., Sterckx, S., Montes, M. J., de Keukelaere, L., and Knaeps, E. (2017). Atmospheric Correction for Inland Waters. In Mishra, D. R., Ogashawara, I., and Gitelson, A. A., editors, *Bio-optical modeling and remote sensing of inland waters*, pages 69–100. Elsevier, Amsterdam.

Moss, B. (2012). Cogs in the endless machine: lakes, climate change and nutrient cycles: a review. *Science of the Total Environment*, 434:130–142.

Mouw, C. B., Greb, S., Aurin, D. A., DiGiacomo, P. M., Lee, Z. P., Twardowski, M., Binding, C. E., Hu, C., Ma, R., Moore, T., Moses, W., and Craig, S. E. (2015). Aquatic color radiometry remote sensing of coastal and inland waters: Challenges and recommendations for future satellite missions. *Remote Sensing of Environment*, 160:15–30.

Mueller, J. L., Morel, A., Frouin, R., Davis, C. O., Arone, R., Carder, K. L., Lee, Z. P., Steward, R. G., Hooker, S., Mobley, C. D., McLean, S., Holben, B., Miller, M., Pietras, C., Knobelspiesse, K. D., Fargion, G. S., Porter, J., and Voss, K. (2003). Ocean Optics Protocols For Satellite Ocean Color Sensor Validation, Revision 4, Volume III: Radiometric Measurements and Data Analysis Protocols: NASA/TM-2003-21621/Rev-Vol III.

Müller-Wilm, U. (2016). S2PAD SEN2COR 2.2.0 –Readme, S2PAD-VEGA-SRN-0001.

Murfitt, J. and Brown, L. C. (2017). Lake ice and temperature trends for Ontario and Manitoba: 2001 to 2014. *Hydrological Processes*, 31(21):3596–3609.

NASA (2015). OceanColor SeaDAS.

Nechad, B., Ruddick, K., Schroeder, T., Oubelkheir, K., Blondeau-Patissier, D., Cherukuru, N., Brando, V. E., Dekker, A. G., Clementson, L. A., Banks, A. C., Maritorena, S., Werdell, P. J., Sá, C., Brotas, V., Caballero de Frutos, I., Ahn, Y.-H., Salama, S., Tilstone, G., Martinez-Vicente, V., Foley, D., McKibben, M., Nahorniak, J., Peterson, T., Siliò-Calzada, A., Röttgers, R., Lee, Z. P., Peters, M., and Brockmann, C. (2015). CoastColour Round Robin data sets: A database to evaluate the performance of algorithms for the retrieval of water quality parameters in coastal waters. *Earth System Science Data*, 7(2):319–348.

Nguy-Robertson, A., Li, L., Tedesco, L. P., Wilson, J. S., and Soyeux, E. (2013). Determination of absorption coefficients for chlorophyll a, phycocyanin, mineral matter and CDOM from three central Indiana reservoirs. *Journal of Great Lakes Research*, 39:151–160.

Odermatt, D., Brockmann, C., Stelzer, K., Danne, O., and Gangkofner, U. (2015). ESA DUE DIVERSITY II - Algorithm Theoretic Baseline Document (ATBD). Official project deliverable.

Odermatt, D., Gitelson, A., Brando, V. E., and Schaepman, M. (2012). Review of constituent retrieval in optically deep and complex waters from satellite imagery. *Remote Sensing of Environment*, 118:116–126.

Ogashawara, I., Li, L., and Moreno-Madriñán, M. J. (2017a). Slope algorithm to map algal blooms in inland waters for Landsat 8/Operational Land Imager images. *Journal of Applied Remote Sensing*, 11(1):012005.

Ogashawara, I., Mishra, D. R., and Gitelson, A. A. (2017b). Remote Sensing of Inland Waters: Background and Current State-of-the-Art. In Mishra, D. R., Ogashawara, I., and Gitelson, A. A., editors, *Bio-optical modeling and remote sensing of inland waters*, pages 1–24. Elsevier, Amsterdam.

Oliver, R. L., Hamilton, D. P., Brookes, J. D., and Ganf, G. G. (2012). Physiology, Blooms and Prediction of Planktonic Cyanobacteria. In Whitton, B. A., editor, *Ecology of cyanobacteria II*, pages 155–194. Springer, Dordrecht and London.

Olmanson, L. G., Brezonik, P. L., Finlay, J. C., and Bauer, M. E. (2016). Comparison of Landsat 8 and Landsat 7 for regional measurements of CDOM and water clarity in lakes. *Remote Sensing of Environment*, 185:119–128.

Oppelt, N., Scheiber, R., Wegmann, M., Taubenböck, H., Gege, P., and Berger, M. (2015). Fundamentals of remote sensing for terrestrial applications: evolution, current state-of-art, and future possibilities. In Thenkabail, P. S., editor, *Remotely sensed data characterization, classification, and accuracies*. Taylor & Francis, Boca Raton, Fl.

Oppelt, N., Schulze, F., Bartsch, I., Doernhoefer, K., and Eisenhardt, I. (2012). Hyperspectral classification approaches for intertidal macroalgae habitat mapping: a case study in Heligoland. *Optical Engineering*, 51(11):111703.

Paerl, H. W., Gardner, W. S., Havens, K. E., Joyner, A. R., McCarthy, M. J., Newell, S. E., Qin, B., and Scott, J. T. (2016). Mitigating cyanobacterial harmful algal blooms in aquatic ecosystems impacted by climate change and anthropogenic nutrients. *Harmful Algae*, 54:213–222.

Pahlevan, N., Lee, Z. P., Wei, J., Schaaf, C. B., Schott, J. R., and Berk, A. (2014). On-orbit radiometric characterization of OLI (Landsat-8) for applications in aquatic remote sensing. *Remote Sensing of Environment*, 154:272–284.

Pahlevan, N., Sarkar, S., and Franz, B. A. (2016). Uncertainties in coastal ocean color products: Impacts of spatial sampling. *Remote Sensing of Environment*, 181:14–26.

Pahlevan, N., Sarkar, S., Franz, B. A., Balasubramanian, S. V., and He, J. (2017). Sentinel-2 MultiSpectral Instrument (MSI) data processing for aquatic science applications: Demonstrations and validations. *Remote Sensing of Environment*, 201:47–56.

Palmer, S. C., Hunter, P. D., Lankester, T., Hubbard, S., Spyrakos, E., Tyler, A. N., Présing, M., Horváth, H., Lamb, A., Balzter, H., and Tóth, V. R. (2015a). Validation of Envisat MERIS algorithms for chlorophyll retrieval in a large, turbid and optically-complex shallow lake. *Remote Sensing of Environment*, 157:158–169.

Palmer, S. C., Kutser, T., and Hunter, P. D. (2015b). Remote sensing of inland waters: Challenges, progress and future directions. *Remote Sensing of Environment*, 157:1–8.

Palmer, S. C., Odermatt, D., Hunter, P. D., Brockmann, C., Présing, M., Balzter, H., and Tóth, V. R. (2015c). Satellite remote sensing of phytoplankton phenology in Lake Balaton using 10 years of MERIS observations. *Remote Sensing of Environment*, 158:441–452.

Pareeth, S., Bresciani, M., Buzzi, F., Leoni, B., Lepori, F., Ludovisi, A., Morabito, G., Adrian, R., Neteler, M., and Salmaso, N. (2017). Warming trends of perialpine lakes from homogenised time series of historical satellite and in-situ data. *Science of the Total Environment*, 578:417–426.

Pareeth, S., Salmaso, N., Adrian, R., and Neteler, M. (2016). Homogenised daily lake surface water temperature data generated from multiple satellite sensors: A long-term case study of a large sub-Alpine lake. *Scientific reports*, 6:31251.

Pasztaleniec, A. (2016). Phytoplankton in the ecological status assessment of European lakes – advantages and constraints. *Ochrona Srodowiska i Zasobów Naturalnych*, 27(1).

Peeters, E. T., Franken, R. J., Jeppesen, E., Moss, B., Bécares, E., Hansson, L.-A., Romo, S., Kairesalo, T., Gross, E. M., van Donk, E., Nõges, T., Irvine, K., Kornijów, R., and Scheffer, M. (2009). Assessing ecological quality of shallow lakes: Does knowledge of transparency suffice? *Basic and Applied Ecology*, 10(1):89–96.

Peng, F. and Effler, S. W. (2012). Mass-specific scattering coefficient for natural minerogenic particle populations: particle size distribution effect and closure analyses. *Applied Optics*, 51(13):2236–2249.

Penning, W. E., Dudley, B. J., Mjelde, M., Hellsten, S., Hanganu, J., Kolada, A., van den Berg, M., Poikane, S., Phillips, G., Willby, N. J., and Ecke, F. (2008). Using aquatic macrophyte community indices to define the ecological status of European lakes. *Aquatic Ecology*, 42(2):253–264.

Philipson, P., Kratzer, S., Ben Mustapha, S., Strömbeck, N., and Stelzer, K. (2016). Satellite-based water quality monitoring in Lake Vänern, Sweden. *International Journal of Remote Sensing*, 37(16):3938–3960.

Pinnel, N. (2006). *A method for mapping submerged macrophytes in lakes using hyperspectral remote sensing*. PhD thesis, TU München, München.

Pitarch, J., Ruiz-Verdú, A., Sendra, M. D., and Santoleri, R. (2017). Evaluation and reformulation of the maximum peak height algorithm (MPH) and application in a hypertrophic lagoon. *Journal of Geophysical Research: Oceans*, 122(2):1206–1221.

Plath, T. (30.9.2014). Igitt: Die Pest am Kummerower See: (Ugh. Pest at Lake Kummerow). *Nordkurier*.

Plath, T. (4.8.2015). Giftige Algenpest am Kummerower See. (Toxic algal bloom at Lake Kummerow). *Nordkurier*.

Poikane, S., Birk, S., Böhmer, J., Carvalho, L., de Hoyos, C., Gassner, H., Hellsten, S., Kelly, M., Solheim, A. L., Olin, M., Pall, K., Phillips, G., Portielje, R., Ritterbusch, D., SANDIN, L., Schartau, A.-K., SOLIMINI, A. G., van den Berg, M., Wolfram, G., and van de Bund, W. (2015). A hitchhiker's guide to European lake ecological assessment and intercalibration. *Ecological Indicators*, 52:533–544.

Poikane, S., Portielje, R., van den Berg, M., Phillips, G., Brucet, S., Carvalho, L., Mischke, U., Ott, I., Soszka, H., van Wichelen, J., and Strecker, A. (2014). Defining ecologically relevant water quality targets for lakes in Europe. *Journal of Applied Ecology*, 51(3):592–602.

Politi, E., Cutler, M. E., and Rowan, J. S. (2015). Evaluating the spatial transferability and temporal repeatability of remote-sensing-based lake water quality retrieval algorithms at the European scale: A meta-analysis approach. *International Journal of Remote Sensing*, 36(11):2995–3023.

Politi, E., Cutler, M. E. J., and Rowan, J. S. (2012). Using the NOAA Advanced Very High Resolution Radiometer to characterise temporal and spatial trends in water temperature of large European lakes. *Remote Sensing of Environment*, 126:1–11.

Politi, E., Rowan, J. S., and Cutler, M. E. J. (2016). Assessing the utility of geospatial technologies to investigate environmental change within lake systems. *Science of the Total Environment*, 543(Pt A):791–806.

Potes, M., Costa, M. J., da Silva, J. C. B., Silva, A. M., and Morais, M. (2011). Remote sensing of water quality parameters over Alqueva Reservoir in the south of Portugal. *International Journal of Remote Sensing*, 32(12):3373–3388.

Pour Kheyrollah, H., Rontu, L., Duguay, C. R., Eerola, K., and Kourzeneva, E. (2014). Impact of satellite-based lake surface observations on the initial state of HIRLAM. Part II: Analysis of lake surface temperature and ice cover. *Tellus A*, 66:671–688.

R Core Team (2016). R: A Language and Environment for Statistical Computing.

Rastogi, R. P., Sinha, R. P., and Incharoensakdi, A. (2014). The cyanotoxin-microcystins: Current overview. *Reviews in Environmental Science and Bio/Technology*, 13(2):215–249.

Reyjol, Y., Argillier, C., Bonne, W., Borja, A., Buijse, A. D., Cardoso, A. C., Daufresne, M., Kernan, M., Ferreira, M. T., Poikane, S., Prat, N., Solheim, A. L., Stroffek, S., Usseglio-Polatera, P., Villeneuve, B., and van de Bund, W. (2014). Assessing the ecological status in the context of the European Water Framework Directive: where do we go now? *Science of the Total Environment*, 497-498:332–344.

Reynaud, A. and Lanzanova, D. (2017). A Global Meta-Analysis of the Value of Ecosystem Services Provided by Lakes. *Ecological Economics*, 137:184–194.

Reynolds, C. S. (2006). *Ecology of phytoplankton*. Ecology, biodiversity, and conservation. Cambridge University Press, Cambridge.

Riedel, S., Gege, P., Schneider, M., Pflug, B., and Oppelt, N. (2016). Comparison of atmospheric parameters derived from in-situ and hyperspectral remote sensing data beautiful Bavarian lakes. In ESA Communications, editor, *Proceedings of the Living Planet Symposium 2016. SP-740 August 2016.*

Riedmüller, U. (2014). *Trophieklassifikation von Seen: Richtlinie zur Ermittlung des Trophie-Index nach LAWA für natürliche Seen, Baggerseen, Talsperren und Speicherseen*. Empfehlungen oberirdische Gewässer. Kulturbuch-Verl., Berlin, stand: 2014 edition.

Robert, E., Kergoat, L., Soumaguel, N., Merlet, S., Martinez, J.-M., Diawara, M., and Grippa, M. (2017). Analysis of Suspended Particulate Matter and Its Drivers in Sahelian Ponds and Lakes by Remote Sensing (Landsat and MODIS): Gourma Region, Mali. *Remote Sensing*, 9(12):1272.

Rodrigues, T., Alcântara, E., Watanabe, F., and Imai, N. (2017). Retrieval of Secchi disk depth from a reservoir using a semi-analytical scheme. *Remote Sensing of Environment*, 198:213–228.

Roessler, S., Wolf, P., Schneider, T., and Melzer, A. (2013). Multispectral Remote Sensing of Invasive Aquatic Plants Using RapidEye. In Krisp, J. M., Meng, L., Pail, R., and Stilla, U., editors, *Earth Observation of Global Changes (EOGC)*, Lecture notes in geoinformation and cartography, pages 109–123. Springer Berlin Heidelberg, Berlin, Heidelberg.

Rose, K. C., Greb, S. R., Diebel, M., and Turner, M. G. (2017). Annual precipitation regulates spatial and temporal drivers of lake water clarity. *Ecological applications : a publication of the Ecological Society of America*, 27(2):632–643.

Rößler, S. (2014). *Methods for multitemporal mapping of submerged aquatic macrophytes using multi- and hyperspectral remote sensing*. PhD thesis, TU München, München.

Rößler, S., Wolf, P., Schneider, T., and Melzer, A. (2012). Monitoring of invasive aquatic plants using multitemporal RapidEye-data. Proceedings of the 1st EARSeL Workshop on Temporal Analysis of Satellite Images, Mykonos, Greece, 23-25 May 2012. In ESA, editor, *Proceedings of the 1st EARSeL Workshop on Temporal Analysis of Satellite Images*, volume 2012.

Rößler, S., Wolf, P., Schneider, T., Zimmermann, S., and Melzer, A. (2013). Water constituent retrieval and littoral bottom mapping using hyperspectral APEX imagery and submersed artificial surfaces. *EARseL eProceedings*, 12:44–57.

Röttgers, R., Heymann, K., and Krasemann, H. (2014). Suspended matter concentrations in coastal waters: Methodological improvements to quantify individual measurement uncertainty. *Estuarine, Coastal and Shelf Science*, 151:148–155.

Rozenstein, O., Qin, Z., Derimian, Y., and Karnieli, A. (2014). Derivation of land surface temperature for Landsat-8 TIRS using a split window algorithm. *Sensors (Basel, Switzerland)*, 14(4):5768–5780.

Salama, M. S. and Su, Z. (2011). Resolving the Subscale Spatial Variability of Apparent and Inherent Optical Properties in Ocean Color Match-Up Sites. *IEEE Transactions on Geoscience and Remote Sensing*, 49(7):2612–2622.

Salem, S., Strand, M., Higa, H., Kim, H., Kazuhiro, K., Oki, K., and Oki, T. (2017). Evaluation of MERIS Chlorophyll-a Retrieval Processors in a Complex Turbid Lake Kasumigaura over a 10-Year Mission. *Remote Sensing*, 9(10):1022.

Santer, R. and Schmechtig, C. (2000). Adjacency effects on water surfaces: Primary scattering approximation and sensitivity study. *Applied Optics*, 39(3):361–375.

Santer, R. and Zagolski, F. (2000). ICOL: Improve Contrast between Ocean and Land." ATBD–MERIS Level-1c, Rev. 1, Rep. D6 (1), University Littoral, France.

Sayers, M., Fahnenstiel, G. L., Shuchman, R. A., and Whitley, M. (2016). Cyanobacteria blooms in three eutrophic basins of the Great Lakes: A comparative analysis using satellite remote sensing. *International Journal of Remote Sensing*, 37(17):4148–4171.

Schaeffer, B. A., Schaeffer, K. G., Keith, D. J., Lunetta, R. S., Conmy, R., and Gould, R. W. (2013). Barriers to adopting satellite remote sensing for water quality management. *International Journal of Remote Sensing*, 34(21):7534–7544.

Schneider, P. and Hook, S. J. (2010). Space observations of inland water bodies show rapid surface warming since 1985. *Geophysical Research Letters*, 37(22):L22405.

Schröder, T. (2005). *Fernerkundung von Wasserinhaltsstoffen in Küstengewässern mit MERIS unter Anwendung expliziter und impliziter Atmosphärenkorrekturverfahren*. PhD thesis, FU Berlin, Berlin.

Schroeder, T., Behnert, I., Schaale, M., Fischer, J., and Doerffer, R. (2007a). Atmospheric correction algorithm for MERIS above case–2 waters. *International Journal of Remote Sensing*, 28(7):1469–1486.

Schroeder, T., Schaale, M., and Fischer, J. (2007b). Retrieval of atmospheric and oceanic properties from MERIS measurements: A new Case–2 water processor for BEAM. *International Journal of Remote Sensing*, 28(24):5627–5632.

Shen, M., Duan, H., Cao, Z., Xue, K., Loiselle, S., and Yesou, H. (2017). Determination of the Downwelling Diffuse Attenuation Coefficient of Lake Water with the Sentinel-3A OLCI. *Remote Sensing*, 9(12):1246.

Shi, K., Zhang, Y., Liu, X., Wang, M., and Qin, B. (2014). Remote sensing of diffuse attenuation coefficient of photosynthetically active radiation in Lake Taihu using MERIS data. *Remote Sensing of Environment*, 140:365–377.

Shi, K., Zhang, Y., Zhu, G., Liu, X., Zhou, Y., Xu, H., Qin, B., Liu, G., and Li, Y. (2015). Long-term remote monitoring of total suspended matter concentration in Lake Taihu using 250 m MODIS-Aqua data. *Remote Sensing of Environment*, 164:43–56.

Shuchman, R. A., Bosse, K. R., Sayers, M. J., Fahnenstiel, G. L., and Leshkevich, G. (2017). SATELLITE OBSERVED WATER QUALITY CHANGES IN THE LAURENTIAN GREAT LAKES DUE TO INVASIVE SPECIES, ANTHROPOGENIC FORCING, AND CLIMATE CHANGE. *ISPRS - International Archives of the Photogrammetry, Remote Sensing and Spatial Information Sciences*, XLII-3/W2:189–195.

Shuchman, R. A., Leshkevich, G., Sayers, M. J., Johengen, T. H., Brooks, C. N., and Pozdnyakov, D. (2013a). An algorithm to retrieve chlorophyll, dissolved organic carbon, and suspended minerals from Great Lakes satellite data. *Journal of Great Lakes Research*, 39:14–33.

Shuchman, R. A., Sayers, M. J., and Brooks, C. N. (2013b). Mapping and monitoring the extent of submerged aquatic vegetation in the Laurentian Great Lakes with multi-scale satellite remote sensing. *Journal of Great Lakes Research*, 39:78–89.

Shuter, B. J., Minns, C. K., and Fung, S. R. (2013). Empirical models for forecasting changes in the phenology of ice cover for Canadian lakes. *Canadian Journal of Fisheries and Aquatic Sciences*, 70(7):982–991.

Sima, S., Ahmadalipour, A., and Tajrishy, M. (2013). Mapping surface temperature in a hyper-saline lake and investigating the effect of temperature distribution on the lake evaporation. *Remote Sensing of Environment*, 136:374–385.

Simon, R. N., Tormos, T., and Danis, P.-A. (2014). Retrieving water surface temperature from archive LANDSAT thermal infrared data: Application of the mono-channel atmospheric correction algorithm over two freshwater reservoirs. *International Journal of Applied Earth Observation and Geoinformation*, 30:247–250.

Slonecker, E. T., Jones, D. K., and Pellerin, B. A. (2016). The new Landsat 8 potential for remote sensing of colored dissolved organic matter (CDOM). *Marine pollution bulletin*, 107:518–527.

Smith, V. H. and Schindler, D. W. (2009). Eutrophication science: where do we go from here? *Trends in ecology & evolution*, 24(4):201–207.

SNAP (2016). ESA Sentinel Application Platform v4.0.

Solheim, A. L., Feld, C. K., Birk, S., Phillips, G., Carvalho, L., Morabito, G., Mischke, U., Willby, N. J., Søndergaard, M., Hellsten, S., Kolada, A., Mjelde, M., Böhmer, J., Miler, O., Pusch, M. T., Argillier, C., Jeppesen, E., Lauridsen, T. L., and Poikane, S. (2013). Ecological status assessment of European lakes: a comparison of metrics for phytoplankton, macrophytes, benthic invertebrates and fish. *Hydrobiologia*, 704(1):57–74.

Søndergaard, M., Johansson, L. S., Lauridsen, T. L., Jørgensen, T. B., Liboriussen, L., and Jeppesen, E. (2010). Submerged macrophytes as indicators of the ecological quality of lakes. *Freshwater Biology*, 55(4):893–908.

Søndergaard, M., Larsen, S. E., Johansson, L. S., Lauridsen, T. L., and Jeppesen, E. (2016). Ecological classification of lakes: Uncertainty and the influence of year-to-year variability. *Ecological Indicators*, 61:248–257.

Spears, B. M., Mackay, E. B., Yasseri, S., Gunn, I. D. M., Waters, K. E., Andrews, C., Cole, S., de Ville, M., Kelly, A., Meis, S., Moore, A. L., Nürnberg, G. K., van Oosterhout, F., Pitt, J.-A., Madgwick, G., Woods, H. J., and Lürling, M. (2016). A meta-analysis of water quality and aquatic macrophyte responses in 18 lakes treated with lanthanum modified bentonite (Phoslock(®)). *Water research*, 97:111–121.

Srivastava, A., Singh, S., Ahn, C.-Y., Oh, H.-M., and Asthana, R. K. (2013). Monitoring approaches for a toxic cyanobacterial bloom. *Environmental Science & Technology*, 47(16):8999–9013.

Stendera, S., Adrian, R., Bonada, N., Cañedo-Argüelles, M., Hugueny, B., Januschke, K., Pletterbauer, F., and Hering, D. (2012). Drivers and stressors of freshwater biodiversity patterns across different ecosystems and scales: a review. *Hydrobiologia*, 696(1):1–28.

Sterckx, S., Knaeps, E., Adriaensen, S., Reusen, I., de Keukelaere, L., Hunter, P., Giardino, C., and Odermatt, D. (2015a). OPERA: An Atmospheric Correction for Land and Water. In Ouwehand, L., editor, *Sentinel-3 for Science Workshop*, ESA SP, 1609-042X. ESA Communications, Noordwijk, The Netherlands.

Sterckx, S., Knaeps, E., Kratzer, S., and Ruddick, K. (2015b). SIMilarity Environment Correction (SIMEC) applied to MERIS data over inland and coastal waters. *Remote Sensing of Environment*, 157:96–110.

Sterckx, S., Knaeps, E., and Ruddick, K. (2011). Detection and correction of adjacency effects in hyperspectral airborne data of coastal and inland waters: The use of the near infrared similarity spectrum. *International Journal of Remote Sensing*, 32(21):6479–6505.

Strömbeck, N. and Pierson, D. C. (2001). The effects of variability in the inherent optical properties on estimations of chlorophyll a by remote sensing in Swedish freshwaters. *Science of the Total Environment*, 268(1-3):123–137.

Stumpf, R. P., Davis, T. W., Wynne, T. T., Graham, J. L., Loftin, K. A., Johengen, T. H., Gossiaux, D., Palladino, D., and Burtner, A. (2016). Challenges for mapping cyanotoxin patterns from remote sensing of cyanobacteria. *Harmful Algae*, 54:160–173.

Sukenik, A., Quesada, A., and Salmaso, N. (2015). Global expansion of toxic and non-toxic cyanobacteria: Effect on ecosystem functioning. *Biodiversity and Conservation*, 24(4):889–908.

Sun, D., Li, Y., Wang, Q., Le, C., Huang, C., and Wang, L. (2009). Parameterization of water component absorption in an inland eutrophic lake and its seasonal variability: A case study in Lake Taihu. *International Journal of Remote Sensing*, 30(13):3549–3571.

Thurman, E. M. (1985). *Organic geochemistry of natural waters*, volume 2 of *Developments in biogeochemistry*. M. Nijholl and Distributors for the U.S. and Canada, Kluwer Academic, Dordrecht and Boston and Hingham, MA, USA, 1st ed. edition.

Toming, K., Kutser, T., Laas, A., Sepp, M., Paavel, B., and Nõges, T. (2016a). First Experiences in Mapping Lake Water Quality Parameters with Sentinel-2 MSI Imagery. *Remote Sensing*, 8(8):640.

Toming, K., Kutser, T., Tuvikene, L., Viik, M., and Nõges, T. (2016b). Dissolved organic carbon and its potential predictors in eutrophic lakes. *Water research*, 102:32–40.

Traganos, D. and Reinartz, P. (2017). Mapping Mediterranean seagrasses with Sentinel-2 imagery. *Marine pollution bulletin*.

Tranvik, L. J., Downing, J. A., Cotner, J. B., Loiselle, S. A., Striegl, R. G., Ballatore, T. J., Dillon, P., Finlay, K., Fortino, K., and Knoll, L. B. (2009). Lakes and reservoirs as regulators of carbon cycling and climate. *Limnology and Oceanography*, 54(6_part_2):2298–2314.

Trees, C. C., Clark, D. K., Bidigare, R. R., Ondrusek, M. E., and Mueller, J. L. (2000). Accessory pigments versus chlorophyll a concentrations within the euphotic zone: A ubiquitous relationship. *Limnology and Oceanography*, 45(5):1130–1143.

Trimble (2012). Datasheet. Trimble Juno SD Handheld GPS device.

TriOS (2015). RAMSES Radiometer.

Tuvikene, L., Nõges, T., and Nõges, P. (2011). Why do phytoplankton species composition and "traditional" water quality parameters indicate different ecological status of a large shallow lake? *Hydrobiologia*, 660(1):3–15.

Tyler, A. N., Hunter, P. D., Spyrakos, E., Groom, S., Constantinescu, A. M., and Kitchen, J. (2016). Developments in Earth observation for the assessment and monitoring of inland, transitional, coastal and shelf-sea waters. *Science of the Total Environment*, 572:1307–1321.

United States Congress House (2002). Federal Water Pollution Control Act.33 U.S.C. 1251-1387.

van Puijenbroek, P., Evers, C., and van Gaalen, F. W. (2015). Evaluation of Water Framework Directive metrics to analyse trends in water quality in the Netherlands. *Sustainability of Water Quality and Ecology*.

Vanhellemont, Q. and Ruddick, K. (2014). Turbid wakes associated with offshore wind turbines observed with Landsat 8. *Remote Sensing of Environment*, 145:105–115.

Vanhellemont, Q. and Ruddick, K. (2015). Advantages of high quality SWIR bands for ocean colour processing: Examples from Landsat-8. *Remote Sensing of Environment*, 161:89–106.

Vanhellemont, Q. and Ruddick, K. (2016). ACOLITE for Sentinel-2: aquatic applications of MSI imagery. In ESA Communications, editor, *Proceedings of the Living Planet Symposium 2016. SP-740 August 2016*.

Verpoorter, C., Kutser, T., Seekell, D. A., and Tranvik, L. J. (2014). A global inventory of lakes based on high-resolution satellite imagery. *Geophysical Research Letters*, 41(18):6396–6402.

Villa, P., Laini, A., Bresciani, M., and Bolpagni, R. (2013). A remote sensing approach to monitor the conservation status of lacustrine Phragmites australis beds. *Wetlands Ecology and Management*, 21(6):399–416.

Vogel, E., Deumlich, D., and Kaupenjohann, M. (2016). Bioenergy maize and soil erosion — Risk assessment and erosion control concepts. *Geoderma*, 261:80–92.

Walshe, T., MacNeil, A., Archer, A., Sweatman, H., Lawrey, E., Bay, L., Addison, P., and Anthony, K. (2014). Integrated Monitoring, modelling and managament of the Great Barrier Reef world heritage area - demonstration case for the Mackay region: Final Report to the Department of the Environment December 2014.

Warne, M. S. J., Batley, G. E., Braga, O., Chapman, J. C., Fox, D. R., Hickey, C. W., Stauber, J. L., and van Dam, R. (2014). Revisions to the derivation of the Australian and New Zealand guidelines for toxicants in fresh and marine waters. *Environmental Science and Pollution Research*, 21(1):51–60.

Weber, H., Riffler, M., Nõges, T., and Wunderle, S. (2016). Lake ice phenology from AVHRR data for European lakes: An automated two-step extraction method. *Remote Sensing of Environment*, 174:329–340.

Wetzel, R. G. (2001). *Limnology: Lake and river ecosystems / Robert G. Wetzel*. Academic, San Diego, Calif. and London, 3rd ed. edition.

Williamson, C. E., Saros, J. E., Vincent, W. F., and Smol, J. P. (2009). Lakes and reservoirs as sentinels, integrators, and regulators of climate change. *Limnology and Oceanography*, 54(6, part 2):2273–2282.

Winder, M. and Schindler, D. E. (2004). Climatic effects on the phenology of lake processes. *Global Change Biology*, 10(11):1844–1856.

Winder, M. and Sommer, U. (2012). Phytoplankton response to a changing climate. *Hydrobiologia*, 698(1):5–16.

Wöbbecke, K., Klett, G., and Rechenberk, B. (2003). Wasserbeschaffenheit der wichtigsten Seen in der Bundesrepublik Deutschland: Datensammlung 1981-2000. Berlin, Germany.

Wolf, P. (2014). *In situ-Messungen als Basis für Wachstums-/Reflexionsmodelle submerser Makrophyten*. PhD thesis, TU München, München.

Wolf, P., Rößler, S., Schneider, T., and Melzer, A. (2013). Collecting in situ remote sensing reflectances of submersed macrophytes to build up a spectral library for lake monitoring. *European Journal of Remote Sensing*, 46:401–416.

Wu, T., Qin, B., Brookes, J. D., Shi, K., Zhu, G., Zhu, M., Yan, W., and Wang, Z. (2015). The influence of changes in wind patterns on the areal extension of surface cyanobacterial blooms in a large shallow lake in China. *Science of the Total Environment*, 518-519:24–30.

Yadav, S., Yoneda, M., Susaki, J., Tamura, M., Ishikawa, K., and Yamashiki, Y. (2017). A Satellite-Based Assessment of the Distribution and Biomass of Submerged Aquatic Vegetation in the Optically Shallow Basin of Lake Biwa. *Remote Sensing*, 9(9):966.

Yang, J., Gong, P., Fu, R., Zhang, M., Chen, J., Liang, S., Xu, B., Shi, J., and Dickinson, R. (2013). The role of satellite remote sensing in climate change studies. *Nature Climate Change*, 3(10):875–883.

Yousef, F., Shuchman, R., Sayers, M., Fahnenstiel, G., and Henareh, A. (2017). Water clarity of the Upper Great Lakes: Tracking changes between 1998–2012. *Journal of Great Lakes Research*, 43(2):239–247.

Yuzugullu, O. and Aksoy, A. (2014). Generation of the bathymetry of a eutrophic shallow lake using WorldView-2 imagery. *Journal of Hydroinformatics*, 16(1):50–59.

Zambrano-Bigiarini, M. (2014). hydroGOF: Goodness-of-fit functions for comparison of simulated and observed hydrological time series: R package version 0.3-8.

Zhang, L. L., Liu, J. L., Yang, Z. F., Li, Y., and Yang, Y. (2013a). Integrated ecosystem health assessment of a macrophyte-dominated lake. *Ecological Modelling*, 252:141–152.

Zhang, Y., Giardino, C., and Li, L. (2017). Water Optics and Water Colour Remote Sensing. *Remote Sensing*, 9(12):818.

Zhang, Y., Liu, X., Osburn, C. L., Wang, M., Qin, B., and Zhou, Y. (2013b). Photobleaching response of different sources of chromophoric dissolved organic matter exposed to natural solar radiation using absorption and excitation-emission matrix spectra. *PloS one*, 8(10):e77515.

Zhang, Y., Liu, X., Qin, B., Shi, K., Deng, J., and Zhou, Y. (2016a). Aquatic vegetation in response to increased eutrophication and degraded light climate in Eastern Lake Taihu: Implications for lake ecological restoration. *Scientific reports*, 6:23867.

Zhang, Y., Ma, R., Duan, H., Loiselle, S., and Xu, J. (2016b). Satellite analysis to identify changes and drivers of CyanoHABs dynamics in Lake Taihu. *Water Science and Technology: Water Supply*, 16(5):1451–1466.

Zhang, Y., Ma, R., Zhang, M., Duan, H., Loiselle, S. A., and Xu, J. (2015). Fourteen-Year Record (2000–2013) of the Spatial and Temporal Dynamics of Floating Algae Blooms in Lake Chaohu, Observed from Time Series of MODIS Images. *Remote Sensing*, 7(8):10523–10542.

Zhang, Y., Shi, K., Zhou, Y., Liu, X., and Qin, B. (2016c). Monitoring the river plume induced by heavy rainfall events in large, shallow, Lake Taihu using MODIS 250m imagery. *Remote Sensing of Environment*, 173:109–121.

Zhang, Y., Zhang, Y., Shi, K., Zha, Y., Zhou, Y., and Liu, M. (2016d). A Landsat 8 OLI-Based, Semianalytical Model for Estimating the Total Suspended Matter Concentration in the Slightly Turbid Xin'anjiang Reservoir (China). *IEEE Journal of Selected Topics in Applied Earth Observations and Remote Sensing*, 9(1):398–413.

Zheng, Z., Ren, J., Li, Y., Huang, C., Liu, G., Du, C., and Lyu, H. (2016). Remote sensing of diffuse attenuation coefficient patterns from Landsat 8 OLI imagery of turbid inland waters: A case study of Dongting Lake. *Science of the Total Environment*, 573:39–54.

Zhong, Y., Notaro, M., Vavrus, S. J., and Foster, M. J. (2016). Recent accelerated warming of the Laurentian Great Lakes: Physical drivers. *Limnology and Oceanography*, 61(5):1762–1786.

Zibordi, G., Ruddick, K., Ansko, I., Moore, G., Kratzer, S., Icely, J., and Reinart, A. (2012). In situ determination of the remote sensing reflectance: An inter-comparison. *Ocean Science Discussions*, 9(2):787–833.

Zimmer, C. (12.8.2014). A Rising 3-Billion-Year-Old Threat. *New York Times*, page D6.

Zolfaghari, K. and Duguay, C. R. (2016). Estimation of Water Quality Parameters in Lake Erie from MERIS Using Linear Mixed Effect Models. *Remote Sensing*, 8(6):473.

Erklärung

Hiermit erkläre ich an Eides statt, dass ich die vorliegende Dissertation, abgesehen von der Beratung durch meine Betreuer/innen, nach Inhalt und Form selbständig verfasst habe und keine weiteren Quellen und Hilfsmittel als die hier angegebenen verwendet habe. Diese Arbeit hat weder ganz noch in Teilen bereits an anderer Stelle im Rahmen eines Prüfungsverfahrens vorgelegen. Als kumulative Dissertation sind Kapitel 3 bis 6 wie zu Beginn der Kapitel vermerkt in den genannten Zeitschriften veröffentlicht. Ich erkläre, dass die vorliegende Arbeit unter Einhaltung der Regeln guter wissenschaftlicher Praxis der Deutschen Forschungsgemeinschaft entstanden ist.

Kiel, den 14.6.2018